



HAL
open science

Study of the coupling of numerical methods for the Vlasov-Maxwell problem

Thomas Respaud

► **To cite this version:**

Thomas Respaud. Study of the coupling of numerical methods for the Vlasov-Maxwell problem. Mathematics [math]. Université de Strasbourg, 2010. English. NNT : 2010STRA6126 . tel-00526817

HAL Id: tel-00526817

<https://theses.hal.science/tel-00526817>

Submitted on 15 Oct 2010

HAL is a multi-disciplinary open access archive for the deposit and dissemination of scientific research documents, whether they are published or not. The documents may come from teaching and research institutions in France or abroad, or from public or private research centers.

L'archive ouverte pluridisciplinaire **HAL**, est destinée au dépôt et à la diffusion de documents scientifiques de niveau recherche, publiés ou non, émanant des établissements d'enseignement et de recherche français ou étrangers, des laboratoires publics ou privés.

INSTITUT DE RECHERCHE MATHÉMATIQUE AVANCÉE
Université de Strasbourg et C.N.R.S. (UMR 7501)
7, rue René Descartes
67084 STRASBOURG Cedex
Discipline: Mathématiques appliquées

Etude du couplage de méthodes numériques pour les équations de Vlasov et Maxwell

par

Thomas RESPAUD

Thèse soutenue le 2 novembre 2010 devant le jury composé de

Eric SONNENDRÜCKER	Directeur de thèse
Mihaï BOSTAN	Rapporteur
Francis FILBET	Rapporteur
Frédéric LAGOUTIÈRE	Examineur
Nicolas CROUSEILLES	Examineur

Remerciements

0.1 Présentation générale : Contexte physique et méthodes numériques

Cette thèse s'ouvre sur une présentation générale du contexte physique et des principales méthodes numériques utilisées pour résoudre le problème considéré.

0.1.1 Contexte physique

Le plasma, tout comme le solide, le liquide ou le gaz, est un état de la matière. Il n'est visible sur Terre qu'à très haute température (au moins 10 K, voire beaucoup plus), quand l'énergie est telle qu'elle réussit à arracher des électrons aux atomes. On obtient alors un mélange globalement neutre des particules chargées, ions et électrons. Le terme plasma, qualifié également de quatrième état de la matière, a été utilisé en physique pour la première fois par le physicien américain Irving Langmuir en 1928 par analogie avec le plasma sanguin.

L'évolution des besoins énergétiques et l'épuisement des combustibles fossiles comme le pétrole imposent le développement de nouvelles sources d'énergie. D'après la fameuse formule $E = mc^2$, on peut produire de l'énergie en réalisant des transformations faisant disparaître de la masse. Deux grands types de réactions nucléaires suivent ce processus. La première est la réaction de fission nucléaire. Celle-ci consiste à générer deux noyaux plus légers à partir du noyau d'un atome lourd (noyau qui contient beaucoup de nucléons, tels les noyaux d'uranium ou de plutonium). La fission est utilisée dans les centrales nucléaires actuelles.

La fusion nucléaire est un processus où deux noyaux atomiques s'assemblent pour former un noyau plus lourd. La fusion de noyaux légers dégage d'énormes quantités d'énergie provenant de l'attraction entre les nucléons due à l'interaction forte. Cette réaction est à l'œuvre naturellement dans le Soleil et la plupart des étoiles de notre univers. En dépit des travaux de recherche réalisés dans le monde entier depuis les années 1950, aucune application industrielle de la fusion à la production d'énergie n'a encore abouti, en dehors du domaine militaire avec la bombe H, étant donné que cette application ne vise aucunement à contenir et maîtriser la réaction produite. Cependant, la réaction de fusion la plus accessible est celle qui implique des noyaux de Deutérium

et de Tritium pour obtenir un atome d'Hélium et un neutron doté d'une très grande énergie qui servira à produire la chaleur nécessaire à fabriquer de l'électricité.

Les travaux pour atteindre cet objectif de fusion contrôlée sur Terre suivent deux approches : la fusion par confinement inertiel qui consiste à atteindre une densité très élevée pendant un temps relativement court en tirant sur une capsule de Deuterium-Tritium avec des faisceaux laser, et la fusion par confinement magnétique qui consiste à confiner le plasma grâce à un champ magnétique à une densité moins élevée mais pendant un temps plus long. C'est cette approche que poursuit le projet ITER, partenariat entre l'Union européenne, le Japon, les Etats-Unis, la Chine, la Corée du Sud, la Russie et l'Inde, dont l'accord international a été signé le 21 novembre 2006 à Paris. Il a pour but de prouver la faisabilité scientifique et technique de la production d'électricité grâce à la fusion. La construction a démarré à Cadarache dans le sud-est de la France. Le réacteur dans lequel est confiné le plasma a une forme toroïdale et s'appelle un tokamak.

Nous nous intéressons à des modèles décrivant l'interaction entre des particules chargées sous l'effet d'un champ électromagnétique extérieur, auto-produit, ou bien souvent les deux. Une particule chargée crée un champ électromagnétique, qui même si son intensité décroît avec la distance à la particule, a un effet dans tout l'espace. Le modèle consiste donc à déterminer le mouvement d'une particule soumise à tous ces champs combinés et éventuellement extérieurs, ceci à l'aide de la Loi de Newton. Vu la quantité gigantesque de particules présentes dans un plasma, il est inconcevable d'utiliser un tel modèle à N corps, ou modèle microscopique pour simuler numériquement le problème. Il est donc nécessaire de recourir à des modèles simplifiés. Nous nous intéresserons au suivant : le modèle mésoscopique ou cinétique dans lequel chaque espèce de particules s du plasma est caractérisée par sa fonction de distribution $f_s(x, v, t)$ qui correspond à une approche statistique de la répartition des particules dans l'espace des phases pour un grand nombre de réalisations. Si l'on suppose les interactions binaires entre particules proches dominantes, on obtient l'équation de Boltzmann. En supposant les interactions entre les particules régies par le champ moyen qu'elles engendrent, on obtient l'équation de Vlasov, non linéairement couplée aux équations de Maxwell qui régissent les champs. L'équation de Vlasov pour une espèce de particules s'écrit :

$$\frac{\partial f}{\partial t} + v(\mathbf{p}) \cdot \nabla_x f + q(\mathbf{E}(t, \mathbf{x}) + v(\mathbf{p}) \times \mathbf{B}(t, \mathbf{x})) \cdot \nabla_p f = 0, \quad (1)$$

avec la vitesse de la particule définie par $\mathbf{v}(\mathbf{p}) = \frac{\mathbf{p}}{m\gamma}$ et le facteur de Lorentz $\gamma = \sqrt{1 + \frac{p_x^2 + p_y^2 + p_z^2}{m^2 c^2}}$ dans le cas relativiste, et $\gamma = 1$ sinon. c est la vitesse de la lumière dans le vide, m la masse de la particule, q sa charge et (\mathbf{E}, \mathbf{B}) les champs électromagnétiques. La fonction f dépend donc de sept variables, trois d'espace : $\mathbf{x} \in \mathbb{R}^3$, trois d'impulsion : $\mathbf{p} \in \mathbb{R}^3$ et le temps $t \in \mathbb{R}$.

Les équations de Maxwell dont les sources sont les densités de charge et de courant, sont calculées à partir des particules :

$$\frac{\partial \mathbf{E}}{\partial t} - c^2 \nabla \times \mathbf{B} = -\frac{\mathbf{J}}{\epsilon_0}, \quad (2)$$

$$\frac{\partial \mathbf{B}}{\partial t} + \nabla \times \mathbf{E} = 0, \quad (3)$$

$$\nabla \cdot \mathbf{E} = \frac{\rho}{\epsilon_0}, \quad (4)$$

$$\nabla \cdot \mathbf{B} = 0, \quad (5)$$

et pour les sources :

$$\rho(\mathbf{x}, t) = \sum_s q_s \int_{\mathbb{R}^3} f_s(\mathbf{x}, \mathbf{p}, t) d\mathbf{p},$$

$$\mathbf{J}(x, t) = \sum_s q_s \int_{\mathbb{R}^3} v(\mathbf{p}) f_s(\mathbf{x}, \mathbf{p}, t) d\mathbf{p}.$$

Dans certains cas particuliers, comme par exemple quand les particules sont à vitesse faible devant celle de la lumière c , on peut supposer que le champ magnétique est stationnaire. On a alors $\nabla \times \mathbf{E} = 0$ d'après (3). Ainsi, le champ électrique dérive d'un potentiel. On obtient ainsi le système de Vlasov-Poisson, où le champ électrique satisfait l'équation de Poisson (4), ou de manière équivalente est solution d'un problème au Laplacien :

$$\mathbf{E} = -\nabla\phi, \quad -\Delta\phi = \frac{\rho}{\epsilon_0}.$$

Les caractéristiques de l'équation de Vlasov (1) sont les fonctions $\mathbf{X}(s; t, \mathbf{x}, \mathbf{p})$, $\mathbf{P}(s; t, \mathbf{x}, \mathbf{p})$ solutions du système d'équations ordinaires suivant avec conditions initiales :

$$\frac{d\mathbf{X}}{ds} = v(\mathbf{P}), \quad \mathbf{X}(t; t, \mathbf{x}, \mathbf{p}) = \mathbf{x},$$

$$\frac{d\mathbf{P}}{ds} = q(\mathbf{E} + v(\mathbf{P}) \times \mathbf{B}), \quad \mathbf{P}(t; t, \mathbf{x}, \mathbf{p}) = \mathbf{p},$$

où $\mathbf{P} = m\gamma(\mathbf{P})\mathbf{V}$. Une propriété du système fait que f est constante le long des caractéristiques, et par conséquent,

$$f(t, \mathbf{x}, \mathbf{p}) = f_0(X(0; t, \mathbf{x}, \mathbf{p}), P(0; t, \mathbf{x}, \mathbf{p})),$$

où f_0 est la fonction de distribution initiale. Ceci fournit d'ailleurs un principe du maximum pour le problème continu.

On a de plus une hypothèse physique dans le modèle continu très importante à respecter au niveau numérique qui est la conservation de la charge, dont l'équation continue est :

$$\frac{\partial \rho}{\partial t} + \nabla \cdot \mathbf{J} = 0.$$

0.1.2 Méthodes numériques

La première méthode à avoir été utilisée pour résoudre numériquement le problème de Vlasov-Maxwell est la méthode PIC. Cette méthode est particulière pour la résolution de l'équation de Vlasov, et on utilise une grille pour résoudre les équations de Maxwell. C'est toujours l'une des méthodes les plus utilisées et elle s'avère très efficace dans certains cas. Cette méthode est de plus assez peu coûteuse au niveau computationnel. Néanmoins, elle présente également des défauts comme la présence inhérente de bruit numérique qui devient problématique dans les

régions à basse densité ou à forte turbulence, et cause un manque de précision relatif dans des cas plus généraux.

La puissance informatique à disposition évoluant sans cesse, avec les années, de nouvelles méthodes numériques pour résoudre Vlasov utilisant une grille de l'espace des phases ont pu voir le jour. Il s'agit des méthodes semi-Lagrangiennes. Ces méthodes sont à la fois Lagrangiennes dans le sens où l'on utilise la constance de la solution le long des caractéristiques de l'équation, et Euleriennes car on utilise les valeurs de la fonction sur une grille de l'espace des phases. Ces méthodes sont plus précises et ne souffrent pas de bruitage numérique. Néanmoins, elles sont beaucoup plus coûteuses, et l'utilisation de la grille de l'espace des phases fait en sorte que pour le moment, la grande majorité des codes semi-Lagrangiens sont 2D, 3D ou 4D. Des codes 5D peuvent être implémentés, mais nécessitent de grandes ressources de calcul. Il existe plusieurs familles de méthodes semi-Lagrangiennes :

La méthode semi-Lagrangienne classique, qui sera appelée BSL tout au long de la thèse pour Backward semi-Lagrangian. Décrivons le principe de la méthode sur un pas de temps. Pour calculer les valeurs de la fonction de distribution sur la grille de l'espace des phases, on suit les caractéristiques de l'équation en reculant dans le temps. On doit donc trouver l'origine des caractéristiques au temps t^n qui aboutissent aux points de la grille en t^{n+1} . Puis, connaissant les valeurs de la fonction au temps t^n sur la grille, on utilise une interpolation pour connaître la valeur au pied de la caractéristique, qui va être transportée sur la grille par la propriété de constance de la fonction de distribution le long des caractéristiques. Cette interpolation est souvent faite en se servant de fonctions de bases appelées les B-splines cubiques. Pour réussir à trouver l'origine des caractéristiques, il faut résoudre un système d'équations différentielles ordinaires dans lequel la valeur des champs doit être calculée. Pour cette résolution, on peut utiliser la méthode numérique de son choix, comme par exemple des algorithmes de type Runge-Kutta. Dans tous les cas, on a besoin des valeurs des champs électromagnétiques au temps t^{n+1} . Pour connaître ces valeurs, il s'agit d'utiliser le solveur Maxwell de son choix. Citons par exemple le schéma de Yee aux différences finies, qui est beaucoup utilisé dans ce cas là. Cette méthode peut être résumée ainsi en 1D :

- pour chaque noeud x_i , calculer $X(t_n; x_i, t^{n+1})$, la valeur de la caractéristique au temps t^n dont la valeur est x_i au temps t^{n+1} .
- comme

$$f^{n+1}(x_i) = f^n(X(t_n; x_i, t^{n+1})),$$

$f^{n+1}(x_i)$ est calculé grâce à une interpolation de $f^n(X(t_n; x_i, t^{n+1}))$.

Il existe également des méthodes semi-Lagrangiennes conservatives qui sont développées grâce à la forme conservative de l'équation de Vlasov, que nous allons donner dans le cas Vlasov-Poisson :

$$\frac{\partial f}{\partial t} + v \frac{\partial f}{\partial x} + \frac{q}{m} E(t, x) \frac{\partial f}{\partial v} = \frac{\partial f}{\partial t} + \nabla \cdot \left(\left(v, \frac{q}{m} E(t, x) \right) f \right).$$

La méthode semi-Lagrangienne conservative peut-être vue comme une méthode de volumes finis, où les flux sont calculés en intégrant la fonction de distribution sur chaque maille au temps t^n . Dans ce cas, l'inconnue devient la valeur moyenne de f sur les mailles : $\frac{1}{V} \int_V f dx dv$, et la méthode numérique peut être décomposée ainsi :

- Reconstruction d'une approximation polynomiale du degré souhaité en utilisant les valeurs moyennes par maille.

- Calcul de l'origine des caractéristiques finissant sur les noeuds de la grille comme dans BSL.
- Calcul de la nouvelle valeur moyenne par maille au temps t^{n+1} utilisant le fait que la valeur $\frac{1}{V} \int_V f dx$ est constante le long des caractéristiques.

Pour finir, il est possible de construire des méthodes semi-Lagrangiennes qui suivent les caractéristiques en avançant dans le temps, qu'on peut appeler méthodes semi-Lagrangiennes en avant et qui seront notées FSL pour Forward semi-Lagrangian. Cette méthode a été mise en place en météorologie par Cotter et Reich [2, 3].

Le but de cette thèse est de construire une méthode semi-Lagrangienne en avant conservant la charge pour le problème de Vlasov-Maxwell. Elle se compose d'une présentation du contexte et d'un état de l'art en ce qui concerne les méthodes numériques usuelles pour résoudre le problème considéré, qui viennent d'être résumés, ainsi que de quatre parties qui sont résumées dans les quatre sections suivantes. La première est dédiée à la mise en place d'une méthode FSL dans des cas 2D de l'espace des phases, et à la validation de cette méthode par des cas tests numériques. La deuxième introduit de nouveaux algorithmes pour résoudre les caractéristiques et propose une analyse du problème de Vlasov-Poisson 1D. La troisième met en place un schéma FSL conservant la charge pour des problèmes 1D, avec des cas tests de validation, et la quatrième ouvre sur un algorithme conservant la charge en 4D de l'espace des phases, utilisant les méthodes semi-Lagrangiennes conservatives.

0.2 La méthode semi-Lagrangienne en avant pour les systèmes de Vlasov-Poisson 1D et Centre Guide.

0.2.1 Petite Introduction.

Les deux modèles étudiés dans cette première partie sont : le modèle Vlasov-Poisson 1D :

$$\frac{\partial f}{\partial t} + v \partial_x f + E(t, x) \partial_v f = 0,$$

$$\partial_x E(t, x) = \rho(t, x) = \int_{\mathbf{R}} f(t, x, v) dv - \rho_i, \quad \int_0^L E(t, x) dx = 0,$$

où ρ représente la densité de charge. L'étude se fera dans l'espace des phases (x, v) .

Et le modèle Centre-Guide, avec une équation de Vlasov :

$$\frac{\partial f}{\partial t} + E^\perp(x, y) \cdot \nabla_{(x, y)} f = 0,$$

où $E^\perp = (E_y, -E_x)$. Notons qu'ici l'espace des phases est en fait un espace physique et qu'il n'y a pas de variable de vitesse. Cette équation est couplée avec l'équation de Poisson 2D pour le champ électrique qui dérive d'un potentiel $\Phi = \Phi(x, y)$:

$$-\Delta \Phi(t, x, y) = f(t, x, y), \quad E(t, x, y) = -\nabla \Phi(t, x, y).$$

L'un des inconvénients de la méthode semi-Lagrangienne classique est que le problème de résolution des caractéristiques est mal posé. En effet, au début d'une étape, dans ce cas là, on connaît x^{n+1} , v^{n+1} et E^n . Or, pour suivre les caractéristiques en arrière, on a besoin tout de suite du champ électrique au temps t^{n+1} . Il est donc nécessaire de chercher une valeur de ce champ à ce temps. Pour ce faire, on peut utiliser des techniques de point fixe comme la méthode de Newton, des méthodes de type prédiction correction, ou encore des algorithmes saute-mouton. L'un des autres désavantages de ces méthodes est que la montée en ordre est assez difficile à obtenir, et coûte très cher. De plus, il semble également ardu d'obtenir des algorithmes conservant la charge avec cette méthode classique. Ceci a motivé l'élaboration d'une méthode semi-Lagrangienne suivant les caractéristiques vers l'avant, technique qui existait déjà dans les équations de météorologie. Les différents objectifs sont donc d'élaborer une méthode explicite facilitant la montée en ordre et qui pourra être utilisée pour construire un schéma conservant la charge discrète.

0.2.2 Présentation de l'algorithme.

L'un des points importants de la méthode est la projection de la fonction de distribution sur un espace de B-splines :

$$f(t, x, y) = \sum_{k,l} \omega_{k,l}^n S(x - X_1(t; x_k, y_l, t^n)) S(y - X_2(t; x_k, y_l, t^n)), \quad \forall t \in [t^n, t^{n+1}], \quad (6)$$

où $X(t; x_k, y_l, t^n) = (X_1, X_2)(t; x_k, y_l, t^n)$ correspond à la solution des caractéristiques au temps t dont la valeur au temps t^n était le point de la grille (x_k, y_l) . La B-splines cubique S est définie ainsi :

$$6S(x) = \begin{cases} (2 - |x|)^3 & \text{si } 1 \leq |x| \leq 2, \\ 4 - 6x^2 + 3|x|^3 & \text{si } 0 \leq |x| \leq 1, \\ 0 & \text{sinon.} \end{cases}$$

Dans l'expression (6), le poids $w_{k,l}^n$ est associé à la particule située au point de la grille (x_k, y_l) au temps t^n . Il correspond au coefficient de la spline cubique déterminé par les conditions d'interpolation suivantes :

$$\begin{aligned} f(t^{n+1}, x_i, y_j) &= \sum_{k,l} \omega_{k,l}^n S(x_i - X_1(t^{n+1}; x_k, y_l, t^n)) S(y_j - X_2(t^{n+1}; x_k, y_l, t^n)), \\ &= \sum_{k,l} \omega_{k,l}^{n+1} S(x_i - x_k) S(y_j - y_l). \end{aligned}$$

Les courbes caractéristiques $X(t, \mathbf{x}, s)$ sont définies de manière générale comme les solutions d'un système d'équations différentielles ordinaires qui peut s'écrire de manière générale :

$$\frac{dX}{dt} = U(X(t), t). \quad (7)$$

avec comme condition initiale $X(s, \mathbf{x}, s) = \mathbf{x}$. L'algorithme total s'écrit alors pour FSL :

- Etape 0 : Initialiser $f_{i,j}^0 = f_0(x_i, y_j)$,

- Etape 1 : Calculer les coefficients de spline $\omega_{k,l}^0$, tels que

$$f_{i,j}^0 = \sum_{k,l} \omega_{k,l}^0 S(x_i - x_k) S(y_j - y_l),$$

- Etape 2 : Résoudre les caractéristiques de t^n à t^{n+1} , avec comme donnée initiale les points de la grille : $X(t^n) = (x_k, y_l)$ pour obtenir $X(t; x_k, y_l, t^n)$ pour $t \in [t^n, t^{n+1}]$, en supposant que la vitesse d'advection U est connue,
- Etape 3 : Projection sur la grille de l'espace des phases utilisant (6) avec $t = t^{n+1}$ pour obtenir $f_{i,j}^{n+1} = f^{n+1}(x_i, y_j)$,
- Etape 4 : Calcul du coefficient de splines cubiques $\omega_{k,l}^{n+1}$ tel que

$$f_{i,j}^{n+1} = \sum_{k,l} \omega_{k,l}^{n+1} S(x_i - x_k) S(y_j - y_l),$$

- Retour à l'étape 2 pour le pas de temps suivant.

Dans ce chapitre, nous utilisons différents algorithmes de résolution des caractéristiques (7) : par exemple l'algorithme de Verlet, mais uniquement pour Vlasov-Poisson car il ne fonctionne pas pour le Centre-Guide. Pour Vlasov-Poisson, on a $U(X(t^n), t^n) = (v^n, E(x^n, t^n))$, et Verlet s'écrit :

- Etape 1 : $\forall k, l, v_{k,l}^{n+\frac{1}{2}} - v_l^n = \frac{\Delta t}{2} E(x_k^n, t^n)$,
- Etape 2 : $\forall k, l, x_{k,l}^{n+1} - x_k^n = \Delta t v_{k,l}^{n+\frac{1}{2}}$,
- Etape 3 : calcul de champ électrique au temps t^{n+1} ,
 - déposition des particules $x_{k,l}^{n+1}$ sur la grille spatiale x_i pour la densité $\rho : \rho(x_i, t^{n+1}) = \sum_{k,l} \omega_{k,l}^n S(x_i - x_{k,l}^{n+1})$,
 - Résoudre l'équation de Poisson sur la grille $x_i : E(x_i, t^{n+1})$,
- Etape 4 : $\forall k, l, v_{k,l}^{n+1} - v_{k,l}^{n+\frac{1}{2}} = \frac{\Delta t}{2} E(x_{k,l}^{n+1}, t^{n+1})$.

Et les algorithmes plus généraux de Runge Kutta d'ordre 2, 3 ou 4. Donnons le détail de l'algorithme de Runge Kutta 2 pour le Centre-Guide où : $U(X^n, t^n) = E^\perp(X^n, t^n)$, avec $E^\perp = (E_y, -E_x)$:

- Etape 1 : $\tilde{X}^{n+1} - X^n = \Delta t E^\perp(X^n, t^n)$,
- Etape 2 : Calcul du champ électrique au temps t^{n+1} ,
 - déposition 2D des particules sur la grille spatiale (x_j, y_i) pour la densité $\rho : \rho(x_j, y_i, t^{n+1}) = \sum_k \omega_k^n S[x_j - \tilde{x}_{k,l}^{n+1}] S[y_i - \tilde{y}_{k,l}^{n+1}]$,
 - Résoudre l'équation de Poisson 2D sur la grille $x_j, y_i : E(x_j, y_i, t_{n+1})$.
- Etape 3 : $X^{n+1} - X^n = \frac{\Delta t}{2} [E^\perp(X^n, t^n) + E^\perp(\tilde{X}^{n+1}, t^{n+1})]$.

0.2.3 Résultats numériques

Afin de valider la méthode développée, elle est testée sur différents cas tests classiques en la comparant avec la méthode BSL qui a déjà fait ses preuves et peut-être prise comme référence. Pour Vlasov-Poisson : les cas tests Landau linéaire, Landau non linéaire, Two Stream Instability et Bump on Tail sont présentés. De nombreuses figures sont présentées, et elles sont toutes en

accord avec la littérature abondante que l'on peut trouver sur le sujet. Le comportement des solutions est extrêmement proche de celui des solutions avec BSL. De plus, sur un cas test assez simple, celui de Hill-Mathieu, nous avons pu retrouver l'ordre en temps de nos schémas de résolution des caractéristiques, et il est conforme aux attentes. Une méthode "hybride" est également testée, sur laquelle on ne fait la déposition que tous les T pas de temps. Les autres étapes se rapprochent du coup d'une méthode PIC sauf que les coefficients de splines sont tout de même actualisés. Quand T augmente, le bruit numérique apparaît, alors qu'il est totalement absent de BSL tout comme de FSL.

Pour le centre-Guide, nous présentons deux cas tests appelés Instabilités de Kelvin Helmholtz 1 et 2. Les résultats numériques sont également tout à fait satisfaisants et en adéquation avec ceux obtenus avec BSL.

Enfin, une étude du temps de calcul est réalisée. Les étapes d'interpolation pour BSL et de déposition pour FSL sont de même complexité, la différence se situe donc dans la résolution des caractéristiques. La méthode en avant avec RK2 est plus lente que la méthode arrière car elle demande une étape de déposition intermédiaire supplémentaire et bien sûr RK4 ne fait qu'accentuer cette différence vu qu'à chaque temps intermédiaire une déposition est faite.

Néanmoins, la méthode remplit ses premiers objectifs, elle est parfaitement explicite et bien posée, la montée en ordre n'a pas posé de problème, et ses similitudes avec les méthodes PIC sont encourageantes dans l'objectif d'un algorithme FSL conservant la charge.

0.3 Analyse d'une nouvelle classe de schémas pour le problème de Vlasov-Poisson 1D.

0.3.1 Petite introduction

Un schéma FSL a été mis en place pour le problème de Vlasov-Poisson. Le schéma de Verlet utilisé entre autres ne peut s'appliquer que dans des cas particuliers comme pour les caractéristiques de Vlasov-Poisson, et non dans d'autres cas plus généraux comme le modèle Centre-Guide ou la gyrocinétique. Les algorithmes de Runge-Kutta, comme on l'a vu sont très coûteux en temps de calcul lorsque l'on souhaite monter en ordre. Ces considérations ont motivé l'élaboration de nouveaux schémas basés sur une procédure de Cauchy-Kovalevsky (CK) qui peut-être écrite à n'importe quel ordre. Dans ce chapitre, nous proposons des méthodes CK d'ordre 2 et 3, et nous donnons une preuve de convergence d'un schéma FSL utilisant ces procédures ou celle de Verlet pour la résolution des caractéristiques et une déposition par splines linéaires. Quelques résultats de convergence de schémas semi-Lagrangiens classiques existent déjà, utilisant la norme L^2 , et une résolution des caractéristiques par une méthode splittée, c'est à dire une méthode pour laquelle les caractéristiques sont approchées par des déplacements horizontaux en x , puis verticaux en v . Or, pour les schémas splittés, il est assez facile de voir que la méthode en avant est exactement la même que la méthode en arrière. Il n'y avait donc pas d'intérêt à travailler dans cette direction. Notre schéma gère les caractéristiques dans le cas général, mais est réalisé en norme L^1 et pour des splines linéaires, résultat donc plus faible à ces niveaux là. La résolution de l'équation de Poisson est faite exactement utilisant une formule avec un noyau de Green. Dans ce chapitre, on donne également une preuve de la conservation

de la masse et du premier moment en vitesse pour les différents schémas considérés.

0.3.2 Problème discret

Tout d'abord, le problème numérique est présenté : Soit $\Omega = [0, L] \times [-R, R]$, et M_h un maillage cartésien de l'espace des phases Ω . M_h est donné par une première suite de points : $(x_i)_{i \in [0..N_x]}$ de l'intervalle $[0, L]$ et une seconde : $(v_j)_{j \in [0..N_v]}$ de l'intervalle $[-R, R]$. Soit $\Delta x_i = x_{i+1} - x_i$ la taille des mailles de l'espace des positions $\Delta v_j = v_{j+1} - v_j$ la taille des mailles de l'espace des vitesses. Pour simplifier l'étude, on considère un maillage régulier, *i.e* $\Delta x_i = \Delta x = \frac{L}{N_x+1}$, et $\Delta v_j = \Delta v = \frac{2R}{N_v}$, où N_x, N_v sont dans \mathbb{N} . Alors h est défini comme $\max(\Delta x, \Delta v)$.

Pour toute fonction g définie sur tous les points $(x_i, v_j) \in M_h$ on notera $g_{i,j} := g(x_i, v_j)$, et ces valeurs sont prolongées à $\mathbb{Z} \times \mathbb{Z}$ par périodicité en x et par 0 en v . L'espace des fonctions L -périodiques en x et à support compact en v sera noté $P(\Omega)$.

Soit $L_h^2(\Omega)$ (resp. $L_h^1(\Omega)$), l'espace des fonctions définies sur la grille dont la norme $\|\cdot\|_{L_h^2(\Omega)}$ (resp $\|\cdot\|_{L_h^1(\Omega)}$) est bornée :

$$\|f\|_{L_h^2(\Omega)} = (\Delta x \Delta v \sum_{i=0}^{N_x-1} \sum_{j=0}^{N_v-1} |f_{i,j}|^2)^{\frac{1}{2}},$$

$$\|f\|_{L_h^1(\Omega)} = \Delta x \Delta v \sum_{i=0}^{N_x-1} \sum_{j=0}^{N_v-1} |f_{i,j}|.$$

La fonction approchée $f_h(t^n)$ est alors donnée partout sur $\mathbb{R}_x \times \mathbb{R}_v$ grâce à un opérateur d'interpolation R_h défini sur une grille uniforme par :

$$R_h : L^1(\Omega) \cap P(\Omega) \longrightarrow L^1(\Omega) \cap P(\Omega),$$

$$f \mapsto R_h f = \sum_{(i,j) \in \mathbb{Z} \times \mathbb{Z}} f_{i,j} \Psi_{i,j},$$

où $\Psi_{i,j}$ seront des produits tensoriels de splines linéaires pour notre étude :

$$S(x) = \begin{cases} (1 - |x|) & \text{si } 0 \leq |x| \leq 1, \\ 0 & \text{sinon.} \end{cases}$$

L'opérateur de calcul du champ électrique lié à une fonction $g \in L^1([0, L] \times \mathbb{R})$ est défini ainsi :

$$E[g](x) = \int_0^L K(x, y) \left(\int_{\mathbb{R}} g(y, v) dv - 1 \right). \quad (8)$$

La fonction approchée f_h est solution de l'équation de Vlasov suivante sur la grille :

$$\frac{\partial f_h}{\partial t}(t, x, v) + v \frac{\partial f_h}{\partial x}(t, x, v) + E_h(t, x) \frac{\partial f_h}{\partial v}(t, x, v) = 0.$$

Cette fonction suit les caractéristiques approchées définies par :

$$\begin{aligned}\frac{dX_h}{dt}(t; (x, v), s) &= V_h(t; (x, v), s), \\ \frac{dV_h}{dt}(t; (x, v), s) &= E_h(t, X(t; (x, v), s)),\end{aligned}\tag{9}$$

où E_h est défini à partir de f_h en utilisant (8) : $E_h = E[f_h](x)$.

Pour les caractéristiques, l'algorithme de Verlet est maintenant connu. Nous avons dérivé des algorithmes suivant une procédure de Cauchy Kovalevsky qui repose sur des développements de Taylor des caractéristiques, puis sur le remplacement des dérivées temporelles par des dérivées spatiales de quantités toutes connues au temps t^n . Cet algorithme s'écrit à l'ordre 3 :

$$\begin{aligned}X^{n+1} &= X^n + \Delta t V^n + \frac{\Delta t^2}{2} E^n(X^n) + \frac{\Delta t^3}{6} (V^n \rho^n(X^n) - J^n(X^n) + \bar{J}), \\ V^{n+1} &= V^n + \Delta t E^n(X^n) + \frac{\Delta t^2}{2} (V^n \rho^n(X^n) - J^n(X^n) + \bar{J}) \\ &\quad + \frac{\Delta t^3}{6} \left(\frac{\partial I_2}{\partial x}(X^n, t^n) - E^n(X^n) - 2V^n \frac{\partial J}{\partial x}(X^n, t^n) + (V^n)^2 \frac{\partial \rho}{\partial x}(X^n, t^n) \right).\end{aligned}$$

Ces algorithmes seront notés plus simplement :

$$\begin{aligned}X^{n+1} &= X^n + \Delta t V^n + \frac{\Delta t^2}{2} E^n(X^n) + \frac{\Delta t^3}{6} \varphi^n(X^n), \\ V^{n+1} &= V^n + \Delta t E^n(X^n) + \frac{\Delta t^2}{2} \varphi^n(X^n) + \frac{\Delta t^3}{6} \phi^n(X^n).\end{aligned}$$

Ensuite, un rappel sur les propriétés a priori des splines est donné :

- $\mathbb{S}_{m+1, h} = \text{Vect}(S_{m+1}(\cdot - x_i) S_{m+1}(\cdot - v_j); \forall (i, j) \in \mathbb{Z})$,
- $\mathbb{S}_{m+1, h} \subset W^{k, p}$ $1 \leq p \leq \infty$ $0 \leq k \leq m$,
- Stabilité $\|R_h f\|_{L^p(\Omega)} \leq C \|f\|_{L^p(\Omega)} \quad \forall f \in L^p(\Omega) \cap P(\Omega), \quad 1 \leq p \leq \infty$ (i),
- Consistance et précision. Il existe $C > 0$ | $\|f - R_h f\|_{W^{k, p}(\Omega)} \leq C h^{m+1-k} \|f\|_{W^{m+1, p}(\Omega)} \quad \forall f \in W^{m+1, p}(\Omega) \cap P(\Omega)$ $1 \leq p \leq \infty$ $0 \leq k \leq m$,
- $\sum_i S_m(\cdot - x_i) = 1, \quad \int S_m(u) du = \Delta x$,
- $\sum_l v_l S_1(v_l - v) = v$.

Après la définition des schémas, une preuve de conservation de la masse et du premier moment en vitesse est donnée pour les schémas de Verlet et CK.

Le théorème de convergence prouvé dans ce chapitre est le suivant :

Théorème :

Supposons $f_0 \in W_{c, \text{per}_x}^{3, \infty}(\mathbb{R}_x \times \mathbb{R}_v)$, positive, périodique en x de période L , à support compact en v . Alors la solution (f_h, E_h) approchée du système de Vlasov-Poisson, calculée à l'aide du schéma numérique présenté, converge vers la solution exacte (f, E) du système de Vlasov-Poisson périodique, et il existe une constante $C = C(\|f\|_{W^{1, \infty}(0, T; W^{2, \infty}(\Omega))})$ indépendante de Δt et de h telle que pour les algorithmes de Verlet et CK2 on ait :

$$\|f - f_h\|_{l^\infty(0, T; L^1(\Omega))} + \|E - E_h\|_{l^\infty(0, T; L^\infty([0, L]))} \leq C(\Delta t^2 + h^2 + \frac{h^2}{\Delta t}).$$

Pour CK3, on a :

$$\|f - f_h\|_{l^\infty(0,T;L^1(\Omega))} + \|E - E_h\|_{l^\infty(0,T;L^\infty([0,L]))} \leq C(\Delta t^3 + h^2 + \frac{h^2}{\Delta t}).$$

Remarque : Pour obtenir ces résultats d'estimation pour CK, on devra supposer $\Delta t \leq \Delta x$.

Ce théorème est prouvé grâce à une utilisation du lemme de Gronwall discret. On doit contrôler l'erreur l^1 au temps $n + 1$:

$$e^{n+1}(i, j) = |f(t^{n+1}, x_i, v_j) - f_h(t^{n+1}, x_i, v_j)| \quad \forall(i, j),$$

$$e^{n+1} = \Delta x \Delta v \sum_{i,j} e^{n+1}(i, j).$$

Alors on décompose $f(t^{n+1}, x_k, v_l) - f_h(t^{n+1}, x_k, v_l)$ ainsi

$$\begin{aligned} f(t^{n+1}, x_k, v_l) - f_h(t^{n+1}, x_k, v_l) &= f(t^{n+1}, x_k, v_l) - R_h f(t^{n+1}, x_k, v_l), \\ &+ R_h f(t^{n+1}, x_k, v_l) - R_h \tilde{f}_h(t^{n+1}, x_k, v_l), \\ &+ R_h \tilde{f}_h(t^{n+1}, x_k, v_l) - R_h f_h(t^{n+1}, x_k, v_l), \end{aligned}$$

où \tilde{f}_h est la fonction f_h au temps t^n mais qui suit les caractéristiques exactes. Comme f_h^{n+1} appartient à l'image de R_h , on a $R_h f_h(t^{n+1}, x_k, v_l) = f_h(t^{n+1}, x_k, v_l)$.

Pour contrôler e^{n+1} en fonction de e^n , une suite de lemmes est prouvée :

Lemma 1. Soit f dans $C(\Omega) \cap P(\Omega)$, alors :

$$\|f - R_h f\|_{L_h^1(\Omega)} \leq Ch^2.$$

Lemma 2. Soit f dans $C(\Omega) \cap P(\Omega)$, alors :

$$\|R_h f^{n+1} - R_h \tilde{f}_h^{n+1}\|_{L_h^1(\Omega)} \leq e^n.$$

Lemma 3. Soit f dans $C(\Omega) \cap P(\Omega)$, alors on a :

$$\begin{aligned} \|R_h \tilde{f}_h^{n+1} - R_h f_h^{n+1}\|_{L_h^1(\Omega)} &\leq C \max_{i,j} (|X(t^{n+1}; (x_i, v_j), t^n) - X_h(t^{n+1}; (x_i, v_j), t^n)|, \\ &+ |V(t^{n+1}; (x_i, v_j), t^n) - V_h(t^{n+1}; (x_i, v_j), t^n)|). \end{aligned}$$

Lemma 4. Verlet

Si $E \in W^{2,\infty}([0, t] \times \mathbb{R})$, avec (X, V) les caractéristiques exactes, et (X_h, V_h) calculées avec E_h et l'algorithme de Verlet :

$$\begin{aligned} |X(t^{n+1}; (x_i, v_j), t^n) - X_h(t^{n+1}; (x_i, v_j), t^n)| + |V(t^{n+1}; (x_i, v_j), t^n) - V_h(t^{n+1}; (x_i, v_j), t^n)| \\ \leq C\Delta t^3 + \Delta t \|(E - E_h)(t^{n+\frac{1}{2}})\|_{L^\infty}. \end{aligned}$$

Lemma 5. : CK3

Si $E \in W^{4,\infty}([0, t] \times \mathbb{R})$, avec (X, V) les caractéristiques exactes, et (X_h, V_h) calculés E_h, ρ_h, J_h et un algorithme CK3 :

$$\begin{aligned} |X(t^{n+1}; (x_i, v_j), t^n) - X_h(t^{n+1}; (x_i, v_j), t^n)| &+ |V(t^{n+1}; (x_i, v_j), t^n) - V_h(t^{n+1}; (x_i, v_j), t^n)| \\ &\leq C\Delta t^4 + C(\Delta t \| (E^n - E_h^n) \|_{l^\infty(\Omega)} + \Delta t^2 \| (\phi^n - \phi_h^n) \|_{l^\infty(\Omega)} \\ &\quad + \Delta t^3 \| (\varphi^n - \varphi_h^n) \|_{l^\infty(\Omega)}). \end{aligned}$$

Lemma 6. : Verlet

Si $E \in W^{2,\infty}([0, t] \times \mathbb{R})$, alors

$$\| (E - E_h)(t^{n+\frac{1}{2}}) \|_{L^\infty(\Omega)} \leq C(h^2 + \Delta t^2 + \Delta t h^2 + e^n).$$

Lemma 7. CK3 : Avec les mêmes hypothèses qu'au lemme 5 :

$$\| R_h \tilde{f}_h^{n+1} - R_h f_h^{n+1} \|_{L_h^1(\Omega)} \leq C(e^n (\Delta t + \frac{\Delta t^3}{\Delta x^2} + \frac{\Delta t^2}{\Delta x}) + \Delta t h^2 + \Delta t^2 \frac{h^2}{\Delta x} + \Delta t^3 \frac{h^2}{\Delta x^2} + \Delta t^4).$$

En appliquant à la suite tous ces lemmes, puis le lemme de Gronwall discret, on montre le théorème. Afin de s'assurer que les algorithmes CK étaient corrects numériquement, on propose également en fin de chapitre quelques tests sur le Two Stream Instability et le Bump on Tail, où ces algorithmes sont comparés à Verlet qui est une référence. Les résultats numériques sont satisfaisants.

0.4 Un schéma préservant la charge pour les équations de Vlasov-Ampère 1D et Vlasov-Maxwell 1D quasi-relativiste

0.4.1 Petite Introduction

Les méthodes numériques classiques présentées jusque là ont un inconvénient majeur au niveau de la physique. Les densités de charge et de courant que l'on calcule ne vérifient pas a priori la relation de conservation de la charge discrète, ce qui est pourtant imposé par la physique. Néanmoins, pour la méthode PIC une stratégie a été mise au point par Villasenor Buneman [5] et généralisée par Barthelmé [1]. Plus récemment, Sircombe et Arber ont réussi à créer un algorithme semi-Lagrangien conservatif 4D qui préserve la charge dans un code nommé VALIS [4]. Grâce aux similitudes de la méthode FSL et de la méthode PIC, la stratégie utilisée pour cette dernière est adaptable assez facilement à FSL. Nous avons donc créé un algorithme préservant la charge pour FSL dans le cas de problèmes 1D : Vlasov-Ampère 1D et Vlasov-Maxwell quasi-relativiste 1D. Si l'on parvient à conserver la charge pour Vlasov-Ampère, ce système devient parfaitement équivalent au système de Vlasov-Poisson. Le but est par la suite de l'adapter en 4D grâce à un splitting d'opérateurs et ainsi de pouvoir la comparer au code VALIS. Dans le cas Vlasov-Ampère, les caractéristiques seront résolues à l'aide de Runge Kutta 2, et des algorithmes de Cauchy-Kovalevsky développés dans la partie précédente, d'ordre 2 et 3. La déposition utilise à nouveau les splines cubiques.

0.4.2 Présentation des modèles et algorithmique

Le modèle de Vlasov-Poisson a déjà été donné, donnons celui de Vlasov-Ampère 1D :

$$\partial_t f + v \partial_x f + E(t, x) \partial_v f = 0,$$

$$\partial_t E(t, x) = -J(t, x) + \bar{J}(t) = - \int_{\mathbb{R}} v f(t, x, v) dv + \frac{1}{L} \int_0^L J(t, x) dx,$$

Le modèle de Vlasov-Maxwell 1D quasi relativiste (QR) est donné par :

$$\frac{\partial f}{\partial t} + v(p) \frac{\partial f}{\partial x} + \left(E_x - \frac{\partial |A|^2}{\partial x} \right) \frac{\partial f}{\partial v} = 0,$$

où $v(p) = \frac{p}{\gamma(p)}$, $\gamma(p) = (1 + p^2)^{\frac{1}{2}}$ étant le facteur de Lorentz quasi-relativiste, et $A = (0, A_y, A_z)$ le potentiel vecteur. Les équations de Vlasov-Maxwell 1D s'écrivent :

$$\frac{\partial E_y(t, x)}{\partial t} = - \frac{\partial B_z(t, x)}{\partial x} + A_y(t, x) \rho_\gamma(t, x),$$

$$\frac{\partial E_z(t, x)}{\partial t} = \frac{\partial B_y(t, x)}{\partial x} + A_z(t, x) \rho_\gamma(t, x),$$

Notons que $\rho_\gamma = \rho$ dans le cas QR.

$$\frac{\partial B_y(t, x)}{\partial t} = \frac{\partial E_z(t, x)}{\partial x},$$

$$\frac{\partial B_z(t, x)}{\partial t} = - \frac{\partial E_y(t, x)}{\partial x}.$$

Les composantes du potentiel vecteur sont ensuite calculées :

$$\frac{\partial A_y(t, x)}{\partial t} = -E_y(t, x),$$

$$\frac{\partial A_z(t, x)}{\partial t} = -E_z(t, x).$$

La composante longitudinale du champ électrique est obtenue grâce à l'équation de Poisson

$$\frac{\partial E_x(t, x)}{\partial x} = \int_{\mathbb{R}} f(t, x, p) dp - 1,$$

ou de manière équivalente par celle d'Ampère :

$$\frac{\partial E_x(t, x)}{\partial t} = -J(t, x) + \bar{J}(t) = - \int_{\mathbb{R}} v(p) f(t, x, p) dp + \frac{1}{L} \int_0^L J(t, x) dx,$$

sous réserve de conservation de la charge continue :

$$\partial_t \rho + \partial_x J = 0.$$

Notons qu'en fait on peut prouver que \bar{J} est indépendant de t . Nous allons donner des détails sur l'algorithmique pour le cas Vlasov-Ampère. L'update du champ électrique peut donc se faire par Ampère :

$$E(t^{n+1}, x_{i+\frac{1}{2}}) = E(t^n, x_{i+\frac{1}{2}}) - \Delta t (J_{i+\frac{1}{2}}^{n+\frac{1}{2}} + \bar{J}),$$

ou de manière équivalente par Poisson :

$$E(t^{n+1}, x_{i+\frac{1}{2}}) = E(t^{n+1}, x_{i-\frac{1}{2}}) + \Delta x \rho_i^{n+1},$$

sous condition de conservation de la charge discrète qui dérive du schéma de Yee :

$$\frac{\rho_i^{n+1} - \rho_i^n}{\Delta t} + \frac{J_{i+\frac{1}{2}}^{n+\frac{1}{2}} - J_{i-\frac{1}{2}}^{n+\frac{1}{2}}}{\Delta x} = 0.$$

Il s'agit d'expliquer comment ρ et J sont calculés pour conserver la charge :

Calcul de ρ Une fois que l'on connaît le bout des caractéristiques en x , on peut calculer ρ classiquement à l'aide d'une déposition :

$$\rho(t^{n+1}, x_i) = \sum_{k,l} \omega_{k,l}^n S(x_i - X(t^{n+1}; (x_k, v_l), t^n)) - 1.$$

En posant $E(t^{n+1}, x_{-1/2}) = 0$, Poisson est initialisée et $E(t^{n+1}, x_{i+\frac{1}{2}})$ peut-être calculé partout en ajoutant une condition de moyenne nulle.

calcul de J On utilise l'équation de conservation de la charge discrète pour calculer J :

$$\begin{aligned} \frac{\rho_i^{n+1} - \rho_i^n}{\Delta t} &= \frac{1}{\Delta t} \int_{t^n}^{t^{n+1}} \partial_t \rho(x_i, t), \\ &= \frac{1}{\Delta t} \sum_{k,l} \omega_{k,l}^n \int_{t^n}^{t^{n+1}} \frac{d}{dt} S^3(x_i - X_{k,l}(t)) dt, \\ &= -\frac{1}{\Delta t \Delta x} \sum_{k,l} \omega_{k,l}^n \int_{t^n}^{t^{n+1}} \frac{dX_{k,l}(t)}{dt} (S^2(x_{i+\frac{1}{2}} - X_{k,l}(t)) - S^2(x_{i-\frac{1}{2}} - X_{k,l}(t))) dt, \\ &= -\left(\frac{J_{i+\frac{1}{2}}^{n+\frac{1}{2}} - J_{i-\frac{1}{2}}^{n+\frac{1}{2}}}{\Delta x} \right), \end{aligned}$$

où $X_{k,l}(t) = X(t; (x_k, v_l), t^n)$, et S^2 la B-spline quadratique. S^2 and S^3 sont liés à travers

$$\frac{dS^3(x)}{dx} = S^2(x + \frac{1}{2}) - S^2(x - \frac{1}{2}).$$

Cet update de ρ dépend de la dérivée de la courbe caractéristique. Ceci est lié à l'algorithme utilisé :

Runge-Kutta. On approche la trajectoire de manière linéaire :

$$X_{k,l}(t) = x_k + \frac{t - t^n}{2} (v_l + \tilde{v}_{k,l}^{n+1}),$$

et donc :

$$\frac{dX_{k,l}(t)}{dt} = \frac{1}{2} (v_l + \tilde{v}_{k,l}^{n+1}).$$

alors :

$$J_{i+\frac{1}{2}}^{n+\frac{1}{2}} = \frac{1}{2\Delta t} \sum_{k,l} \omega_{k,l}^n (v_l + \tilde{v}_{k,l}^{n+1}) \int_{t^n}^{t^{n+1}} S^2(x_{i+\frac{1}{2}} - X_{k,l}(t)) dt.$$

Cauchy-Kovalevsky. On utilise également une approximation linéaire

$$X_{k,l}(t) = x_k + (t - t^n)v_l + \Delta t(t - t^n)E^n(x_k) + \frac{\Delta t^2}{2}(t - t^n)\varphi^n(x_k, v_l),$$

ainsi :

$$\frac{dX_{k,l}(t)}{dt} = v_l + \Delta t E^n(x_k) + \frac{\Delta t^2}{2}\varphi^n(x_k, v_l).$$

Et donc

$$J_{i+\frac{1}{2}}^{n+\frac{1}{2}} = \frac{1}{\Delta t} \sum_{k,l} \omega_{k,l}^n (v_l + \Delta t E^n(x_k) + \frac{\Delta t^2}{2}\varphi^n(x_k, v_l)) \int_{t^n}^{t^{n+1}} S^2(x_{i+\frac{1}{2}} - X_{k,l}(t)) dt.$$

Il reste alors juste à calculer exactement cette intégrale, et pour ce faire, on peut utiliser une formule de Gauss à deux points en s'assurant que le déplacement ne peut excéder une maille par pas de temps, et ainsi l'intégrande sera un polynôme de degré 2. Cette condition est assurée si on se soumet à la contrainte CFL suivante : $v_{\max}\Delta t \leq \Delta x$. La formule de Gauss donne :

$$\begin{aligned} \int_{t^n}^{t^{n+1}} S^2(x_{i+\frac{1}{2}} - X_{k,l}(t)) dt &= \frac{\Delta t}{2} \int_{-1}^1 S^2(x_{i+\frac{1}{2}} - X_{k,l}(\frac{\Delta t}{2}u + t^{n+\frac{1}{2}})) du, \\ &= \frac{\Delta t}{2} (S^2(x_{i+\frac{1}{2}} - X_{k,l}(t^{n+\frac{1}{2}} + \frac{\Delta t}{2\sqrt{3}})) + S^2(x_{i+\frac{1}{2}} - X_{k,l}(t^{n+\frac{1}{2}} - \frac{\Delta t}{2\sqrt{3}}))). \end{aligned}$$

Si ρ et J sont calculés ainsi, on a bien conservation de la charge discrète, et équivalence entre Vlasov-Poisson et Vlasov-Ampère. La stratégie utilisée pour Vlasov-Maxwell avec RK2 est la même.

0.4.3 Résultats numériques

Tout d'abord, pour Vlasov-Ampère, on vérifie sur les mêmes cas test que dans le chapitre de développement de FSL que la méthode est efficace, et qu'elle est effectivement bien soumise à une condition CFL. Les résultats sont entièrement satisfaisants, la charge est conservée à 10^{-15} , et les résultats sont en adéquation avec la méthode qui ne conserve pas la charge. Néanmoins, comme

dans le modèle de Vlasov-Poisson, il n'est pas nécessaire de conserver la charge, la méthode ne se comporte pas mieux que les autres. Par contre, on effectue également un cas test poussé sur le problème de Vlasov-Maxwell 1D dans lequel la charge doit être préservée. On compare sur ce cas test notre FSL avec conservation de la charge avec un BSL classique, et les résultats numériques vont clairement en faveur de notre nouvel algorithme, par conséquent, l'objectif est atteint.

0.5 Algorithme semi-Lagrangien conservatif qui conserve la charge pour les équations de Vlasov-Maxwell 4D relativistes

0.5.1 Petite introduction

Dans la partie précédente, nous avons créé un algorithme qui conserve la charge pour des problèmes 1D, le but étant de l'adapter au modèle 4D pour comparer les résultats à ceux de Sircombe et Arber dans le code VALIS. Afin de pouvoir effectuer les comparaisons, il nous faut construire un algorithme utilisant les méthodes conservatives qui va préserver la charge pour le modèle de Vlasov-Maxwell 4D relativiste.

0.5.2 Modèle

Les équations de Vlasov-Maxwell 4D relativistes s'écrivent :

$$\frac{\partial f}{\partial t} + \mathbf{v}(\mathbf{p}) \cdot \nabla_x f + q(\mathbf{E}(t, x) + v(\mathbf{p}) \times \mathbf{B}(t, x)) \cdot \nabla_p f = 0,$$

où la vitesse de la particule est définie par $\mathbf{v}(\mathbf{p}) = \frac{\mathbf{p}}{m\gamma}$ et le facteur de Lorentz $\gamma = \sqrt{1 + \frac{p_x^2 + p_y^2}{m^2 c^2}}$, avec c la vitesse de la lumière dans le vide.

$$\begin{aligned} \frac{\partial \mathbf{E}}{\partial t} - c^2 \nabla \times \mathbf{B} &= -\frac{\mathbf{J}}{\epsilon_0}, \\ \frac{\partial \mathbf{B}}{\partial t} + \nabla \times \mathbf{E} &= 0, \\ \nabla \cdot \mathbf{E} &= \frac{\rho}{\epsilon_0}, \\ \nabla \cdot \mathbf{B} &= 0, \end{aligned}$$

où ϵ_0 est la permittivité électrique dans le vide. Et pour les sources :

$$\rho(t, \mathbf{x}) = q \left(\int f(t, \mathbf{x}, \mathbf{p}) d\mathbf{p} - n_b(\mathbf{x}) \right), \quad \mathbf{J}(t, \mathbf{x}) = q \int f(t, \mathbf{x}, \mathbf{p}) v(\mathbf{p}) d\mathbf{p}.$$

0.5.3 Formulation Volume Fini des schémas semi-Lagrangiens

Si l'on considère une équation de transport 1D :

$$\frac{\partial f}{\partial t} + a \frac{\partial f}{\partial x} = 0.$$

Les inconnues pour ce type de schéma sont les valeurs moyennes par maille : $f_j^n = \frac{1}{\Delta x} \int_{x_{j-1/2}}^{x_{j+1/2}} f(t^n, x) dx$.
On calcule ensuite :

$$\begin{aligned} f_{i+1/2}^{n+1/2} &= \frac{1}{\Delta t} \int_{t_n}^{t_{n+1}} f(t, x_{i+1/2}) dt, \\ &= \frac{1}{\Delta t} \int_{t_n}^{t_{n+1}} f(x_{i+1/2} - a(t - t_n)) dt, \\ &= \frac{1}{a\Delta t} \int_{x_{i+1/2}-a\Delta t}^{x_{i+1/2}} f^R(x) dx. \end{aligned}$$

Puis en intégrant l'équation de transport sur une cellule entre t^n et t^{n+1} , on obtient :

$$f_i^{n+1} = f_i^n - \frac{a\Delta t}{\Delta x} (f_{i+1/2}^{n+1/2} - f_{i-1/2}^{n+1/2}).$$

D'autre part pour un schéma conservatif : la fonction de distribution est actualisée ainsi :

$$\begin{aligned} f_i^{n+1} &= \frac{1}{\Delta x} \int_{x_{i-1/2}-a\Delta t}^{x_{i+1/2}-a\Delta t} f(x) dx, \\ &= \frac{1}{\Delta x} \left(\int_{x_{i-1/2}-a\Delta t}^{x_{i-1/2}} f(x) dx + \int_{x_{i-1/2}}^{x_{i+1/2}} f(x) dx - \int_{x_{i+1/2}-a\Delta t}^{x_{i+1/2}} f(x) dx \right), \\ &= f_i^n + \frac{1}{\Delta x} \left(\int_{x_{i-1/2}-a\Delta t}^{x_{i-1/2}} f(x) dx - \int_{x_{i+1/2}-a\Delta t}^{x_{i+1/2}} f(x) dx \right), \end{aligned}$$

ce qui est le même schéma que la forme Volume Fini. Précisons que dans les deux cas, on est amené à calculer la primitive de la fonction de distribution, et que cette reconstruction peut s'effectuer par exemple avec une méthode PSM, PFC ou PPM.

0.5.4 Schéma Volume Fini conservant la charge

Une équation de conservation de la charge discrète est toujours liée au solveur utilisé pour les équations de Maxwell. Nous utiliserons ici le schéma de Yee 2D :

$$\begin{aligned} \frac{B_{z_{i+1/2,j+1/2}}^{n+1/2} - B_{z_{i+1/2,j+1/2}}^{n-1/2}}{\Delta t} &= \frac{E_{x_{i+1/2,j+1}}^n - E_{x_{i+1/2,j}}^n}{\Delta y} - \frac{E_{y_{i+1,j+1/2}}^n - E_{y_{i,j+1/2}}^n}{\Delta x}, \\ \frac{E_{x_{i+1/2,j}}^{n+1} - E_{x_{i+1/2,j}}^n}{\Delta t} &= c^2 \frac{B_{z_{i+1/2,j+1/2}}^{n+1/2} - B_{z_{i+1/2,j-1/2}}^{n+1/2}}{\Delta y} - \frac{1}{\epsilon_0} J_{x_{i+1/2,j}}^{n+1/2}, \\ \frac{E_{y_{i,j+1/2}}^{n+1} - E_{y_{i,j+1/2}}^n}{\Delta t} &= -c^2 \frac{B_{z_{i+1/2,j+1/2}}^{n+1/2} - B_{z_{i-1/2,j+1/2}}^{n+1/2}}{\Delta x} - \frac{1}{\epsilon_0} J_{y_{i,j+1/2}}^{n+1/2}. \end{aligned}$$

et l'équation de conservation de la charge discrète associée :

$$\frac{\rho_{i,j}^{n+1} - \rho_{i,j}^n}{\Delta t} + \frac{J_{x_{i+1/2,j}}^{n+1/2} - J_{x_{i-1/2,j}}^{n+1/2}}{\Delta x} + \frac{J_{y_{i,j+1/2}}^{n+1/2} - J_{y_{i,j-1/2}}^{n+1/2}}{\Delta y} = 0,$$

Utilisant un splitting, le schéma d'update de f s'écrit :

$$\begin{aligned} f_{i,j,k,l}^{n,1} &= f_{i,j,k,l}^n - \frac{v_x(\mathbf{p}_{k,l})\Delta t}{2\Delta x} (f_{i+1/2,j,k,l}^{n,1/2} - f_{i-1/2,j,k,l}^{n,1/2}), \\ f_{i,j,k,l}^{n,2} &= f_{i,j,k,l}^{n,1} - \frac{v_y(\mathbf{p}_{k,l})\Delta t}{2\Delta y} (f_{i,j+1/2,k,l}^{n,3/2} - f_{i,j-1/2,k,l}^{n,3/2}), \\ f_{i,j,k,l}^{n,3} &\leftarrow f_{i,j,k,l}^{n,2} \text{ utilisant une advection conservative dans l'espace des } \mathbf{p}, \\ f_{i,j,k,l}^{n,4} &= f_{i,j,k,l}^{n,3} - \frac{v_y(\mathbf{p}_{k,l})\Delta t}{2\Delta y} (f_{i,j+1/2,k,l}^{n,7/2} - f_{i,j-1/2,k,l}^{n,7/2}), \\ f_{i,j,k,l}^{n+1} &= f_{i,j,k,l}^{n,4} - \frac{v_x(\mathbf{p}_{k,l})\Delta t}{2\Delta x} (f_{i+1/2,j,k,l}^{n,9/2} - f_{i-1/2,j,k,l}^{n,9/2}). \end{aligned}$$

où

$$\begin{aligned} f_{i+1/2,j,k,l}^{n,1/2} &= \frac{2}{v_x(\mathbf{p}_{k,l})\Delta t} \int_{x_{i+\frac{1}{2}} - v_x(\mathbf{p}_{k,l})\frac{\Delta t}{2}}^{x_{i+\frac{1}{2}}} f^n(x, y_j, v_{x_k}, v_{y_l}) dx, \\ f_{i,j+1/2,k,l}^{n,3/2} &= \frac{2}{v_y(\mathbf{p}_{k,l})\Delta t} \int_{y_{j+\frac{1}{2}} - v_y(\mathbf{p}_{k,l})\frac{\Delta t}{2}}^{y_{j+\frac{1}{2}}} f^{n,1}(x_i, y, v_{x_k}, v_{y_l}) dy, \\ f_{i,j+1/2,k,l}^{n,7/2} &= \frac{2}{v_y(\mathbf{p}_{k,l})\Delta t} \int_{y_{j+\frac{1}{2}} - v_y(\mathbf{p}_{k,l})\frac{\Delta t}{2}}^{y_{j+\frac{1}{2}}} f^{n,3}(x_i, y, v_{x_k}, v_{y_l}) dy, \\ f_{i+1/2,j,k,l}^{n,9/2} &= \frac{2}{v_x(\mathbf{p}_{k,l})\Delta t} \int_{x_{i+\frac{1}{2}} - v_x(\mathbf{p}_{k,l})\frac{\Delta t}{2}}^{x_{i+\frac{1}{2}}} f^{n,4}(x, y_j, v_{x_k}, v_{y_l}) dx. \end{aligned}$$

Quelques calculs montrent que

$$\begin{aligned} \frac{1}{q\Delta p_x \Delta p_y} \rho_{i,j}^{n+1} &= \sum_{k,l} f_{i,j,k,l}^n - \frac{\Delta t}{2\Delta y} \sum_{k,l} (v_y(\mathbf{p}_{k,l}) (f_{i,j+1/2,k,l}^{n,7/2} + f_{i,j+1/2,k,l}^{n,3/2} - f_{i,j-1/2,k,l}^{n,7/2} - f_{i,j-1/2,k,l}^{n,3/2})) \\ &\quad - \frac{\Delta t}{2\Delta x} \sum_{k,l} (v_x(\mathbf{p}_{k,l}) (f_{i+1/2,j,k,l}^{n,9/2} + f_{i+1/2,j,k,l}^{n,1/2} - f_{i-1/2,j,k,l}^{n,9/2} - f_{i-1/2,j,k,l}^{n,1/2})). \end{aligned}$$

Et ainsi, en posant :

$$\begin{aligned} J_{x_{i+1/2,j}}^{n+1/2} &= q\Delta p_x \Delta p_y \sum_{k,l} v_x(\mathbf{p}_{k,l}) \cdot \frac{1}{2} (f_{i+1/2,j,k,l}^{n,9/2} + f_{i+1/2,j,k,l}^{n,1/2}), \\ J_{y_{i,j+1/2}}^{n+1/2} &= q\Delta p_x \Delta p_y \sum_{k,l} v_y(\mathbf{p}_{k,l}) \cdot \frac{1}{2} (f_{i,j+1/2,k,l}^{n,7/2} + f_{i,j+1/2,k,l}^{n,3/2}), \end{aligned}$$

on a bien conservation de la charge discrète.

0.5.5 Résultats numériques et perspectives

On donne ici simplement quelques résultats numériques pour la méthode PSM pour le cas test du Landau linéaire, qui sont encourageants pour la suite. Nous essaierons aussi d'implémenter PPM, et PFC. Il restera ensuite à construire un algorithme FSL 4D qui conserve la charge afin de pouvoir comparer les résultats.

0.6 Articles

Cette thèse est basée principalement sur les trois articles qui en sont issus :

N. Crouseilles, T. Respaud, E. Sonnendrücker, *A forward semi-Lagrangian method for the numerical solution of the Vlasov equation*, *Comput. Phys. Comm.*, **180** (10), pp. 1730–1745, (2009).

T. Respaud, E. Sonnendrücker, *Analysis of a new class of Forward semi-Lagrangian schemes for the 1D Vlasov-Poisson Equations*, *Soumis Numerische Mathematike*.

N. Crouseilles, T. Respaud, *A charge preserving scheme for the numerical resolution of the Vlasov-Ampère equations*. *Soumis CiCP*

Bibliographie

- [1] R. BARTHELMÉ, *Le problème de conservation de la charge dans le couplage des équations de Vlasov et de Maxwell*, Thèse de l'Université Louis Pasteur, 2005.
- [2] C.J. COTTER, J. FRANK, S. REICH *The remapped particle-mesh semi-Lagrangian advection scheme*, Q. J. Meteorol. Soc., **133**, pp. 251-260, (2007).
- [3] S. REICH, *An explicit and conservative remapping strategy for semi-Lagrangian advection*, Atmospheric Science Letters **8**, pp. 58-63, (2007).
- [4] N.J. SIRCOMBE, T.D. ARBER, *VALIS : A split-conservative scheme for the relativistic 2D* ; J. Comput. Phys., **228**, pp. 4773-4788 (2009).
- [5] J. VILLASENOR, O. BUNEMAN, *Rigorous charge conservation for local electromagnetic field solvers*, Comp. Phys. Comm. **69**, pp. 306-316, (1992).

Table des matières

Remerciements	i
Résumé	iii
0.1 Présentation générale :	
Contexte physique et méthodes numériques	iii
0.1.1 Contexte physique	iii
0.1.2 Méthodes numériques	v
0.2 FSL pour Vlasov-Poisson 1D et Centre Guide	vii
0.2.1 Petite Introduction.	vii
0.2.2 Présentation de l’algorithme.	viii
0.2.3 Résultats numériques	ix
0.3 Analyse d’une nouvelle classe de schémas pour le problème de Vlasov-Poisson 1D.	x
0.3.1 Petite introduction	x
0.3.2 Problème discret	xi
0.4 Schéma FSL conservant la charge	xiv
0.4.1 Petite Introduction	xiv
0.4.2 Présentation des modèles et algorithmique	xv
0.4.3 Résultats numériques	xvii
0.5 Conservation de la charge pour Vlasov-Maxwell 4D relativiste	xviii
0.5.1 Petite introduction	xviii
0.5.2 Modèle	xviii
0.5.3 Formulation Volume Fini des schémas semi-Lagrangiens	xviii
0.5.4 Schéma Volume Fini conservant la charge	xix
0.5.5 Résultats numériques et perspectives	xx
0.6 Articles	xxi
1 Introduction	1
1.1 Physical context	1
1.1.1 Plasmas	1
1.1.2 Controlled thermonuclear fusion	2
1.1.3 Modeling and equations	5
1.1.4 Plasmas modeling	5
1.1.5 The Vlasov-Maxwell system	5

1.2	A few a priori properties of the system.	6
1.2.1	The characteristics of the Vlasov equation.	6
1.2.2	Charge conservation	7
1.2.3	Energy conservation	7
1.3	Existence of solutions for the Vlasov-Poisson system	9
1.3.1	Non relativistic case	9
1.3.2	Relativistic case	10
1.4	Existence of solutions for the Vlasov-Maxwell system	10
1.4.1	Non relativistic case	11
1.4.2	Relativistic case	11
2	Numerical methods for the solving of Vlasov-Poisson and Vlasov-Maxwell systems	15
2.1	Numerical resolution of the Vlasov equation	15
2.1.1	Introduction	15
2.1.2	The particle methods	16
2.1.3	The semi-Lagrangian methods	19
2.2	Numerical resolution of the Maxwell's equations	22
2.2.1	Introduction	22
2.2.2	Finite difference	23
2.2.3	Finite Volume methods	24
2.2.4	Finite Element methods	25
2.3	Convergence results	25
2.3.1	PIC Algorithms	25
2.3.2	Semi-Lagrangian methods	27
2.4	Numerical charge conservation	28
3	Forward semi-Lagrangian for numerical Vlasov-Poisson	37
3.1	Introduction	37
3.2	Models in plasma physics	39
3.2.1	Vlasov-Poisson model	39
3.2.2	Guiding-center model	39
3.2.3	Characteristic curves	40
3.3	The forward semi-Lagrangian method	40
3.3.1	General algorithm	40
3.3.2	FSL: An explicit solution of the characteristics	42
3.3.3	FSL - BSL Cubic Spline Interpolation	44
3.3.4	Basic differences between FSL and BSL	46
3.4	Numerical results	47
3.4.1	Hill's equation	47
3.4.2	Vlasov-Poisson case	48
3.4.3	Guiding-center case	57
3.5	Conclusion and perspectives	62
3.6	Appendix I: Linearized Vlasov Poisson and Landau damping	63

3.7	Appendix II: Solution of Poisson in the Guided Center model	64
3.7.1	Find ϕ	64
3.7.2	Find E	65
4	1D Analysis of a Forward semi-Lagrangian scheme	71
4.1	Introduction	71
4.2	The continuous problem	72
4.2.1	The Vlasov-Poisson model	72
4.2.2	Existence, uniqueness and regularity of the solution of the continuous problem	74
4.3	The discrete problem	74
4.3.1	Definitions and notations	74
4.3.2	The numerical scheme	75
4.3.3	Exact conservation of number of particles and momentum	79
4.4	Convergence analysis	85
4.4.1	Decomposition of the error	85
4.4.2	A priori estimates	85
4.4.3	End of the proof	97
4.5	Numerical results	98
4.6	Conclusion	101
5	1D Charge preserving semi-Lagrangian scheme	105
5.1	Introduction	105
5.2	The continuous problem	107
5.2.1	The Vlasov-Ampère and Vlasov-Poisson models	107
5.2.2	The quasi-relativistic Vlasov-Maxwell model	108
5.3	The discrete problems	110
5.3.1	Deposition step	110
5.3.2	General time algorithms	111
5.4	The charge preserving algorithms	114
5.4.1	Solving the electric field, Ampère vs Poisson	114
5.4.2	Charge conservation	115
5.5	Numerical results	118
5.5.1	Introduction	118
5.5.2	Linear Landau damping	118
5.5.3	Two stream instability	121
5.5.4	Bump on Tail	124
5.5.5	QR Vlasov-Maxwell test case	127
5.5.6	Numerical Synthesis	133
5.6	Conclusion	133

6	Charge conserving conservative semi-Lagrangian methods	139
6.1	Introduction	139
6.2	The relativistic Vlasov-Maxwell equations	140
6.3	Finite Volume form of a semi-Lagrangian scheme	141
6.3.1	Description of the conservative semi-Lagrangian scheme for constant co-efficient advection in a Finite Volume formalism	141
6.3.2	Examples of reconstruction	143
6.4	Charge conserving Finite Volume schemes	144
6.5	Numerical results	149
6.6	Conclusion and perspectives	150

Introduction

1.1 Physical context

1.1.1 Plasmas

Plasma, like solid, liquid and gas is a state of matter. On Earth, you can only see it if temperature is really high (at least 10 K, but often far more), when energy is so strong that some electrons are extracted from the atoms. Thus, a globally neutral combination of the different charged particles is obtained (ions and electrons). The word plasma, also qualified as the "fourth state of matter", was used for the first time in physics by the physicist Irving Langmuir in 1928, due to its analogy with blood plasma.

In usual conditions, a gas environment does not permit the electricity conduction. When this environment is submitted to a weak electric field, a pure gas can be regarded as a perfect insulator, since it contains no free charged particles at all (neither electrons nor positive ions). These two kinds of particles shall appear if this gas is submitted to an electric field with strong intensity, or to high enough temperatures, and also if it is being shelled with particles, or submitted to a very intensive magnetic field. When ionization is so important that the number of electrons per volume unit is equivalent to the one of neutral molecules, the gas becomes then a very conductive fluid, which is called a plasma.

Originally, plasma referred to an ionized and globally neutral gas, and then the definition spread to partially ionized gas, which behavior differs from the one of a neutral gas. Those non neutral plasmas are often obtained imposing a really big potential difference, in order to extract some ions or some electrons from a well chosen metal. Plasmas are extremely scattered in our universe, since it represents more than 99% from the know matter. Nevertheless, you cannot see them in our casual environment, "the Earth", since its conditions of apparition are very far from the ones needed for living on Earth.

Thus, you can distinguish two different kinds of plasmas, natural and artificial ones: The most common examples for natural plasmas are stars, gas nebulas, quasar, pulsar, northern lights, flash of lightning, ionosphere or solar wind (Fig. 1.1.1).



Figure 1.1.1: Plasmas.

As for artificial ones, with which we are daily surrounded, we can cite televisions, electric shocks like in high-tension circuit breaker, discharge tubes (lamps, screens, X-ray production). There are also treatment plasmas for deposits, engraving, surface modification or ionic implantation doping. And, to conclude, controlled thermonuclear fusion. Other applications, which are still in laboratories shall also be quoted, like radars, combustion improvement, rubbish treatment, sterilization a.s.o.

1.1.2 Controlled thermonuclear fusion

The evolution of energy needs and the exhaustion of fossil fuels like oil make it necessary to develop new energy sources. Using the famous formula $E = mc^2$, you can produce energy with transformations where mass is decreasing. Two big kinds of nuclear reactions follow this process.

The first one is the reaction of nuclear fission. The induced nuclear fission was described on december the 17th 1938 by two chemists from the Kaiser-Wilhelm-Institut für Chemie from Berlin: Otto Hahn and his young assistant Fritz Strassmann. The austrian physicist Lise Meitner had also taken part to the work, but being jewish, she had fled from Germany to Sweden in July 1938. Although she kept on working with them by letters, she could not be cited in the publication. Nuclear fission consists in generating two lighter nuclei from one heavier atom that contains many nucleons such as uranium or plutonium nuclei. Nuclear fission is currently used in nuclear power plants.

Nuclear fusion is a process where two nuclei gather in order to create a heavier nucleus. The fusion of lighter nuclei gives off huge quantities of energy, coming from the attraction between the nuclei, due to strong interaction. This reaction is the one that happens naturally inside the sun, and most of the stars of our universe. Despite all the work realized since the 50's by the whole world, no industrial application of nuclear fusion has been achieved yet, except the military field with the H. Bomb. Nevertheless, this application obviously does not aim at containing and

overcoming the produced reaction. Yet, the fusion reaction that may be the most accessible is the one that implicates nuclei of Deuterium and Tritium which create a Helium atom and one neutron which is gifted with a huge amount of energy that will be used in order to produce electricity (see Fig. 1.1.2). The required temperatures for such a reaction need to be larger than one hundred million degrees. With such temperatures, the electrons are extracted from an atom, and a plasma is obtained. If you want to produce some energy, it is obvious that you need to have an amplification factor Q superior than 1, where Q is defined by the ratio between produced energy and exterior power that has to be brought. An energetic budget leads to the Lawson criterion, which ensures that the amplification factor Q is proportional to the product nTt_E , where n is the density, T the temperature, t_E the confining time.

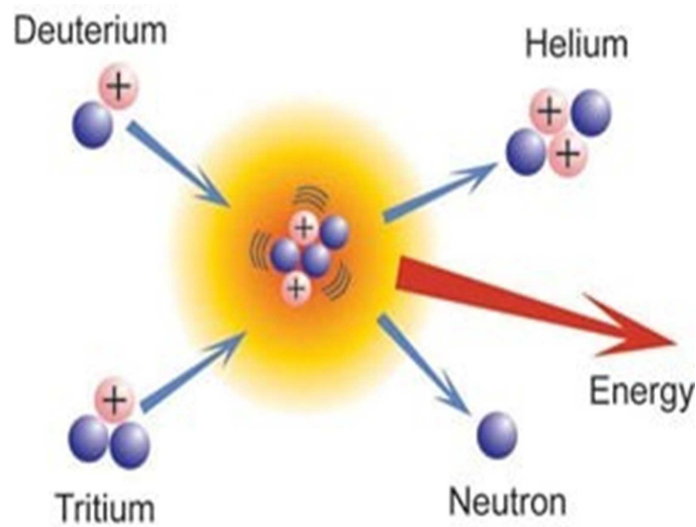


Figure 1.1.2: Fusion reaction.

One of the main interests of nuclear fusion is that theoretically this reaction could produce a lot more energy than fission (from 3 to 4 times more), given an equal mass of fuel. Moreover, the oceans are naturally full of Deuterium which could supply the whole planet with energy during a few hundreds of millenaries. Contrarily to nuclear fission, the fusion products (mainly Helium 4) are not radioactive. Nevertheless, when the reaction produces fast neutrons, these ones can alter nuclei that capture them in isotopes that might be radioactive.

The work done in order to achieve this goal of controlled thermonuclear fusion on Earth follows two approaches. Inertial confinement fusion, in which a very high density is reached during a quite short time, shooting on a Deuterium-Tritium cartridge with laser; and magnetic confinement fusion, in which the plasma is confined at lower densities, but during a longer time. This approach is the one followed by the ITER project, partnership between the European Union, Japan, the United States, China, South Korea, Russia and India. The agreement was signed on november 26th 2006 in Paris. It aims at proving the scientific and technical feasibility of producing energy thanks to fusion. The construction has started in Cadarache in South East

of France. The reactor in which the plasma is confined is of toroidal shape and is called a tokamak (Fig. 1.1.3).

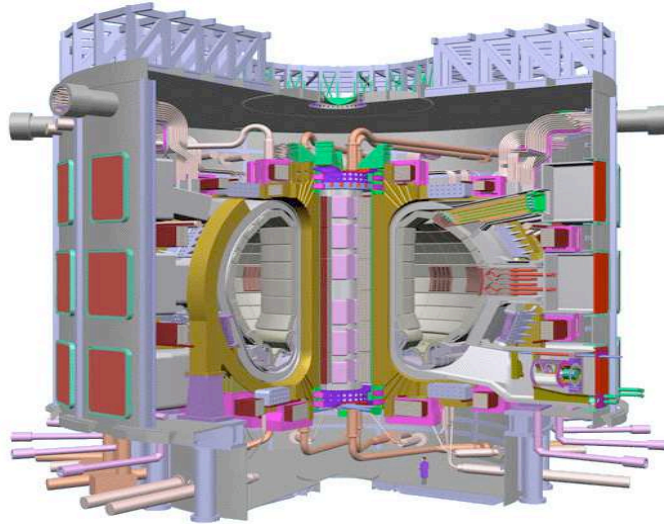


Figure 1.1.3: ITER tokamak

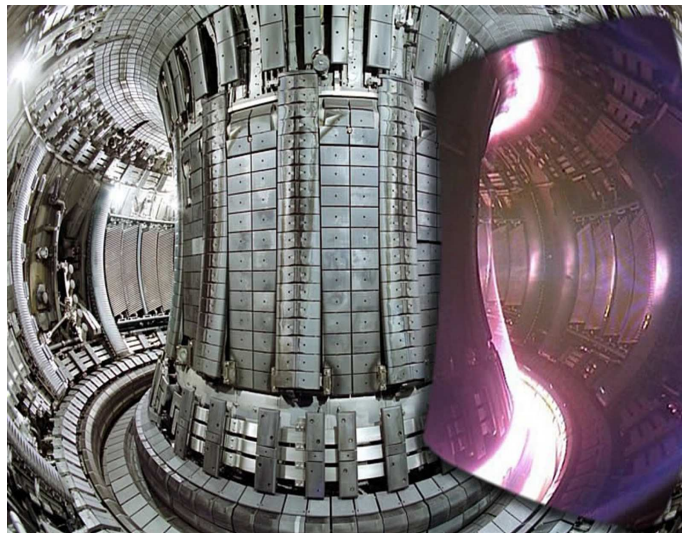


Figure 1.1.4: JET tokamak

The current world record of amplification factor is $Q = 0.64$, and was reached in the English tokamak called JET (Fig. 1.1.4). It is well known now that in order to reach higher amplification factors, it will be necessary to build a far bigger tokamak, like ITER which will be five times

bigger and from which an amplification factor Q superior than 10 is awaited.

1.1.3 Modeling and equations

1.1.4 Plasmas modeling

We are interested in models describing the interaction between charged particles under the effects of exterior electromagnetic field, or self-consistent ones, or often both. One charged particle generates an electromagnetic field, and even though its intensity decreases with the distance to the particle, it has an effect on the whole space. The model then consists in determining the movement of one particle submitted to one of the previously called electromagnetic field, using the Newton's law. Since there is a huge number of particles in a plasma, it is impossible to use a N-bodies problem, or microscopic one to simulate the problem. Therefore it is necessary to use simplified models.

The macroscopic model, or fluid one can be used when the plasma is near its equilibrium. It is the sufficient to describe it with its density, its mean speed, its temperature, which follow fluid equations like the Euler one.

The mesoscopic or kinetic model in which each kind of particles s of the plasma is characterized by its distribution function $f_s(x, v, t)$, which represents a statistical approach of the particles repartition in the phase space for a big number of realizations. If the interactions between the nearest particles dominate, the Boltzmann equation is found. If the interactions between particles are ruled by the mean field they generate, the Vlasov equation appears, and is non linearly coupled with the Maxwell's equations that rule the fields. This model is the one we will study. The distribution function contains far more information than the fluid description, because it enables to have a description of the repartition of the particles in velocity. The kinetic model is necessary when the distribution function is far from the Maxwell-Boltzmann distribution, corresponding to the state of thermodynamical equilibrium of the plasma. Otherwise, the fluid description is enough.

1.1.5 The Vlasov-Maxwell system

We are interested in the most frequently used model in plasmas evolution ; the kinetic one based on the Vlasov equation which describes the space and velocity repartition of charged particles, submitted to electromagnetic fields, which may be exterior, self-consistent, or both. It writes, for one kind of particle:

$$\frac{\partial f}{\partial t} + \mathbf{v}(\mathbf{p}) \cdot \nabla_x f + q(\mathbf{E}(t, \mathbf{x}) + \mathbf{v}(\mathbf{p}) \times \mathbf{B}(t, \mathbf{x})) \cdot \nabla_p f = 0, \quad (1.1)$$

where the particle velocity is defined by $\mathbf{v}(\mathbf{p}) = \frac{\mathbf{p}}{m\gamma}$ and the Lorentz factor $\gamma = \sqrt{1 + \frac{p_x^2 + p_y^2 + p_z^2}{m^2 c^2}}$ in the relativistic case, and $\gamma = 1$ in the non relativistic case. c is the speed of light in vacuum, m is the particle mass, q its charge, and (\mathbf{E}, \mathbf{B}) the electric and magnetic fields. The function f_s depends on seven variables, the position, $\mathbf{x} \in \mathbb{R}^3$, the impulsion $\mathbf{p} \in \mathbb{R}^3$, and time $t \in \mathbb{R}$.

A plasma is globally neutral, thus, it is composed with different kinds of particles. You have one Vlasov equation for each kind of particles.

The self-consistent electromagnetic field (\mathbf{E}, \mathbf{B}) , can be computed thanks to a coupling with the Maxwell's equations. Their sources are the charge density and the current density, computed thanks to the particles.

$$\frac{\partial \mathbf{E}}{\partial t} - c^2 \nabla \times \mathbf{B} = -\frac{\mathbf{J}}{\epsilon_0}, \quad (1.2)$$

$$\frac{\partial \mathbf{B}}{\partial t} + \nabla \times \mathbf{E} = 0, \quad (1.3)$$

$$\nabla \cdot \mathbf{E} = \frac{\rho}{\epsilon_0}, \quad (1.4)$$

$$\nabla \cdot \mathbf{B} = 0. \quad (1.5)$$

and for the sources:

$$\rho(\mathbf{x}, t) = \sum_s q_s \int_{\mathbb{R}^3} f_s(\mathbf{x}, \mathbf{p}, t) d\mathbf{p},$$

$$\mathbf{J}(\mathbf{x}, t) = \sum_s q_s \int_{\mathbb{R}^3} \mathbf{p} f_s(\mathbf{x}, \mathbf{p}, t) d\mathbf{p}.$$

where c is the light velocity, and ϵ_0 the electric permittivity of vacuum. In a few particular cases, like for example when the particles have a low velocity compared to the one of light, you can suppose that the magnetic field is stationary. So you have: $\nabla \times \mathbf{E} = 0$ using (1.3). You get the Vlasov-Poisson system, where the electric field satisfies the Poisson's equation (1.4), or equivalently is solution of a Laplace problem:

$$\mathbf{E} = -\nabla\phi, \quad -\Delta\phi = \frac{\rho}{\epsilon_0}.$$

Plasmas are really complex objects, involving numerous instabilities, and turbulence phenomena, which make its containment very tricky. The way towards nuclear fusion gets through a really accurate understanding of the plasmas thanks to well suited models, and numerical simulations of these models.

The 3D resolution of the system represents a real challenge, at least because of the big size of this system coming from the fact that the problem is a 6D space problem, adding time. Therefore it may be useful to simplify the problems in order to get reduced ones that might be accurate enough.

1.2 A few a priori properties of the system.

1.2.1 The characteristics of the Vlasov equation.

Definition 1.2.1. *The characteristics of the Vlasov equation (1.1) are the functions $\mathbf{X}(s; t, \mathbf{x}, \mathbf{p})$, $\mathbf{P}(s; t, \mathbf{x}, \mathbf{p})$ solutions of the system of ordinary differential equations with initial conditions:*

$$\frac{d\mathbf{X}}{ds} = v(\mathbf{P}), \quad \mathbf{X}(t; t, \mathbf{x}, \mathbf{p}) = \mathbf{x},$$

$$\frac{d\mathbf{P}}{ds} = q(\mathbf{E} + v(\mathbf{P}) \times \mathbf{B}), \quad \mathbf{P}(t; t, \mathbf{x}, \mathbf{p}) = \mathbf{p},$$

where $v(\mathbf{P}) = \frac{\mathbf{P}}{m\gamma(\mathbf{P})}$.

Since

$$\frac{d}{ds} f(s, \mathbf{X}(s; t, \mathbf{x}, \mathbf{p}), \mathbf{P}(s; t, \mathbf{x}, \mathbf{p})) = \frac{\partial f}{\partial s} + \frac{d\mathbf{X}}{ds} \cdot \nabla_x f + \frac{d\mathbf{P}}{ds} \cdot \nabla_p f = 0,$$

it can be concluded that f is constant along the characteristic curves, and then

$$f(t, \mathbf{x}, \mathbf{p}) = f_0(\mathbf{X}(0; t, \mathbf{x}, \mathbf{p}), P(0; t, \mathbf{x}, \mathbf{p})),$$

where f_0 is the initial distribution function.

It follows that if f_0 is bounded, there is a maximum principle:

$$0 \leq f(t, \mathbf{x}, \mathbf{p}) \leq \sup_{(\mathbf{x}, \mathbf{p})} f_0(\mathbf{x}, \mathbf{p}) \quad \forall (t, \mathbf{x}, \mathbf{p}) \in \mathbb{R} \times \mathbb{R}^3 \times \mathbb{R}^3.$$

1.2.2 Charge conservation

Let us notice first that since $\nabla_x \cdot v(\mathbf{p}) = 0$ and $\nabla_p \cdot (\mathbf{E} + v(\mathbf{p}) \times \mathbf{B}) = 0$, the Vlasov equation (1.1) can write:

$$\frac{\partial f}{\partial t} + \nabla_x \cdot (v(\mathbf{p})f) + q\nabla_p \cdot ((\mathbf{E} + v(\mathbf{p}) \times \mathbf{B})f) = 0, \quad (1.6)$$

If the functions \mathbf{E}, \mathbf{B} are supposed regular enough, and tend to zero quickly enough at infinite, integrating (1.6) with respect to \mathbf{p} you get:

$$\frac{\partial \rho}{\partial t} + \nabla \cdot \mathbf{J} = 0.$$

that is a consequence of the Vlasov equation. The charge conservation allows the Vlasov-Maxwell problem to be well posed since the right hand sides of (1.2) and (1.4) are compatible.

Integrating once more with respect to \mathbf{x} , you get:

$$\frac{d}{dt} \int \int f d\mathbf{p} d\mathbf{x} = 0,$$

which means that total mass and total charge are also preserved.

Remark 1. *If the Vlasov equation is multiplied with f^{q-1} and integrated with respect to x and v , you similarly have the conservation of the L^q norm of f , q integer, $1 \leq q < \infty$.*

1.2.3 Energy conservation

Let us define the relativistic kinetic energy

$$E_{cin}^R(t) = mc^2 \int \int (\gamma - 1) f(\mathbf{x}, \mathbf{p}, t) d\mathbf{x} d\mathbf{p},$$

the non relativistic kinetic energy:

$$E_{cin}^{NR}(t) = \frac{m}{2} \int \int |\mathbf{v}|^2 f(\mathbf{x}, \mathbf{v}, t) d\mathbf{x} d\mathbf{v},$$

and the electromagnetic energy:

$$E_{field}(t) = \frac{\epsilon_0}{2} \int (|\mathbf{E}(\mathbf{x}, t)|^2 + c^2 |\mathbf{B}(\mathbf{x}, t)|^2) d\mathbf{x}.$$

Proposition 1.2.2. *For both systems of non relativistic Vlasov-Poisson and Vlasov-Maxwell models, we have:*

$$\frac{d}{dt}(E_{cin}^{NR}(t) + E_{field}(t)) = 0.$$

For both systems of relativistic Vlasov-Poisson and Vlasov-Maxwell models, we have:

$$\frac{d}{dt}(E_{cin}^R(t) + E_{field}(t)) = 0.$$

Proof: The functions E, B and f will be supposed regular enough, tending to zero at infinite. In the non relativistic case, we have:

$$\begin{aligned} \frac{dE_{cin}^R}{dt} &= \frac{m}{2} \int \int |\mathbf{v}|^2 \frac{\partial f}{\partial t}(\mathbf{x}, \mathbf{v}, t) d\mathbf{x} d\mathbf{v}, \\ &= -\frac{m}{2} \int \int |\mathbf{v}|^2 (\nabla_x \cdot (\mathbf{v}f) + \frac{q}{m} \nabla_v \cdot ((\mathbf{E} + v(\mathbf{p}) \times \mathbf{B})f)) d\mathbf{x} d\mathbf{v}, \\ &= \frac{m}{2} \int \int \nabla_v (|\mathbf{v}|^2) \cdot \frac{q}{m} ((\mathbf{E} + v(\mathbf{p}) \times \mathbf{B})f) d\mathbf{x} d\mathbf{v}, \\ &= \int \int \mathbf{v} \cdot q(\mathbf{E} + v(\mathbf{p}) \times \mathbf{B})f d\mathbf{x} d\mathbf{v}, \\ &= \int \int q\mathbf{v}f \cdot \mathbf{E} d\mathbf{x} d\mathbf{v}, \\ &= \int \mathbf{J} \cdot \mathbf{E} d\mathbf{x}. \end{aligned}$$

In the relativistic case, we have:

$$\begin{aligned} \frac{dE_{cin}^{NR}}{dt} &= mc^2 \int \int (\gamma - 1) \frac{\partial f}{\partial t}(\mathbf{x}, \mathbf{p}, t) d\mathbf{x} d\mathbf{p}, \\ &= -mc^2 \int \int (\gamma - 1) (\nabla_x \cdot (\mathbf{v}f) + \frac{q}{m} \nabla_p \cdot ((\mathbf{E} + v(\mathbf{p}) \times \mathbf{B})f)) d\mathbf{x} d\mathbf{p}, \\ &= mc^2 \int \int \nabla_p (\gamma - 1) \cdot (q(\mathbf{E} + v(\mathbf{p}) \times \mathbf{B})f) d\mathbf{x} d\mathbf{p}, \\ &= \int \int \frac{\mathbf{P}}{m\gamma} \cdot q(\mathbf{E} + v(\mathbf{p}) \times \mathbf{B})f d\mathbf{x} d\mathbf{p}, \\ &= \int \int q\mathbf{v}f \cdot \mathbf{E} d\mathbf{x} d\mathbf{p}, \\ &= \int \mathbf{J} \cdot \mathbf{E} d\mathbf{x}. \end{aligned}$$

Thanks to the solving of the Maxwell's equation, we have:

$$\begin{aligned} \frac{dE_{field}^{NR}}{dt} &= \epsilon_0 \int \left(\frac{\partial \mathbf{E}}{\partial t} \cdot \mathbf{E} + c^2 \frac{\partial \mathbf{B}}{\partial t} \cdot \mathbf{B} \right) d\mathbf{x}, \\ &= \epsilon_0 \int \left(c^2 \nabla \times \mathbf{B} \cdot \mathbf{E} - c^2 \nabla \times \mathbf{E} \cdot \mathbf{B} - \frac{1}{\epsilon_0} \mathbf{J} \cdot \mathbf{E} \right) d\mathbf{x}, \\ &= - \int \mathbf{J} \cdot \mathbf{E} d\mathbf{x}. \end{aligned}$$

and thanks to the solving of the Poisson's equation, where the magnetic field is zero, we have:

$$\begin{aligned} \frac{dE_{field}^{NR}}{dt} &= \epsilon_0 \int \frac{\partial \mathbf{E}}{\partial t} \cdot \mathbf{E} d\mathbf{x}, \\ &= \epsilon_0 \int \frac{\partial \nabla \phi}{\partial t} \cdot \nabla \phi d\mathbf{x}, \\ &= -\epsilon_0 \int \frac{\partial \Delta \phi}{\partial t} \phi d\mathbf{x}, \\ &= \int \frac{\partial \rho}{\partial t} \phi d\mathbf{x}, \\ &= - \int \nabla \cdot \mathbf{J} \phi d\mathbf{x}, \\ &= \int \mathbf{J} \cdot \nabla \phi d\mathbf{x}, \\ &= - \int \mathbf{J} \cdot \mathbf{E} d\mathbf{x}. \end{aligned}$$

In all cases, the total energy is conserved all through the time.

1.3 Existence of solutions for the Vlasov-Poisson system

Let us be given the following Cauchy problem:

$$\begin{cases} \frac{\partial f}{\partial t} + v(\mathbf{p}) \cdot \nabla_x f + q(\mathbf{E} + v(\mathbf{p}) \times \mathbf{B}) \cdot \nabla_p f = 0, \\ \rho = q \int f d\mathbf{p}, \\ \nabla \times \mathbf{E} = 0, \\ \nabla \cdot \mathbf{E} = \frac{\rho}{\epsilon_0}, \\ f(.,., 0) = f_0, \end{cases}$$

with $\mathbf{p} = m\gamma v(\mathbf{p})$. This problem will be denoted (RVP) for relativistic Vlasov-Poisson when $\gamma = (1 + (\frac{|\mathbf{p}|}{mc})^2)^{\frac{1}{2}}$ and (VP) for the non relativistic case where $\mathbf{p} = mv(\mathbf{p})$.

1.3.1 Non relativistic case

Weak solutions: The weak solutions of the (VP) problem are functions that check this problem in the distribution sense. Arsen'ev [1] in 1975 proved the global existence of weak solutions but the uniqueness remains an open question.

Classical solutions: Kurth, in 1952, [20] is the first one who managed to prove the existence of local regular solution to the (VP) problem. The global existence was proved later for particular initial data:

- for spherical symmetric initial data: Batt in 1977 [3],
- for cylinder-shaped symmetric initial data: Horst in 1982 [17],
- for small initial data: Bardos-Degond in 1985 [2],
- for nearly symmetric initial data: Schaeffer in 1987 [27].

Global existence for the 2D case was proved in 1978 by Okabe-Ukai [23]. In 1990, Pfaffelmoser [24] managed to prove global existence of regular solutions for the 3D problem with general initial data. We will give as an example the Schaeffer version [28] who simplified the Pfaffelmoser version in 1991:

Let us settle $Q(t) = 1 + \sup\{|v| : \exists(x, \tau) \in \mathbb{R}^3 \times [0, t] \text{ so that } f(x, v, \tau) \neq 0\}$.

Theorem 1 (Schaeffer). *Let us suppose the initial data f_0 C^1 positive and compactly supported. Then, the (VP) problem admits one unique solution f C^1 . Moreover, $\forall p > \frac{33}{16}, \exists C_p$ so that*

$$Q(t) \leq C_p(1 + T)^p.$$

Other simplifications were brought by Horst in 1993 [18] and by Lions-Perthame in 1991 [21]

1.3.2 Relativistic case

For the moment there is no proof of the existence of global classical solutions for the relativistic case. Nevertheless, Glassey-Schaeffer in 1985 [9] proved the existence of global classical solutions with spherical symmetries.

1.4 Existence of solutions for the Vlasov-Maxwell system

Let us consider this Cauchy problem:

$$\left\{ \begin{array}{l} \frac{\partial f}{\partial t} + v(\mathbf{p}) \cdot \nabla_x f + q(\mathbf{E} + v(\mathbf{p}) \times \mathbf{B}) \cdot \nabla_p f = 0, \\ \mathbf{J} = q \int v(\mathbf{p}) f d\mathbf{p}, \\ \partial_t \mathbf{E} - c^2 \nabla \times \mathbf{B} = \frac{\mathbf{J}}{\epsilon_0}, \\ \partial_t \mathbf{B} + \nabla \times \mathbf{E} = 0, \\ f(\cdot, \cdot, 0) = f_0, \quad \mathbf{E}(\cdot, 0) = \mathbf{E}_0, \quad \mathbf{B}(\cdot, 0) = \mathbf{B}_0, \\ \nabla \cdot \mathbf{E}_0 = \frac{\rho(\cdot, 0)}{\epsilon_0}, \quad \nabla \cdot \mathbf{B}_0 = 0, \end{array} \right.$$

It will be denoted (RVM) for relativistic Vlasov-Maxwell in the same case as Vlasov-Poisson and VM for non relativistic Vlasov-Maxwell.

1.4.1 Non relativistic case

Weak solutions: The first result of global existence for (VM 3D) was obtained by DiPernia-Lions [7] in 1989. Their proof is also valid in the relativistic case. Their theorem will be displayed, but let us first introduce the following Banach spaces: for $p \geq 1$ and Ω an open from \mathbb{R}^n , $n \in \mathbb{N}^*$:

$$\begin{aligned} L^p(\Omega) &= \{f : \Omega \rightarrow \mathbb{R}: \text{measurable and } \int_{\Omega} |f|^p dx < \infty\} \\ L^\infty(\Omega) &= \{f : \Omega \rightarrow \mathbb{R}: \text{measurable and } \exists C > 0, |f(x)| \leq C \text{ a.e. } x \in \Omega\}. \end{aligned}$$

Theorem 2 (DiPernia-Lions). *Let us suppose f_0 positive and in $L^1 \cap L^\infty(\mathbb{R}^3 \times \mathbb{R}^3)$ and f_0, E_0, B_0 check:*

$$\int \int |v|^2 f_0 dx dv + \frac{1}{2} \int (|E_0|^2 + |B_0|^2) dx < \infty.$$

Then, there exists a weak solution to the VM problem $f \in C^0(\mathbb{R}^+, L^\infty(\mathbb{R}^3 \times \mathbb{R}^3) - w^)$ and $E, B \in C^0(\mathbb{R}^+, L^2(\mathbb{R}^3) - w)$.*

The notations $-w$ and $-w^*$ are here to recall that the functions are obtained as weak or weak * limits of functions in the quoted spaces.

Let us also speak about the work of Guo [16], who showed in 1993 the global existence of weak solutions to the VM problem, with limit conditions in the relativistic and the non relativistic case.

Classical solutions: The first 1D results were issued from the work of Cooper-Klimas [6] in 1980, and for 1D1/2 case, the work by Neunzert-Petry in 1980 [22]. Local existence and uniqueness of classical solutions to the VM3D problem was proved by Wollmann [29] in 1984.

1.4.2 Relativistic case

Weak solutions: The global existence of weak solutions is included in the demonstration by DiPernia-Lions in 1985 (see non relativistic case) and was more simply proved by Rein in 2004 [26]. The uniqueness of weak solutions remains an open question.

Classical solutions: Global existence and uniqueness of regular enough solutions is still an open problem. Yet, Glassey-Strauss [14] in 1986 proved a result of local existence and uniqueness of classical solutions, with regular compactly supported initial data. The solutions become global if the support in the p^{th} -moment is controlled:

Theorem 3 (Glassey-Strauss). *Let us suppose $f_0 \geq 0$, $f_0 \in C^1$ and compactly supported, $E_0, B_0 \in C^2$. An a priori estimate is made about the approximation of the solution: there exists $\beta(t)$ a continuous function so that:*

$$f(x, v, t) = 0, \forall x \in \mathbb{R}^3, |v| > \beta(t).$$

So the RVM problem admits a unique solution $f \in C^1(\mathbb{R}^3 \times \mathbb{R}^3 \times \mathbb{R}^+)$. Moreover, $E, B \in C^1(\mathbb{R}^3 \times \mathbb{R}^+)$.

This condition is verified when data are small (Glassey-Strauss in 1987 [15]), quasi-neutral (Glassey-Strauss in 1988 [10]), or nearly-spheric symmetrical (Rein in 1990 [25]). In lower dimensions, classical global solutions exist for general initial data (Glassey-Schaeffer [11, 12, 13]).

The Glassey-Strauss theorem led to new demonstrations. In 2002, Klainerman Staffilani [19] proved the theorem using Fourier transform, and gave a new version of it:

Theorem 4 (Klainerman-Staffilani). *Let us suppose that the initial data check: $f_0 \geq 0$, $f_0 \in C^1$ and compactly supported, $E_0, B_0 \in C^1$, and $\exists C, \forall T > 0$,*

$$\|(E, B)\|_{L^\infty([0, T] \times \mathbb{R}^3)} \leq C.$$

So the RVM problem admits a unique solution $f \in C^1(\mathbb{R}^3 \times \mathbb{R}^3 \times [0, T])$. Moreover, $E, B \in C^1(\mathbb{R}^3 \times [0, T])$.

In 2003, Bouchut-Golse-Pallard [4] gave a shorter proof of Glassey-Strauss theorem.

Bibliography

- [1] A. ARSEN'EV, *Global existence of a weak solution of Vlasov's system of equations*, USSR Comp. Math. Phys. **15**, pp. 131-143, (1975).
- [2] C. BARDOS, P. DEGOND, *Global existence for the Vlasov-Poisson equation in three variables with small initial data* Ann. Inst. Henri Poincaré, Analyse non linéaire, **2**, pp.101-118, (1985).
- [3] J.BATT, *Global symmetric solutions of the initial value problem of stellar dynamics*, Jour. of Diff. Eq. **25**, pp. 342-364, (1977).
- [4] F.BOUCHUT, G. GOLSE, C. PALLARD, *Classical solutions and the Glassey-Strauss Theorem for the 3D Vlasov-Maxwell system*, Arch. Rational Mech. Anal. **170**, no.1, pp. 1-15, (2003).
- [5] F.BOUCHUT, G. GOLSE, M. PULVIRENTI, *Kinetic equations and asymptotic theory*, Series in Applied Mathematics, Gauthier-Villars (2000).
- [6] J. COOPER, A. KLIMAS, *Boundary value problems for the Vlasov-Maxwell equation in one dimension*, J. Math. Anal. Appl. **75**, pp. 306-329, (1980).
- [7] R. DIPERNA, P.L. LIONS, *Global weak solutions of Vlasov-Maxwell systems*, Comm. Pure Appl. Math. **42**, pp. 729-757, (1989).
- [8] R. GLASSEY *The Cauchy problem in kinetic theory*, SIAM, Philadelphia (1996).
- [9] R. GLASSEY, J. SCHAEFFER *On symmetric solutions of the relativistic Vlasov-Poisson system*, Comm. Math. Phys. **101**, pp. 459-473, (1985).
- [10] R. GLASSEY, J. SCHAEFFER *Global existence for the relativistic Vlasov-Maxwell system with nearly neutral initial data*, Comm. Math. Phys. **119**, pp. 353-384, (1988).
- [11] R. GLASSEY, J. SCHAEFFER *On the 'one and one-half dimensional' relativistic Vlasov-Maxwell system*, Math. Meth. APPL. Sci **13**, pp. 169-179, (1990).
- [12] R. GLASSEY, J. SCHAEFFER *The 'two and one-half dimensional' relativistic Vlasov-Maxwell system*, Comm. Math. Phys. **185**, pp. 257-284, (1997).
- [13] R. GLASSEY, J. SCHAEFFER *The relativistic Vlasov-Maxwell system in two space dimensions: Part I and II*, Arch. Rational. mech. Anal. **141**, pp.331-354 , 355-374, (1998).

- [14] R. GLASSEY, W. STRAUSS *Singularity formation in a collisionless plasma could only occur at high velocities*, Arch. Rational. mech. Anal. **92**, pp. 56-90, (1986).
- [15] R. GLASSEY, W. STRAUSS *Absence of shocks in an initially dilute collisionless plasma*, Comm. Math. Phys. **113**, pp. 191-208, (1987).
- [16] Y. GUO *Global weak solutions of the Vlasov-Maxwell system with boundary conditions*, Comm. Math. Phys. **154**, pp. 245-263, (1993).
- [17] E. HORST *On the classical solutions of the initial value problem for the unmodified non-linear Vlasov equation Part II*, Math. Meth. Appl. Sci. **4**, pp. 19-32, (1982).
- [18] E. HORST *On the asymptotic growth of the solutions of the Vlasov-Poisson system*, Math. Meth. Appl. Sci. **16**, pp.75-82, (1993).
- [19] S. KLAINERMAN, G. STAFFILANI, *A new approach to study the Vlasov-Maxwell system* Comm. Pure Appl Anal. **1**, no.1, pp. 103-125, (2002).
- [20] R. KURTH, *Das Anfangswertproblem der Stelldynamik*, Z. Astrophys. **30**, pp. 213-229, (1952).
- [21] P.L. LIONS, B. PERTHAME, *Propagation of moments and regularity of solutions for the 3 dimensional Vlasov-Poisson system*, Invent. Math. **105**, pp. 415-430, (1991).
- [22] H. NEUNZERT, K.H. PETRY, *Ein Existenzsatz für die Vlasov-Gleichung mit selbstkonsistentem Magnetfeld*, Math. Meth Appl. Sci. **2**, pp. 429-444, (1980).
- [23] T. UKAI, S. OKABE, *On classical solutions in the large in time of two-dimensional Vlasov's equation*, Osaka J. Math. **15**, pp. 245-261, (1978).
- [24] K. PFAFFELMOSE, *Global classical solutions of the Vlasov-Poisson system in three dimensions for general initial data*, Jour. of Diff. Eq. **95**, pp. 281-303, (1992).
- [25] G. REIN, *Generic global solutions of the relativistic Vlasov-Maxwell system of plasma physics*, Comm. Math. Phys. **135**, pp. 41-78, (1990).
- [26] G. REIN, *Global weak solutions to the relativistic Vlasov-Maxwell system revisited*, Comm. Math. Sci. **Vol. 2**, No. 2, pp. 145-158, (2004).
- [27] J. SCHAEFFER, *Global existence for the Poisson-Vlasov system with nearly symmetric data*, Jour. of Diff. Eq. **69**, pp. 111-148, (1987).
- [28] J. SCHAEFFER, *Global existence of smooth solutions to the Vlasov-Poisson system in three dimensions*, Communications in P.D.E. **16**, pp. 1313-1335, (1991).
- [29] S. WOLLMAN, *An existence and uniqueness theorem for the Vlasov-Maxwell system*, Comm. Pure Pll. Math. **37**, pp. 457-462, (1984).

Numerical methods for the solving of Vlasov-Poisson and Vlasov-Maxwell systems

2.1 Numerical resolution of the Vlasov equation

2.1.1 Introduction

Different kinds of methods are used for the resolution of the Vlasov equation, coupled with either the Poisson or the Maxwell's equations. The most used method is by far the particle method, other methods, like Fourier or Hermite developments of the distribution function exist, and methods using a phase space grid are also used. Historically, the unstopping evolution of computational power makes people have to find always new and better numerical methods, which are able to solve more complex and accurate problems. Hence, the outgoing of numerical methods is historically linked to the power available at that time. That is why, at the beginning, in the 1960's and 1970's, only 1D problems could be solved, and many methods were invented, each one having its advantages and drawbacks. Then, in the 1980's and 1990's, one of these methods, the PIC one (for Particle In Cell), was nearly the only one used in practice, since it enabled to have quite good physical results with a reasonable computational cost. Since the end of the 1990's, the increasing computational power allowed to create methods using a phase space grid. These methods lead to a really better accuracy in general cases. The methods that will be developed and used in this work all belong to the so-called semi-Lagrangian methods. Semi means in fact semi Eulerian because of the use of a grid, and semi Lagrangian since the invariance of the distribution function along the characteristics will also be fully used. It is obvious that as time will go by, these methods will be improved, and new ones will arise always in order to be able to follow the power of the machines. We shall not forget to speak about finite volume methods about which many details can be found in [36, 37, 20, 14]. Their theoretical study in the particular case of Vlasov-Poisson 1D was done by Filbet in [38]. Even though they are known to be robust, these methods are quite dissipative and suffer from the fact that they

are constrained by a severe CFL condition on the time step. We will not give further details about these methods.

2.1.2 The particle methods

Introduction

As we said, the first particle method which has been used is the PIC one, and this method is still one of the most commonly used in order to solve the problems of Vlasov-Poisson or Vlasov-Maxwell. This method consists in a coupling of a particle method for Vlasov, and a grid method for Poisson or Maxwell that will be discussed later. The principle of the particle method is to discretize the distribution function through a set of macro-particles, which represent the initial state of the data $f_0(x, v)$, normalized so that it can be regarded as a density probability function. The coupling with the fields is done through the sources ρ and \mathbf{J} , thanks to a regularization method. Then any algorithm concerning the fields can be done, and in order to finish the step, you just have to know the values of the fields at the position of the particles, which can be inherent to the method, or shall require an interpolation method. Like that, you can move your particles, and start again. There exists huge literature concerning PIC methods. For a more physical point of view, there are two books by Birdsall and Langdon [12] and by Hockney and Eastwood [45]. For a more mathematical point of view, you can find some results of convergence in particular cases for example by Neunzert and Wick [56, 57], Cottet and Raviart [27], Victory and Allen [71, 72], and Wollman [74].

There exists also a little variant of the PIC method, which is called the δf method. It can be used when the physical environment is near an equilibrium configuration, like in tokamaks or particle accelerators. The principle is to set $f = f_0 + \delta f$, and only take care of δf through a PIC method.

The PIC method

It consists in representing the distribution function f with a finite number N of macro-particles, given their position $\mathbf{x}_k(t) \in \mathbb{R}^3$ and their impulsion $\mathbf{p}_k(t) \in \mathbb{R}^3$, which weight will be denoted ω_k .

Let us write the initial density $f^0 = f(., ., 0)$:

$$f_N^0(\mathbf{x}, \mathbf{p}) = \sum_{k=1}^N \omega_k \delta(\mathbf{x} - \mathbf{x}_k^0) \delta(\mathbf{p} - \mathbf{p}_k^0),$$

where $(\mathbf{x}_k^0, \mathbf{p}_k^0)$ are the initial position and impulsion of the N macro-particles and δ represent Dirac mass. In the mathematical context of measures, the following proposition by Raviart [60] will be recalled:

Proposition 2.1.1. *Let us suppose that the Vlasov equation coefficients $v(\mathbf{p}), \mathbf{E} + v(\mathbf{p}) \times \mathbf{B}$ belong to the space: $L^\infty(0, T; W^{1,p}(\mathbb{R}^6)) \cap C^0(\mathbb{R}^6 \times [0, T])$. So, there exists a unique measure f_N*

solution of the Vlasov equation with f_N^0 as the initial data, and it writes

$$f_N(\mathbf{x}, \mathbf{p}, t) = \sum_{k=1}^N \omega_k \delta(\mathbf{x} - \mathbf{x}_k(t)) \delta(\mathbf{p} - \mathbf{p}_k(t)),$$

where $(\mathbf{x}_k(t), \mathbf{p}_k(t))$ are the solutions of the following differential system:

$$\begin{cases} \frac{d\mathbf{x}_k}{dt}(t) = v(\mathbf{p}_k(t)), & \mathbf{x}_k(0) = \mathbf{x}_k^0 \\ \frac{d\mathbf{p}_k}{dt}(t) = \mathbf{E}(\mathbf{x}_k(t), t) + v(\mathbf{p}_k(t)) \times \mathbf{B}(\mathbf{x}_k(t), t), & \mathbf{p}_k(0) = \mathbf{p}_k^0 \end{cases}$$

Thus, if the movement equation can be solved exactly (which happens for example if the fields are easy enough), the PIC method gives the exact solution for an initial data given under a Dirac mass sum way.

The charge and current densities write:

$$\rho_N(\mathbf{x}, t) = q \int_{\mathbb{R}^3} f_N(\mathbf{x}, \mathbf{p}, t) d\mathbf{p} = q \sum_{k=1}^N \omega_k \delta(\mathbf{x} - \mathbf{x}_k(t)),$$

$$\mathbf{J}_N(\mathbf{x}, t) = q \int_{\mathbb{R}^3} v(\mathbf{p}) f_N(\mathbf{x}, \mathbf{p}, t) d\mathbf{p} = q \sum_{k=1}^N \omega_k v(\mathbf{p}_k(t)) \delta(\mathbf{x} - \mathbf{x}_k(t)).$$

In order to fully describe a particle method, the way the initial data is chosen, how the coupling between the particles and the grid is done, and the way the characteristics are solved are needed.

Choice of the initial data

- determinist method: A uniform or not phase space grid must be settled. Then the initial position and impulsion of the particles $(\mathbf{x}_k^0, \mathbf{p}_k^0)$ are chosen as the barycenter of the mesh, with the integral of f_0 on this mesh as associated weight.
- Monte Carlo method: The initial position and impulsion of the particles are chosen randomly or pseudo randomly, being given the density of probability associated to f_0 .

Coupling particles-mesh

The particle approximation does not enable to have the values of the densities on the mesh. So, in order to couple this method with a field solver, a regularization has to be done. In that goal, at all nodes \mathbf{x}_i , a form function of form factor S_i is introduced. S_i is integrable and compactly supported. So the phase: particles \rightarrow mesh can be exposed like that:

$$\rho_h(\mathbf{x}_i, t) = q \int_{\mathbb{R}^3} \rho_N(\mathbf{x}, t) S_i(\mathbf{x}) d\mathbf{x} = q \sum_{k=1}^N \omega_k S_i(\mathbf{x}_k(t)),$$

$$\mathbf{J}_h(\mathbf{x}_i, t) = q \int_{\mathbb{R}^3} \mathbf{J}_N(\mathbf{x}, t) S_i(\mathbf{x}) d\mathbf{x} = q \sum_{k=1}^N \omega_k v(\mathbf{p}_k(t)) S_i(\mathbf{x}_k(t)).$$

In order to ensure total charge conservation, it has to be imposed that:

$$\sum_i V_i S_i(\mathbf{x}) = 1, \quad \forall \mathbf{x} \in \mathbb{R}^3,$$

where V_i represents the volume of the mesh associated to x_i . So, we have:

$$\sum_i V_i \rho_h(\mathbf{x}_i, t) = q \sum_k \omega_k, \quad \forall t \geq 0.$$

There remains the phase: grid \rightarrow particles. The fields need to be evaluated at the position of each particle, knowing their values on the mesh. Hockney and Eastwood [45] suggest to use the same form functions S_i , in order to avoid self-forces. It follows:

$$\mathbf{E}(\mathbf{x}_k(t)) = \sum_i V_i E(\mathbf{x}_i, t) S_i(\mathbf{x}_k(t)),$$

$$B(\mathbf{x}_k(t)) = \sum_i V_i B(\mathbf{x}_i, t) S_i(\mathbf{x}_k(t)),$$

In the particular case of a uniform cartesian mesh used to solve Maxwell, the S_i functions are translated from one unique form function $S : \mathbb{R}^3 \rightarrow \mathbb{R}$:

$$S_i(\mathbf{x}) = S(\mathbf{x}_i - \mathbf{x}), \quad \forall \mathbf{x} \in \mathbb{R}^3.$$

In that case, the densities approximation can be regarded as convolution products:

$$\rho_h(\mathbf{x}_i, t) = q \int_{\mathbb{R}^3} \rho_N(\mathbf{x}, t) S(\mathbf{x}_i - \mathbf{x}) d\mathbf{x} = (\rho_N *_{\mathbf{x}} S)(\mathbf{x}_i, t),$$

$$\mathbf{J}_h(\mathbf{x}_i, t) = q \int_{\mathbb{R}^3} \mathbf{J}_N(\mathbf{x}, t) S(\mathbf{x}_i - \mathbf{x}) d\mathbf{x} = (\mathbf{J}_N *_{\mathbf{x}} S)(\mathbf{x}_i, t).$$

The examples of form function that will be used during all this work will be B -splines. Let us introduce them now:

These B -splines are defined recurrently. The function used for the initialization will be denoted S^0 :

$$S^0(x) = \begin{cases} \frac{1}{\Delta x} & \text{if } x \in] -\frac{\Delta x}{2}, \frac{\Delta x}{2} [, \\ 0 & \text{else.} \end{cases}$$

The B -splines of superior degrees are then given by:

$$\forall m \in \mathbb{N}^*, S^m(x) = (S^0)^{*m}(x) = S_0 * S_{m-1}(x) = \frac{1}{\Delta x} \int_{x-\frac{\Delta x}{2}}^{x+\frac{\Delta x}{2}} S^{m-1}(u) du;$$

In particular, this work deals with the three first degrees, let us remind them:

$$S^1(x) = \begin{cases} (1 - \frac{|x|}{\Delta x}) & \text{if } |x| < \Delta x, \\ 0 & \text{else.} \end{cases}$$

$$S^2(x) = \begin{cases} \left(\frac{1}{2}\left(\frac{3}{2} - \frac{|x|}{\Delta x}\right)^2\right) & \text{if } \frac{1}{2}\Delta x < |x| < \frac{3}{2}\Delta x, \\ \left(\frac{3}{4} - \left(\frac{x}{\Delta x}\right)^2\right) & \text{if } |x| < \frac{1}{2}\Delta x, \\ 0 & \text{else.} \end{cases}$$

$$S^3(x) = \begin{cases} \frac{1}{6}\left(2 - \frac{|x|}{\Delta x}\right)^3 & \text{if } \Delta x < |x| < 2\Delta x, \\ \frac{1}{6}\left(4 - 6\left(\frac{x}{\Delta x}\right)^2 + 3\left(\frac{|x|}{\Delta x}\right)^3\right) & \text{if } 0 \leq |x| < \Delta x, \\ 0 & \text{else.} \end{cases}$$

Some basic properties should be added to help understanding why these functions were chosen:

- Density: $\int S^m(x)dx = \Delta x$,
- Partition of unity: for $x_j = j\Delta x$, $\sum_j S(x - x_j) = 1$,
- Oddity: $S^m(-x) = S^m(x)$.

Solving of the characteristics

We will give two examples of algorithms used to solve the characteristics, one for non relativistic Vlasov-Maxwell, one for non relativistic Vlasov-Poisson:

- Leap frog of second order algorithm for Vlasov-Maxwell:

$$\begin{cases} \frac{\mathbf{x}_k^{n+1} - \mathbf{x}_k^n}{\Delta t} = \mathbf{v}_k^{n+\frac{1}{2}}, \\ \frac{\mathbf{v}_k^{n+\frac{1}{2}} - \mathbf{v}_k^{n-\frac{1}{2}}}{\Delta t} = \frac{q}{m}(\mathbf{E}_k^n + \frac{\mathbf{v}_k^{n+\frac{1}{2}} + \mathbf{v}_k^{n-\frac{1}{2}}}{2} \times \mathbf{B}_k^n), \end{cases}$$

- Second order Verlet algorithm for Vlasov-Poisson:

$$\begin{cases} \frac{\mathbf{v}_k^{n+\frac{1}{2}} - \mathbf{v}_k^n}{\Delta t} = \frac{q}{2m}\mathbf{E}_k^n(\mathbf{x}_k^n), \\ \frac{\mathbf{x}_k^{n+1} - \mathbf{x}_k^n}{\Delta t} = \mathbf{v}_k^{n+\frac{1}{2}}, \\ \frac{\mathbf{v}_k^{n+1} - \mathbf{v}_k^{n+\frac{1}{2}}}{\Delta t} = \frac{q}{2m}\mathbf{E}_k^{n+1}(\mathbf{x}_k^{n+1}). \end{cases}$$

2.1.3 The semi-Lagrangian methods

As it was already said, the semi-Lagrangian methods appeared really later than the particle ones. They remain less used, but have become classical anyway thanks to their bigger accuracy and the lack of numerical noise. These methods use a phase space grid, which explains that for the moment, it can be computed only in smaller dimension (2D or 4D), since it is unreasonable for the moment to try to construct a 6D grid, with consequent dimensions in each direction. The originality of semi-Lagrangian methods, comparing to classical grid methods for solving partial differential equations is that it takes benefit from the constance of the distribution function along the characteristics in order to update the unknown from one time step to the other. There exists big families of semi-Lagrangian methods: classical backward, volumic and forward. We will briefly present them. All these methods use an interpolation step, and often like in this work, an interpolation thanks to cubic B -spline. Let us first present this method of interpolation:

Cubic B-spline Interpolation

The process will be explained in 1D. How to deal higher dimensions will be precised. Let us be given a uniform mesh of the interval $[a, b]$: $x_i = a + ih$, $i \in \{1, \dots, N\}$, with $h = \frac{b-a}{N}$. If a function f is supposed C^k , $k \geq 0$, its cubic B-spline interpolant f_h is defined through: $f_h(x_i) = f(x_i)$, $f_h \in \mathbb{P}_3[X]([x_i, x_{i+1}])$, $\forall i \in \{0, \dots, N\}$, and $f_h \in C^2([a, b])$.

If the domain is periodical, that is to say that $[a, b]$ is one period of the functions f and f_h , these relations are sufficient to define f_h uniquely. Otherwise, limit conditions have to be added: for example, Hermite conditions where $f'_h(a)$ and $f'_h(b)$ are also given, or natural conditions, where $f''_h(a)$ and $f''_h(b)$ are set to 0.

Now, f_h has to be written on a B-spline basis. Let us display only the periodical case. All considered functions are periodical of period $b - a$. So, $f^p(a) = f^p(b)$, $p \in \{0, 1, 2\}$, and then the point x_N is in fact exactly the point x_0 . The writing of f on the B-spline basis is:

$$f_h(x) = \sum_{k=0}^{N-1} \alpha_k S^3(x - x_k),$$

where α_k are the unknown, which will be called spline coefficients. They are determined through the interpolation conditions:

$$f(x_i) = f_h(x_i) = \sum_{k=0}^{N-1} \alpha_k S^3(x_i - x_k), \quad \forall i \in \{0, \dots, N-1\}.$$

Using the spline properties, this system of equations has to be solved:

$$\alpha_{i-1} + 4\alpha_i + \alpha_{i+1} = 6f(x_i),$$

with $\alpha_{-1} = \alpha_{N-1}$ and $\alpha_0 = \alpha_N$ using periodicity. This system can be rewritten under a matricial linear system form: $\mathbf{A}\alpha = \beta$ with:

$$\mathbf{A} = \begin{pmatrix} 4 & 1 & 0 & \dots & 0 & 1 \\ 1 & 4 & 1 & 0 & \dots & 0 \\ 0 & \ddots & \ddots & \ddots & \ddots & 0 \\ \vdots & \ddots & \ddots & \ddots & \ddots & 0 \\ 0 & \dots & 0 & 1 & 4 & 1 \\ 1 & 0 & \dots & 0 & 1 & 4 \end{pmatrix}, \quad \alpha = \begin{pmatrix} \alpha_0 \\ \vdots \\ \alpha_{N-1} \end{pmatrix}, \quad \beta = 6 \begin{pmatrix} f(x_0) \\ \vdots \\ f(x_{N-1}) \end{pmatrix}$$

\mathbf{A} is a strictly dominant diagonal matrix, and so is invertible. The resolution of the system gives a unique solution α , and consequently, a unique f_h function.

In order to interpolate in higher dimensions, tensorial products of B-splines will be used.

Classical Backward semi-Lagrangian (BSL)

In order to update the distribution function from step n to step $n + 1$, the method can be decomposed in two steps.

- For each node x_i , compute $X(t_n; x_i, t^{n+1})$, the value of the characteristic at time t^n which value is x_i at time t^{n+1} . That is why the method is called backward, since time is followed backwardly.
- As

$$f^{n+1}(x_i) = f^n(X(t_n; x_i, t^{n+1})),$$

$f^{n+1}(x_i)$ can be computed through an interpolation of $f^n(X(t_n; x_i, t^{n+1}))$, since $X(t_n; x_i, t^{n+1})$ is not necessarily a node of the mesh.

Historically, this method was first introduced by Cheng and Knorr [20] for the Vlasov-Poisson model, solved with a splitting of Strang method. We will briefly explain how the splitting works for this problem, since this will be dealt with in this work.

Splitting of Strang The non relativistic Vlasov-Poisson equation can be written in a conservative way:

$$\frac{\partial f}{\partial t} + v \frac{\partial f}{\partial x} + \frac{q}{m} E(t, x) \frac{\partial f}{\partial v} = \frac{\partial f}{\partial t} + \nabla \cdot \left(\left(v, \frac{q}{m} E(t, x) \right) f \right) = 0,$$

since $\partial_x v = \partial_v \left(\frac{q}{m} E(t, x) \right) = 0$. Thus, this equation can be splitted in two equations, which are still conservative

$$\frac{\partial f}{\partial t} + v \frac{\partial f}{\partial x} = 0,$$

$$\frac{\partial f}{\partial x} + \frac{q}{m} E(t, x) \frac{\partial f}{\partial v} = 0.$$

The splitting of Strang consists in solving the first equation over half a time step, then the second one over one time step, and once more the first equation over half a time step. The splitting of Strang is of second order with regards to time, and in this particular case enables to solve explicitly the characteristics, since simple transport with constant coefficients equations are dealt with. This enables to simplify the algorithm.

Nevertheless, this remains a simplification, and it is not always relevant to give priority to the axes directions. Therefore, non splitted semi-Lagrangian methods had to be developed.

The backward semi-Lagrangian methods needs to find the origin of the characteristics. At time n , you know f^n and E^n on the mesh, and their values at time $n + 1$ have to be found. An algorithm of second order can be written like that:

- Step one: Find a value \tilde{E}^{n+1} of the electric field at time $n + 1$ through a fixed point method like Newton or a predictor corrector method.
- Step two: For each mesh point $(x_i, v_j) = (X^{n+1}, V^{n+1})$, compute:

$$\begin{cases} V^{n+\frac{1}{2}} = V^{n+1} - \frac{\Delta t}{2} \tilde{E}^{n+1}(X^{n+1}), \\ X^n = X^{n+1} - \Delta t V^{n+\frac{1}{2}}, \\ V^n = V^{n+\frac{1}{2}} - \frac{\Delta t}{2} E^n(X^n). \end{cases}$$

- Step three: Use the computed approximation $f^{n+1}(x_i, v_j)$ to get a new value of E^{n+1} , and start again the iteration if necessary.

For a comparison between Eulerian solvers for Vlasov, refer to [37]. For more details about BSL, see [66, 41, 42, 35]

Conservative semi-Lagrangian method

Conservative numerical methods can also be naturally derived from the conservative form of the Vlasov equation. Classical semi-Lagrangian with splitting is also conservative, but this is an a posteriori result. The conservative semi-Lagrangian method can be regarded as a finite volume method, where the flux computation is made integrating the considered function over one mesh at a time t^n . In that case, the unknown is the mean value of f over one mesh: $\frac{1}{V} \int_V f dx$, and the numerical method can be decomposed like that:

- Reconstruction of a polynomial approximation of required degree using the mean values per mesh.
- Computation of the origin of the characteristics ending at the nodes of the mesh. (Like in classical method)
- Computation of the mean value per mesh at time t^{n+1} using the fact that $\frac{1}{V} \int_V f dx$ is constant along the characteristics.

The reconstruction of a polynomial approximation can be made using the PFC method [36], PPM1 [23], PPM2, [24] or PSM [78]. For more details, refer to [28, 42, 70, 77].

Forward semi-Lagrangian

This method was introduced by Reich et al [61, 25] in meteorology. This method adapted to the Vlasov equation is developed in this work. Let us just explain the basic principle of this method for Vlasov-Poisson. Suppose at time t^n , you know f^n, E^n .

- Find the location of $X(t^{n+1}, x_i, t^n)$ for all mesh nodes solving explicitly the characteristics.
- Deposit the known value on the nearest grid points depending on the degree of the form functions.

There are two main things to do, which will be widely explained: how characteristics are solved and how the values are deposited.

2.2 Numerical resolution of the Maxwell's equations

2.2.1 Introduction

The Maxwell's equations

$$\frac{\partial \mathbf{E}}{\partial t} - c^2 \nabla \times \mathbf{B} = -\frac{\mathbf{J}}{\epsilon_0}, \quad (2.1)$$

$$\frac{\partial \mathbf{B}}{\partial t} + \nabla \times \mathbf{E} = 0, \quad (2.2)$$

$$\nabla \cdot \mathbf{E} = \frac{\rho}{\epsilon_0}, \quad (2.3)$$

$$\nabla \cdot \mathbf{B} = 0. \quad (2.4)$$

describe the evolution of the electromagnetic fields $(\mathbf{E}(t, \mathbf{x}), \mathbf{B}(t, \mathbf{x}))$, knowing the charge density ρ and the charge current \mathbf{J} :

$$\rho(\mathbf{x}, t) = \sum_s q_s \int_{\mathbb{R}^3} f(\mathbf{x}, \mathbf{p}, t) d\mathbf{p},$$

$$\mathbf{J}(\mathbf{x}, t) = \sum_s q_s \int_{\mathbb{R}^3} v(\mathbf{p}) f(\mathbf{x}, \mathbf{p}, t) d\mathbf{p}.$$

through the coupling with the Vlasov equation.

The system of Maxwell's equation is well posed if and only if the charge conservation equation

$$\frac{\partial \rho}{\partial t} + \nabla \cdot \mathbf{J} = 0,$$

is satisfied. Indeed, you get it summing the derivative of (2.3) and the divergence of equation (2.1). Whether this equation is not verified, the Maxwell's system has too many unknowns.

The mathematical study of the Maxwell's equation is done for example in [2, 5, 29].

2.2.2 Finite difference

Yee

The original paper by Yee was written in the 1960's [76]. This scheme has been used a lot and keeps on being used a lot because of good properties (of second order in time and space, stable under CFL condition...), but also because it is very simple. You will find complete reference in [68, 76]. As an example, the Transverse Electric mode for Maxwell 2D (TE) will be written:

$$\frac{(B_z)_{i+\frac{1}{2}, j+\frac{1}{2}}^{n+\frac{1}{2}} - (B_z)_{i+\frac{1}{2}, j+\frac{1}{2}}^{n-\frac{1}{2}}}{\Delta t} = -\frac{(E_y)_{i+1, j+\frac{1}{2}}^n - (E_y)_{i, j+\frac{1}{2}}^n}{\Delta x} + \frac{(E_x)_{i+\frac{1}{2}, j+1}^n - (E_x)_{i+\frac{1}{2}, j}^n}{\Delta y},$$

$$\frac{(E_x)_{i+\frac{1}{2}, j}^{n+1} - (E_x)_{i+\frac{1}{2}, j}^n}{\Delta t} = -\frac{1}{\epsilon_0} (J_x)_{i+\frac{1}{2}, j}^{n+\frac{1}{2}} + c^2 \frac{(B_z)_{i+\frac{1}{2}, j+\frac{1}{2}}^{n+\frac{1}{2}} - (B_z)_{i+\frac{1}{2}, j-\frac{1}{2}}^{n+\frac{1}{2}}}{\Delta y},$$

$$\frac{(E_y)_{i, j+\frac{1}{2}}^{n+1} - (E_y)_{i, j+\frac{1}{2}}^n}{\Delta t} = -\frac{1}{\epsilon_0} (J_y)_{i, j+\frac{1}{2}}^{n+\frac{1}{2}} - c^2 \frac{(B_z)_{i+\frac{1}{2}, j+\frac{1}{2}}^{n+\frac{1}{2}} - (B_z)_{i-\frac{1}{2}, j+\frac{1}{2}}^{n+\frac{1}{2}}}{\Delta x}.$$

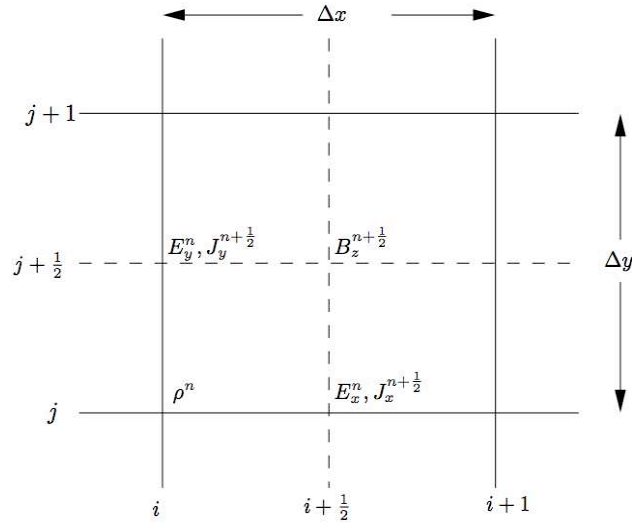


Figure 2.2.1: Positions of the fields and the densities for the 4D Yee scheme for Maxwell TE

This scheme is convergent under CFL condition: $c^2 \Delta t^2 \left(\frac{1}{\Delta x^2} + \frac{1}{\Delta y^2} \right) \leq 1$. One of the main advantages of this method is that discrete differential operators still satisfy: $div_h rot_h = 0$, and so, if charge conservation is checked and divergence constraints are checked initially, then they are exactly checked at every time.

Other algorithms or extensions

Some methods of superior orders can be computed, with conditions over the derivatives, see for example [22].

Nevertheless, one of the main drawbacks of finite difference methods is that non rectilinear frontiers will be badly represented. If you don't want to lose second order, you have few solutions. The first one is to refine in order to improve the representation of the boarder. But this leads to huge number of degrees of freedom, and so the method loses its efficiency. Another technique was developed in [31], consisting in particular interpolation on the exterior mesh. This technique is used in commercial codes like Microwave Studio [48].

2.2.3 Finite Volume methods

One of the most famous method is the one by Hermeline. His method, of second order numerically, but only proved of first order, is an extension of Yee on non orthogonal mesh. It is fully described in the original article by Hermeline: [44].

The Remaki's method should also be quoted. This method is the simple application of classical finite volume method to the conservative form of the two equations of Faraday and Ampere (2.1),(2.2). This method is called like that because of its application to the Maxwell's problem by Remaki at INRIA [62].

The main drawback of the Hermeline's method is that its order cannot be improved. With the Remaki's method, you can reach higher orders. Some variants can be found in Munz et al [50]. Generally, all variants are finite volume methods that can be applied to conservative laws: [13] for example.

2.2.4 Finite Element methods

We will start with the Assous et al. method, which consists in taking care of the divergence constraints with Lagrange multipliers. It is fully described in [4]. The finite elements used for spatial discretization are the ones of Taylor-Hood. This scheme is of second order in time and space, convergent under CFL condition, and in 1D, it degenerates in a Yee centered finite difference scheme.

Then, the edge finite elements of Raviart-Thomas-Nédelec, which were based on a work by Nédelec [55]. The second order formulation of the Maxwell's equations is used. The finite elements used are conform in $H(\text{rot})$, which ensures the continuity of the tangential components between two elements, whereas the normal components are discontinuous. The method is generally of first order, but of second order on uniform mesh. Many edge finite elements set exist. The scheme is stable under CFL condition, and like the Yee scheme, the method satisfies $\text{div}_h(\text{rot}_h) = 0$. The divergence constraints are taken into account implicitly, if charge conservation is checked by the sources.

The Cohen Monk finite elements should also be quoted [49] for their good numerical behavior. Extensions to higher order finite element families can be found in [30, 59, 1, 64].

Eventually, discontinuous Galerkin methods should not be forgotten. As examples, we will quote the works of Ferrières-Cohen-Pernet [21], Sonnendrücker [67], Piperno [58].

2.3 Convergence results

2.3.1 PIC Algorithms

Vlasov-Poisson

The first results of convergence of particle methods for the Vlasov-Poisson system were proved by Neunzert and Wick [56, 57] in 1972, for the 1D problem, for an asymptotic distribution of the initial set of particles, thanks to measure theory.

In 1984, Cottet and Raviart [27] studied the convergence of a 1D particle method for the 1D periodical problem, when particles are uniformly initialized in the phase space. Let us present their result. The form functions used are B-splines. The initial distribution is given this way. A uniform mesh of the phase space is given, with Δx and Δv as discretization parameters. $\beta := \sqrt{\Delta x^2 + \Delta v^2}$. At the center of each cell, a particle is settled, and its weight is defined by the value of f_0 at this point multiplied by the mesh volume $\Delta x \Delta v$. Let S be the spline used to reconstruct the densities with a convolution product. Let ϵ be the length of the spline support. Eventually, let $(x_k^h(t), v_k^h(t))_{k \in \{1, \dots, N\}}$ and $(x_k(t), v_k(t))_{k \in \{1, \dots, N\}}$ be the approached and exact trajectories of the particles, E_h and E the approached and exact electric fields. The Cottet Raviart theorem writes:

Theorem 5 (Cottet-Raviart). *Let us suppose that:*

- $\frac{\beta}{\epsilon}$ is bounded when β and $\epsilon \rightarrow 0$,
- $\exists m \in \mathbb{N}, S \in W^{m,\infty}$,
- $f^0 \in C^{\max(m+1,2)}(\mathbb{R}^2)$ is periodical in x and checks:

$$\forall \alpha \in \mathbb{N}^2, |\alpha| \leq \max(m+1, 2), |D^\alpha f_0(x, v)| \leq C(1 + |v|)^{-\gamma}, \quad \gamma > 1,$$

so, $\forall T > 0$, and $\beta \leq \beta_0, \epsilon \leq \epsilon_0, \exists C(T) > 0, \forall 0 \leq t \leq T$:

$$\max_{1 \leq k \leq N} (|x_k^h(t) - x_k(t)| + |v_k^h(t) - v_k(t)|) + \|(E^h - E)(\cdot, t)\|_{L^\infty(\mathbb{R})} \leq C(T)(\epsilon^2 + \frac{\beta^{m+1}}{\epsilon^m}).$$

More recently, Wollman and Ozizmir [74] showed that a particle method converges for the 1D problem, without regularization of the field, and with more general initialization of the weight of the particles.

The 3D problem was treated by Schaeffer in 1987 [63], for a model with spherical symmetries. A great work was done by Victory Jr. and his colleagues. In the articles [39, 71, 72], the authors generalized the results of Cottet-Raviart for uniform repartition of the particles. The convergence for a Neunzert-Wick type of initial repartition was generalized in [40]. Wollman [75] showed the convergence of a 3D particle methods with more general initial repartition.

Cohen-Perthame's [26] article can also be consulted, they proposed modifications to the Raviart [60] method, and got better order of convergence.

Relativistic Vlasov-Maxwell

Only a 1D and a half case was treated by Glassey and Schaeffer [43] in 1990. The variables are (x, p_x, p_y) . Their theorem is recalled here:

Let $\Delta x, \Delta p$ be the numerical parameters. The particles are supposed to be uniformly spread. $\beta = \max(\Delta x, \Delta p)$. Only the form function S^1 will be used. Let ϵ be its support length. Let $(x_k^h(t), p_{x_k}^h(t), p_{y_k}^h(t)), (x_k(t), p_{x_k}(t), p_{y_k}(t)), k \in \{1, \dots, N\}$ be the approached and exact trajectories of the particles and $(E_x^h, E_y^h, B_z^h), (E_x, E_y, B_z)$ the approached and exact electromagnetic fields. The initial data will be supposed smooth enough. The Glassey-Schaeffer theorem writes:

Theorem 6 (Glassey-Schaeffer). *Being given $C_1 > 0$. There exists $C : \mathbb{R}^+ \rightarrow \mathbb{R}^+$ so that, $\forall \epsilon, \beta$ with $\beta < C_1 \epsilon$ and $\epsilon \sup_{x,t} |B_z(t, x)| < 1$, there exists $T_{\epsilon, \beta}$ so that:*

$$\begin{aligned} & \sup_{k, 0 \leq \tau \leq t} (|x_k^h(t) - x_k(t)| + |p_{x_k}^h(t) - p_{x_k}(t)| + |p_{y_k}^h(t) - p_{y_k}(t)|) \\ & + \sup_{0 \leq \tau \leq t} (\|E_x(\tau, \cdot) - E_x^h(\tau, \cdot)\|_{L^\infty(\mathbb{R})} + \|E_y(\tau, \cdot) - E_y^h(\tau, \cdot)\|_{L^\infty(\mathbb{R})}) \\ & + \|B_z(\tau, \cdot) - B_z^h(\tau, \cdot)\|_{L^\infty(\mathbb{R})} \leq C(t)(\epsilon + \frac{\beta^2}{\epsilon}), \end{aligned}$$

$\forall 0 \leq t \leq T_{\epsilon, \beta}$. Moreover, $T_{\epsilon, \beta} \rightarrow \infty$ when $\epsilon \rightarrow 0^+, \beta < C_1 \epsilon$.

2.3.2 Semi-Lagrangian methods

Semi-Lagrangian methods, as already said, are a lot more recent than particle ones. Few rigorous mathematical results of convergence analysis of semi-Lagrangian methods have been stated. Although interesting a priori estimates have been pointed out in [6, 7, 34], a lot of work still remains in order to give complete and rigorous results in more general situations. The most difficult step in the convergence analysis of semi-Lagrangian methods is to obtain a stability result for the interpolation operators. If stability results in the L^∞ norm seem out of reach for high order interpolation operators because of the Runge phenomena (artificial oscillations, which amplitude increases with the degree of the polynomial in the case of Lagrange interpolation appear at the edges of finite elements). A more appropriate mathematical framework is L^2 stability. If Fourier analysis tools as Fourier series are useful for proving L^2 stability in the case of grids, convenient mathematical tools are lacking for unstructured meshes such as triangulation and have to be developed in the future. Nevertheless results on the convergence analysis of classes of high order algorithms for the 1D Vlasov-Poisson problem have been done by Besse [8, 9, 10, 11]. Mehrenberger and Campos-Pinto extended the result to adaptative schemes in [18].

As an example, we will give one of the latest theorem found in [11]. They solve the periodical case. The distribution function and the field are supposed periodical in x , and compactly supported in v . Moreover a splitting method is used. Their theorem writes:

Theorem 7 (Besse-Mehrenberger). *Assume that $f_0 \in W_{c,per_x}^{m+1,\infty}(\mathbb{R}_x \times \mathbb{R}_v)$, positive, periodic with respect to the variable x of period L , and compactly supported in velocity. In addition, we assume that the interpolation operator R_h satisfies:*

- *Consistency and high order accuracy: Let m, p and k be some integers such that $m \geq 0$, $1 \leq p \leq \infty$, and $0 \leq k \leq 1$, then the following interpolation error estimates holds:*

$$\|f - R_h f\|_{W^{k,p}(\Omega)} \leq Ch^{m+1-k} \|f\|_{W^{m+1,p}(\Omega)}, \forall f \in W^{m+1,p}(\Omega) \cap Per(\Omega).$$

- *Stability: Let f belong to $C(\Omega) \cap P(\Omega)$, then we have:*

$$c \|f\|_{L_h^2(\Omega)} \leq \|R_h f\|_{L^2(\Omega)} \leq C \|f\|_{L_h^2(\Omega)},$$

with c and C independent of h , $\|R_h f\|_{L_h^2, \Delta_h^{0,\beta}} \leq \|f\|_{L_h^2(\Omega)}$, $\|R_h f\|_{L_h^2, \Delta_h^{\alpha,0}} \leq \|f\|_{L_h^2(\Omega)}$.

Then, the numerical solution of the Vlasov-Poisson system (f_h, E_h) converges towards the solution (f, E) of the periodical Vlasov-Poisson system, and there exists a constant

$$C = C(\|f\|_{W^{2,\infty}(0,T;W^{m+1,\infty}(\Omega))})$$

independent of Δt and h such that:

$$\|f - f_h\|_{l^\infty(0,T;L^2(\Omega))} + \|E - E_h\|_{l^\infty(0,T;L^\infty([0,L]))} \leq C(\Delta t^2 + h^{m+1} + \frac{h^{m+1}}{\Delta t}).$$

A work on another model should not be forgotten, the result by Bostan and Crouseilles in 2008, [16] about the 1D Vlasov-Maxwell relativistic and quasi relativistic model. These models have also been theoretically studied in [19, 17]

2.4 Numerical charge conservation

It was seen that the numerical solutions of Ampère and Faraday automatically check the discrete electric and magnetic divergence conditions if:

- The discrete operators check $div_h rot_h = 0$,
- The initial data satisfy $div_h(E_0) = \frac{\rho^{(\cdot,0)}}{\epsilon_0}$ and $div_h B_0 = 0$,
- The discrete charge conservation is checked.

It has to be noticed that the discrete charge conservation depends on the numerical scheme computed. We will only give the finite difference examples derived from Yee, in one and two dimensions:

$$\frac{\rho_i^{n+1} - \rho_i^n}{\Delta t} + \frac{J_{i+\frac{1}{2}}^{n+\frac{1}{2}} - J_{i-\frac{1}{2}}^{n+\frac{1}{2}}}{\Delta x} = 0,$$

in one dimension and

$$\frac{\rho_{i,j}^{n+1} - \rho_{i,j}^n}{\Delta t} + \frac{J_{i+\frac{1}{2},j}^{n+\frac{1}{2}} - J_{i-\frac{1}{2},j}^{n+\frac{1}{2}}}{\Delta x} + \frac{J_{i,j+\frac{1}{2}}^{n+\frac{1}{2}} - J_{i,j-\frac{1}{2}}^{n+\frac{1}{2}}}{\Delta y} = 0.$$

in two dimensions.

Unfortunately, the described classical numerical methods do not automatically verify this charge equation. The numerical solution of Ampère and Faraday is not solution of the Maxwell's system: the electric divergence constraint is not satisfied. That means that in numerical simulations, unphysical solutions might appear if the problem is not solved.

Two main issues have been explored in the literature, mainly in the PIC context.

The first one is to modify the Maxwell's equations in order to link the Ampère's equation to the electric field divergence constraint. This will be called correction methods. There are different kind of corrections. We can cite the one of Boris [12, 15]. It consists in correcting at each time step the computed electric field thanks to a potential in order to enforce Gauss' law to be verified. This method is very efficient, and is widely used, nevertheless, it is necessary in this method to solve a Laplacian problem at each time step, which is numerically very expensive. We can also cite the Marder/Langdon correction. In 1987 Marder (see [47]) introduced a pseudo-current in the Ampère's equation, and Langdon in 1989 (see [46]) proposed an amelioration taking into account the Gauss' law. In this paper he also showed that his method is equivalent to making an iteration of the Jacobi's algorithm in order to invert the Laplacian in the correction of Boris. A good overview of the different correction methods can be found in the PhD thesis of Barthelmé [3]. Other interesting papers about charge conservation issues about the Maxwell's equation are the ones of Munz et al. ([51, 52]).

The other way of tackling the problem is to compute charge and current densities which automatically verify the discrete charge conservation equation. The first ones who managed to do that were Villasenor and Buneman [73]. Their method consists in linearly approximating the trajectories of the particles over each time step, and counting how many frontiers the particle

is crossing in order to be able to compute the current properly. Their result is done for uniform mesh and for B-splines of degree 0. Their method is generalized in [3] to non uniform mesh and to higher orders, and compared to the one of Esirkepov in 2001 [33] which splits the particles trajectories following the coordinate axis, and can be derived with any form function. Barthelmé also compared these methods to a more recent "zigzag" method introduced by Umeda et al. [69] for an interpolation of ρ of degree one. In this method, the particle trajectories are approached by piecewise linear trajectories over each time step. It was created in order to simplify the implementation and to speed up computational time.

We shall not forget to speak about the work of Eastwood in 1990 [32], who proposed different current conserving particle-mesh algorithms for solving the coupled relativistic Vlasov-Maxwell set of equations, using finite elements in both space and time.

More recently, Sircombe and Arber were the first to find a way to preserve charge in a semi-Lagrangian scheme. Their method is quite natural since they take full benefits from conservative semi-Lagrangian methods in the VALIS code. For details, see [65].

The work developed further tries to use the fact that forward semi-Lagrangian methods have lot in common with a PIC method, which shall be used in this work.

Bibliography

- [1] M. AINSWORTH, J. COYLE, *Hierarchical hp-edge element families for Maxwell's equations on hybrid quadrilateral/triangular meshes*, Comp. Meth. Appl. Mech. Engng, **190**, pp. 6709–6733, (2001).
- [2] F. ASSOUS, P. CIARLET, *Modèles et méthodes pour les équations de Maxwell*, Rapport de recherche ENSTA 347 (2001).
- [3] R. BARTHELMÉ, *Le problème de conservation de la charge dans le couplage des équations de Vlasov et de Maxwell*, Thèse de l'Université Louis Pasteur, 2005.
- [4] F. ASSOUS, P. DEGOND, E. HEINTZE, P.A RAVIART, J. SEGRÉ, *On a finite-element Method for solving the three-dimensionnal Maxwell equations*, J. Comput. Physics, **109**, pp. 222–237, (1993).
- [5] H. BARUCQ, *Etude asymptotique du système de Maxwell avec conditions aux limites absorbantes*, Thèse de l'université de Bordeaux I (1993).
- [6] R. BERMEJO, *Analysis of an algorithm for the Galerkin-characteristic method*, Numer. Math., **60**, pp. 163–194, (1991).
- [7] R. BERMEJO, *Analysis of a class of quasi-monotone and conservative semi-Lagrangian advection schemes*, Numer. Math., **87**, pp. 597–623 (2001).
- [8] N. BESSE, *Etude mathématique et numérique de l'équation de Vlasov non linéaire sur des maillages non structurés de l'espace des phases*, Ph.D. thesis, Institut de Recherche Mathématique Avancée, Université Louis Pasteur, Strasbourg, France, (2003).
- [9] N. BESSE, *Convergence of a semi-Lagrangian scheme for the one-dimensional Vlasov-Poisson system* SIAM J. Numer. Anal, **42** no1, pp. 350-382 (2004).
- [10] N. BESSE, *Convergence of a High Order semi-Lagrangian Scheme with Propagation of Gradients for the Vlasov-Poisson System*, SIAM J. Numer. Anal, **46** no2, pp. 639-670, (2009).
- [11] N. BESSE, M. MEHRENBERGER, *Convergence of classes of high order semi-Lagrangian schemes for the Vlasov-Poisson system*, Math. Comput., **77**, pp. 93-123, (2008).
- [12] C. K. BIRDSALL, A. B. LANGDON, *Plasma physics via computer simulation*, Institute of Physics, Bristol (1991).

- [13] B. BIDÉGARRAY, J.M. GHIDAGLIA, *Multidimensional corrections to cell-centered finite volume methods for Maxwell equations*, Appl. Num. Maths, **44**, pp. 281–298, (2003).
- [14] J.-P. BORIS, D.L. BOOK, *Solution of continuity equations by the method of flux-corrected transport*, J. Comput. Phys. **20**, pp. 397-431, (1976).
- [15] J. P. BORIS, *Relativistic plasma simulations - Optimization of a hybrid code*, Proc. 4th Conf. Num. Sim. of Plasmas (NRL Washington, Washington DC, 1970) pp. 3-67.
- [16] M. BOSTAN, N. CROUSEILLES, *Convergence of a semi-Lagrangian scheme for the reduced Vlasov-Maxwell system for laser-plasma interaction*, Numer. Math. **112**, no2, pp. 169-195, (2009).
- [17] M. BOSTAN, *Mild solutions for the relativistic Vlasov-Maxwell system for laser-plasma interaction*, Quart. Appl. **LXV**, pp. 163-187 (2007).
- [18] M. CAMPOS-PINTO, M. MEHREBERGER *Convergence of an adaptive scheme for the one-dimensional Vlasov-Poisson system*, Numer. Math. **108**, no3, pp. 407-444, (2008).
- [19] CARILLO, S. LABRUNIE, *Global solutions for the one-dimensional Vlasov-Maxwell system for laser-plasma interaction*, Math. Models Methods Appl. Sci. **16**, pp. 19-57, (2006).
- [20] C. Z. CHENG, G. KNORR, *The integration of the Vlasov equation in configuration space*, J. Comput. Phys, **22**, pp. 330-3351, (1976).
- [21] G. COHEN, X. FERRIÈRES, S. PERNET, *A spatial high-order hexahedral discontinuous Galerkin method to solve Maxwell's equations in time domain*, J. Comput. Phys., **217**, Issue 2, pp. 340-363, (2006).
- [22] G. COHEN, P. JOLY, *Construction Analysis of Fourth-Order Finite Difference Schemes for the Acoustic Wave Equation in Nonhomogeneous Media*, SIAM J. Num. Anal., **33**, pp. 1266–1302, (1996).
- [23] P. COLELLA, P.R. WOODWARD, *The Piecewise Parabolic Method (PPM) for gas-dynamical simulations*, J. Comput. Phys. **54** (1984) 174–201.
- [24] P. COLELLA, M. D. SEKORA, *A limiter for PPM that preserves accuracy at smooth extrema*, J. Comput. Phys., **227**, 7069-7076, (2008).
- [25] C.J. COTTER, J. FRANK, S. REICH *The remapped particle-mesh semi-Lagrangian advection scheme*, Q. J. Meteorol. Soc., **133**, pp. 251-260, (2007).
- [26] G. COHEN, B. PERTHAME, *Optimal approximations of transport equations by particle and pseudoparticle methods*, SIAM J. Num. Anal., **32**, Issue 3, pp. 616-636 (2000).
- [27] G.-H COTTET, P.-A RAVIART, *Particle methods for the one-dimensional Vlasov-Poisson equations*, Siam J. Num. Anal. **21**, pp. 52-75, (1984).
- [28] N. CROUSEILLES, M. MEHREBERGER, E. SONNEDRÜCKER, *Conservative semi-Lagrangian schemes for the Vlasov equation*, J. Comp. Phys., **229**, no6, pp. 1927-1953 (2010).

- [29] R. DAUTRAY, J.L. LIONS *Analyse mathématique et calcul numérique pour les sciences et les techniques*, Volume 8, Masson, Paris (1988).
- [30] L. DEMKOWICZ, L. VARDAPETYAN, *Modeling of electromagnetic absorption/scattering problems using hp-adaptive finite elements*, *Comp. Meth. in Appl. Mech. and Eng.*, **152**, pp. 103–124, (1998).
- [31] A. DITKOWSKI, K. DRIDI, J.S. HESTHAVEN, *Convergent Cartesian Grid Methods for Maxwell's Equations in Complex Geometries*, *J. Comput. Phys.*, **170**, pp. 39–80, (2001).
- [32] J.W. EASTWOOD, *Virtual particle methods*, *Comp. Phys. Comm.*, **64**, Issue 2, pp. 252-266, (1991).
- [33] T. ZH. ESIRKEPOV, *Exact charge conservation scheme for Particle-in-Cell simulation with an arbitrary form-factor*, *Comp. Phys. Comm.* **135**, pp. 144-153, (2001).
- [34] M. FALCONE, R. FERRETTI, *Convergence analysis for a class of high-order semi-Lagrangian advection schemes*, *SIAM J. Numer. Anal.*, **35**, pp. 909–940, (1998).
- [35] M. R. FEIX, P. BERTRAND, AND A. GHIZZO, *Eulerian codes for the Vlasov equation*, *Series on Advances in Math. for Appl. Sci.* **22**. *Kinetic Theory and Computing*, edited by B. Perthame (1994).
- [36] F. FILBET, E. SONNENDRÜCKER, P. BERTRAND, *Conservative numerical schemes for the Vlasov equation*, *J. Comput. Phys.* **172**, pp. 166-187, (2001).
- [37] F. FILBET, E. SONNENDRÜCKER, *Comparison of Eulerian Vlasov solvers*, *Comput. Phys. Comm.*, **151**, pp. 247-266, (2003).
- [38] F. FILBET, *Convergence of a finite volume scheme for the Vlasov–Poisson system*, *SIAM J. Numer. Anal.*, **39**, pp. 1146–1169, (2001).
- [39] K. GANGULY, H.D. VICTORY JR., *On the convergence of particle methods for multidimensional Vlasov-Poisson systems*, *SIAM J. Numer. Anal.*, **26**, pp. 249-288, (1989).
- [40] K. GANGULY, J. T. LEE, H. D. VICTORY JR., *On simulation methods for Vlasov-Poisson systems with particles initially asymptotically distributed*, *SIAM J. Numer. Anal.*, **28**, pp. 1574-1609, (1991).
- [41] A. GHIZZO, P. BERTRAND, M. SHOUCRI, T. W. JOHNSTON, E. FILJAKOW, AND M. R. FEIX, *A Vlasov code for the numerical simulation of stimulated Raman scattering*, *J. Comput. Phys.* **90**, 431 (1990).
- [42] A. GHIZZO, P. BERTRAND, M. L. BEGUE, T. W. JOHNSTON, AND M. SHOUCRI, *A Hilbert–Vlasov code for the study of high-frequency plasma beatwave accelerator*, *IEEE Trans. Plasma Sci.* **24**, 370 (1996).
- [43] R. GLASSEY, J. SCHAEFFER, *Convergence of a particle method for the relativistic Vlasov-Maxwell system*, *SIAM J. Numer. Anal.*, **28**. No1, pp. 1-25, (1991).

- [44] F. HERMELINE, *Two Coupled Particle-Finite Volume Methods Using Delaunay-Voronoi Meshes for the Approximation of Vlasov-Poisson and Vlasov-Maxwell Equations*, J. Comput. Phys., **106**, pp. 1–18, (1993).
- [45] R.W. HOCKNEY, J.W. EASTWOOD, *Computer Simulation Using Particles*, Taylor and Francis, (1989).
- [46] A. B. LANGDON, *On enforcing Gauss' law in electromagnetic particle-in-cell codes*, Comp. Phys. Comm. **70**, pp. 447-450, (1992).
- [47] B. MARDER, *A method for incorporating Gauss's law into electromagnetic PIC codes*, J. Comput. Phys. **68**, pp. 48-55, (1987).
- [48] MICROWAVE STUDIO, Computer Simulation Technology.
- [49] G. COHEN, P. MONK, *Mur-Nedelec finite element schemes for Maxwell's equations*, Comp. Meth. in Appl. Mech. Eng., **169**, 197–217, (1999).
- [50] C.-D. MUNZ, P. OMNES, R. SCHNEIDER, *A three-dimensional finite-volume solver for the Maxwell equations with divergence cleaning on unstructured meshes*, Comp. Phys. Comm., **130**, pp. 83–117, (2000).
- [51] C.-D. MUNZ, P. OMNES, R. SCHNEIDER, E. SONNENDRÜCKER, U. VOSS, *Divergence Correction Techniques for Maxwell Solvers Based on a Hyperbolic Model*, J. Comput. Phys., **161**, Issue 2, pp. 484-511, (2000).
- [52] C-D. MUNZ, R. SCHNEIDER, E. SONNENDRÜCKER, U. VOSS, *Maxwell's equations when the charge conservation is not satisfied*, Comptes Rendus de l'Académie des Sciences - Series I - Mathematics **328**, Issue 5, pp. 431-436, (1999).
- [53] T. NAKAMURA, R. TANAKA, T. YABE, K. TAKIZAWA, *Exactly conservative semi-Lagrangian scheme for multi-dimensional hyperbolic equations with directional splitting technique*, J. Comput. Phys., **174**, pp. 171-207, (2001).
- [54] T.NAKAMURA, T.YABE, *Cubic Interpolated Propagation Scheme for Solving the Hyper-Dimensional Vlasov-Poisson Equation in Phase Space*, Comput. Phys. Comm., **120**, pp.122-154 (1999).
- [55] J-C. NÉDELEC, *Mixed finite elements in \mathbb{R}^3* , Numer. Math., **35**, pp. 315–341, (1980).
- [56] H. NEUNZERT, J. WICK, *Theoretische und numerische Ergebnisse zur nicht linearen Vlasov-Gleichung*, in *Numerische Lösung nichtlinearen partiellen Differential - unnr Integro differential gleichungen*, Lecture Notes in Math. **267**, Springer Verlag, New Tork, Berlin (1972).
- [57] H. NEUNZERT, J. WICK, *Die Theorie der Asymptotischen Verteilung une dir Numerische Lösung von Integrodifferentialgleichungen*, Numer. Math., **21**, pp. 234-243, (1973).

- [58] N. CANOUE, L. FEZOU, S. PIPERNO, *3D Maxwell's equations and orthogonal nonconforming meshes: a hp-type Discontinuous Galerkin method*, Research report INRIA-4912, (2003).
- [59] W. RACHOWICZ, L. DEMKOWICZ, *An hp-adaptive finite element method for electromagnetics: Part 1: Data structure and constrained approximation*, Comp. Meth. in Appl. Mech. and Engi., **187**, pp. 307–335, (2000).
- [60] P.A. RAVIART, *An analysis of particle methods*, Numer. Meth. in Fluids Dyn., Lecture Notes in Math. **1127**, Springer Verlag, Berlin, New York, pp. 243-324, (1985).
- [61] S. REICH, *An explicit and conservative remapping strategy for semi-Lagrangian advection*, Atmospheric Science Letters **8**, pp. 58-63, (2007).
- [62] M. REMAKI, *Méthodes numériques pour les équations de Maxwell instationnaires en milieu hétérogène*, Thèse Mathématiques Appliquées, CERMICS, Ponts et Chaussées, 178pp, (1999).
- [63] J. SCHAEFFER, *Discrete approximation of the Vlasov-Poisson system*, Quart. Appl. Math., **45**, pp. 59-73, (1987).
- [64] J. SCHOBEL, S. ZAGLMAYR, *High Order Nedelec Elements with local complete sequence properties*, Int. J for Computation and Maths in Electrical and Electronic Eng COMPEL, (2005).
- [65] N.J. SIRCOMBE, T.D. ARBER, *VALIS: A split-conservative scheme for the relativistic 2D*; J. Comput. Phys., **228**, pp. 4773-4788.
- [66] E. SONNENDRÜCKER, J. ROCHE, P. BERTRAND, A. GHIZZO *The semi-Lagrangian method for the numerical resolution of the Vlasov equation*, J. Comput. Phys., **149**, pp. 201-220, (1999).
- [67] E. SONNENDRÜCKER, P. NAVARO, *Développement du code Maxwell-Vlasov PIC parallèle Brennus: Mise en œuvre d'un solveur Maxwell 2D par la méthode de Galerkin Discontinu*, rapport CEA, (2006).
- [68] A. TAFLOVE, *Computational Electrodynamics: The Finite-Difference Time-Domain Method*, Norwood, MA: Artech House, (1995).
- [69] T. UMEDA, Y. OMURA, T. TOMINAGA, H. MATSUMOTO, *A new charge conservation method in electromagnetic particle-in-cell simulations*, Comp. Phys. Comm **156**, Issue1, pp. 73-85, (2003).
- [70] T. UMEDA, M. ASHOUR-ABDALLA, D. SCHRIVER, *Comparison of numerical interpolation schemes for one-dimensional electrostatic Vlasov code*, J. Plasma Phys., **72**, pp. 1057-1060, (2006).
- [71] H.D. VICTORY JR., E. J. ALLEN, *The convergence theory of particle-in-cell for multidimensional Vlasov-Poisson systems*, SIAM J. Numer. Anal., **28** No. 5, pp. 1207-1241, (1991).

- [72] H.D. VICTORY JR., E. J. ALLEN, *The convergence analysis of fully discretized particle methods for solving Vlasov-Poisson systems*, SIAM J. Numer. Anal., **28** No. 4, pp. 955-989, (1991).
- [73] J. VILLASENOR, O. BUNEMAN, *Rigorous charge conservation for local electromagnetic field solvers*, Comp. Phys. Comm. **69**, pp. 306-316, (1992).
- [74] S. WOLLMAN, E. OZIZMIR, *Numerical approximation of the one-dimensional Vlasov-Poisson system with periodic boundary conditions*, SIAM J. Numer. Anal., **33**, pp. 1377-1409, (1996).
- [75] S. WOLLMAN *On the approximation of the Vlasov-Poisson system by particle methods* SIAM J. Numer. Anal., **37**, pp. 1369-1398, (2000).
- [76] K.S. YEE , *Numerical solution of initial boundary value problems involving Maxwell's equations in isotropic media*, IEEE Trans. Antennas Propag., **14**, pp. 302–307, (1966).
- [77] M. ZERROUKAT, N. WOOD, A. STANIFORTH, *A monotonic and positive-definite filter for a Semi-Lagrangian Inherently Conserving and Efficient (SLICE) scheme*, Q.J.R. Meteorol. Soc., **131**, pp 2923-2936, (2005).
- [78] M. ZERROUKAT, N. WOOD, A. STANIFORTH, *The Parabolic Spline Method (PSM) for conservative transport problems*, Int. J. Numer. Meth. Fluids, **51**, pp. 1297-1318, (2006).

A forward semi-Lagrangian method for the numerical solution of the Vlasov equation

3.1 Introduction

Understanding the dynamics of charged particles in a plasma is of great importance for a large variety of physical phenomena, such as the confinement of strongly magnetized plasmas, or laser-plasma interaction problems for example. Thanks to recent developments in computational science and in numerical methods, meaningful comparisons between experience and numerics become possible.

An accurate model for the motion of charged particles, is given by the Vlasov equation. It is based on a phase space description so that non-equilibrium dynamics can be accurately investigated. The unknown $f(t, x, v)$ depends on the time t , the space x and the velocity v . The electromagnetic fields are computed self-consistently through the Maxwell or Poisson equations, which leads to the nonlinear Vlasov-Maxwell or Vlasov-Poisson system.

The numerical solution of such systems is most of the time performed using Particle In Cell (PIC) methods, in which the plasma is approximated by macro-particles (see [5]). They are advanced in time with the electromagnetic fields which are computed on a grid. However, despite their capability to treat complex problems, PIC methods are inherently noisy, which becomes problematic when low density or highly turbulent regions are studied. Hence, numerical methods which discretize the Vlasov equation on a grid of the phase space can offer a good alternative to PIC methods (see [8, 12, 13, 30, 7]). The so-called Eulerian methods can deal with strongly nonlinear processes without additional complexity, and are well suited for parallel computation (see [16]). Moreover, semi-Lagrangian methods which have first been introduced in meteorology (see [29, 33, 34]), try to take advantage of both Lagrangian and Eulerian approaches. Indeed, they allow a relatively accurate description of the phase space using a fixed mesh and avoid traditional step size restriction using the invariance of the distribution function along the

trajectories. Standard semi-Lagrangian methods calculate departure points of the characteristics ending at the grid point backward in time; an interpolation step enables to update the unknown.

In this work, we consider the numerical solution of the two-dimensional Vlasov equation on a mesh of the phase space using a forward semi-Lagrangian numerical scheme. In the present method, the characteristic curves are advanced in time and a deposition procedure on the phase space grid, similar to the procedure used in PIC methods for the configuration space only, enables to update the distribution function.

With Backward semi-Lagrangian methods (BSL), a leap-frog algorithm is usually performed. An important problem with non split Backward semi-Lagrangian (BSL) solvers is that they generally rely on a leap-frog algorithm which consists in updating f^{n+1} from f^{n-1} and storing two distribution functions at successive times. This procedure enables to regain second order accuracy but the two distribution functions can deviate for long time simulations. Moreover, the fields have to be computed iteratively, with Newton fixed point methods, or prediction correction algorithms. This is due to an implicit way of solving the characteristics (see [30] for details). This strategy makes high order methods quite difficult and expensive. Making the problem explicit enables to get rid of the two drawbacks and to use for example high order Runge Kutta methods more easily. This is one of the main advantages of the present Forward semi-Lagrangian (FSL) method. Once the new position of the particles computed, a remapping (or a deposition) step has to be performed. This issue is achieved using cubic spline polynomials which deposit the contribution of the Lagrangian particles on the uniform Eulerian mesh. This step is similar to the deposition step which occurs in PIC codes but in our case, the deposition is performed in the whole phase space grid. Similarities can also be found in strategies developed in [9, 20, 22] for meteorology applications.

In order to take benefit from the advantages of PIC and semi-Lagrangian methods, and since the two methods (PIC and FSL) really look like each other, except the deposition step, we have also developed a hybrid method, where the deposition step is not performed at each time step, but every T time steps. During the other time steps, the fields are computed directly at the new position of the particles. It shall be noticed that however the present method is not a real PIC method, since the particle weights are not constant. Indeed, in this method based on a description of the unknown using cubic spline polynomials, the spline coefficients play the role of the particle weights, and are updated at each time step. This kind of hybrid approach has been developed recently in a slightly different framework in [31] inspired by [10, 23]. Applications can also be found in [2, 28].

This paper is organized as follows. In the next section, the two Vlasov equations which will be dealt with are presented. Then, we shall introduce the Forward semi-Lagrangian (FSL) method, always regarding it comparatively to Backward semi-Lagrangian (BSL) methods. Afterward, numerical results for several test cases are shown and discussed. Eventually, some specific details are given in two appendices, one for the computation of an exact solution to the Landau damping problem, another about the solution of the Poisson's equation for the Guiding-Center model.

3.2 Models in plasma physics

In this section, we briefly present two typical reduced models from plasma physics for the description of the time evolution of charged particles. These two-dimensional models are relevant for more complex problems we are interested in and shall be used to validate our new method.

3.2.1 Vlasov-Poisson model

We consider here the classical 1D Vlasov-Poisson model, the unknown of which $f = f(t, x, v)$ is the electron distribution function. It depends on the space variable $x \in [0, L]$ where $L > 0$ is the size of the domain, the velocity variable $v \in \mathbb{R}$ and the time $t \geq 0$. The Vlasov equation which translates the invariance of the distribution function along the characteristics then writes

$$\frac{\partial f}{\partial t} + v \partial_x f + E(t, x) \partial_v f = 0, \quad (3.1)$$

with a given initial condition $f(0, x, v) = f_0(x, v)$. The self-consistent electric field $E(t, x)$ is computed thanks to the distribution function f

$$\partial_x E(t, x) = \int_{\mathbb{R}} f(t, x, v) dv - \rho_i, \quad \int_0^L E(t, x) dx = 0, \quad (3.2)$$

where ρ_i denotes the ion density which forms a uniform and motionless background in the plasma.

The Vlasov-Poisson model constitutes a nonlinear self-consistent system as the electric field determines f with (3.1) and is in turn determined by it in (3.2). It presents several conserved quantities as the total number of particles, the L^p norms ($p \geq 1$) defined by $\|f\|_{L^p} = (\iint |f|^p dx dv)^{1/p}$, the momentum and the total energy, as follows:

$$\begin{aligned} \frac{d}{dt} \iint f(t, x, v) dx dv &= \frac{d}{dt} \|f(t)\|_{L^1} = \frac{d}{dt} \iint v f(t, x, v) dx dv \\ &= \frac{d}{dt} \left[\iint v^2 f(t, x, v) dx dv + \int E(t, x)^2 dx dv \right] \\ &= 0. \end{aligned}$$

One of the main features of the present work is to develop accurate numerical methods which are able to preserve these conserved quantities exactly or approximately for long times.

3.2.2 Guiding-center model

We are also interested in other kinds of Vlasov equations. For instance, in the guiding-center approximation. Charged particles in magnetized tokamak plasmas can be modeled by the density $f = f(t, x, y)$ in the 2 dimensional poloidal plane by

$$\frac{\partial f}{\partial t} + E^\perp(x, y) \cdot \nabla_{(x,y)} f = 0, \quad (3.3)$$

coupled self-consistently to Poisson's equation for the electric field which derives from a potential $\Phi = \Phi(x, y)$

$$-\Delta\Phi(t, x, y) = f(t, x, y), \quad E(t, x, y) = -\nabla\Phi(t, x, y). \quad (3.4)$$

In equation (3.3), the advection term $E^\perp = (E_y, -E_x)$ depends on (x, y) and the time-splitting cannot be simply applied like in the Vlasov-Poisson case. Hence, this simple model appears to be interesting in order to test numerical methods.

The guiding-center model (3.3)-(3.4) also presents conserved quantities as the total number of particles and L^2 norm of f (enstrophy) and E (energy)

$$\frac{d}{dt} \iint f(t, x, y) dx dy = \frac{d\|f(t)\|_{L^2}^2}{dt} = \frac{d\|E(t)\|_{L^2}^2}{dt} = 0. \quad (3.5)$$

3.2.3 Characteristic curves

We can re-write Vlasov equations in a more general context by introducing the characteristic curves

$$\frac{dX}{dt} = U(X(t), t). \quad (3.6)$$

Let us introduce $X(t, x, s)$ as the solution of this dynamical system, at time t which value is x at time s . These are called the characteristics of the equation. With $X(t)$ a solution of (3.6), we obtain:

$$\frac{d}{dt}(f(X(t), t)) = \frac{\partial f}{\partial t} + \frac{dX}{dt} \cdot \nabla_X f = \frac{\partial f}{\partial t} + U(X(t), t) \cdot \nabla_X f = 0. \quad (3.7)$$

which means that f is constant along the characteristics. Using the notations of [30] $X(t; x, s)$ which the characteristic at time t which was in the phase space position x at time s , it can be written

$$f(X(t; x, s), t) = f(X(s; x, s), s) = f(x, s)$$

for any times t and s , and any phase space coordinate x . This is the key property used to define semi-Lagrangian methods for the solution of a discrete problem.

3.3 The forward semi-Lagrangian method

In this section, we present the different stages of the forward semi-Lagrangian method (FSL) and try to emphasize the differences with the traditional backward semi-Lagrangian method (BSL).

3.3.1 General algorithm

Let us consider a grid of the studied space (possibly phase-space) with N_x and N_y the number of points in the x direction $[0, L_x]$ and in the y direction $[0, L_y]$. We then define

$$\Delta x = L_x/N_x, \quad \Delta y = L_y/N_y, \quad x_i = i\Delta x, \quad y_j = j\Delta y,$$

for $i = 0, \dots, N_x$ and $j = 0, \dots, N_y$. One important point of the present method is the definition of the approximate distribution functions which are projected on a cubic B-splines basis:

$$f(t, x, y) = \sum_{k,l} \omega_{k,l}^n S(x - X_1(t; x_k, y_l, t^n)) S(y - X_2(t; x_k, y_l, t^n)), \quad (3.8)$$

where $X(t; x_k, y_l, t^n) = (X_1, X_2)(t; x_k, y_l, t^n)$ corresponds to the solution of the characteristics at time t (of the two dimensional system (3.6)) whose value at time t^n was the grid point (x_k, y_l) . The cubic B-spline S is defined as follows

$$6S(x) = \begin{cases} (2 - |x|/\Delta x)^3 & \text{if } \Delta x \leq |x| \leq 2\Delta x, \\ 4 - 6(x/\Delta x)^2 + 3(|x|/\Delta x)^3 & \text{if } 0 \leq |x| \leq \Delta x, \\ 0 & \text{otherwise.} \end{cases}$$

In the expression (3.8), the weight $w_{k,l}^n$ is associated to the particle located at the grid point (x_k, y_l) at time t^n ; it corresponds to the coefficient of the cubic spline determined by the following interpolation conditions

$$\begin{aligned} f(t^n, x_i, y_j) &= \sum_{k,l} \omega_{k,l}^n S(x_i - X_1(t^n; x_k, y_l, t^n)) S(y_j - X_2(t^n; x_k, y_l, t^n)) \\ &= \sum_{k,l} \omega_{k,l}^n S(x_i - x_k) S(y_j - y_l). \end{aligned}$$

Adding boundary conditions (for example the value of the normal derivative of f at the boundaries, we obtain a set of linear systems in each direction from which the weights $\omega_{k,l}^n$ can be computed as in [30, 16]).

We can now express the full algorithm for the forward semi-Lagrangian method

- Step 0: Initialize $f_{i,j}^0 = f_0(x_i, y_j)$
- Step 1: Compute the cubic splines coefficients $\omega_{k,l}^0$ such that

$$f_{i,j}^0 = \sum_{k,l} \omega_{k,l}^0 S(x_i - x_k) S(y_j - y_l),$$

- Step 2: Integrate (3.6) from t^n to t^{n+1} , given as initial data the grid points $X(t^n) = (x_k, y_l)$ to get $X(t; x_k, y_l, t^n)$ for $t \in [t^n, t^{n+1}]$, assuming the advection velocity U is known. We shall explain in the sequel how it is computed for our typical examples.
- Step 3: Project on the phase space grid using (3.8) with $t = t^{n+1}$ to get $f_{i,j}^{n+1} = f^{n+1}(x_i, y_j)$
- Step 4: Compute the cubic spline coefficients $\omega_{k,l}^{n+1}$ such that

$$f_{i,j}^{n+1} = \sum_{k,l} \omega_{k,l}^{n+1} S(x_i - x_k) S(y_j - y_l).$$

- Go to Step 2 for the next time step.

3.3.2 FSL: An explicit solution of the characteristics

For BSL, especially for the solution of the characteristics, it is possible to choose algorithms based on two time steps with field estimations at intermediate times. Generally, you have to use a fixed-point algorithm, a Newton-Raphson method (see [30]), a prediction correction one or also Taylor expansions (see [16]) in order to find the foot of the characteristics. This step of the global algorithm costs a lot (see [30]). It is no longer needed in FSL, where the starting point of the characteristics is known so that traditional methods to solve ODEs, like Runge-Kutta algorithms can be incorporated to achieve high order accuracy in time. Let us show the details of this explicit solution of the characteristics, in Vlasov-Poisson and Guiding-Center models.

In both cases, the dynamical system (3.6) has to be solved. With FSL, $X(t^n)$, $U(X(t^n), t^n)$ are known. You can choose your favorite way of solving this system on each time step, since the initial conditions are explicit. This leads to the knowledge of $X(t^{n+1})$ and $U(X(t^{n+1}), t^{n+1})$ so that Step 2 of the previous global algorithm is completed.

As examples of forward solvers for the characteristic curves, the second-order Verlet algorithm, Runge-Kutta 2 and Runge-Kutta 4 will be proposed for Vlasov-Poisson, and, as Verlet cannot be applied, only Runge-Kutta 2 and 4 will be used for the Guiding-Center model.

For Vlasov-Poisson, we denote by $X(t^n) = (X_1(t^n), X_2(t^n)) = (x^n, v^n)$ the mesh of the phase space, and $U(X(t^n), t^n) = (v^n, E(x^n, t^n))$ the advection velocity. The Verlet algorithm can be written

- Step 1: $\forall k, l, v_{k,l}^{n+\frac{1}{2}} - v_l^n = \frac{\Delta t}{2} E(x_k^n, t^n)$,
- Step 2: $\forall k, l, x_{k,l}^{n+1} - x_k^n = \Delta t v_{k,l}^{n+\frac{1}{2}}$,
- Step 3: compute the electric field at time t^{n+1}
 - deposition of the particles $x_{k,l}^{n+1}$ on the spatial grid x_i for the density ρ : $\rho(x_i, t^{n+1}) = \sum_{k,l} \omega_{k,l}^n S(x_i - x_{k,l}^{n+1})$, like in a PIC method.
 - solve the Poisson equation on the grid x_i : $E(x_i, t^{n+1})$.
- Step 4: $\forall k, l, v_{k,l}^{n+1} - v_{k,l}^{n+\frac{1}{2}} = \frac{\Delta t}{2} E(x_{k,l}^{n+1}, t^{n+1})$.

Let us remark that the particles (which are in our case the grid points) move in the two-dimensional phase space; hence a double index (k, l) is necessary to denote the position and the velocity of the particles.

A second or fourth order Runge-Kutta algorithm can also be used to solve the characteristic curves of the Vlasov-Poisson system forward in time. The fourth order Runge-Kutta algorithm needs to compute intermediate values in time of the density and the electric field. Let us detail the algorithm omitting the indices k, l for the sake of simplicity

- Step 1: $k_1 = (v^n, E(x^n, t^n)) = (k_1(1), k_1(2))$,
- Step 2: compute the electric field at intermediate time t_1 :

- deposition of the particles on the spatial grid x_i for the density ρ : $\rho(x_i, t_1) = \sum_{k,l} \omega_{k,l}^n \mathcal{S}[x_i - (x_k^n + \Delta t/2 k_1(1))]$.
- solve the Poisson equation on the grid x_i : $E(x_i, t_1)$.
- Step 3: compute $k_2 = (v^n + \frac{\Delta t}{2} k_1(2), E(x^n + \frac{\Delta t}{2} k_1(1), t_1))$
- Step 4: compute the electric field at intermediate time t_2 :
 - deposition of the particles on the spatial grid x_i for the density ρ : $\rho(x_i, t_2) = \sum_{k,l} \omega_{k,l}^n \mathcal{S}[x_i - (x_k^n + \Delta t/2 k_2(1))]$.
 - solve the Poisson equation on the grid x_i : $E(x_i, t_2)$.
- Step 5: compute $k_3 = (v^n + \frac{\Delta t}{2} k_2(2), E(x^n + \frac{\Delta t}{2} k_2(1), t_2))$
- Step 6: compute the electric field at intermediate time t_3 :
 - deposition of the particles on the spatial grid x_i for the density ρ : $\rho(x_i, t_3) = \sum_{k,l} \omega_{k,l}^n \mathcal{S}[x_i - (x_k^n + \Delta t k_3(1))]$.
 - solve the Poisson equation on the grid x_i : $E(x_i, t_3)$.
- Step 7: compute $k_4 = (v^n + \Delta t k_3(2), E(x^n + \Delta t k_3(1), t_3))$
- Step 8: $X^{n+1} - X^n = \frac{\Delta t}{6} [k_1 + 2k_2 + 2k_3 + k_4]$

In both Verlet and Runge-Kutta algorithms, the value of E at intermediate time steps is needed (step 3 for Verlet and steps 3, 5 and 7 for Runge-Kutta 4). This is achieved as in PIC algorithms by advancing the particles (which coincide at time t^n with the mesh in this method) up to the required intermediate time. Using a deposition step, the density is computed thanks to cubic splines of coefficients w_i^n on the mesh at the right time, and thus the electric field can also be computed at the same time thanks to the Poisson's equation. Using an interpolation operator, the electric field is then evaluated at the required location (in steps 3, 5 and 7). Let us remark that this step involves a high order interpolation operator (cubic spline for example) which has been proved in our experiments to be more accurate than a linear interpolation (see section 4).

For the Guiding-Center equation, the explicit Euler method, and also Runge-Kutta type methods (of order 2, 3 and 4) have been implemented. There is no technical difficulty with computing high order methods. This is one of the general interests of forward methods. The time algorithm for solving the characteristics at the fourth order is similar to those presented in the Vlasov-Poisson case. However, there is an additional difficulty in the deposition step which enables to evaluate the density at intermediate time steps; indeed, the deposition is two-dimensional since the unknown does not depend on the velocity variable in this case.

Let us summarize the main steps of the second order Runge-Kutta method applied to the guiding center model of variables $X^n = (x^n, y^n)$ and of advection field $U(X^n, t^n) = E^\perp(X^n, t^n)$

- Step 1: $\tilde{X}^{n+1} - X^n = \Delta t E^\perp(X^n, t^n)$

- Step 2: Compute the electric field at time t^{n+1}
 - two-dimensional deposition of the particles on the spatial grid (x_j, y_i) for the density ρ : $\rho(x_j, y_i, t^{n+1}) = \sum_k \omega_k^n S[x_j - x_{k,l}^{n+1}] S[y_i - y_{k,l}^{n+1}]$
 - solve the two-dimensional Poisson equation on the grid x_j : $E(x_j, y_i, t_{n+1})$.
- Step 3: $X^{n+1} - X^n = \frac{\Delta t}{2} [E^\perp(X^n, t^n) + E^\perp(\tilde{X}^{n+1}, t^{n+1})]$

Here, the numerical solution of the two-dimensional Poisson's equation is based on Fourier transform coupled with finite difference method. See details in Appendix II.

3.3.3 FSL - BSL Cubic Spline Interpolation

We are going to compare how spline coefficients are computed recurrently, for one dimensional transport problems, for the sake of simplicity.

FSL: deposition principle On our mesh, the grid points $x_i = i\Delta x, i = 0, \dots, N_x$ at a time n can be regarded as particles. We have a distribution function which is projected onto a cubic splines basis. Thus, we know $f(t^n, x), \forall x$, then the particles move forward, and we have to compute $f(t^{n+1}, x_i), i = 0, \dots, N_x$, call that f is constant along the characteristics, and that the particles follow characteristics between t^n and t^{n+1} .

In fact, to each mesh point x_i , a spline coefficient ω_i is linked. The thing to understand, is that these coefficients are transported up to the deposition phase. The key is then to compute them recurrently as follows:

- Deposition step

$$\begin{aligned} f^{n+1}(x_i) &= \sum_k \omega_k^n S(x_i - X(t^{n+1}; x_k, t^n)) \\ &= \sum_{k/X(t^{n+1}; x_k, t^n) \in [x_{i-2}, x_{i+2}]} \omega_k^n S(x_i - X(t^{n+1}; x_k, t^n)), \end{aligned}$$

- Update of the splines coefficients ω_k^{n+1} using the interpolation conditions

$$f^{n+1}(x_i) = \sum_{k=i-2}^{i+2} \omega_k^{n+1} S(x_i - x_k),$$

The number of points which actually take part in the new value of $f^{n+1}(x_i)$ (here 4) is directly linked with the spline degree you choose. A p-Spline for example has a $(p + 1)$ points support.

In 1D, mass conservation follows from the computation:

$$\begin{aligned} m^{n+1} &= \Delta x \sum_i f^{n+1}(x_i) \\ &= \Delta x \sum_i \sum_k \omega_k^n S(x_i - X(t^{n+1}; x_k, t^n)) \\ &= \Delta x \sum_k \omega_k^n = \Delta x \sum_i f^n(x_i) = m^n, \end{aligned}$$

using the spline property of unit partition $\sum_i S(x - x_i) = 1$ for all x . This extends easily to more dimensions using tensor product splines.

BSL: interpolation principle Let us introduce some notations. The foot of the characteristics $X(t^n, x_i, t^{n+1})$ belongs to the interval $[x_l, x_{l+1}[$. Then the reconstructed distribution function can be written

- Interpolation step

$$\begin{aligned} f^{n+1}(x_i) &= f^n(X(t^n; x_i, t^{n+1})) \\ &= \sum_{k=l-2}^{l+2} \omega_k^n S(X(t^n; x_i, t^{n+1}) - x_k) \end{aligned}$$

- Update of the splines coefficients ω_k^{n+1} using the interpolation conditions

$$f^{n+1}(x_i) = \sum_{k=i-2}^{i+2} \omega_k^{n+1} S(x_i - x_k)$$

Here, we denoted by $X(t^n; x_i, t^{n+1})$ the foot of the characteristic coming from x_i . The reader is referred to [27, 30, 16] for more details on BSL interpolation.

In both cases, a linear system has to be solved, of equivalent complexity, so our method is as efficient at this level as BSL is.

If the linear transport equation

$$\frac{\partial f}{\partial t} + v \frac{\partial f}{\partial x} = 0,$$

for fixed v is solved, we can prove that FSL and BSL are in fact identical. The characteristic curve is for FSL:

$$X(t^{n+1}; x_k, t^n) = x_k + v\Delta t = x_k + \xi$$

whereas for BSL we have

$$X(t^n; x_k, t^{n+1}) = x_k - v\Delta t = x_k - \xi$$

Keeping the same notations as previously, we get for FSL:

$$f(t^{n+1}, x_i) = \sum_k \omega_k^n S(x_i - x_k - \xi)$$

In the BSL case, it comes:

$$\begin{aligned} f(t^{n+1}, x_i) &= \sum_k \omega_k^n S(x_k - (x_i - \xi)) \\ &= \sum_k \omega_k^n S(x_i - x_k - \xi) \end{aligned}$$

as the spline is even. So, if a splitting method where each transport phase is with constant velocity is used, actually, both FSL and BSL are exactly the same, and enjoy the same convergence and especially the stability properties. These have been proved for BSL in [4], Theorem 4.2 p.18-19-20.



Figure 3.3.1: Principle of FSL (left) and BSL (right) for linear splines.

3.3.4 Basic differences between FSL and BSL

Let us now explain the basic differences between forward and backward semi-Lagrangian methods. In both cases, a finite set of mesh points $(x_m)_{m=1..N}$ is used, and the values of the function f at the mesh points at a given time step t^n are considered. The aim is to find the new values of f on the grid at the next time step t^{n+1} .

BSL For BSL, in order to find the $(n + 1)$ -th value of f at x_m , we follow the characteristic curve which goes through x_m , backward in time, until time t^n . The arrival point will be called the foot of the characteristics and does not necessarily coincide with a mesh point. Hence, we use any interpolation technique to compute f at this point, knowing all the values of the mesh at this time. This leads to the new value of $f(x_m)$. Let us summarize:

- find the foot of the characteristics $X(t^n)$ knowing $X(t^{n+1}) = x_m$ (mesh point)
- interpolate using the grid function which is known at time t^n .

FSL For FSL, the principle is quite different. The characteristics beginning at time t^n on the grid points are followed, during one time step, and the end of the characteristics (*i.e.* at time t^{n+1}) is found. At this moment, the known value is deposited to the nearest grid points (depending on the chosen method). This deposition step is also performed in PIC codes on the spatial grid only, in order to get the sources for the computation of the electromagnetic field. Once every grid points has been followed, the new value of f is obtained by summing all contributions. The FSL method can be summarized as follows

- find the end of the characteristics $X(t^{n+1})$ leaving from $X(t^n) = x_m$ (mesh point)
- deposit on the grid and compute the new particle weights.

3.4 Numerical results

This section is devoted to the numerical implementation of the forward semi-Lagrangian method. In particular, comparisons with the backward semi-Lagrangian method will be performed to validate the new approach.

3.4.1 Hill's equation

In order to check that high orders time algorithms are really reached, a particularly easy model can be used, in which there are no self-consistent fields. Indeed, we want to verify that the fourth order Runge-Kutta algorithm is well implemented in the FSL method. We consider a 1D model with an external force field written $-a(t)x$, where a is a given periodic function. The Vlasov equation becomes:

$$\frac{\partial f}{\partial t} + v\partial_x f - a(t)x\partial_v f = 0, \quad (3.9)$$

The solution of this equation is seen through its characteristics, solutions of

$$\frac{dX}{dt} = V, \quad \frac{dV}{dt} = -a(t)X \quad (3.10)$$

thus, X is solution of Hill's equation:

$$\frac{d^2 X}{dt^2} + a(t)X = 0 \quad (3.11)$$

Let's note that this equation can be written in a general way $\frac{du}{dt} = A(t)u$, where A is a matrix valued periodic function. Since this is a 2D linear system, its solution is a 2D vector space and it is sufficient to find two independent solutions.

Let $\omega, \psi \in C^2(\mathbb{R}^+, \mathbb{R})$, with $\omega(t) > 0 \quad \forall t \in \mathbb{R}^+$, so that ω is solution of the differential equation

$$\frac{d^2 \omega}{dt^2} + a(t)\omega - \frac{1}{\omega^3} = 0 \quad \frac{d\psi}{dt} = \frac{1}{\omega^2} \quad (3.12)$$

So $u(t) = \omega(t)e^{i\psi(t)}$ and $v(t) = \omega(t)e^{-i\psi(t)}$ are two independent solutions of Hill's equation (see [18] for more details) which can be determined numerically.

For this test case, the initial distribution function will be:

$$f_0(x, v) = e^{-\frac{x^2}{2\omega^2} - \frac{\omega^2 v^2}{2}}, \quad \forall (x, v) \in [-12, 12]^2.$$

The associated solution $f(x, v, t)$ will depend only on $A\omega(t)$. In particular, f will have the same periodicity as a and ω . This is what will be used for testing the code. For different orders (2 and 4), and different Δt , $x_{rms}(t) = \sqrt{\int x^2 f(x, v, t) dx dv}$ will be displayed on Fig 3.4.1. This function should be periodic, and thus should reach the same test value $x_{rms}(0)$ at each period.

The error will be measured between the ten first computed values and the exact one, for the ten first periods. Then these errors will be summed, so that a L^1 norm of the error is dealt with:

$$err = \sum_{k=0}^{k=10} e_k, \quad \text{with } e_k = |x_{rms}(2k\pi) - x_{rms}(0)|.$$

The order of the method is checked in Figure 3.4.1. Note that $N_x = N_v = 1024$ to make sure that convergence is achieved for the interpolation step. The expected order is achieved for a certain Δt interval. If Δt becomes too small, a kind of saturation happens. This is due to the term in $\frac{h^{m+1}}{\Delta t}$ (where $h = \Delta x = \Delta v$) in the theoretical estimation of the error for backward methods ([4]), which becomes too high and prevents us from keeping the correct order. A forthcoming paper will try to do the same kind of error estimation for the forward method.

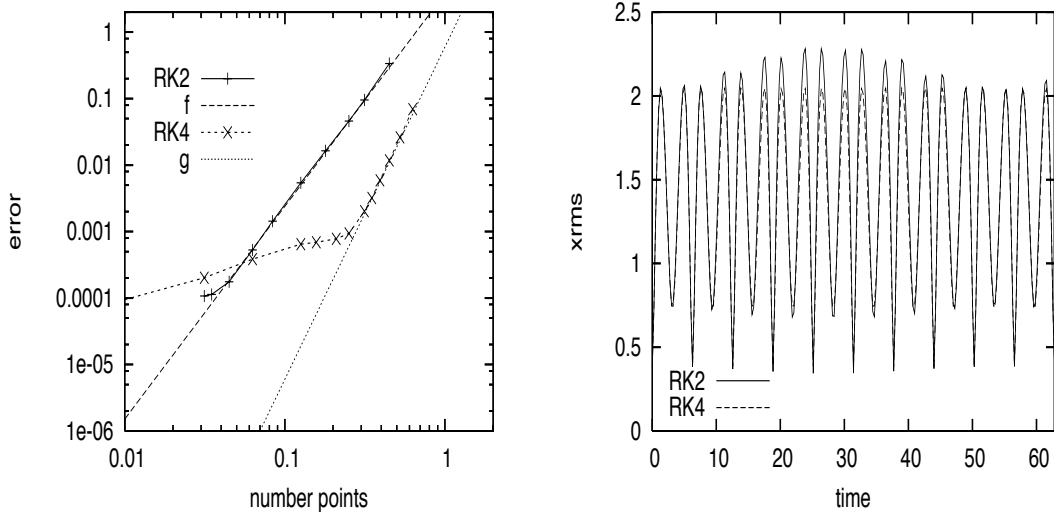


Figure 3.4.1: Error as a function of Δt for RK2 and RK4 (left) and x_{rms} as a function of time, for $\Delta t = 2\pi/25$, RK2 and RK4 (right).

3.4.2 Vlasov-Poisson case

Landau damping The initial condition associated to the scaled Vlasov-Poisson equation (3.1)-(3.2) has the following form

$$f_0(x, v) = \frac{1}{\sqrt{2\pi}} \exp(-v^2/2)(1 + \alpha \cos(kx)), \quad (x, v) \in [0, 2\pi/k] \times \mathbb{R}, \quad (3.13)$$

where $k = 0.5$ is the wave number and $\alpha = 0.001$ is the amplitude of the perturbation, so that linear regimes are considered here. A cartesian mesh is used to represent the phase space with a computational domain $[0, 2\pi/k] \times [-v_{max}, v_{max}]$, $v_{max} = 6$. The number of mesh points in the spatial and velocity directions is designated by $N_x = 64$ and $N_v = 64$ respectively. Finally, the time step is equal to $\Delta t = 0.1$ and the Verlet algorithm is used to compute the characteristics for good accuracy.

In this context, it is possible to find an exact value of the dominant mode solution of the linearized Vlasov-Poisson equation (see Appendix I for some details). The exact electric field corresponding to the dominant mode reads

$$E(x, t) = 4\alpha \times 0.3677e^{-0.1533t} \sin(0.5x) \cos(1.4156t - 0.5326245).$$

On Fig. 3.4.2, the analytical solution of the L^2 norm of the electric field and the implemented one are plotted. It can be observed that the two curves are very close to each other. In particular, the damping rate and the frequency of the wave are well recovered ($\gamma = -0.1533$ and $\omega = 1.4156$) by the method. Similar precision is achieved for different values of k leading to different value of the damping rate and of the frequency (see Fig. 3.4.2).

The recurrence effect that occurs with the present velocity discretization on a uniform grid, at $T_R \approx 80 \omega_p^{-1}$ can also be remarked. This value is in good agreement with the theoretical recurrence time which can be predicted in the free-streaming case (see [21]) $T_R = \frac{2\pi}{k\Delta v}$.

This test case has also been solved with the “hybrid” method in which the deposition step is only performed every T time steps. In all other steps, the remapping (or deposition) step is not performed, therefore, it can be linked with a PIC method. As it was already said, it is not really a PIC method since the spline coefficients are different on the phase space grid and are updated at each remapping step, whereas in classical PIC methods, these coefficients (called *weights*) are constant equal to $\frac{n_0}{N_{part}}$ where N_{part} is the number of particles. On Fig. 3.4.3, the electric field is plotted again, for different values of T , and $\Delta t = 0.1$, with $N_x = N_v = 128$ points. As expected, the method works well, even for large values of T . Only a kind of saturation can be observed, and it can be seen that values smaller than 2^{-18} are not well treated, because of the lack of accuracy of the hybrid method. Nevertheless, the results are convincing: the computation gets faster as T gets larger, and a good accuracy is reached for the linear problem treated.

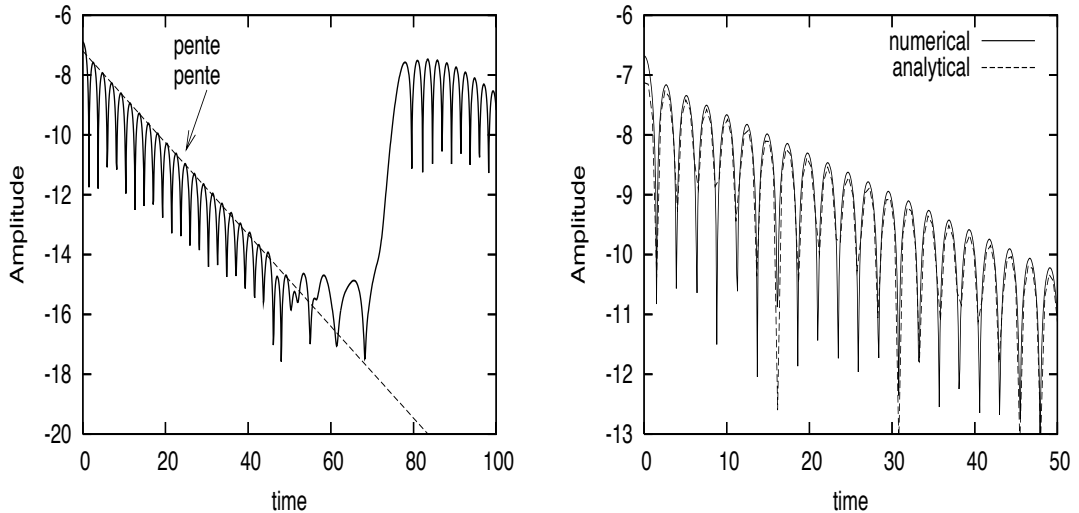


Figure 3.4.2: Linear Landau damping for $k = 0.5$ (left) and $k = 0.4$ (right)

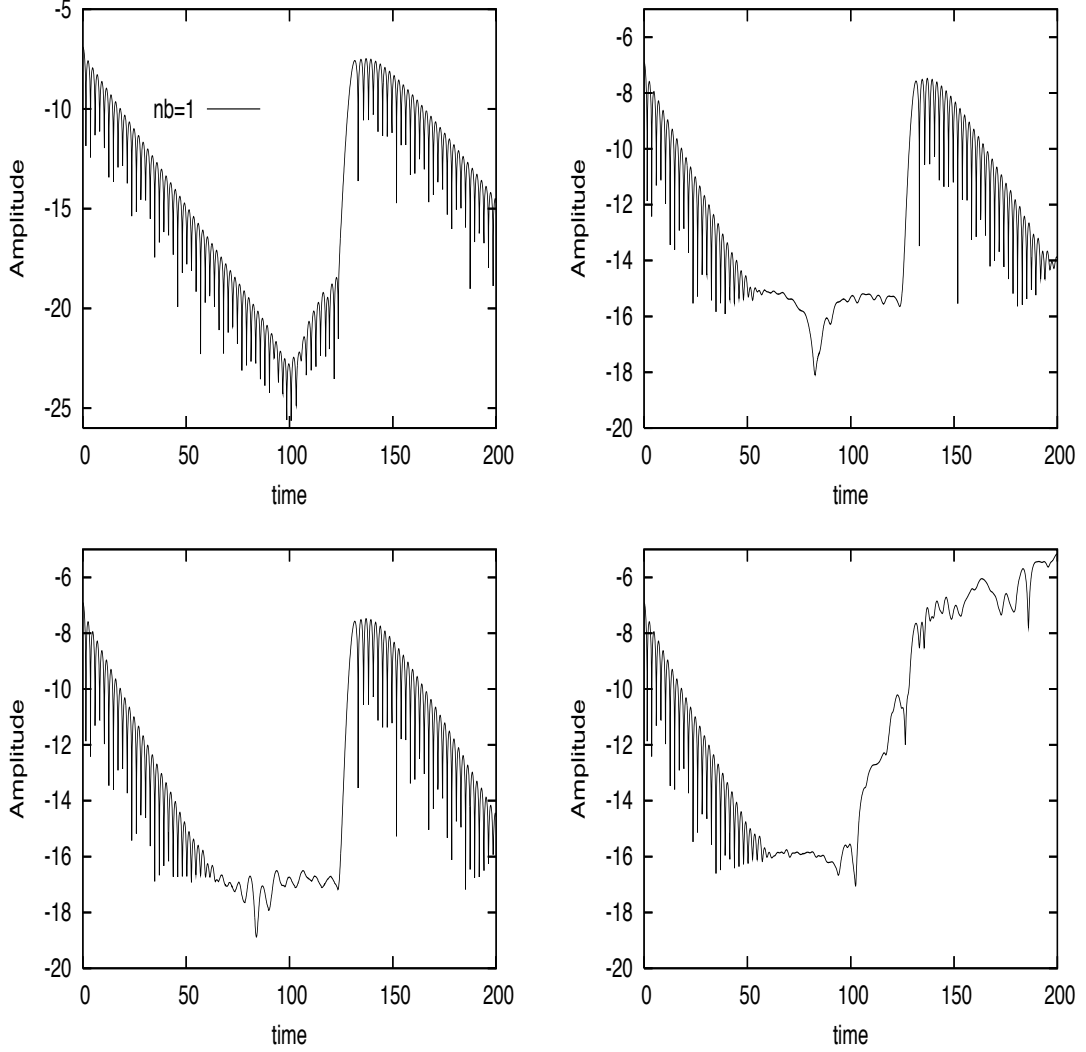


Figure 3.4.3: Linear Landau damping for $k = 0.5$ and for different number of T : from top to bottom and left to right: $T = 1, T = 2, T = 16, T = 256$.

Nonlinear Landau damping Next, we can apply the scheme to the nonlinear Landau damping test case for which the initial condition writes

$$f_0(x, v) = \frac{1}{\sqrt{2\pi}} \exp(-v^2/2)[1 + \alpha \cos(kx)], \quad (x, v) \in [0, 2\pi/k] \times \mathbb{R},$$

with $\alpha = 0.05, k = 0.4$, as in [19]. The numerical parameters are $N_x = 256, N_v = 256, v_{max} = 7, \Delta t = 0.1$.

We are interested in the time evolution of the spatially integrated distribution function

$$F(t, v) = \int_0^{2\pi/k} f(t, x, v) dx,$$

and in the time history of the electric energy $1/2\|E(t)\|_{L^2}^2$. The forward and backward methods will be compared. Let us remark that FSL requires a Runge-Kutta 4 algorithm for the computation of the characteristics.

We report the results of the time evolution of the electric field in Figures 3.4.4, for the BSL and FSL methods; the electric field does not decrease indefinitely, but oscillates around a constant value. Linear Landau damping can be captured until $t \approx 25\omega_p^{-1}$ for which the damping rate is $\gamma = 0.07$ (the theoretical value is $\gamma = 0.0661$). We can observe on Fig. 3.4.5 the spatially integrated distribution function at $t = 2000\omega_p^{-1}$. As in [19], the distribution function shows a bump around the phase space velocity $v_\phi = \omega/k \approx \pm 3.21$. This results in the low frequency amplitude oscillations of the electric field observed in Fig. 3.4.4. These observations are also in agreement with [6, 26].

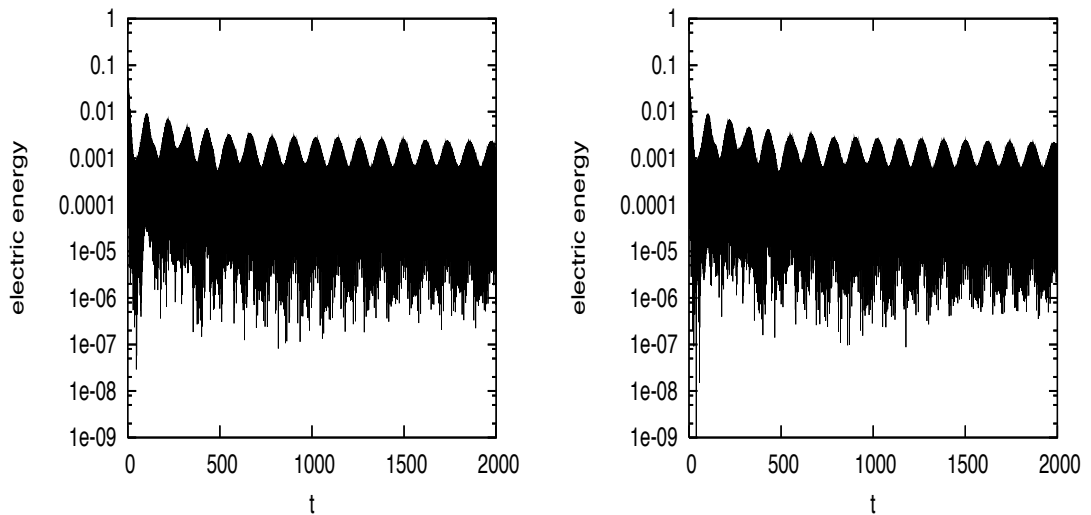


Figure 3.4.4: Nonlinear Landau damping: time evolution of the electric energy in logscale for FSL (left) and BSL (right).

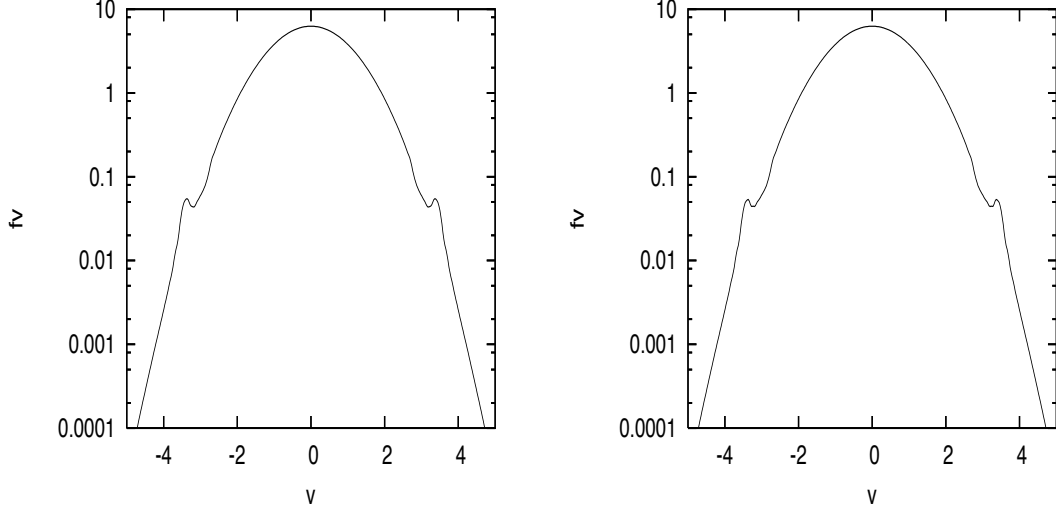


Figure 3.4.5: Nonlinear Landau damping: spatially integrated distribution function in log scale for FSL (left) and BSL (right).

Two stream instability This test case simulates two beams with opposite velocities that encounter (see [13, 21]). The corresponding initial condition can be given by

$$f_0(x, v) = \mathcal{M}(v)v^2[1 - \alpha \cos(kx)], \quad \mathcal{M}(v) = \frac{1}{\sqrt{2\pi}} \exp\left(-\frac{v^2}{2}\right),$$

with $k = 0.5$ and $\alpha = 0.05$. The computational domain is $[0, 2\pi/k] \times [-9, 9]$ which is sampled by $N_x = N_v = 128$ points. The Verlet algorithm is used to compute the characteristics with $\Delta t = 0.5$.

We are interested in the following diagnostics: the first three modes of the electric field, the electric energy $1/2\|E(t)\|_{L^2}^2$ and the time evolution of the phase space distribution function.

On Fig. 3.4.6, we plot the time history of the first three Fourier modes of the electric field: $|E_1|, |E_2|, |E_3|$ denotes the amplitudes of $\hat{E}(k = 0.5)$, $\hat{E}(k = 1)$ and $\hat{E}(k = 1.5)$ respectively. We observe that after an initial phase, the first mode exponentially increases to reach its maximum at $T \approx 18 \omega_p^{-1}$. After this phase and until the end of the simulation, a periodic behavior is observed which translates the oscillation of the trapped particles in the electric field; in particular, a vortex rotates with a period of about $18 \omega_p^{-1}$. The other modes $|E_2|$ and $|E_3|$ also grow exponentially and oscillate after the saturation. However, their amplitude remains inferior to that of the first mode. Similar observations can be performed for the electric energy which reaches its maximum at $T \approx 18 \omega_p^{-1}$ after an important and fast increase (from $t = 8$ to $t = 18 \omega_p^{-1}$).

This test case was also solved with the hybrid method to test the capability in the nonlinear regime. On Fig. 3.4.7, the first Fourier mode of the electric field is displayed for different T , with $\Delta t = 0.5$, and 128 points in each direction. It can be observed that during the first phase, which is a linear one, even for big T , the results are quite accurate for all values of T . The hybrid method seems to have more difficulty after this linear phase. Numerical noise, one of the main drawbacks of PIC methods can be observed as T gets higher. The phenomenon can

be understood looking at the distribution function. On Fig. 3.4.7 the noise clearly appears on f . Noisy values quickly reach high values which prevent the method from being accurate enough. They are more important in our hybrid method than in classical PIC ones, because of the deposition step, where the particles weight play their role. Indeed, if particles with very different weights are located at the same place, the deposition does not take into account properly the particles of low weights compared to those of heavy weights. On Fig. 3.4.7, it can be seen that the vortex which appears at the middle of the distribution and should stay there slowly leaves out of the domain. This can be explained as a kind of diffusion. Nevertheless, if T remains very small ($2 - 4$), the results are really good. It can also be noticed that Δt plays an important role, actually, when a smaller Δt is chosen, the results remain good for bigger T . As an example, if $\Delta t = 0.1$, results remain acceptable until $T = 16$.

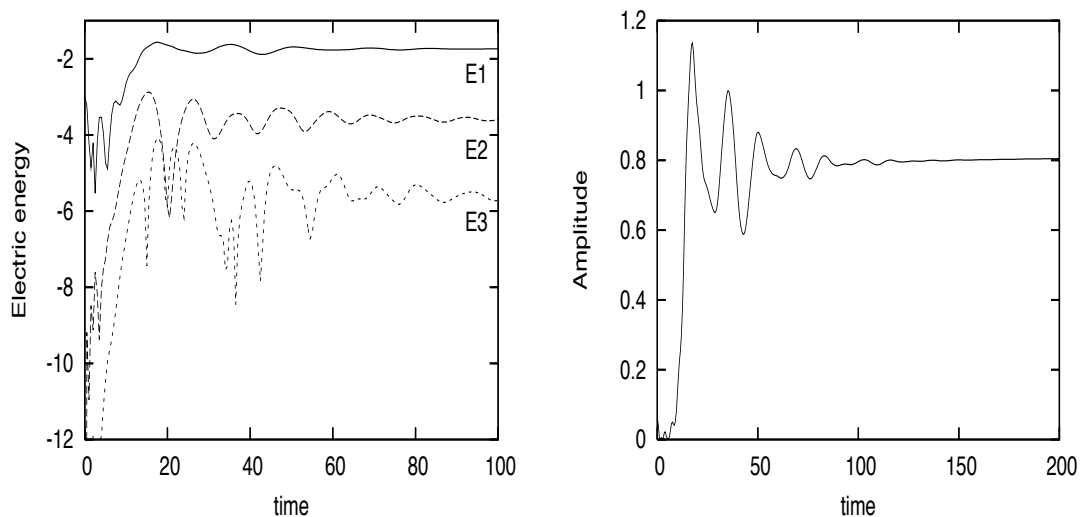


Figure 3.4.6: Two stream instability: Time evolution of the three first modes of the electric field (left) and of the electric energy (right).

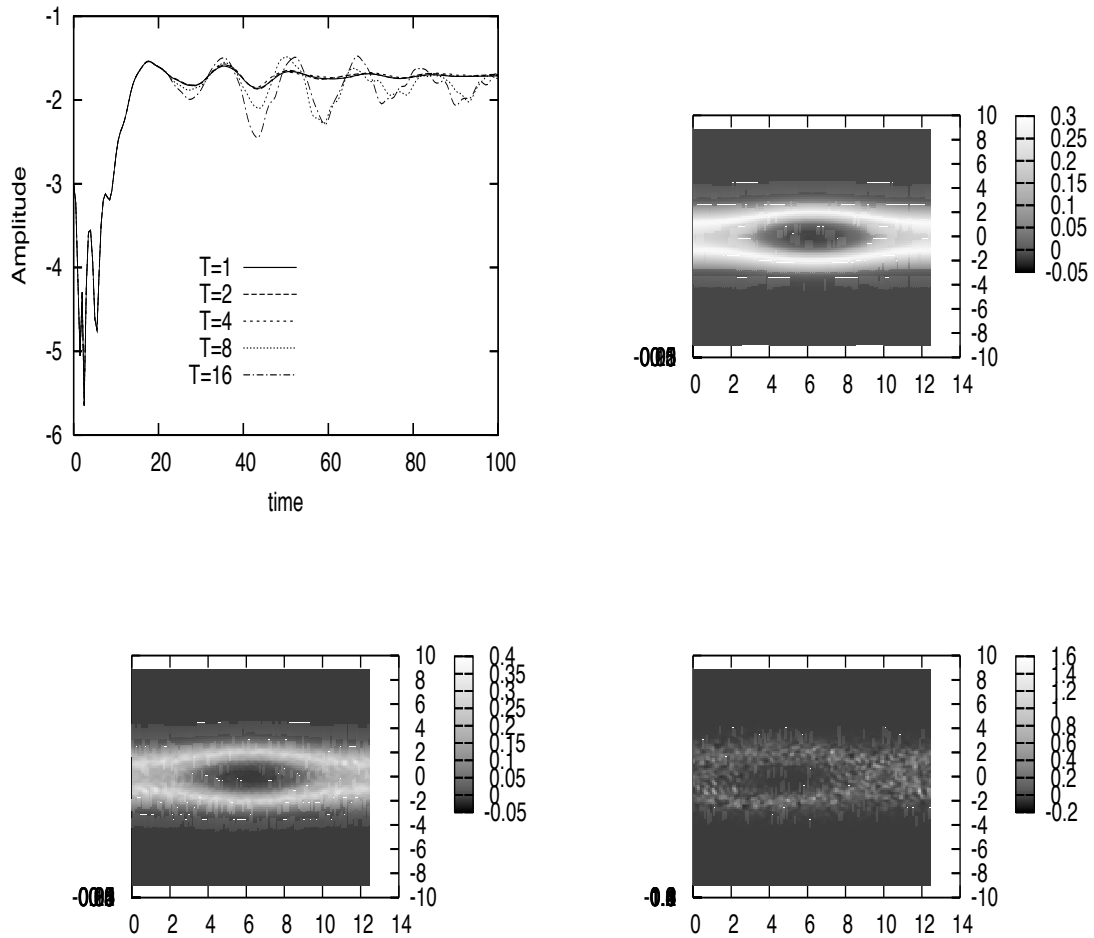


Figure 3.4.7: Two stream instability: Time evolution of the first mode of the electric field (up and left) and distribution function at time $t = 100 \omega_p^{-1}$ for $T = 1, 4, 8$.

Bump on tail Next, we can apply the scheme to the bump-on-tail instability test case for which the initial condition writes (see [24])

$$f_0(x, v) = \tilde{f}(v)[1 + \alpha \cos(kx)],$$

with $\alpha = 0.04$, $k = 0.3$ and

$$\tilde{f}(v) = \frac{n_p}{\sqrt{2\pi}} \exp(-v^2/2) + \frac{n_b}{\sqrt{2\pi}} \exp\left(-\frac{|v-u|^2}{2v_t^2}\right)$$

on the interval $[0, 20\pi]$, with periodic conditions in space. The initial condition f_0 is a Maxwellian distribution function which has a bump on the Maxwell distribution tail; the parameters of this

bump are the following

$$n_p = 0.9, n_b = 0.2, u = 4.5, v_t = 0.5,$$

whereas the numerical parameters are $N_x = 128, N_v = 128, v_{max} = 9, \Delta t = 0.05$. The Runge-Kutta 4 algorithm is used to compute the characteristics.

We are interested in the time evolution of the spatially integrated distribution function

$$F(t, v) = \int_0^{20\pi} f(t, x, v) dx,$$

and in the time history of the electric energy $1/2\|E(t)\|_{L^2}^2$. For this latter diagnostic, we expect oscillatory behavior of frequency equal to 1.05; moreover, since an instability will be declared, the electric energy has to increase up to saturation at $t \approx 20.95$ and to converge for large times (see [21, 24]).

On Figures 3.4.8, we plot the electric energy as a function of time. We can observe that oscillations appear, the frequency of which can be evaluated to 1.; then the maximum value is reached at $t \approx 21$ and the corresponding amplitude is about 9, which is in very good agreement with the results presented in [21, 24]. Then the amplitude of the electric energy is different: it presents a slower oscillation due to the particle trapping on which is superimposed the oscillation of the system at the frequency ω . Finally, it converges to an amplitude of about 2.8 which is very close to the results of the literature. FSL using time integrator algorithms of order two (Runge-Kutta 2 or Verlet algorithms) also leads to good results, and the difference is hard to see on this kind of diagnostic. We also test Runge-Kutta 3 for the solving of the characteristics; as mentioned in [20], it represents a good compromise between accuracy and efficiency. However, Runge-Kutta 4 algorithm seems to remain stable for larger values of Δt . The results obtained by BSL (see Fig. 3.4.8) are very close to those obtained by FSL using Runge-Kutta 4. Moreover, it has been remarked that linear interpolation of the electric field is not sufficient to obtain accurate results with FSL-Runge-Kutta 4 and cubic spline are used to that purpose.

Fig. 3.4.9 and Fig. 3.4.10 show the time development of the spatially integrated distribution function for FSL and BSL. After a strong deformation (around $t = 0 - 40\omega_p^{-1}$), the distribution function reaches an asymptotic state. The distribution function has a bump on tail and presents a minimum at $v = v_\phi \approx 3.5$. This corresponds to BGK equilibrium (see [24, 3]).

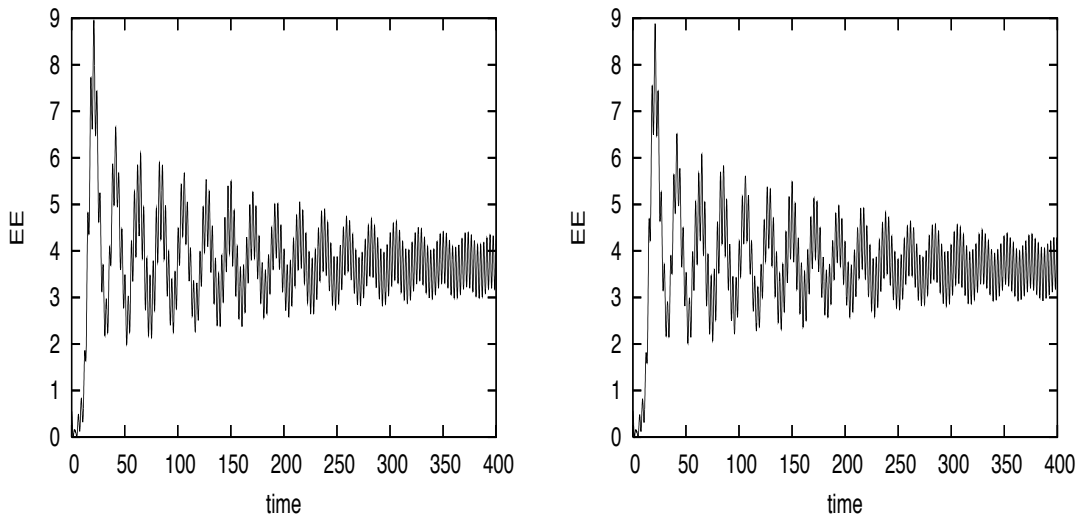


Figure 3.4.8: Bump on tail instability: time evolution of the electric energy for FSL (left) and BSL (right).

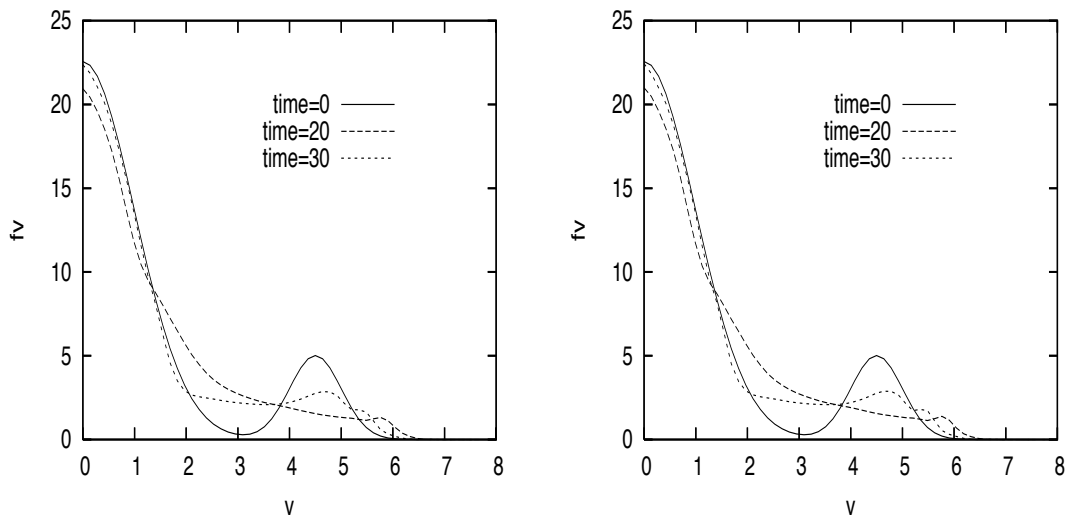


Figure 3.4.9: Bump on tail instability: time development of the spatially integrated distribution function for FSL (left) and BSL (right).

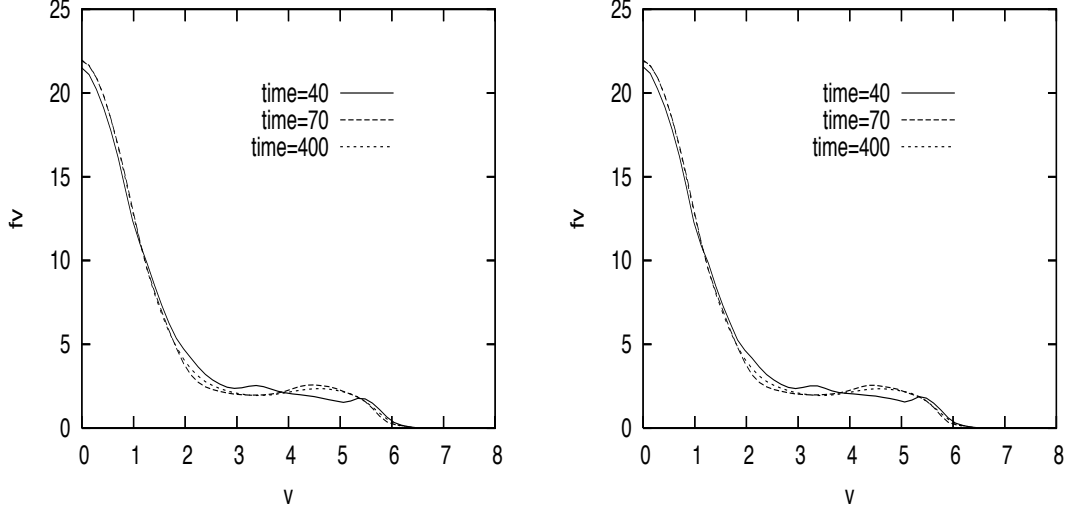


Figure 3.4.10: Bump on tail instability: time development of the spatially integrated distribution function for FSL (left) and BSL (right).

3.4.3 Guiding-center case

Kelvin-Helmoltz instability In order to validate our guiding-center code, we used two test cases introduced in [25] and [15].

First test case

The corresponding initial condition is

$$\rho(x, y, t = 0) = \rho^0(y) + \epsilon \rho^1(y) \cos(kx)$$

coupled with Poisson's equation:

$$\phi = \phi^0(y) + \epsilon \phi^1(y) \cos(kx)$$

The instability is created choosing an appropriate ρ^1 which will perturb the solution around the equilibrium one (ρ^0, ϕ^0) . Using the the work of Shoucri, we will take:

$$\rho(x, y, t = 0) = \sin(y) + 0.015 \sin\left(\frac{y}{2}\right) \cos(kx)$$

where $k = \frac{2\pi}{L_x}$ and L_x the length of the domain in the x -direction

The numerical parameters are:

$$N_x = N_y = 128, \Delta t = 0.5.$$

The domain size has an impact on the solution. The interval $[0, 2\pi]$ will be used on the y -direction, and respectively $L_x = 7$ and $L_x = 10$. This leads to real different configurations:

With $L_x = 7$, Shoucri proved that the stable case should be dealt with. That is what was observed with this code.

With $L_x = 10$, the unstable case is faced. The results prove it on figure Fig. 3.4.11 and 3.4.12.

For this test case, the evolution of the energy $\int E^2 dx dy$ and enstrophy $\int \rho^2 dx dy$ will also be plotted on Fig. 3.4.13. These should be theoretically invariants of the system. Like for other semi-Lagrangian methods, the energy lowers during the first phase, which is the smoothing one, where micro-structures can not be solved properly. Nevertheless, the energy is well conserved. Moreover, on Fig. 3.4.13, FSL using second and fourth order Runge-Kutta's methods are compared to the BSL method. As observed in the bump-on-tail test, the Runge-Kutta 4 leads to more accurate results and is then very close to BSL. However, BSL seems to present slightly better behavior compared to FSL-Runge-Kutta 4. But FSL-Runge-Kutta 4 enables to simulate such complex problems using higher values of Δt (see Fig. 3.4.14). We observed for example that the use of $\Delta t = 1$ gives rise to very reasonable results since the L^2 norm of the electric field E decreases of about 4%. Let us remark that the leap-frog algorithm for BSL leads to a uncoupled dynamics when $\Delta t \geq 0.7$.

Finally, we give an indication on the computational cost of the different methods. The FSL method is dependent on the order of the Runge-Kutta algorithm; indeed, since the deposition step and the interpolation step are roughly similar, the difference between the FSL and BSL methods comes from the computation of the characteristic curves. Hence, the Runge-Kutta 2 algorithm which involves a deposition to compute the intermediate density is slightly more expensive than BSL. Obviously, the tendency is amplified for the Runge-Kutta 4 algorithm in which the electric field has to be computed at the intermediate times. However, other ODE solvers based on multiple time steps or Taylor expansion might be more efficient computationally.

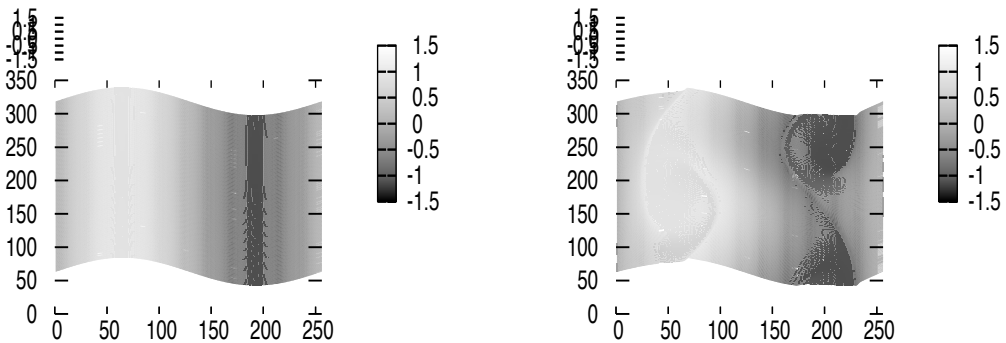


Figure 3.4.11: Kelvin Helmholtz instability 1: distribution function at time $t = 0, 20 \omega_p^{-1}$

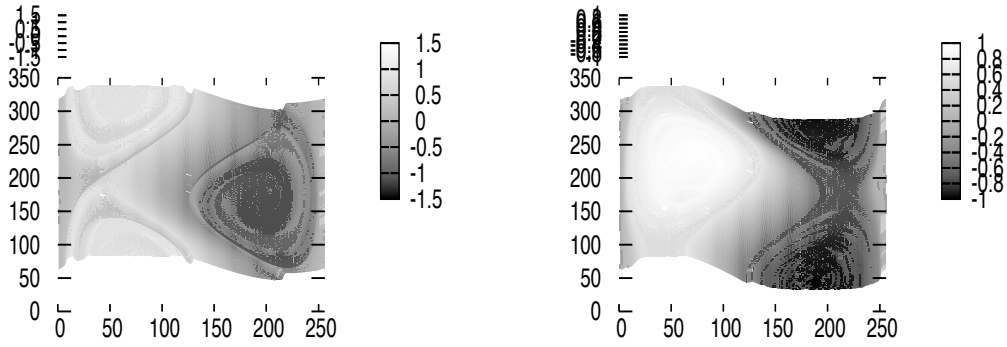


Figure 3.4.12: Kelvin Helmholtz instability 1: distribution function at time $t = 50,500 \omega_p^{-1}$

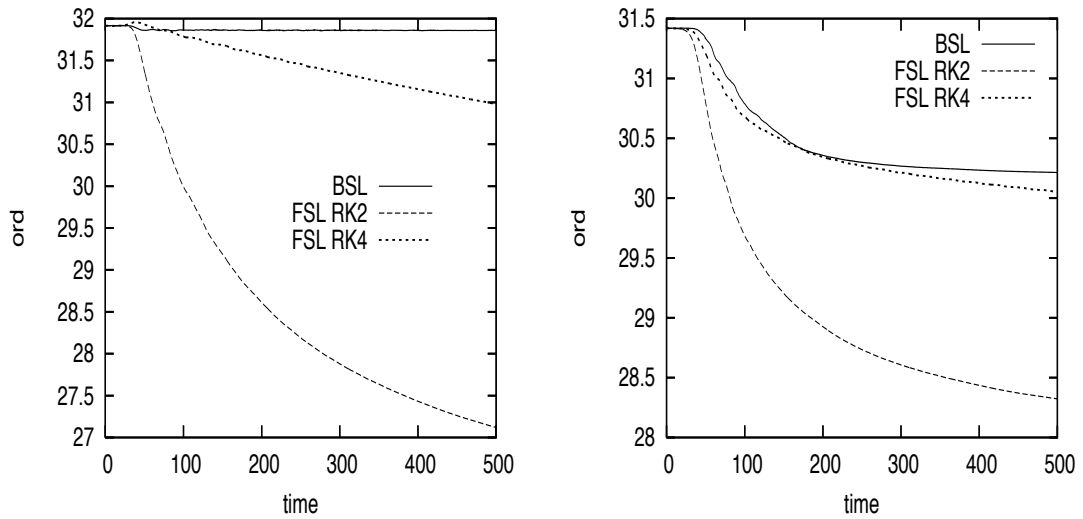


Figure 3.4.13: Kelvin Helmholtz instability 1: time history of L^2 norms of E (left) and of ρ (right). Comparison between FSL and BSL.

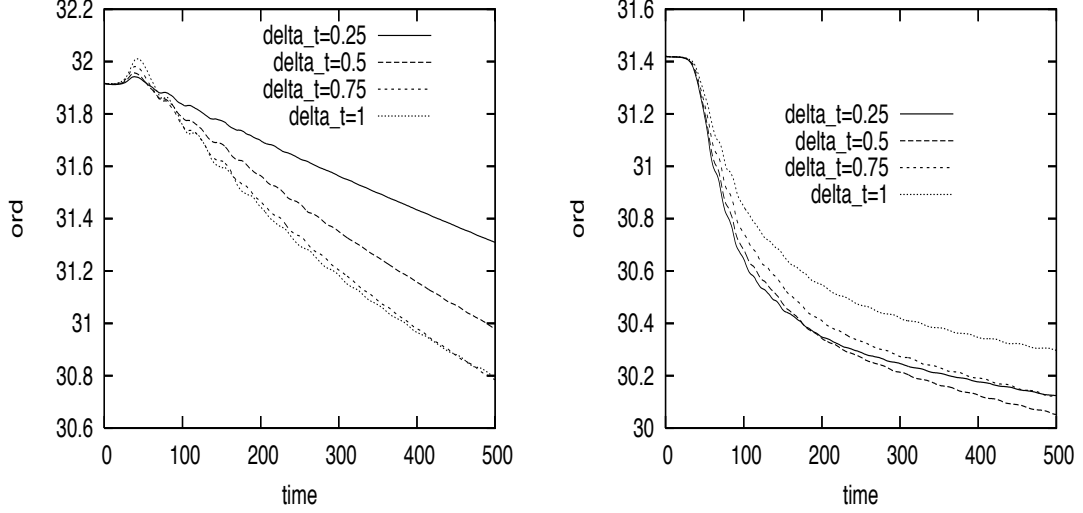


Figure 3.4.14: Kelvin Helmholtz instability 1: time history of L^2 norms of E (left) and of ρ (right). Comparison of the results for RK4 for different values of Δt .

FSL RK2	13.5 s.
FSL RK4	30 s.
BSL	9 s.

Figure 3.4.15: Comparison of computational cost for the guiding-center model: 3 iterations with 64 points in each direction.

Second test case

In this test case, the initial condition will be:

$$\rho(x, y, t = 0) = 1.5 \operatorname{sech}\left(\frac{y}{0.9}\right) (1 + 0.08 \sin(2k_0 x)).$$

The numerical parameters are:

$$N_x = N_y = 128, \Delta t = 0.1.$$

The domain will be taken equal to $0 \leq x \leq 40$, $-5 \leq y \leq 5$. The results with RK2 will be displayed.

Fig. 3.4.16 to 3.4.18 represent the evolution of the distribution function. The instability begins at $t \approx 20$, with two circular rolling-up vortices. Then, a smoothing phase happens, before the start of a second instability, where two structures emerge and roll up around each other, and finally, a smoothing phase occurs.

We also display, on Fig. 3.4.19 the mass and the L^2 norm of the function, $\int \rho^2 dx dy$ which should be invariants of the system. The first one decreases slowly during the two unstable

phases, but is really well conserved anyway. The second one decreases stronger twice, and is otherwise stable. In all our test cases, this is due to the bad resolution of microstructures as they become smaller than a cell. Nevertheless, the results are in good shape with the literature.

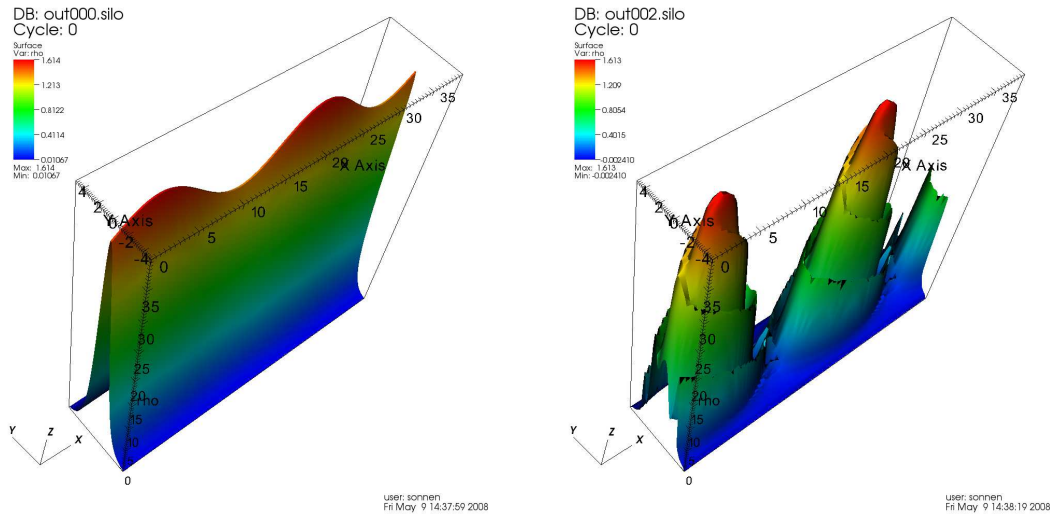


Figure 3.4.16: Distribution function at times $t=0,20$, $N_x = N_y = 128$, $\Delta t = 0.1$

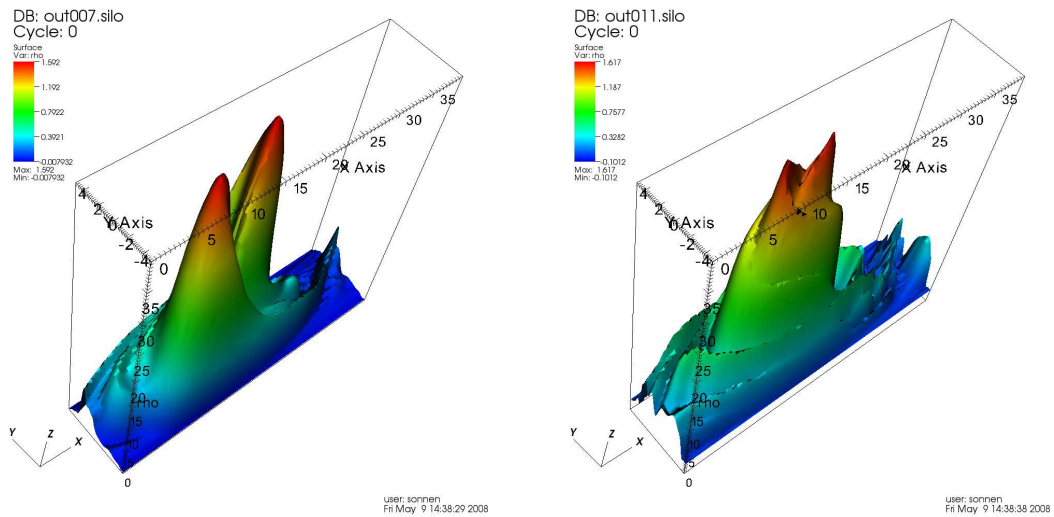
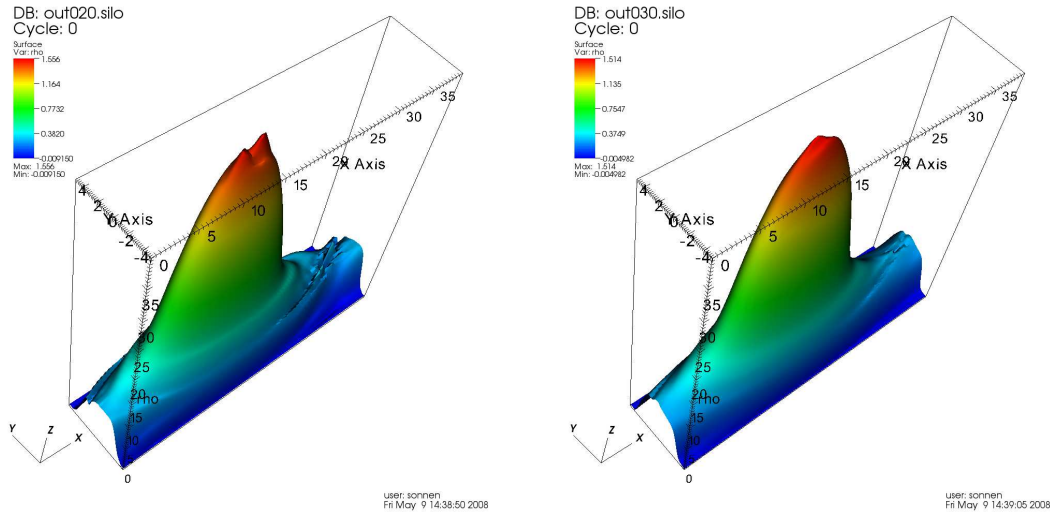
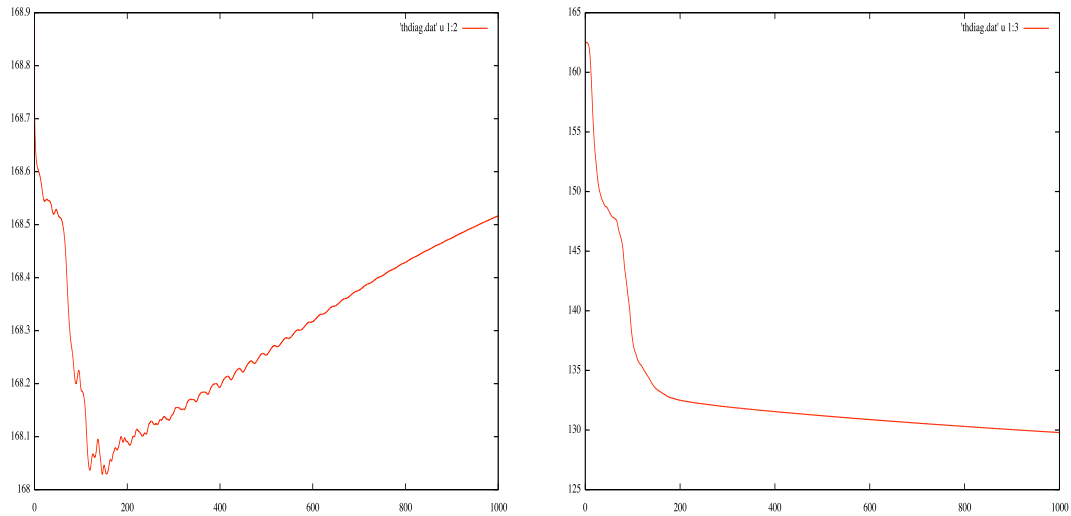


Figure 3.4.17: Distribution function at times $t=70,110$, $N_x = N_y = 128$, $\Delta t = 0.1$

Figure 3.4.18: Distribution function at times $t=200,300$, $N_x = N_y = 128$, $\Delta t = 0.1$ Figure 3.4.19: Mass and L^2 norm of the distribution function, $N_x = N_y = 128$, $\Delta t = 0.1$

3.5 Conclusion and perspectives

In this paper, we introduced the forward semi-Lagrangian method for Vlasov equations. The method has been tested on two different models, the one-dimensional Vlasov-Poisson one, and the guiding-center one. Different test cases have been simulated, and they are quite satisfying. The results are in some cases a bit less accurate, with respect to the conservation of invariants, than with the classical BSL method, but enable the use of very large time steps without being

unstable and recover a good global behavior. No iterative methods are needed, and high order time schemes can be used in a straightforward manner. Moreover, the coupling of the method with adaptive meshes seems to be achievable since the prediction of the mesh is natural. Another next step will be to test the method with the Vlasov-Maxwell model, in which we will try to solve properly the charge conservation problem, which is the ultimate goal. The similarity between PIC and FSL time advance and deposition should enable us to use charge conserving deposition scheme, like [32].

We will try to use PIC results about that conservation, for example in [1]. We will also try to prove theoretically the convergence and stability of this method for physically relevant models.

3.6 Appendix I: Linearized Vlasov Poisson and Landau damping

In classical plasma physics textbooks, only the dispersion relations are computed for the linearized Vlasov-Poisson equation. However using the Fourier and Laplace transforms as for the computation of the dispersion relation and inverting them, it is straightforward to obtain an exact expression for each mode of the electric field (and also the distribution function if needed). Note that each mode corresponds to a zero of the dispersion relation.

The solution of the Landau damping problem is obtained by solving the linearized Vlasov-Poisson equation with a perturbation around a Maxwellian equilibrium, which corresponds to the initial condition $f_0(x, v) = (1 + \epsilon \cos(kx)) / \sqrt{2\pi} e^{-v^2/2}$. Let us introduce the plasma dispersion function Z of Fried and Conte [14]

$$Z(\eta) = \sqrt{\pi} e^{-\eta^2} [i - \text{erfi}(\eta)], \quad \text{where } \text{erfi}(\eta) = \frac{2}{\pi} \int_0^\eta e^{t^2} dt.$$

We also have, $Z'(\eta) = -2(\eta Z(\eta) + 1)$. Then, denoting by $\widehat{E}(k, t)$ the Fourier transform of E and by $\widetilde{E}(k, \omega)$ the Laplace transform of \widehat{E} , the electric field, solution of linearized Vlasov-Poisson satisfies:

$$\widehat{E}(k, t) = \sum_j \text{Res}_{\omega=\omega_j} \widetilde{E}(k, \omega) e^{-i\omega t}$$

where

$$\widetilde{E}(k, \omega) = \frac{N(k, \omega)}{D(k, \omega)}$$

$$D(k, \omega) = 1 - \frac{1}{2k^2} Z'\left(\frac{\omega}{\sqrt{2}k}\right), \quad N(k, \omega) = \frac{i}{2\sqrt{2}k^2} Z\left(\frac{\omega}{\sqrt{2}k}\right)$$

The dispersion relation corresponds to

$$D(k, \omega) = 0.$$

For each fixed k , this equation has different roots ω_j , and to which are associated the residues defining $\widehat{E}(k, t)$ that can be computed with Maple. These residues take in fact the values

$$\text{Res}_{\omega=\omega_j} (\widetilde{E}(k, \omega)) = \frac{N(k, \omega_j)}{\frac{\partial D}{\partial \omega}(k, \omega)}. \quad (3.14)$$

Let us denote by $\omega_r = \text{Re}(\omega_j)$, $\omega_i = \text{Im}(\omega_j)$, r will be the amplitude of (3.14) and φ its phase.

Remark: For each root $\omega = \omega_r + i\omega_i$, linked to $re^{i\varphi}$, there is another: $-\omega_r + i\omega_i$ linked to $re^{-i\varphi}$. Then keeping only the roots in which ω_i is the largest, which are the dominating ones after a short time, we get:

$$\widehat{E}(k, t) \approx re^{i\varphi} e^{-i(\omega_r + i\omega_i)t} + re^{-i\varphi} e^{-i(-\omega_r + i\omega_i)t} = 2re^{\omega_i t} \cos(\omega_r t - \varphi)$$

Taking the inverse Fourier transform, we finally get an analytical expression for the dominating mode of the electric field, which we use to benchmark our numerical solution:

$$E(x, t) \approx 4\epsilon r e^{\omega_i t} \sin(kx) \cos(\omega_r t - \varphi)$$

Remark This is not the exact solution, because we have kept only the highest Laplace mode. Nevertheless, after about one period in time, this is an excellent approximation of E , because the other modes decay very fast.

3.7 Appendix II: Solution of Poisson in the Guided Center model

3.7.1 Find ϕ

We have to solve:

$$-\Delta\phi(x, y) = \rho(x, y)$$

using a high order method (as in [17]). A Fourier transform in the x direction is performed. This leads, for $i \in [1, N_x]$:

$$\frac{\partial^2 \widehat{\phi}_i(y)}{\partial y^2} = \xi^2 \widehat{\phi}_i(y) - \widehat{\rho}_i(y)$$

Let us introduce the notation δ for the second order discrete derivative in y . A Taylor Young formula leads to

$$\delta u_i = \frac{u_{i+1} - 2u_i + u_{i-1}}{\Delta y^2} = \left(1 + \frac{\Delta y^2}{12} \frac{\partial^2}{\partial y^2}\right) \frac{\partial^2 u_i}{\partial y^2} + \mathcal{O}(\Delta y^2).$$

Let us apply this to $\widehat{\phi}_i$

$$\delta \widehat{\phi}_i = \left(1 + \frac{\Delta y^2}{12} \frac{\partial^2}{\partial y^2}\right) (\xi^2 \widehat{\phi}_i - \widehat{\rho}_i) + \mathcal{O}(\Delta y^2) = \xi^2 \widehat{\phi}_i - \widehat{\rho}_i + \frac{\Delta y^2}{12} (\xi^2 \delta \widehat{\phi}_i - \delta \widehat{\rho}_i) + \mathcal{O}(\Delta y^2).$$

Now, factorizing all of it, we get:

$$\widehat{\phi}_{i+1} \left(1 - \frac{\xi^2 \Delta y^2}{12}\right) + \widehat{\phi}_i \left(-2 + \frac{10\xi^2 \Delta y^2}{12}\right) + \widehat{\phi}_{i-1} \left(1 - \frac{\xi^2 \Delta y^2}{12}\right) = -\Delta y^2 (\widehat{\rho}_{i+1} + 10\widehat{\rho}_i + \widehat{\rho}_{i-1}) + \mathcal{O}(\Delta y^4).$$

This is nothing but the solution of a linear system, which has already been derived in [17]

$$A\widehat{\phi} = R,$$

where A is a tridiagonal and symmetric matrix and R is a modified right hand side which allows to achieve a fourth order approximation.

3.7.2 Find E

To compute the electric field from the electric potential, we have to solve $E = -\nabla\phi$. To achieve this task, a quadrature formula is used.

In the x direction, which is the periodic one, a third order Simpson method is used

$$\int_{x_{i-1}}^{x_{i+1}} E(x, y) dx = -\phi(x_{i+1}, y) + \phi(x_{i-1}, y) \approx \frac{1}{6}E_{i-1}(y) + \frac{1}{6}E_{i+1}(y) + \frac{2}{3}E_i(y)$$

where the $(\phi_i)_i$ is given by previous step. There is no problem with extreme values, since the system is periodic. We then find the values of the electric field E solving another tridiagonal linear system.

Whereas on the y -direction, Dirichlet conditions are imposed at the boundary. So, we can use the same strategy within the domain, but not on the two boundary points. Since we have a third order solution everywhere, we want to have the same order there, therefore we cannot be satisfied with a midpoint quadrature rule which is of second order. So we will add corrective terms, in order to gain one order accuracy. Here is how we do this.

$$\int_{y_0}^{y_1} E(x, y) dy = -\phi(x, 1) + \phi(x, 0) \approx \frac{dy}{2}(E(x, 0) + E(x, 1)) - \frac{dy^2}{12}(\rho(x, 1) - \rho(x, 0)) + f_\phi$$

where

$$f_\phi = \mathbb{F}_y^{-1} \left(\frac{\Delta_y^2}{12} \xi^2 (\widehat{\phi(\xi, 1)} - \widehat{\phi(\xi, 0)}) \right) = \frac{\Delta_y^2}{12} [-\partial_{xx}(\phi(x, 1) - \phi(x, 0))].$$

We want to find the precision of this method, thus, we would like to evaluate the following difference which is denoted by A :

$$A = \phi(x, 0) - \phi(x, 1) - \frac{dy}{2}(E(x, 0) + E(x, 1)) + \frac{dy^2}{12}(\rho(x, 1) - \rho(x, 0)) - f_\phi.$$

Using the Poisson equation and Taylor expansion, we have

$$\begin{aligned} A + E(x, 0) + E(x, 1) &= -\frac{2}{dy}(\phi(x, 1) - \phi(x, 0)) + \frac{dy}{6}(\rho(x, 1) - \rho(x, 0)) + \frac{dy}{6}(\partial_{xx}(\phi(x, 1) - \phi(x, 0))) \\ &= -\frac{2}{dy}(\phi(x, 1) - \phi(x, 0)) - \frac{dy}{6}(\partial_{yy}(\phi(x, 1) - \phi(x, 0))) \\ &= -\frac{2}{dy}(\phi(x, 1) - \phi(x, 0)) - \frac{dy^2}{6}(\partial_{yyy}\phi(x, \xi_1) + \mathcal{O}(\Delta_y^3)) \end{aligned}$$

where $\xi_1 \in [y_0, y_1]$. Thus, we finally obtain

$$A + E(x, 0) + E(x, 1) = -\frac{2}{dy}(\phi(x, 1) - \phi(x, 0)) + \frac{dy^2}{6} \frac{\partial^2}{\partial y^2} E(x, \xi_1) + \mathcal{O}(\Delta_y^3)$$

Moreover, classical quadrature theory gives us the existence of $\xi_2 \in [y_0, y_1]$ such as

$$\int_{y_0}^{y_1} E(x, y) dy = \frac{dy}{2}(E(x, 0) + E(x, 1)) - \frac{dy^3}{12} \frac{\partial^2}{\partial y^2} E(x, \xi_2).$$

Replacing $E(x, \xi_1)$ by $E(x, \xi_2)$, which is of first order in our computation leads to

$$A + E(x, 0) + E(x, 1) = -\frac{2}{dy}(\phi(x, 1) - \phi(x, 0)) - \frac{2}{dy} \int_{y_0}^{y_1} E(x, y) dy + (E(x, 0) + E(x, 1)) + \mathcal{O}(\Delta_y^3)$$

so that $A = \mathcal{O}(\Delta_y^3)$ which is what was expected.

Bibliography

- [1] R. BARTHELMÉ, *Charge conservation in PIC codes*, C. R. Acad. Sc., **341**, pp. 689-694, (2005).
- [2] O. V. BATISHCHEV, A. A. BATICHEVA, J. ZHANG, *Hybrid Vlasov/Fokker-Planck-PIC method*, <http://web.mit.edu/ned/ICNSP/abstracts.html>, Proc. 18th Conf. Num. Simul. Plasmas, Cape Cod, USA, Sept. 2003.
- [3] I. B. BERNSTEIN, J. M. GREENE, M. D. KRUSKAL, *Exact Nonlinear Plasma Oscillations*, Phys. Rev. **108**, p. 546, (1957).
- [4] N. BESSE, M. MEHRENBERGER, *Convergence of classes of high order semi-Lagrangian schemes for the Vlasov-Poisson system*, Math. Comput., **77**, pp. 93-123, (2008).
- [5] C.K. BIRDSALL, A.B. LANGDON, *Plasma Physics via Computer Simulation*, Inst. of Phys. Publishing, Bristol/Philadelphia, 1991.
- [6] M. BUCHANAN, J. DORNING, *Nonlinear electrostatic waves in collisionless plasmas*, Phys. Rev. E **52**, 3015, (1995).
- [7] J.-A. CARILLO, F. VECIL, *Non oscillatory interpolation methods applied to Vlasov-based models*, SIAM Journal of Sc. Comput. **29**, pp. 1179-1206, (2007).
- [8] C. Z. CHENG, G. KNORR, *The integration of the Vlasov equation in configuration space*, J. Comput. Phys, **22**, pp. 330-3351, (1976).
- [9] C.J. COTTER, J. FRANK, S. REICH *The remapped particle-mesh semi-Lagrangian advection scheme*, Q. J. Meteorol. Soc., **133**, pp. 251-260, (2007)
- [10] J. DENAVIT, *Numerical simulation of plasmas with periodic smoothing in phase space*, J. Comput. Phys., **9**, pp. 75-98, 1972.
- [11] J. W. EASTWOOD, *The stability and accuracy of EPIC algorithms*, Comput. Phys; Comm. **44**, p. 73-82, (1987).
- [12] F. FILBET, E. SONNENDRÜCKER, P. BERTRAND, *Conservative numerical schemes for the Vlasov equation*, J. Comput. Phys., **172**, pp. 166-187, (2001).
- [13] F. FILBET, E. SONNENDRÜCKER, *Comparison of Eulerian Vlasov solvers*, Comput. Phys. Comm., **151**, pp. 247-266, (2003).

- [14] B. D. FRIED, S. D. COMTE, *The plasma dispersion function*, Academic Press, New York, 1961.
- [15] A. GHIZZO, P. BERTRAND, M.L. BEGUE, T.W. JOHNSTON, M. SHOUCRI, *A Hilbert-Vlasov code for the study of high-frequency plasma beatwave accelerator*, IEEE Transaction on Plasma Science, **24**, p. 370, (1996).
- [16] V. GRANDGIRARD, M. BRUNETTI, P. BERTRAND, N. BESSE, X. GARBET, P. GHENDRIH, G. MANFREDI, Y. SARRAZIN, O. SAUTER, E. SONNENDRÜCKER, J. VACLAVIK, L. VILLARD, *A drift-kinetic semi-Lagrangian 4D code for ion turbulence simulation*, J. Comput. Phys., **217**, pp. 395-423, (2006).
- [17] G. KNORR, A. JOYCE, J. MARCUS, *Fourth-order Poisson solver for the simulation of bounded plasmas*, J. Comput. Phys., **38**, p. 227, (1980).
- [18] W. MAGNUS, S. WINKLER, *Hill's equation*, John Wiley and sons, (1966).
- [19] G. MANFREDI, *Long time behaviour of the nonlinear Landau damping*, Phys. Rev. Let. **79**, 2815, (1997).
- [20] R.D. NAIR, J.S. SCROGGS, F. H.M. SEMAZZI, *A forward-trajectory global semi-Lagrangian transport scheme*, J. Comput. Phys., **190**, pp. 275-294, (2003).
- [21] T. NAKAMURA, T. YABE, *Cubic interpolated propagation scheme for solving the hyper-dimensional Vlasov-Poisson equation in phase space*, Comput. Phys. Comm., **120**, pp. 122-154, (1999).
- [22] S. REICH, *An explicit and conservative remapping strategy for semi-Lagrangian advection*, Atmospheric Science Letters **8**, pp. 58-63, (2007).
- [23] P. H. SAKANAKA, C. K. CHU, T. C. MARSHALL *Formation of ion-acoustic collisionless shocks*, Phys. Fluids **14**, 611, 1971.
- [24] M. SHOUCRI, *Nonlinear evolution of the bump-on-tail instability*, Phys. Fluids **22**, 2038, (1979).
- [25] M. SHOUCRI, *A two-level implicit scheme for the numerical solution of the linearized vorticity equation*, Int. J. Numer. Meth. Eng. **17**, p. 1525 (1981).
- [26] M. SHOUCRI, R. GAGNÉ, *Nonlinear behavior of a monochromatic wave in a one-dimensional Vlasov plasma*, Phys. Fluids **21**, 1168, (1978).
- [27] M. SHOUCRI, H. GERHAUSER, K. FINKEN, *Integration of the Vlasov equation along characteristics in one and two dimensions*, Comput; Phys. Comm. **154**, p. 65-75, (2003).
- [28] N. SINGH, *Computer experiments on the formation and dynamics of electric double layers (in plasma)*, Plasma Phys. **22**, 1, (1980).
- [29] A. STANIFORTH, J. COTÉ, *Semi-Lagrangian integration schemes for atmospheric models - A review*, Mon. Weather Rev. **119**, pp. 2206-2223, (1991).

- [30] E. SONNENDRÜCKER, J. ROCHE, P. BERTRAND, A. GHIZZO *The semi-Lagrangian method for the numerical resolution of the Vlasov equation*, J. Comput. Phys., **149**, pp. 201-220, (1999).
- [31] S. VADLAMANI, S. E. PARKER, Y. CHEN, C. KIM, *The particle-continuum method: an algorithmic unification particle in cell and continuum methods*, Comput. Phys. Comm. **164**, pp. 209-213, (2004).
- [32] J. VILLASENOR, O. BUNEMAN, *Rigorous charge conservation for electromagnetic field solvers*, J. Comput. Phys., **69**, pp. 306-316, (1992).
- [33] M. ZERROUKAT, N. WOOD, A. STANFORTH, *A monotonic and positive-definite filter for a Semi-Lagrangian Inherently Conserving and Efficient (SLICE) scheme*, Q.J.R. Meteorol. Soc., **131**, pp 2923-2936, (2005).
- [34] M. ZERROUKAT, N. WOOD, A. STANFORTH, *The Parabolic Spline Method (PSM) for conservative transport problems*, Int. J. Numer. Meth. Fluids, **51**, pp. 1297-1318, (2006).

Analysis of a new class of Forward semi-Lagrangian schemes for the 1D Vlasov-Poisson Equations

4.1 Introduction

The Vlasov equation describes the dynamics of charged particles in a plasma or in a propagating beam. The unknown $f(t, x, v)$ which depends on the time t , the space x and the velocity v represents the distribution function of the studied particles. The coupling with the self-consistent electric fields is taken into account through the Poisson's equation.

The numerical solution of such systems is most of the time performed using Particle In Cell (PIC) methods, in which the plasma is approximated by macro-particles (see [4]). They are advanced in time with the electromagnetic fields which are computed on a grid. However, despite their capability to treat complex problems, PIC methods are inherently noisy, which becomes problematic when low density or highly turbulent regions are studied. Hence, numerical methods which discretize the Vlasov equation on a grid of the phase space can offer a good alternative to PIC methods (see [6, 11, 12, 17, 5]). The so-called Eulerian methods can deal with strongly nonlinear processes without additional complexity, and are well suited for parallel computation (see [14]). Moreover, semi-Lagrangian methods which have first been introduced in meteorology (see [16, 18, 19]), try to take advantage of both Lagrangian and Eulerian approaches. Indeed, they allow a relatively accurate description of the phase space using a fixed mesh and avoid traditional step size restriction using the invariance of the distribution function along the trajectories.

Traditional semi-Lagrangian schemes follow the characteristics backward in time. In [7], following the idea of Reich [15], we introduced a forward semi-Lagrangian scheme for the Vlasov-Poisson system based on a forward numerical solution of the characteristics using a classical Verlet or Runge-Kutta (order 2 and 4) scheme. The Verlet scheme can only be applied for specific differential equations, as for example the characteristics of the Vlasov-Poisson system,

but not for more general cases, as the characteristics of the guiding center or the gyrokinetic approximation of the Vlasov equation. Therefore an alternative to Verlet is necessary. On the other hand, Runge-Kutta schemes, which can be used in the general case, are very costly in our context, especially when going to higher order, as they require a deposition of the charge and the solution of the Poisson's equation at intermediate time steps. We propose here, a new scheme for the characteristics based on a Cauchy-Kowalevsky (CK) procedure, that can be performed up to an arbitrary order. Second and third order are developed in the present paper. We shall also discuss the conservation of the first moment for both Verlet and CK algorithms.

A proof of the convergence of PIC method for the Vlasov-Poisson system was performed by Cottet and Raviart [9]. Proofs of convergence and stability of the classical semi-Lagrangian method applied to the same model were obtained by Besse and Mehrenberger [1]. These estimates are made in L^2 norm, since L^∞ seems out of reach as they explain. They manage to do it because they deal with split methods, and thus only consider constant coefficient transport at each split step. In order to prove convergence in more general cases, the L^1 norm seems appropriate, as it enables to use the partition of unity property of the splines. Moreover, Després [10] explains possible advantages of studying L^1 convergence instead of more common L^2 .

We propose here a proof of L^1 convergence of the forward semi-Lagrangian scheme with both Verlet and CK solution of the characteristics in the particular case of linear spline interpolation. We also obtain second order error estimates in time and space.

This paper is organized as follows. In the first part, the continuous problem is presented. In the second part, the discrete problem and the numerical scheme to solve it are explained. We also prove the exact conservation of the first moment with respect to v at the discrete level for both CK and Verlet schemes. Then the convergence of our numerical schemes is proved and finally the schemes are validated and compared on a couple of classical test problems.

4.2 The continuous problem

4.2.1 The Vlasov-Poisson model

Let us consider $f(t, x, v) \geq 0$ the distribution function of positively charged particles in phase-space, and $E(t, x)$ the self consistent electric field. The dimensionless Vlasov-Poisson system reads

$$\frac{\partial f}{\partial t} + v\partial_x f + E(t, x)\partial_v f = 0, \quad (4.1)$$

$$\partial_x E(t, x) = \rho(t, x) = \int_{\mathbb{R}} f(t, x, v) dv - 1, \quad (4.2)$$

where x and v are the phase space independent variables. A periodic plasma of period L is considered. So $x \in [0, L]$, $v \in \mathbb{R}$, $t \geq 0$. The functions f and E are submitted to the following conditions

$$f(t, 0, v) = f(t, L, v), \forall v \in \mathbb{R}, t \geq 0, \quad (4.3)$$

$$E(t, 0) = E(t, L) \Leftrightarrow \frac{1}{L} \int_0^L \int_{\mathbb{R}} f(t, x, v) dv dx = 1, \forall t \geq 0, \quad (4.4)$$

which translates the global neutrality of the plasma. In order to get a well-posed problem, a zero-mean electrostatic condition has to be added, which corresponds to a periodic electric potential:

$$\int_0^L E(t, x) dx = 0, \quad \forall t \geq 0, \quad (4.5)$$

and an initial condition

$$f(0, x, v) = f_0(x, v), \quad \forall x \in [0, L], v \in \mathbb{R}. \quad (4.6)$$

Assuming that the electric field is smooth enough, equations (4.1), (4.3) and (4.6) can be solved in the classical sense as follows.

The first order differential system

$$\begin{aligned} \frac{dX}{dt}(t; (x, v), s) &= V(t; (x, v), s), \\ \frac{dV}{dt}(t; (x, v), s) &= E(t, X(t; (x, v), s)), \end{aligned} \quad (4.7)$$

where $(X(t; (x, v), s), V(t; (x, v), s))$ are the characteristic curves, solutions of (4.7) at time t with the initial condition

$$X(s; (x, v), s) = x, V(s; (x, v), s) = v. \quad (4.8)$$

For the existence, the uniqueness and the regularity of the solutions of this differential system, the reader is referred to [3]. The solution of problem (4.1), (4.6) is then given by

$$f(t, x, v) = f_0(X(0; (x, v), t), V(0; (x, v), t)), \quad \forall x \in [0, L], v \in \mathbb{R}, t \geq 0. \quad (4.9)$$

Since

$$\frac{\partial(X, V)}{\partial(x, v)} = 1,$$

the conservation of particles is ensured for all times:

$$\frac{1}{L} \int_0^L \int_{\mathbb{R}} f(t, x, v) dv dx = \frac{1}{L} \int_0^L \int_{\mathbb{R}} f_0(x, v) dv dx = 1.$$

According to previous considerations, an equivalent form of the Vlasov-Poisson periodic problem is to find (f, E) , smooth enough, periodic with respect to x , with period L , and solving the equations (2.2), (4.7), (4.8) and (4.9). Introducing the electrostatic potential $\varphi \equiv \varphi(t, x)$ such that $E(t, x) = -\partial_x \varphi(t, x)$, and setting $G = G(x, y)$ the fundamental solution of the Laplacian operator in one dimension. That is $-\partial_x^2 G(x, y) = \delta_0(x - y)$ with periodic boundary conditions. It comes

$$E(t, x) = \int_0^L K(x, y) \left(\int_{\mathbb{R}} f(t, y, v) dv - 1 \right) dy,$$

where

$$\begin{aligned} K(x, y) = -\partial_x G(x, y) &= \left(\frac{y}{L} - 1 \right), \quad 0 \leq x < y, \\ &= \frac{y}{L}, \quad y < x \leq L. \end{aligned}$$

4.2.2 Existence, uniqueness and regularity of the solution of the continuous problem

Theorem 8. *Assuming that $f_0 \in W_{c,per_x}^{1,\infty}(\mathbb{R}_x \times \mathbb{R}_v)$ ($W_{c,per_x}^{1,\infty}(\mathbb{R}_x \times \mathbb{R}_v)$ being the Sobolev space of functions with first derivatives in L^∞ , compactly supported in v and periodic in x), positive, periodic with respect to the variable x with period L , and $Q(0) \leq R$, with $R > 0$ defined as follows*

$$Q(t) := 1 + \sup |v| : x \in [0, L], \tau \in [0, t] | f(\tau, x, v) \neq 0,$$

and

$$\frac{1}{L} \int_0^L \int_{\mathbb{R}} f_0(x, v) dv dx = 1,$$

then the periodic Vlasov-Poisson system has a unique classical solution (f, E) , periodic in x , with period L , for all t in $[0, T]$, such that

$$f \in W^{1,\infty}(0, T; W_{c,per_x}^{1,\infty}(\mathbb{R}_x \times \mathbb{R}_v)),$$

$$E \in W^{1,\infty}(0, T; W_{per_x}^{1,\infty}(\mathbb{R})),$$

and there exists a constant $C = C(R, f_0)$ dependent of R and f_0 such that

$$Q(T) \leq CT.$$

Moreover if we assume that $f_0 \in W_{c,per_x}^{m,\infty}(\mathbb{R}_x \times \mathbb{R}_v)$, then $(f, E) \in W^{m,\infty}(0, T; W_{c,per_x}^{m,\infty}(\mathbb{R}_x \times \mathbb{R}_v)) \times W^{1,\infty}(0, T; W_{per_x}^{1,\infty}(\mathbb{R}))$, for all finite time T .

For the proof, the reader is referred to the references [3, 13].

4.3 The discrete problem

4.3.1 Definitions and notations

Let $\Omega = [0, L] \times [-R, R]$, with $R > Q(T)$, and M_h a cartesian mesh of the phase-space Ω . M_h is given by a first increasing sequence $(x_i)_{i \in [0..N_x]}$ of the interval $[0, L]$ and a second one $(v_j)_{j \in [0..N_v]}$ of the interval $[-R, R]$. Let $\Delta x_i = x_{i+1} - x_i$ the physical space cell width and $\Delta v_j = v_{j+1} - v_j$ the velocity space cell width. In order to simplify the study, a regular mesh will be used, i.e $\Delta x_i = \Delta x = \frac{L}{N_x+1}$, and $\Delta v_j = \Delta v = \frac{2R}{N_v}$, where N_x, N_v belong to \mathbb{N} . Then h is defined being $\max(\Delta x, \Delta v)$.

For each function g defined on all the points $(x_i, v_j) \in M_h$ we will set $g_{i,j} := g(x_i, v_j)$, and the sequence is completed on $\mathbb{Z} \times \mathbb{Z}$ by periodicity in x and by 0 in v . The sequence (x_i, v_j) will also be defined on the whole set $\mathbb{Z} \times \mathbb{Z}$, by $x_i := i\Delta x$, and $v_j := -R + j\Delta v$. The set of all L -periodic functions in x and compactly supported in v will be denoted $P(\Omega)$.

Now let $f = (f_{i,j})_{(i,j) \in \mathbb{Z} \times \mathbb{Z}}$ be a continuous grid-function, periodic in the x direction and compactly supported in the v direction, with a support included in $[-R, R]$. If f is a function defined on the points M_h , a discrete grid-function f can be defined by $f_{i,j} := f(x_i, v_j)$ for all

$(i, j) \in [0, N_x] \times [0, N_v]$. In order to lighten notations, f will be kept instead of \tilde{f} . Let $L_h^2(\Omega)$ (resp. $L_h^1(\Omega)$), the set of grid-functions whose $\|\cdot\|_{L_h^2(\Omega)}$ (resp $\|\cdot\|_{L_h^1(\Omega)}$) is bounded

$$\|f\|_{L_h^2(\Omega)} = (\Delta x \Delta v \sum_{i=0}^{N_x} \sum_{j=0}^{N_v} |f_{i,j}|^2)^{\frac{1}{2}},$$

$$\|f\|_{L_h^1(\Omega)} = \Delta x \Delta v \sum_{i=0}^{N_x} \sum_{j=0}^{N_v} |f_{i,j}|.$$

As was precised in the introduction, a L^2 convergence analysis for backward semi-Lagrangian scheme, in the case of a Strang split time advance, was performed in [1]. In paper [7], it is explained that for split methods, where the split steps consist of constant coefficient transport, forward and backward methods are exactly the same. So all the L^2 results exposed in [1] are also valid for our method when time splitting is used. In this paper, we shall consider the convergence of a non split method, and the L^1 norm seems more appropriate for this kind of study.

Remark 2. If $f \in L_h^2(\Omega)$, then $f \in L_h^1(\Omega)$ thanks to the Cauchy Schwarz inequality, as Ω is bounded.

In the sequel, a final time T is fixed, as well as a uniform time discretization $(t^n)_{n \leq N_T}$ of the interval $[0, T]$, with time step $\Delta t = t^{n+1} - t^n$. At each point $(x_i, v_j) \in M_h$, an approximation $f_h(t^n, x_i, v_j)$ of the exact distribution function $f(t^n, x_i, v_j)$ at time $t^n = n\Delta t$ is defined. The approximation function $f_h(t^n)$ is then given at each point of $\mathbb{R}_x \times \mathbb{R}_v$ thanks to an interpolation operator R_h defined on a uniform grid:

$$R_h : L^1(\Omega) \cap P(\Omega) \longrightarrow L^1(\Omega) \cap P(\Omega),$$

$$f \mapsto R_h f = \sum_{(i,j) \in \mathbb{Z} \times \mathbb{Z}} f_{i,j} \Psi_{i,j},$$

where $\Psi_{i,j}$ will be linear spline functions for our study. In numerical results, since linear interpolation is quite diffusive, cubic splines will be used. In order to get a convergent scheme, the operator R_h must satisfy some approximation properties which will be detailed later.

4.3.2 The numerical scheme

The electric field operator for the real-valued function $g \in L^1([0, L] \times \mathbb{R})$ is defined this way:

$$E[g](x) = \int_0^L K(x, y) \left(\int_{\mathbb{R}} g(y, v) dv - 1 \right). \quad (4.10)$$

The approximate function f_h is solution on the grid of the following Vlasov equation:

$$\frac{\partial f_h}{\partial t}(t, x, v) + v \frac{\partial f_h}{\partial x}(t, x, v) + E_h(t, x) \frac{\partial f_h}{\partial v}(t, x, v) = 0.$$

This function follows approximate characteristics, solutions of

$$\begin{aligned}\frac{dX_h}{dt}(t; (x, v), s) &= V_h(t; (x, v), s), \\ \frac{dV_h}{dt}(t; (x, v), s) &= E_h(t, X(t; (x, v), s)),\end{aligned}\tag{4.11}$$

where E_h is defined exactly from f_h using (4.10): $E_h = E[f_h](x)$. So we get:

$$\forall t \in [t^n, t^{n+1}[: f_h(t, x, v) = \sum_{k,l} \omega_{k,l}^n S_h(x - X_h(t; (x_k, v_l), t^n)) S_h(v - V_h(t, (x_k, v_l), t^n)),$$

so that f_h is given on the mesh at time t^n by:

$$f_h(t^n, x_i, v_j) = \sum_{k,l} \omega_{k,l}^n S_h(x_i - x_k) S_h(v_j - v_l) \quad \forall n.$$

These are the interpolation conditions enabling to define f_h everywhere. The computation of $(\omega_{k,l}^n)_{k,l}$ from the grid values amounts to solving a linear system, which is trivial in the case of linear splines, where $\omega_{k,l}^n = f_h(t^n, x_k, v_l)$.

Let us recall that the normalized linear B-spline S , which will be used in this chapter is defined as follows

$$S(x) = \begin{cases} (1 - |x|/h) & \text{if } 0 \leq |x| \leq h, \\ 0 & \text{otherwise.} \end{cases}$$

with $h = \Delta x$ for splines in the x variable and $h = \Delta v$ for splines in the v variable.

The distribution function is updated this way: The ending point of the characteristic starting from (x_i, v_j) is computed: $(X_h(t^{n+1}; (x_i, v_j), t^n), V_h(t^{n+1}; (x_i, v_j), t^n)), \forall (i, j)$. Then, since f_h is constant along the approximate characteristics, the value is deposited on the nearest grid points, the number of which depending on the degree of the splines used for the interpolation. This amounts to computing f_h at time t_{n+1} at the grid points using the following formula.

$$f_h(t^{n+1}, x_i, v_j) = \sum_{k,l} f_h(t^n, x_k, v_l) S(x_i - X_h(t^{n+1}; (x_k, v_l), t^n)) S(v_j - V_h(t^{n+1}; (x_k, v_l), t^n)) \quad \forall (i, j),$$

Note that

$$(X_h(t^{n+1}; (x_i, v_j), t^n), V_h(t^{n+1}; (x_i, v_j), t^n)), \forall (i, j),$$

are computed by a numerical solution of the differential system (4.11). Since this requires an explicit solution of that system, any standard ODE solver such as Verlet, Runge-Kutta or others can be used. Our analysis will be based on the Verlet algorithm, which is second order accurate, and on a Cauchy Kovalevsky procedure, which can be of any order, as an alternative to more costly Runge-Kutta solvers. But we will consider only the second and third order, because higher ones would not increase accuracy in our case, as we will explain.

Verlet algorithm

Starting at time t^n from the grid point (x_k, v_l)

- Step 1: $\forall k, l, x_{k,l}^{n+\frac{1}{2}} - x_k = \frac{\Delta t}{2} v_l,$
- Step 2: compute the electric field at time $t^{n+\frac{1}{2}}$
 - deposition of the particles $x_{k,l}^{n+\frac{1}{2}}$ on the spatial grid x_i for the density ρ_h : $\rho_h(x_i, t^{n+\frac{1}{2}}) = \sum_{k,l} \omega_{k,l}^n S(x_i - x_{k,l}^{n+\frac{1}{2}})$, like in a PIC method.
 - solve the Poisson equation on the grid x_i : $E(x_i, t^{n+\frac{1}{2}})$.
- Step 3: $\forall k, l, v_{k,l}^{n+1} - v_l = \Delta t E(x_{k,l}^{n+\frac{1}{2}}, t^{n+\frac{1}{2}}),$
- Step 4: $\forall k, l, x_{k,l}^{n+1} - x_{k,l}^{n+\frac{1}{2}} = \frac{\Delta t}{2} v_{k,l}^{n+1}.$

This is the way the algorithm is implemented. In our convergence study, the slight difference is that an exact solution of Poisson's equation, based on the Green formula (4.10), is used.

Cauchy Kovalevsky procedure

The idea is to get high order approximations of the characteristics using Taylor expansions in time. And then, using the charge conservation equation, and higher velocity moments of the Vlasov equation, to replace time derivatives with terms containing only spatial derivatives and moments at time t_n which can be easily computed. Up to third order, these Taylor expansions in time lead to

$$\begin{aligned} X^{n+1} &= X^n + \Delta t V^n + \frac{\Delta t^2}{2} E^n(X^n) + \frac{\Delta t^3}{6} \frac{d}{dt} E(X(t), t)|_{t=t^n}. \\ V^{n+1} &= V^n + \Delta t E^n(X^n) + \frac{\Delta t^2}{2} \frac{d}{dt} E(X(t), t)|_{t=t^n} + \frac{\Delta t^3}{6} \frac{d^2}{dt^2} E(X(t), t)|_{t=t^n}. \end{aligned}$$

In order to be able to compute all terms of these expansions, the two first total time derivatives of $E(X(t), t)$ are needed.

$$\begin{aligned} \frac{d}{dt} E(X(t), t) &= \frac{\partial E}{\partial t}(X(t), t) + \frac{dX}{dt}(t) \frac{\partial E}{\partial x}(X(t), t) \\ &= -J(X(t), t) + \bar{J}(t) + V(t) \rho(X(t), t), \end{aligned}$$

where $\rho(x, t) = \int f(x, v, t) dv - 1$, $J(x, t) = \int f(x, v, t) v dv$ and $\bar{J}(t) = \frac{1}{L} \int_0^L J(x, t) dx$. Indeed, the Poisson's equation yields $\frac{\partial E}{\partial x} = \rho$ and integrating the Vlasov equation with respect to velocity, yields the charge conservation equation $\frac{\partial \rho}{\partial t} + \frac{\partial J}{\partial x} = 0$. Hence taking the derivative of the Poisson's equation with respect to time and using this equation we get

$$\frac{\partial}{\partial x} \left(\frac{\partial E}{\partial t} + J \right) = 0.$$

From which we obtain, as $\int_0^L E(x, t) dx = 0$, that

$$\frac{\partial E}{\partial t} = -J + \bar{J}.$$

The second order total derivative in time of E reads

$$\begin{aligned} \frac{d^2}{dt^2} E(X(t), t) &= -\frac{\partial J}{\partial t}(X(t), t) - V(t) \frac{\partial J}{\partial x}(X(t), t) + \frac{d\bar{J}}{dt}(t) \\ &+ E(X(t), t) \rho(X(t), t) + V(t) \left(\frac{\partial \rho}{\partial t}(X(t), t) + V(t) \frac{\partial \rho}{\partial x}(X(t), t) \right). \end{aligned}$$

In order to use this expression, we need $\frac{\partial J}{\partial t}, \frac{\partial J}{\partial x}, \frac{\partial \rho}{\partial t}, \frac{\partial \rho}{\partial x}, \frac{d\bar{J}}{dt}$.

The Cauchy-Kovalevsky procedure consists in getting rid of time derivatives, replacing them with space derivatives obtained from the equation, in our case, we use the velocity moments of the Vlasov equation. First for ρ , we use the charge conservation equation:

$$\frac{\partial \rho}{\partial t}(X(t), t) = -\frac{\partial J}{\partial x}(X(t), t). \quad (4.12)$$

In order to get the time derivative of the current J , we need to use the Vlasov equation, multiply it with v , and integrate it with respect to v , so that we get:

$$\frac{\partial J}{\partial t} + \frac{\partial}{\partial x} I_2 + E \int_{\mathbb{R}} \frac{\partial f}{\partial v} v dv = 0,$$

where $I_n(x, t) = \int_{\mathbb{R}} f(x, v, t) v^n dv$ so that, using that f is compactly supported and integrating by parts:

$$\frac{\partial J}{\partial t}(X(t), t) = -\frac{\partial I_2}{\partial x}(X(t), t) + E(X(t), t)(1 + \rho(X(t), t)). \quad (4.13)$$

Let us prove that $\frac{d\bar{J}}{dt}(t) = 0$

$$\begin{aligned} \frac{d\bar{J}}{dt}(t) &= \frac{1}{L} \int_0^L \frac{\partial J}{\partial t}(t, x) dx \\ &= \frac{1}{L} \int_0^L \left(-\frac{\partial I_2}{\partial x}(t, x) + E(t, x)(1 + \rho(t, x)) \right) dx \\ &= \frac{1}{L} ([I_2(t, 0) - I_2(t, L)] + \int_0^L E(t, x) dx + \int_0^L E(t, x) \rho(t, x) dx) \\ &= \frac{1}{L} [E^2(t, L) - E^2(t, 0)] \\ &= 0. \end{aligned}$$

thanks to periodicity, in fact (4.3), (4.5). We will see later, that numerically this value is also zero.

We finally get the following third order Cauchy Kovalevsky (CK3) time algorithm, using (4.12), (4.13):

$$\begin{aligned} X^{n+1} &= X^n + \Delta t V^n + \frac{\Delta t^2}{2} E^n(X^n) + \frac{\Delta t^3}{6} (V^n \rho^n(X^n) - J^n(X^n) + \bar{J}), \\ V^{n+1} &= V^n + \Delta t E^n(X^n) + \frac{\Delta t^2}{2} (V^n \rho^n(X^n) - J^n(X^n) + \bar{J}) \\ &+ \frac{\Delta t^3}{6} \left(\frac{\partial I_2}{\partial x}(X^n, t^n) - E^n(X^n) - 2V^n \frac{\partial J}{\partial x}(X^n, t^n) + (V^n)^2 \frac{\partial \rho}{\partial x}(X^n, t^n) \right). \end{aligned}$$

Let us now introduce a notation, which will be useful later:

$$X^{n+1} = X^n + \Delta t V^n + \frac{\Delta t^2}{2} E^n(X^n) + \frac{\Delta t^3}{6} \phi^n(X^n, V^n),$$

and

$$V^{n+1} = V^n + \Delta t E^n(X^n) + \frac{\Delta t^2}{2} \phi^n(X^n, V^n) + \frac{\Delta t^3}{6} \varphi^n(X^n, V^n),$$

where ϕ, φ are naturally defined.

Remark 3. Obviously, in order to get a second order algorithm (CK2), we just keep the terms until Δt^2 included.

4.3.3 Exact conservation of number of particles and momentum

B-spline interpolation

First, let us recall some useful properties of B-splines interpolation. The linear space of B-splines of order $m + 1$ writes, denoting by $s^{(m)}$ the m^{th} derivative of s

$$S_{m+1, \Delta x} = \{s(x) \in C^{m-1}(\mathbb{R}), \quad s^{(m+1)}(x) = 0, \forall x \in (x_i, x_{i+1}), \forall i \in \mathbb{R}\},$$

if $m + 1$ is even, and

$$S_{m+1, \Delta x} = \{s(x) \in C^{m-1}(\mathbb{R}), \quad s^{(m+1)}(x) = 0, \forall x \in (x_{i-\frac{1}{2}}, x_{i+\frac{1}{2}}), \forall i \in \mathbb{R}\},$$

if $m + 1$ is odd.

The space of B-spline functions in two dimensions is defined as the tensor product of 1D spaces. Let us precise the interpolation operator:

$$R_{h_{i,j}}(f)(x, v) = \omega_{i,j}(f) S(x - x_i) S(v - v_j),$$

$$R_h f(x, v) = \sum_{i,j} R_{h_{i,j}}(f)(x, v).$$

Now come the properties:

- $\mathbb{S}_{m+1, h} = \text{Span}(S_{m+1}(\cdot - x_i) S_{m+1}(\cdot - v_j); \forall (i, j) \in \mathbb{Z}),$

- $\mathbb{S}_{m+1,h} \subset W^{k,p}$ $1 \leq p \leq \infty$ $0 \leq k \leq m$,
- Stability :

$$\|R_h f\|_{L^p(\Omega)} \leq C \|f\|_{L^p(\Omega)} \quad \forall f \in L^p(\Omega) \cap P(\Omega), \quad 1 \leq p \leq \infty \quad (\text{i}),$$
- Consistency and accuracy:
There exists $C > 0$ | $\|f - R_h f\|_{W^{k,p}(\Omega)} \leq Ch^{m+1-k} \|f\|_{W^{m+1,p}(\Omega)} \quad \forall f \in W^{m+1,p}(\Omega) \cap P(\Omega)$ $1 \leq p \leq \infty$ $0 \leq k \leq m$ (ii),
- $\sum_i S_m(\cdot - x_i) = 1$ (iii), $\int S_m(u) du = h$ (iv).
- $\sum_l v_l S_1(v_l - v) = v$. (v)

For the last item, we will give the proof: Let us suppose $v = v_p + \alpha \Delta v$, $\alpha \in [0, 1[$

$$\begin{aligned} \sum_l v_l S_1(v_l - v) &= v_p S_1(\alpha \Delta v) + v_{p+1} S_1(\Delta v - \alpha \Delta v) \\ &= (p + \alpha \Delta v) \\ &= v \end{aligned}$$

Let us also precise particle and momentum conservation. The proof for the mass is independent from the spline degree, and the one for the first moment will only be shown for linear splines, even though it has been checked for the first three splines.

Particle conservation

The discrete algorithm preserves the total number of particles, as the following computation shows:

$$\begin{aligned} m^{n+1} &= \int f_h(t^{n+1}, x, v) dx dv, \\ &= \sum_{i,j} \omega_{i,j}^{n+1} \int S(x - x_i) S(v - v_j) dx dv, \\ &= \Delta x \Delta v \sum_{i,j} f_h^{n+1}(x_i, v_j), \\ &= \Delta x \Delta v \sum_{i,j} \sum_{k,l} \omega_{k,l}^n S(x_i - X(t^{n+1}; (x_k, v_l), t^n)) S(v_j - V(t^{n+1}; (x_k, v_l), t^n)), \\ &= \Delta x \Delta v \sum_{k,l} \omega_{k,l}^n = \Delta x \Delta v \sum_{i,j} f^n(x_i, v_j) = m^n, \end{aligned}$$

thanks to partition of unity property (iii).

Let us precise the way the interpolation operator acts, in fact:

$$\begin{aligned} f_h(t^{n+1}, x, v) &= R_h \left(\sum_{i,j} \omega_{i,j}^n S(x - X_h(t^{n+1}; (x_i, v_j), t^n)) S(v - V_h(t^{n+1}; (x_i, v_j), t^n)) \right), \\ &= \sum_{i,j} \omega_{i,j}^{n+1} S(x - x_i) S(v - v_j), \end{aligned} \quad (4.14)$$

by definition of $\omega_{i,j}^n$. This implies a kind of continuity of f_h at time t^n on the grid points.

Momentum conservation

Let us precise that in this paragraph $(X_h(t; (x_i, v_j), t^n), V_h(t; (x_i, v_j), t^n))$ will be denoted $(X_{i,j}(t), V_{i,j}(t))$, and that Poisson will not be solved exactly. The aim here is to prove that $\forall n$

$$\sum_{i,j} v_j f_h(t^n, x_i, v_j) = \sum_{i,j} v_j f_h(t^{n+1}, x_i, v_j). \quad (4.15)$$

Let us distinguish two phases: the transport one and the deposition one. Let us start with the deposition phase, where we have to get:

$$\sum_{i,j,k,l} \omega_{i,j}^{n+1} v_l S_1(x_k - x_i) S_1(v_l - v_j) = \sum_{i,j,k,l} \omega_{i,j}^n v_l S_1(x_k - X_{i,j}(t^{n+1})) S_1(v_l - V_{i,j}(t^{n+1}))$$

$$\begin{aligned} \sum_{i,j,k,l} \omega_{i,j}^{n+1} v_l S_1(x_k - x_i) S_1(v_l - v_j) &= \sum_{i,j} \omega_{i,j}^{n+1} \sum_l v_l S_1(v_l - v_j) \\ &= \sum_{i,j} \omega_{i,j}^{n+1} v_j \end{aligned}$$

thanks to the property (v) of linear splines. Moreover

$$\sum_l v_l S_1(v_l - V_{i,j}(t^{n+1})) = V_{i,j}(t^{n+1}),$$

thanks to the same property. So we finally get for the deposition phase:

$$\sum_{i,j} \omega_{i,j}^{n+1} v_j = \sum_{i,j} \omega_{i,j}^n V(t^{n+1}; (x_i, v_j), t^n). \quad (4.16)$$

Remark 4. *This proof is given for linear splines, but was also checked for quadratic and cubic ones. The transport phase is independent from the spline degree.*

There remains to prove that

$$\sum_{i,j} \omega_{i,j}^n v_j = \sum_{i,j} \omega_{i,j}^n V(t^{n+1}; (x_i, v_j), t^n) \quad (4.17)$$

which corresponds to the transport phase. Note that this phase exists also in PIC methods, and the following proof of conservation of moments is adapted from [4].

Verlet We have with our Verlet algorithm:

$$V(t^{n+1}; (x_i, v_j), t^n) = v_j + \Delta t E^{n+\frac{1}{2}}(X(t^{n+\frac{1}{2}}, (x_i, v_j), t^n)). \quad (4.18)$$

The electric field is only known on the mesh. In order to know it everywhere, we use a convolution between a spline function and the discrete E .

$$E^{n+\frac{1}{2}}(X(t^{n+\frac{1}{2}}, (x_i, v_j), t^n)) = \sum_k E^{n+\frac{1}{2}}(x_k) S(x_k - X(t^{n+\frac{1}{2}}, (x_i, v_j), t^n)).$$

To get (4.17) using (4.18) we just have to prove that

$$\sum_{i,j,k} \omega_{i,j}^n E^{n+\frac{1}{2}}(x_k) S(x_k - X(t^{n+\frac{1}{2}}, (x_i, v_j), t^n)) = 0,$$

and

$$\begin{aligned} \sum_{i,j,k} \omega_{i,j}^n E^{n+\frac{1}{2}}(x_k) S(x_k - X(t^{n+\frac{1}{2}}, (x_i, v_j), t^n)) &= \sum_k E^{n+\frac{1}{2}}(x_k) \sum_{i,j} \omega_{i,j}^n S(x_k - X(t^{n+\frac{1}{2}}, (x_i, v_j), t^n)), \\ &= \sum_k E^{n+\frac{1}{2}}(x_k) \rho^{n+\frac{1}{2}}(x_k), \\ &= 0, \end{aligned}$$

for most of the centered algorithms used to solve Poisson numerically, like the following centered finite difference one on staggered mesh, with linear regularization:

$$E^{n+\frac{1}{2}}(x_{k+\frac{1}{2}}) - E^{n+\frac{1}{2}}(x_{k-\frac{1}{2}}) = \Delta x \rho^{n+\frac{1}{2}}(x_k) \quad \forall k,$$

and

$$E^{n+\frac{1}{2}}(x) = \sum_i E^{n+\frac{1}{2}}(x_i) S_1(x - x_i).$$

Indeed, we get:

$$\begin{aligned} \sum_k E^{n+\frac{1}{2}}(x_k) \rho^{n+\frac{1}{2}}(x_k) &= \sum_k \sum_i E^{n+\frac{1}{2}}(x_k) E^{n+\frac{1}{2}}(x_i) ((S_1(x_{k+\frac{1}{2}} - x_i) - S_1(x_{k-\frac{1}{2}} - x_i))), \\ &= \sum_i E^{n+\frac{1}{2}}(x_i) \left(\frac{E^{n+\frac{1}{2}}(x_{i-1}) - E^{n+\frac{1}{2}}(x_{i+1})}{2} \right), \\ &= \frac{1}{2} \left(\sum_i E^{n+\frac{1}{2}}(x_i) E^{n+\frac{1}{2}}(x_{i+1}) - \sum_i E^{n+\frac{1}{2}}(x_i) E^{n+\frac{1}{2}}(x_{i-1}) \right), \\ &= 0, \end{aligned}$$

thanks to periodicity.

To conclude, using (4.16) and (4.17), we get (4.15), which is what was wanted.

CK algorithm. We still have to prove that:

$$\sum_{i,j} \omega_{i,j}^n v_j = \sum_{i,j} \omega_{i,j}^n V(t^{n+1}; (x_i, v_j), t^n)$$

That means for the third order scheme:

$$\begin{aligned} \sum_{i,j} \omega_{i,j}^n E^n(x_i) &= 0 \quad (i) \\ \sum_{i,j} \omega_{i,j}^n \varphi^n(x_i, v_j) &= 0 \quad (ii) \\ \sum_{i,j} \omega_{i,j}^n \phi^n(x_i, v_j) &= 0 \quad (iii) \end{aligned}$$

each number being linked with the order of the algorithm.

First order. Using the same strategy (regularization of the electric field and centered algorithm):

$$\begin{aligned} \sum_{i,j} \omega_{i,j}^n E^n(x_i) &= \sum_{i,j,k,l} \omega_{i,j}^n E^n(x_k) S(x_i - x_k), \\ &= \sum_{k,l} E^n(x_k) \rho^n(x_k) = 0. \end{aligned} \quad (4.19)$$

Second order. For the second order, we need J_i^n, ρ_i^n, \bar{J}

$$\begin{aligned} \rho_i^n &= \Delta v \sum_{k,l} \omega_{k,l}^n S(x_i - x_k) - 1, \\ J_i^n - \bar{J} &= \Delta v \sum_{k,l} \omega_{k,l}^n v_l S(x_i - x_k) - \frac{\Delta x \Delta v}{L} \sum_{k,l} \omega_{k,l}^n v_l, \\ \sum_{i,j} \omega_{i,j}^n v_j \rho^n(x_i) &= \Delta v \sum_{i,j,k,l} \omega_{i,j}^n \omega_{k,l}^n v_j S(x_i - x_k) - \sum_{i,j} \omega_{i,j}^n v_j, \end{aligned} \quad (4.20)$$

$$\begin{aligned} \sum_{i,j} \omega_{i,j}^n J^n(x_i) &= \Delta v \sum_{i,j,k,l} \omega_{i,j}^n \omega_{k,l}^n v_l S(x_i - x_k) - \frac{\Delta x \Delta v}{L} \sum_{i,j,k,l} \omega_{k,l}^n \omega_{i,j}^n v_l, \\ &= \Delta v \sum_{i,j,k,l} \omega_{i,j}^n \omega_{k,l}^n v_j S(x_i - x_k) - \sum_{k,l} \omega_{k,l}^n v_l, \end{aligned} \quad (4.21)$$

using mass conservation and $\sum_{i,j} \omega_{i,j}^0 = L$ (4.20) and (4.21) are the same, just exchanging (i, j) and (k, l) . So

$$\sum_{i,j} \omega_{i,j}^n \varphi^n(x_i, v_j) = 0.$$

Third order. Here we need $I_2^n(x_i)$

$$\begin{aligned}
I_2(t^n, x_i) &= \int_{\mathbb{R}} v^2 \sum_{k,l} \omega_{k,l}^n S(x_k - x_i) S(v - v_l) dv, \\
&= \sum_{k,l} \omega_{k,l}^n S(x_k - x_i) \int_{\mathbb{R}} (v^2 S(v) + 2vv_l S(v) + v_l^2 S(v)) dv, \\
&= \sum_{k,l} \omega_{k,l}^n S(x_k - x_i) (\alpha + \Delta v v_l^2).
\end{aligned}$$

In Φ we still have $\sum_{i,j} \omega_{i,j}^n E^n(x_i) = 0$. We also have three terms in $\frac{\partial}{\partial x}$ which will be approached with a centered finite difference formula:

$$\begin{aligned}
\sum_{i,j} \omega_{i,j}^n \frac{\partial}{\partial x} I_2(t^n, x_i) &= \frac{1}{2\Delta x} \sum_{i,j} \omega_{i,j}^n (I_2(t^n, x_{i+1}) - I_2(t^n, x_{i-1})), \\
&= \frac{1}{2\Delta x} \sum_{i,j,k,l} \omega_{i,j}^n \omega_{k,l}^n (\alpha + v_l^2) (S(x_{i+1} - x_k) - S(x_{i-1} - x_k)), \quad (4.22)
\end{aligned}$$

$$2 \sum_{i,j} \omega_{i,j}^n v_j \frac{\partial J}{\partial x}(t^n, x_i) = \frac{1}{\Delta x} \sum_{i,j,k,l} \omega_{i,j}^n \omega_{k,l}^n v_j v_l (S(x_{i+1} - x_k) - S(x_{i-1} - x_k)), \quad (4.23)$$

$$\sum_{i,j} \omega_{i,j}^n v_j^2 \frac{\partial \rho}{\partial x}(t^n, x_i) = \frac{1}{2\Delta x} \sum_{i,j,k,l} \omega_{i,j}^n \omega_{k,l}^n v_j^2 (S(x_{i+1} - x_k) - S(x_{i-1} - x_k)). \quad (4.24)$$

Adding (4.22), (4.23) and (4.24) and using (4.19) we have:

$$\sum_{i,j} \omega_{i,j}^n \phi^n(x_i) = \frac{1}{\Delta x} \sum_{i,j,k,l} \omega_{i,j}^n \omega_{k,l}^n (\alpha + v_l^2 + 2v_j v_l + v_j^2) (S(x_{i+1} - x_k) - S(x_{i-1} - x_k)),$$

$$\begin{aligned}
\sum_{i,j,k,l} \omega_{i,j}^n \omega_{k,l}^n (\alpha + v_l^2 + 2v_j v_l + v_j^2) S(x_{i+1} - x_k) &= \sum_{i,j,k,l} \omega_{k,l}^n \omega_{i,j}^n (\alpha + v_l^2 + 2v_j v_l + v_j^2) S(x_{k+1} - x_i) \\
&= \sum_{i,j,k,l} \omega_{i,j}^n \omega_{k,l}^n (\alpha + v_l^2 + 2v_j v_l + v_j^2) S(x_k - x_{i-1}),
\end{aligned}$$

just changing (i, j) and (k, l) and $S(x_{k+1} - x_i) = S(x_k - x_{i-1})$. So we get:

$$\sum_{i,j} \omega_{i,j}^n \phi^n(x_i) = 0.$$

Remark 5. We can see that the conservation of the first moment in v implies that numerically $\frac{dJ}{dt} = 0$, which means that $\frac{\Delta x \Delta v}{L} \sum_{i,j} \omega_{i,j}^n v_j$ is constant.

4.4 Convergence analysis

Theorem 9. *Assume that $f_0 \in W_{c,per_x}^{3,\infty}(\mathbb{R}_x \times \mathbb{R}_v)$, positive, periodic with respect to the variable x , with period L , and compactly supported in velocity.*

Then the numerical solution of the Vlasov-Poisson system (f_h, E_h) , computed by the numerical scheme introduced in section 3.2 converges towards the solution (f, E) of the periodic Vlasov-Poisson system, and there exists a constant $C = C(\|f\|_{W^{1,\infty}(0,T;W^{2,\infty}(\Omega))})$ independent of Δt and h such that for Verlet and CK2 algorithms:

$$\|f - f_h\|_{l^\infty(0,T;L^1(\Omega))} + \|E - E_h\|_{l^\infty(0,T;L^\infty([0,L]))} \leq C(\Delta t^2 + h^2 + \frac{h^2}{\Delta t}).$$

For CK3, we have:

$$\|f - f_h\|_{l^\infty(0,T;L^1(\Omega))} + \|E - E_h\|_{l^\infty(0,T;L^\infty([0,L]))} \leq C(\Delta t^3 + h^2 + \frac{h^2}{\Delta t}).$$

Remark 6. *In order to get these estimates for CK, we will have to assume $\Delta t \leq \Delta x$.*

4.4.1 Decomposition of the error

Let f be the exact solution of the Vlasov-Poisson equation and f_h the approximate solution previously defined. In order to apply a discrete Gronwall inequality we express the l^1 error at time t^{n+1}

$$e^{n+1}(i, j) = |f(t^{n+1}, x_i, v_j) - f_h(t^{n+1}, x_i, v_j)| \quad \forall(i, j),$$

$$e^{n+1} = \Delta x \Delta v \sum_{i,j} e^{n+1}(i, j).$$

Then $f(t^{n+1}, x_k, v_l) - f_h(t^{n+1}, x_k, v_l)$ can be decomposed as

$$\begin{aligned} f(t^{n+1}, x_k, v_l) - f_h(t^{n+1}, x_k, v_l) &= f(t^{n+1}, x_k, v_l) - R_h f(t^{n+1}, x_k, v_l) + \\ &R_h f(t^{n+1}, x_k, v_l) - R_h \tilde{f}_h(t^{n+1}, x_k, v_l) + \\ &R_h \tilde{f}_h(t^{n+1}, x_k, v_l) - R_h f_h(t^{n+1}, x_k, v_l), \end{aligned} \quad (4.25)$$

where \tilde{f}_h is the function f_h at time t^n but then follows the exact characteristics. Since f_h^{n+1} already belongs to the image of R_h , we have $R_h f_h(t^{n+1}, x_k, v_l) = f_h(t^{n+1}, x_k, v_l)$.

In order to estimate e^{n+1} , the three terms of the right hand side of the previous equation have to be dealt with. These estimations are developed in the following subsection.

4.4.2 A priori estimates

Stability for linear splines

Let us translate the useful spline properties in this case, and give a few more results about the operator R_h .

Lemma 8. *The R_h operator is consistent, that is, using property (i), for $1 \leq p \leq \infty$, and $0 \leq k \leq 1$*

$$\exists C > 0 \quad | \quad \|f - R_h f\|_{W^{k,p}(\Omega)} \leq Ch^{2-k} \|f\|_{W^{2,p}(\Omega)} \quad \forall f \in W^{2,p}(\Omega) \cap P(\Omega).$$

This result is a classical property of B-splines.

Lemma 9. *With linear splines, if $\omega_{i,j}(f_0) \geq 0 \quad \forall (i,j)$ then $\forall n \quad \omega_{i,j}(f^n) \geq 0 \quad \forall (i,j)$.*

Proof: With linear interpolation, we get in fact $\omega_{i,j}(f^n) = f^n(x_i, v_j)$, so if f_0 is positive, $\omega_{i,j}(f_0)$ is also, and since $f^{n+1}(x_i, v_j)$ is a sum of positive contributions coming from the $f^n(x_k, v_l)$ which are positive by a recurrence hypothesis, it will also be positive, and so $\omega_{i,j}(f^{n+1})$ is positive for all (i,j) , and recurrently for all n .

Lemma 10. *Stability: Let f belong to $C(\Omega) \cap P(\Omega)$, then we have:*

$$\|R_h f\|_{L^1(\Omega)} = \|f\|_{L_h^1(\Omega)}.$$

Proof:

$$\begin{aligned} \|R_h f\|_{L^1(\Omega)} &= \int_0^L \int_{\mathbb{R}} |R_h f(x, v)| \, dv \, dx, \\ &= \int_0^L \int_{\mathbb{R}} \sum_{i,j} \omega_{i,j}(f) S(x - x_i) S(v - v_j), \\ &= \Delta x \Delta v \sum_{i,j} \omega_{i,j}(f), \\ &= \|f\|_{L_h^1(\Omega)}, \end{aligned}$$

using $\int S(x) dx = \Delta x$, the positivity of f thanks to Lemma 9 and the positivity of f_0 .

Towards Gronwall

Let us precise that in this subsection, some lemmas are valid for all the time algorithms we use, and when they are not, the lemmas will be proved in each case successively. For the Cauchy Kovalevsky procedure, the proofs will be done for (CK 3), since their adaptation to lower orders is trivial. We will now give estimates about the three right-hand side terms of the error e^{n+1} (4.25):

Lemma 11. *Let f belong to $C(\Omega) \cap P(\Omega)$, then we have:*

$$\|f - R_h f\|_{L_h^1(\Omega)} \leq Ch^2. \tag{4.26}$$

Proof: Thanks to Lemma 10

$$\begin{aligned} \|f - R_h f\|_{L_h^1(\Omega)} &= \|R_h(f - R_h f)\|_{L^1(\Omega)}, \\ &\leq C \|f - R_h f\|_{L^1(\Omega)}, \\ &\leq C' (\|f\|_{L^\infty(0,T;W^{2,\infty}(\Omega))}) h^2, \end{aligned}$$

thanks to the property (ii) of spline interpolation and the fact that the domain is bounded.

Lemma 12. *Let f belong to $C(\Omega) \cap P(\Omega)$, then we have:*

$$\|R_h f^{n+1} - R_h \tilde{f}_h^{n+1}\|_{L_h^1(\Omega)} \leq e^n. \quad (4.27)$$

Proof: We compute

$$\begin{aligned} \|R_h f^{n+1} - R_h \tilde{f}_h^{n+1}\|_{L_h^1(\Omega)} &= \Delta x \Delta v \sum_{k,l} |(R_h f^{n+1} - R_h \tilde{f}_h^{n+1})(x_k, v_l)|, \\ &= \Delta x \Delta v \sum_{k,l} \left| \sum_{i,j} (f^{n+1}(x_i, v_j) - \tilde{f}_h^{n+1}(x_i, v_j)) S(x_k - x_i) S(v_l - v_j) \right|, \\ &\leq \Delta x \Delta v \sum_{i,j} |\omega_{i,j}(f^n) - \omega_{i,j}(f_h^n)| \sum_{k,l} |S(x_k - X(t^{n+1}; (x_i, v_j), t^n)) S(v_l - V(t^{n+1}; (x_i, v_j), t^n))|, \\ &\leq \Delta x \Delta v \sum_{i,j} |\omega_{i,j}(f^n) - \omega_{i,j}(f_h^n)|, \\ &\leq e^n, \end{aligned}$$

thanks once more to the partition of unity (iii) and $f(x_i, v_j, t^n) = \omega_{i,j}(f^n)$.

Lemma 13. *Let f belong to $C(\Omega) \cap P(\Omega)$, then we have:*

$$\begin{aligned} \|R_h \tilde{f}_h^{n+1} - R_h f_h^{n+1}\|_{L_h^1(\Omega)} &\leq C \max_{i,j} (|X(t^{n+1}; (x_i, v_j), t^n) - X_h(t^{n+1}; (x_i, v_j), t^n)|, \\ &\quad + |V(t^{n+1}; (x_i, v_j), t^n) - V_h(t^{n+1}; (x_i, v_j), t^n)|). \end{aligned} \quad (4.28)$$

Proof:

$$\begin{aligned} \|R_h \tilde{f}_h^{n+1} - R_h f_h^{n+1}\|_{L_h^1(\Omega)} &= \Delta x \Delta v \sum_{k,l} |(R_h \tilde{f}_h^{n+1} - R_h f_h^{n+1})(x_k, v_l)|, \\ &= \Delta x \Delta v \sum_{k,l} \left| \sum_{i,j} \omega_{i,j}(f_h^n) (S(x_k - X(t^{n+1}; (x_i, v_j), t^n)) S(v_l - V(t^{n+1}; (x_i, v_j), t^n)) \right. \\ &\quad \left. - S(x_k - X_h(t^{n+1}; (x_i, v_j), t^n)) S(v_l - V_h(t^{n+1}; (x_i, v_j), t^n))) \right|. \end{aligned}$$

We can rewrite

$$\begin{aligned} &(S(x_k - X(t^{n+1}; (x_i, v_j), t^n)) S(v_l - V(t^{n+1}; (x_i, v_j), t^n)) \\ &\quad - S(x_k - X_h(t^{n+1}; (x_i, v_j), t^n)) S(v_l - V_h(t^{n+1}; (x_i, v_j), t^n))) \\ &= (S(x_k - X(t^{n+1}; (x_i, v_j), t^n)) - S(x_k - X_h(t^{n+1}; (x_i, v_j), t^n))) S(v_l - V(t^{n+1}; (x_i, v_j), t^n)) \\ &\quad - (S(v_l - V(t^{n+1}; (x_i, v_j), t^n)) - S(v_l - V_h(t^{n+1}; (x_i, v_j), t^n))) S(x_k - X_h(t^{n+1}; (x_i, v_j), t^n)). \end{aligned}$$

Then, we use the fact that S_1 is 1-Lipschitzian, compactly supported, and the property (i):

$$\begin{aligned} \sum_{k,l} |(S(x_k - X(t^{n+1}; (x_i, v_j), t^n)) - S(x_k - X_h(t^{n+1}; (x_i, v_j), t^n))) S(v_l - V(t^{n+1}; (x_i, v_j), t^n))| \\ \leq |X(t^{n+1}; (x_i, v_j), t^n) - X_h(t^{n+1}; (x_i, v_j), t^n)|, \end{aligned}$$

and

$$\begin{aligned} \sum_{k,l} |(S(v_l - V(t^{n+1}; (x_i, v_j), t^n)) - S(v_l - V_h(t^{n+1}; (x_i, v_j), t^n)))S(x_k - X_h(t^{n+1}; (x_i, v_j), t^n))| \\ \leq |V(t^{n+1}; (x_i, v_j), t^n) - V_h(t^{n+1}; (x_i, v_j), t^n)|. \end{aligned}$$

So that we get:

$$\begin{aligned} \|R_h \tilde{f}_h^{n+1} - R_h f_h^{n+1}\|_{L_h^1(\Omega)} &\leq \Delta x \Delta v \sum_{i,j} |\omega_{i,j}(f_h^n)| (|X(t^{n+1}; (x_i, v_j), t^n) - X_h(t^{n+1}; (x_i, v_j), t^n)| \\ &\quad + |V(t^{n+1}; (x_i, v_j), t^n) - V_h(t^{n+1}; (x_i, v_j), t^n)|), \\ &\leq C \max_{i,j} (|X(t^{n+1}; (x_i, v_j), t^n) - X_h(t^{n+1}; (x_i, v_j), t^n)| + |V(t^{n+1}; (x_i, v_j), t^n) - V_h(t^{n+1}; (x_i, v_j), t^n)|). \end{aligned}$$

thanks to particle conservation ($\sum_{i,j} \omega_{i,j}(f_h^n) = \sum_{i,j} \omega_{i,j}(f_0)$) and positivity of $\omega_{i,j}(f_h^n)$, where (X, V) are the exact characteristics, solution of the differential system (4.7), and (X_h, V_h) the approximate characteristics defined in (4.11).

To move on, we need another lemma which enables to control the difference between exact and computed characteristics. It clearly depends on the algorithm we use. Let us first give the lemma for the Verlet algorithm.

Lemma 14. : *Verlet*

If $E \in W^{2,\infty}([0, t] \times \mathbb{R})$, and with (X, V) calculated exactly with the differential system (4.7), and (X_h, V_h) computed with E_h and a Verlet algorithm:

$$\begin{aligned} |X(t^{n+1}; (x_i, v_j), t^n) - X_h(t^{n+1}; (x_i, v_j), t^n)| + |V(t^{n+1}; (x_i, v_j), t^n) - V_h(t^{n+1}; (x_i, v_j), t^n)| \\ \leq C \Delta t^3 + \Delta t \|(E - E_h)(t^{n+\frac{1}{2}})\|_{L^\infty}. \end{aligned}$$

Proof: The strategy follows the work of M. Bostan and N. Crouseilles ([2]).

Let us recall how $(x, v)^{n+1}$ is computed from $(x, v)^n$ with the Verlet algorithm

$$\begin{aligned} x^{n+\frac{1}{2}} &= x^n + \frac{\Delta t}{2} v^n, \\ v^{n+1} &= v^n + \Delta t E_h(t^{n+\frac{1}{2}}, x^n + \frac{\Delta t}{2} v^n), \\ x^{n+1} &= x^{n+\frac{1}{2}} + \frac{\Delta t}{2} v^{n+1}. \end{aligned}$$

Then we define $X_h(t^{n+1}, (x^n, v^n), t^n) = x^{n+1}$ and $V_h(t^{n+1}, (x^n, v^n), t^n) = v^{n+1}$.

Let us begin with the characteristics in v :

$$\begin{aligned} (V_h - V)(t^{n+1}; (x^n, v^n), t^n) &= v^n + \Delta t E_h(t^{n+\frac{1}{2}}, x^n + \frac{\Delta t}{2} v^n) - v^n - \int_{t^n}^{t^{n+1}} E(s, X(s; (x^n, v^n), t^n)) ds, \\ &= - \int_{t^n}^{t^{n+1}} (E(s, X(s; (x^n, v^n), t^n)) - E(t^{n+\frac{1}{2}}, X(t^{n+\frac{1}{2}}; (x^n, v^n), t^n))) ds, \\ &\quad - \Delta t (E(t^{n+\frac{1}{2}}, X(t^{n+\frac{1}{2}}; (x^n, v^n), t^n)) - E_h(t^{n+\frac{1}{2}}, x^n + \frac{\Delta t}{2} v^n)). \quad (4.29) \end{aligned}$$

Let us take care of the integral term in (4.29), using a Taylor expansion around $s = t^{n+\frac{1}{2}}$ of $s \mapsto E(s, X(s; (x^n, v^n), t^n))$.

$$\begin{aligned} E(s, X(s; (x^n, v^n), t^n)) &= E(t^{n+\frac{1}{2}}, X(t^{n+\frac{1}{2}}; (x^n, v^n), t^n)) + (s - t^{n+\frac{1}{2}})E'(t^{n+\frac{1}{2}}, X(t^{n+\frac{1}{2}}; (x^n, v^n), t^n)) \\ &\quad + \int_{t^{n+\frac{1}{2}}}^s (s - u)E''(u, X(u; (x^n, v^n), t^n)) du. \end{aligned} \quad (4.30)$$

Let us precise that $E'(s, X(s)) = \frac{d}{ds}E(s, X(s))$, $E''(s, X(s)) = \frac{d}{ds}E'(s, X(s))$. Then using (4.30) in (4.29), we get

$$\begin{aligned} \int_{t^n}^{t^{n+1}} (E(s, X(s; (x^n, v^n), t^n)) - E(t^{n+\frac{1}{2}}, X(t^{n+\frac{1}{2}}; (x^n, v^n), t^n))) ds, \\ = E'(t^{n+\frac{1}{2}}, X(t^{n+\frac{1}{2}}; (x^n, v^n), t^n)) \left[\left(\frac{s - t^{n+\frac{1}{2}}}{2} \right)^2 \right]_{t^n}^{t^{n+1}}, \\ + \int_{t^n}^{t^{n+1}} \int_{t^{n+\frac{1}{2}}}^s (s - u)E''(u, X(u; (x, v), t^n)) du ds. \end{aligned}$$

There are here two terms to control. The first one is zero, and for the second one, we have,

$$\begin{aligned} \left| \int_{t^n}^{t^{n+1}} \int_{t^{n+\frac{1}{2}}}^s (s - u)E''(u, X(u; (x^n, v^n), t^n)) du ds \right| &\leq \|E''\|_{L^\infty} \int_{t^n}^{t^{n+1}} \int_{t^{n+\frac{1}{2}}}^s (s - u) du ds, \\ &\leq \|E''\|_{L^\infty} \int_{t^n}^{t^{n+1}} \left[-\left(\frac{s - u}{2} \right)^2 \right]_{t^{n+\frac{1}{2}}}^s ds, \\ &\leq \frac{1}{2} \|E''\|_{L^\infty} \int_{t^n}^{t^{n+1}} (s - t^{n+\frac{1}{2}})^2 ds, \\ &\leq \frac{\Delta t^3}{24} \|E''\|_{L^\infty} \leq C \|E''\|_{L^\infty} \Delta t^3. \end{aligned} \quad (4.31)$$

Now let us deal with the second term of (4.29). Since E is bounded:

$$\begin{aligned} \left| x^n + \frac{\Delta t}{2} v^n - X(t^{n+\frac{1}{2}}; (x^n, v^n), t^n) \right| &= \left| \int_{t^n}^{t^{n+\frac{1}{2}}} v^n - V(s; (x^n, v^n), t^n) ds \right|, \\ &\leq \int_{t^n}^{t^{n+\frac{1}{2}}} (s - t^n) V'(u; (x^n, v^n), t^n) ds \quad u \in [t^n, s], \\ &\leq C(\|E\|_{L^\infty}) \int_{t^n}^{t^{n+\frac{1}{2}}} (s - t^n) ds \leq C' \Delta t^2. \end{aligned} \quad (4.32)$$

and thus, since E' is bounded, using the zero mean theorem:

$$\begin{aligned} |E(t^{n+\frac{1}{2}}, X(t^{n+\frac{1}{2}}; (x^n, v^n), t^n)) - E(t^{n+\frac{1}{2}}, x^{n+\frac{1}{2}})| &\leq C(\|E'\|_{L^\infty}) |X(t^{n+\frac{1}{2}}; (x^n, v^n), t^n) - x^{n+\frac{1}{2}}|, \\ &\leq C(\|E'\|_{L^\infty}) \Delta t^2. \end{aligned} \quad (4.33)$$

Finally the second term of (4.29) can be controlled by

$$\begin{aligned} |E(t^{n+\frac{1}{2}}, X(t^{n+\frac{1}{2}}; (x^n, v^n), t^n)) - E_h(t^{n+\frac{1}{2}}, x^{n+\frac{1}{2}})| &\leq \|(E - E_h)(t^{n+\frac{1}{2}})\|_\infty \\ &+ |E(t^{n+\frac{1}{2}}, X(t^{n+\frac{1}{2}}; (x^n, v^n), t^n)) - E(t^{n+\frac{1}{2}}, x^{n+\frac{1}{2}})| \end{aligned} \quad (4.34)$$

So, using (4.31), (4.33) and (4.34), we get

$$|(V_h - V)(t^{n+1}; (x, v), t^n)| \leq C\Delta t^3 + \Delta t \|(E - E_h)(t^{n+\frac{1}{2}})\|_{L^\infty(\Omega)}. \quad (4.35)$$

Let us now deal with the characteristics in X :

$$\begin{aligned} (X_h - X)(t^{n+1}; (x^n, v^n), t^n) &= \frac{\Delta t}{2}v^n + \frac{\Delta t}{2}v^{n+1} - \int_{t^n}^{t^{n+1}} V(s; (x^n, v^n), t^n) ds, \\ &= -\Delta t(V(t^{n+\frac{1}{2}}; (x^n, v^n), t^n) - \frac{1}{2}v^n - \frac{1}{2}v^{n+1}), \\ &- \int_{t^n}^{t^{n+1}} (V(s; (x^n, v^n), t^n) - V(t^{n+\frac{1}{2}}; (x^n, v^n), t^n)) ds \end{aligned} \quad (4.36)$$

so once again we have to control two terms.

For the first one, thanks to Taylor's inequality, like for X , it comes:

$$|\int_{t^n}^{t^{n+1}} (V(s; (x^n, v^n), t^n) - V(t^{n+\frac{1}{2}}; (x^n, v^n), t^n)) ds| \leq C(\|E\|_{L^\infty})\Delta t^3. \quad (4.37)$$

Let us precise that this is nothing else than the error in the mid-point rule for numerical integration. Now, the second term in (4.36):

$$\begin{aligned} V(t^{n+\frac{1}{2}}; (x^n, v^n), t^n) &= v^n + \int_{t^n}^{t^{n+\frac{1}{2}}} E(s, X(s; (x^n, v^n), t^n)) ds, \\ &= v^n + \frac{\Delta t}{2}E(t^{n+\frac{1}{2}}, X(t^{n+\frac{1}{2}}; (x^n, v^n), t^n)), \\ &+ \int_{t^n}^{t^{n+\frac{1}{2}}} (E(s, X(s; (x^n, v^n), t^n)) - E(t^{n+\frac{1}{2}}, X(t^{n+\frac{1}{2}}; (x^n, v^n), t^n))) ds, \end{aligned}$$

and

$$|\int_{t^n}^{t^{n+\frac{1}{2}}} (E(s, X(s; (x^n, v^n), t^n)) - E(t^{n+\frac{1}{2}}, X(t^{n+\frac{1}{2}}; (x^n, v^n), t^n))) ds| \leq C(\|E'\|_{L^\infty})\Delta t^2,$$

with the error formula for the rectangle rule. On the other hand

$$\begin{aligned} V(t^{n+\frac{1}{2}}; (x^n, v^n), t^n) - \frac{1}{2}v^n - \frac{1}{2}v^{n+1} &= \frac{1}{2}v^n - \frac{1}{2}v^{n+1} \\ &+ \frac{\Delta t}{2}E(t^{n+\frac{1}{2}}, X(t^{n+\frac{1}{2}}; (x^n, v^n), t^n)) + O(\Delta t^2). \end{aligned}$$

Since

$$\frac{1}{2}(v^n - v^{n+1}) = -\frac{\Delta t}{2}E_h(t^{n+\frac{1}{2}}, x^{n+\frac{1}{2}}),$$

we have, proceeding as for (4.33)-(4.34)

$$\begin{aligned} |V(t^{n+\frac{1}{2}}; (x^n, v^n), t^n) - \frac{1}{2}v^n - \frac{1}{2}v^{n+1}| &= \left| \frac{\Delta t}{2}(E(t^{n+\frac{1}{2}}, X(t^{n+\frac{1}{2}}; (x^n, v^n), t^n)) - E_h(t^{n+\frac{1}{2}}, x^{n+\frac{1}{2}})) \right. \\ &\quad \left. + O(\Delta t^2) \right|, \\ &\leq \frac{\Delta t}{2}(\|(E - E_h)(t^{n+\frac{1}{2}})\|_{L^\infty(\Omega)} + C\Delta t^2). \end{aligned} \quad (4.38)$$

To conclude, using (4.37), (4.38), we have:

$$|(X_h - X)(t^{n+1}; (x, v), t^n)| \leq C\Delta t^3 + C\Delta t^2\|(E - E_h)(t^{n+\frac{1}{2}})\|_{L^\infty(\Omega)}. \quad (4.39)$$

Finally, using (4.35) and (4.39), we get the estimation of Lemma 7, and using (4.28), this also implies

$$\|R_h \tilde{f}_h^{n+1} - R_h f_h^{n+1}\|_{L_h^1(\Omega)} \leq C\Delta t^3 + \Delta t\|(E - E_h)(t^{n+\frac{1}{2}})\|_{L^\infty}.$$

Lemma 15. : CK3

If $E \in W^{4,\infty}([0, t] \times \mathbb{R})$, and with (X, V) calculated exactly with the differential system (4.7), and (X_h, V_h) computed with E_h, ρ_h, J_h and a CK3 algorithm:

$$\begin{aligned} |X(t^{n+1}; (x_i, v_j), t^n) - X_h(t^{n+1}; (x_i, v_j), t^n)| + |V(t^{n+1}; (x_i, v_j), t^n) - V_h(t^{n+1}; (x_i, v_j), t^n)| \\ \leq C\Delta t^4 + C(\Delta t\|(E^n - E_h^n)\|_{l^\infty(\Omega)} + \Delta t^2\|(\phi^n - \phi_h^n)\|_{l^\infty(\Omega)} \\ + \Delta t^3\|(\varphi^n - \varphi_h^n)\|_{l^\infty(\Omega)}). \end{aligned}$$

Proof: This proof just relies on Taylor expansions and computations already made:

$$X(t^{n+1}; (x_i, v_j), t^n) = x_i + \Delta t v_j + \frac{\Delta t^2}{2}E^n(x_i) + \frac{\Delta t^3}{6}\phi^n(x_i, v_j) + O(\Delta t^4),$$

$$X_h(t^{n+1}; (x_i, v_j), t^n) = x_i + \Delta t v_j + \frac{\Delta t^2}{2}E_h^n(x_i) + \frac{\Delta t^3}{6}\phi_h^n(x_i, v_j),$$

and

$$V(t^{n+1}; (x_i, v_j), t^n) = v_j + \Delta t E^n(x_i) + \frac{\Delta t^2}{2}\phi^n(x_i, v_j) + \frac{\Delta t^3}{6}\varphi^n(x_i, v_j) + O(\Delta t^4),$$

$$V_h(t^{n+1}; (x_i, v_j), t^n) = v_j + \Delta t E_h^n(x_i) + \frac{\Delta t^2}{2}\phi_h^n(x_i, v_j) + \frac{\Delta t^3}{6}\varphi_h^n(x_i, v_j),$$

and the lemma follows by simple subtraction.

In both cases we need to control the difference between the exact and approximate fields. Let us begin with Verlet algorithm.

Lemma 16. : *Verlet*

If $E \in W^{2,\infty}([0, t] \times \mathbb{R})$, it comes

$$\|(E - E_h)(t^{n+\frac{1}{2}})\|_{L^\infty(\Omega)} \leq C(h^2 + \Delta t^2 + \Delta t h^2 + e^n)$$

Proof: First

$$E(t^{n+\frac{1}{2}}, x) = \int_0^L K(x, y) \left(\int_{\mathbb{R}} f(t^{n+\frac{1}{2}}, y, v) dv - 1 \right) dy,$$

$$E_h(t^{n+\frac{1}{2}}, x) = \int_0^L K(x, y) \left(\int_{\mathbb{R}} f_h(t^{n+\frac{1}{2}}, y, v) dv - 1 \right) dy.$$

Hence

$$\begin{aligned} E(t^{n+\frac{1}{2}}, x) - E_h(t^{n+\frac{1}{2}}, x) &= \int_0^L K(x, y) \left(\int_{\mathbb{R}} (f(t^{n+\frac{1}{2}}, y, v) - f_h(t^{n+\frac{1}{2}}, y, v)) dv \right) dy, \\ &= \int_0^L K(x, y) \left(\int_{\mathbb{R}} (f(t^{n+\frac{1}{2}}, y, v) - R_h f(t^{n+\frac{1}{2}}, y, v)) dv \right) dy, \\ &+ \int_0^L K(x, y) \left(\int_{\mathbb{R}} (R_h f(t^{n+\frac{1}{2}}, y, v) - \bar{f}(t^{n+\frac{1}{2}}, y, v)) dv \right) dy, \\ &+ \int_0^L K(x, y) \left(\int_{\mathbb{R}} (\bar{f}(t^{n+\frac{1}{2}}, y, v) - \tilde{f}_h(t^{n+\frac{1}{2}}, y, v)) dv \right) dy, \\ &+ \int_0^L K(x, y) \left(\int_{\mathbb{R}} (\tilde{f}_h(t^{n+\frac{1}{2}}, y, v) - f_h(t^{n+\frac{1}{2}}, y, v)) dv \right) dy, \end{aligned} \quad (4.40)$$

where

$$\bar{f}(t^{n+\frac{1}{2}}, y, v) = \sum_{k,l} \omega_{k,l}(f^n) S(y - X(t^{n+\frac{1}{2}}; (x_k, v_l), t^n)) S(v - V(t^{n+\frac{1}{2}}; (x_k, v_l), t^n))$$

and

$$\tilde{f}_h(t^{n+\frac{1}{2}}, y, v) = \sum_{k,l} \omega_{k,l}(f_h^n) S(y - X(t^{n+\frac{1}{2}}; (x_k, v_l), t^n)) S(v - V(t^{n+\frac{1}{2}}; (x_k, v_l), t^n)).$$

In order to lighten notations, $X(t^{n+\frac{1}{2}}; (x_k, v_l), t^n)$ and $V(t^{n+\frac{1}{2}}; (x_k, v_l), t^n)$ will be denoted $X_{k,l}^{n+\frac{1}{2}}$ and $V_{k,l}^{n+\frac{1}{2}}$. We have four terms to control.

The first one is controlled using property (ii) of consistency and accuracy:

$$\left| \int_0^L K(x, y) \left(\int_{\mathbb{R}} (f(t^{n+\frac{1}{2}}, y, v) - R_h f(t^{n+\frac{1}{2}}, y, v)) dv \right) dy \right| \leq C \|K\|_{\infty} h^2. \quad (4.41)$$

Now, the second term of (4.40).

$$\begin{aligned} &\int_0^L K(x, y) \left(\int_{\mathbb{R}} (R_h f(t^{n+\frac{1}{2}}, y, v) - \bar{f}(t^{n+\frac{1}{2}}, y, v)) dv \right) dy, \\ &= \int_0^L K(x, y) \left(\int_{\mathbb{R}} \left(\sum_{k,l} (\omega_{k,l}^{n+\frac{1}{2}} S(y - x_k) S(v - v_l) - \omega_{k,l}^n S(y - X_{k,l}^{n+\frac{1}{2}}) S(v - V_{k,l}^{n+\frac{1}{2}})) \right) dv \right) dy. \end{aligned}$$

We have, using Taylor expansion and Vlasov equation:

$$\begin{aligned}\omega_{k,l}^{n+\frac{1}{2}} &= f^{n+\frac{1}{2}}(x_k, v_l) = f^n(x_k, v_l) + \frac{\Delta t}{2} \frac{\partial f}{\partial t}(x_k, v_l) + O(\Delta t^2), \\ &= f^n(x_k, v_l) - \frac{\Delta t}{2} (v_l \frac{\partial f}{\partial x}(x_k, v_l) + E^n(x_k) \frac{\partial f}{\partial v}(x_k, v_l)) + O(\Delta t^2).\end{aligned}$$

Moreover, since S is piecewise polynomial of degree one and continuous, we have almost everywhere (which is enough as we are going to integrate these expressions)

$$\begin{aligned}S(y - X_{k,l}^{n+\frac{1}{2}}) &= S(y - x_k - \frac{\Delta t}{2} v_l + O(\Delta t^2)) = S(y - x_k) - \frac{\Delta t}{2} v_l S'(y - x_k) + O(\Delta t^2). \\ S(v - V_{k,l}^{n+\frac{1}{2}}) &= S(v - v_l - \frac{\Delta t}{2} E^n(x_k) + O(\Delta t^2)) = S(v - v_l) - \frac{\Delta t}{2} v_l S'(v - v_l) + O(\Delta t^2).\end{aligned}$$

Using, these expansions, we get:

$$\begin{aligned}&\int_0^L K(x, y) \left(\int_{\mathbb{R}} \left(\sum_{k,l} (\omega_{k,l}^{n+\frac{1}{2}} S(y - x_k) S(v - v_l) - \omega_{k,l}^n S(y - X_{k,l}^{n+\frac{1}{2}}) S(v - V_{k,l}^{n+\frac{1}{2}})) \right) dv \right) dy, \\ &= \frac{\Delta t}{2} \left(\int_0^L K(x, y) \left(\int_{\mathbb{R}} \left(\sum_{k,l} v_l S(v - v_l) (f^n(x_k, v_l) S'(y - x_k) - \frac{\partial f^n}{\partial x}(x_k, v_l) S(y - x_k)) \right. \right. \right. \\ &\left. \left. \left. + \sum_{k,l} E^n(x_k) S(y - x_k) (f^n(x_k, v_l) S'(v - v_l) - \frac{\partial f^n}{\partial x}(x_k, v_l) S(v - v_l)) \right) dv \right) dy \right) + O(\Delta t^2). \quad (4.42)\end{aligned}$$

There are two terms in (4.42). They will be dealt with similarly using mid-point quadrature, which is of second order. For the first term, it writes

$$\begin{aligned}&\int_0^L K(x, y) \left(\int_{\mathbb{R}} \left(\sum_{k,l} v_l S(v - v_l) (f^n(x_k, v_l) S'(y - x_k) - \frac{\partial f^n}{\partial x}(x_k, v_l) S(y - x_k)) \right) dv \right) dy, \\ &= \Delta v \sum_{k,l} v_l \int_0^L K(x, y) (f^n(x_k, v_l) S'(y - x_k) - \frac{\partial f^n}{\partial x}(x_k, v_l) S(y - x_k)) dy, \\ &= \Delta v \sum_{i,k,l} (v_l K(x, x_{i+\frac{1}{2}}) (f^n(x_k, v_l) S'(x_{i+\frac{1}{2}} - x_k) - \frac{\partial f^n}{\partial x}(x_k, v_l) S(x_{i+\frac{1}{2}} - x_k))).\end{aligned}$$

Here, we have to use the properties of linear splines. $S'(x_{i+\frac{1}{2}} - x_k)$ and $S(x_{i+\frac{1}{2}} - x_k)$ are non zero only if $k = i$ or $k = i + 1$. Then, we have: $S'(x_{i+\frac{1}{2}} - x_i) = \frac{-1}{\Delta x}$, $S'(x_{i+\frac{1}{2}} - x_{i+1}) = \frac{1}{\Delta x}$ and $S(x_{i+\frac{1}{2}} - x_i) = S(x_{i+\frac{1}{2}} - x_{i+1}) = \frac{1}{2}$. Using that, we get

$$\begin{aligned}&\Delta v \sum_{i,k,l} (v_l K(x, x_{i+\frac{1}{2}}) (f^n(x_k, v_l) S'(x_{i+\frac{1}{2}} - x_k) - \frac{\partial f^n}{\partial x}(x_k, v_l) S(x_{i+\frac{1}{2}} - x_k)), \\ &= \Delta v \sum_{i,l} v_l K(x, x_{i+\frac{1}{2}}) \left(\frac{f^n(x_{i+1}, v_l) - f^n(x_i, v_l)}{\Delta x} - \frac{1}{2} \left(\frac{\partial f^n}{\partial x}(x_i, v_l) + \frac{\partial f^n}{\partial x}(x_{i+1}, v_l) \right) \right).\end{aligned}$$

Using Taylor expansions with respect to x , we easily get:

$$\frac{f(x_{i+1}, v_l) - f(x_i, v_l)}{\Delta x} = \frac{\partial f^n}{\partial x}(x_{i+\frac{1}{2}}, v_l) + O(\Delta x^2).$$

and

$$\frac{1}{2} \left(\frac{\partial f^n}{\partial x}(x_i, v_l) + \frac{\partial f^n}{\partial x}(x_{i+1}, v_l) \right) = \frac{\partial f^n}{\partial x}(x_{i+\frac{1}{2}}, v_l) + O(\Delta x^2),$$

since $f \in W_{c,per_x}^{3,\infty}(\mathbb{R}_x \times \mathbb{R}_v)$. And to conclude for the first term of (4.42):

$$\left| \int_0^L K(x, y) \left(\int_{\mathbb{R}} \sum_{k,l} v_l S(v - v_l) (f^n(x_k, v_l) S'(y - x_k) - \frac{\partial f^n}{\partial x}(x_k, v_l) S(y - x_k)) dv dy \right) \right| \leq C \Delta x^2.$$

For the second term of (4.42), with a mid-point quadrature for the integral with respect to v , and the same properties of splines:

$$\begin{aligned} & \int_0^L K(x, y) \left(\int_{\mathbb{R}} \sum_{k,l} E^n(x_k) S(y - x_k) (f^n(x_k, v_l) S'(v - v_l) - \frac{\partial f^n}{\partial x}(x_k, v_l) S(v - v_l)) dv \right) dy, \\ &= \Delta v \sum_{k,l} E^n(x_k) \int_0^L K(x, y) S(y - x_k) dy \sum_j (f^n(x_k, v_l) S'(v_{j+\frac{1}{2}} - v_l) - \frac{\partial f^n}{\partial x}(x_k, v_l) S(v_{j+\frac{1}{2}} - v_l)), \\ &\leq \Delta x \Delta v \|K\|_{L^\infty} \sum_{k,j} |E^n(x_k)| \left| \frac{f^n(x_k, v_{j+1}) - f^n(x_k, v_j)}{\Delta v} - \frac{1}{2} \left(\frac{\partial f^n}{\partial v}(x_k, v_{j+1}) + \frac{\partial f^n}{\partial v}(x_k, v_j) \right) \right|. \end{aligned}$$

Using again Taylors expansions, with respect to v , we get:

$$\begin{aligned} & \left| \int_0^L K(x, y) \left(\int_{\mathbb{R}} \sum_{k,l} E^n(x_k) S(y - x_k) (f^n(x_k, v_l) S'(v - v_l) - \frac{\partial f^n}{\partial x}(x_k, v_l) S(v - v_l)) dv \right) dy \right|, \\ &\leq \Delta x \Delta v \|K\|_{L^\infty} \sum_{k,j} |E^n(x_k)| \Delta v^2, \\ &\leq C \|E^n\|_{L^\infty([0,L])} \Delta v^2 \leq C' \Delta v^2, \end{aligned}$$

since $E \in W^{2,\infty}([0,t] \times \mathbb{R})$. To conclude, the second term of (4.40) can be bounded like that:

$$\left| \int_0^L K(x, y) \left(\int_{\mathbb{R}} (R_h f(t^{n+\frac{1}{2}}, y, v) - \bar{f}(t^{n+\frac{1}{2}}, y, v)) dv \right) dy \right| \leq C(\Delta t h^2 + \Delta t^2). \quad (4.43)$$

For the third term of (4.40):

$$\begin{aligned} & \left| \int_0^L K(x, y) \left(\int_{\mathbb{R}} (\bar{f}(t^{n+\frac{1}{2}}, y, v) - \tilde{f}_h(t^{n+\frac{1}{2}}, y, v)) dv \right) dy \right|, \\ &= \left| \int_0^L K(x, y) \left(\int_{\mathbb{R}} \sum_{k,l} (\omega_{k,l}(f^n) - \omega_{k,l}(f_h^n)) S(y - X_{k,l}^{n+\frac{1}{2}}) S(v - V_{k,l}^{n+\frac{1}{2}}) dv \right) dy \right|, \\ &\leq \Delta v \sum_{k,l} |\omega_{k,l}(f^n) - \omega_{k,l}(f_h^n)| \int_0^L |K(x, y)| S(y - X_{k,l}^{n+\frac{1}{2}}) dy, \\ &\leq \|K\|_\infty \Delta x \Delta v \sum_{k,l} |f^n(x_k, v_l) - f_h^n(x_k, v_l)| \leq C e^n. \end{aligned} \quad (4.44)$$

Eventually, the last term of (4.40):

$$\begin{aligned}
& \left| \int_0^L K(x, y) \left(\int_{\mathbb{R}} (\tilde{f}_h(t^{n+\frac{1}{2}}, y, v) - f_h(t^{n+\frac{1}{2}}, y, v)) dv \right) dy \right|, \\
& = \left| \int_0^L K(x, y) \left(\int_{\mathbb{R}} \sum_{k,l} \omega_{k,l}(f_h^n) (S(y - X_{k,l}^{n+\frac{1}{2}}) S(v - V_{k,l}^{n+\frac{1}{2}}) - S(y - X_{h;k,l}^{n+\frac{1}{2}}) S(v - V_{h;k,l}^{n+\frac{1}{2}})) dv \right) dy \right|, \\
& \leq \Delta v \sum_{k,l} \omega_{k,l}(f_h^n) \int_0^L K(x, y) (S(y - X_{k,l}^{n+\frac{1}{2}}) - S(y - X_{h;k,l}^{n+\frac{1}{2}})) dy, \\
& \leq \|K\|_{\infty} \Delta x \Delta v \sum_{k,l} \omega_{k,l}(f_h^n) |X_{k,l}^{n+\frac{1}{2}} - X_{h;k,l}^{n+\frac{1}{2}}|, \\
& \leq C \Delta t^2, \tag{4.45}
\end{aligned}$$

using successively the positivity of f_h , mass conservation, f_h is 1-lipschitzian and a result in Lemma 14: (4.32), where obviously, $(X_{h;(k,l)}^{n+\frac{1}{2}}, V_{h;(k,l)}^{n+\frac{1}{2}})$ are the approximate characteristic curves at time $t^{n+\frac{1}{2}}$ beginning at time t^n at (x_k, v_l) .

To conclude, using (4.41), (4.43), (4.44) and (4.45) we get:

$$\|(E - E_h)(t^{n+\frac{1}{2}})\|_{L^\infty(\Omega)} \leq C(h^2 + \Delta t^2 + e^n + \Delta t h^2),$$

which is what was expected.

Lemma 17. *CK3 With the same hypothesis as in Lemma 15, we have :*

$$\|R_h \tilde{f}_h^{n+1} - R_h f_h^{n+1}\|_{L_h^1(\Omega)} \leq C(e^n (\Delta t + \frac{\Delta t^3}{\Delta x^2} + \frac{\Delta t^2}{\Delta x}) + \Delta t h^2 + \Delta t^2 \frac{h^2}{\Delta x} + \Delta t^3 \frac{h^2}{\Delta x^2} + \Delta t^4).$$

Proof: Here, we need to evaluate the difference between the $l^\infty(\Omega)$ norms of the exact and approximate values of ϕ, φ and ψ , so to say the one between:

- E^n and E_h^n , ρ^n and ρ_h^n , J^n and J_h^n ,
- their first spatial derivative and the one of I_2^n and I_{2h}^n .

Let us start with

$$\begin{aligned}
(E^n - E_h^n)(x_i) &= \int_0^L K(x_i, y) \left(\int_{\mathbb{R}} (f(t^n, y, v) - f_h(t^n, y, v)) dv \right) dy, \\
&\leq C(e^n + h^2).
\end{aligned}$$

simply using a quadrature with the mesh points, which will also be of second order thanks to periodicity, and the fact that K is bounded. So that:

$$\|E^n - E_h^n\|_{l^\infty([0,L])} \leq C(e^n + h^2), \tag{4.46}$$

$$\begin{aligned} \|\rho^n - \rho_h^n\|_{L_h^1([0,L])} &= \Delta x \sum_i \left| \int_{\mathbb{R}} (f^n - f_h^n)(x_i, v) dv \right|, \\ &\leq C(e^n + h^2). \end{aligned}$$

So that using the equivalence of discrete norms, carefully noticing that

$$\|\cdot\|_{l^\infty([0,L])} \leq \frac{1}{\Delta x} \|\cdot\|_{L_h^1([0,L])}$$

we get:

$$\begin{aligned} \|\rho^n - \rho_h^n\|_{l^\infty([0,L])} &\leq \frac{1}{\Delta x} \|\rho^n - \rho_h^n\|_{L_h^1([0,L])}, \\ &\leq \frac{C}{\Delta x} (e^n + h^2), \end{aligned}$$

and

$$\begin{aligned} \|J^n - J_h^n\|_{L_h^1([0,L])} &= \Delta x \sum_i \left| \int_{\mathbb{R}} v (f^n - f_h^n)(x_i, v) dv \right|, \\ &\leq C(e^n + h^2), \end{aligned}$$

using the same arguments and the fact that f is compactly supported, so that:

$$\begin{aligned} \|J^n - J_h^n\|_{l^\infty([0,L])} &\leq \frac{1}{\Delta x} \|J^n - J_h^n\|_{L_h^1([0,L])}, \\ &\leq \frac{C}{\Delta x} (e^n + h^2). \end{aligned}$$

Let us precise that the same bound is obviously also valid for \bar{J} . So that we get, still using that Ω is bounded:

$$\|\phi^n - \phi_h^n\|_{l^\infty([0,L])} \leq \frac{C}{\Delta x} (e^n + h^2).$$

For the first spatial derivative of these three terms, we can use the same strategy of finite difference. Let us do it with E .

$$\frac{\partial(E - E_h)}{\partial x}(t^n, x_i) = \frac{(E_{i+1}^n - E_{i+1,h}^n) - (E_{i-1}^n - E_{i-1,h}^n)}{2\Delta x} + O(\Delta x^2),$$

so that using (4.46) we get:

$$\left\| \frac{\partial(E - E_h)}{\partial x}(t^n) \right\|_{l^\infty([0,L])} \leq \frac{C}{\Delta x} (e^n + h^2).$$

For ρ^n , J^n and for I_2^n just bounding v, v^2 in its integral definition, the same strategy leads to

$$\|\varphi^n - \varphi_h^n\|_{l^\infty([0,L])} \leq \frac{C}{\Delta x^2} (e^n + h^2).$$

Plugging these estimates into Lemma 15 and then Lemma 13 completes the proof.

4.4.3 End of the proof

For the sake of simplicity, and since we are interested in $\Delta t, \Delta x$ tend to 0, we will assume $\Delta t \leq 1$. We can now apply Gronwall inequality since

Verlet For Verlet, using Lemmas 11, 12, 14, 16, we get,

$$\begin{aligned} e^{n+1} &\leq C(h^2 + \Delta t^3 + (\Delta t^2 + \Delta t)(h^2 + h^2 \Delta t \Delta t^2 + e^n)) + e^n, \\ &\leq (1 + C\Delta t)e^n + C(h^2 + \Delta t^3 + (\Delta t^2 + \Delta t)(h^2 + \Delta t^2)), \end{aligned}$$

So that

$$e^n \leq \exp(C'T)e^0 + C(h^2 + \Delta t^2 + \frac{h^2}{\Delta t}),$$

which is what was expected. Taking $\Delta t = Ch^\alpha$, we find the best global order with $\alpha = \frac{2}{3}$ being $\frac{4}{3}$.

CK2 For CK2, using Lemmas 11, 12, 15, 17, we get

$$\begin{aligned} e^{n+1} &\leq C(h^2 + \Delta t^3 + (\frac{\Delta t^2}{\Delta x} + \Delta t)(h^2 + e^n)) + e^n, \\ &\leq (1 + C(\Delta t + \frac{\Delta t^2}{\Delta x}))e^n + C(h^2 + \Delta t^3 + \Delta t h^2 + \frac{\Delta t^2}{\Delta x} h^2), \end{aligned}$$

Here, assuming $\Delta t \leq \Delta x$, we have :

$$e^n \leq \exp(C'T)e^0 + C(h^2 + \Delta t^2 + \frac{h^2}{\Delta t}),$$

If you want to look for the best global order here, you find the same result as in Verlet, nevertheless, this cannot fit with the other assumption $\Delta t \leq \Delta x$. Therefore, the only way is to take $\Delta t = \Delta x$, and the global order is 1.

CK3 For CK3, using the same lemmas as for CK2:

$$\begin{aligned} e^{n+1} &\leq C(h^2 + \Delta t^4 + e^n(\Delta t + \frac{\Delta t^2}{\Delta x} + \frac{\Delta t^3}{\Delta x^2}) + \Delta t h^2 + \Delta t^2 \frac{h^2}{\Delta x} + \Delta t^3 \frac{h^2}{\Delta x^2}) + e^n, \\ &\leq e^n(1 + C(\Delta t + \frac{\Delta t^2}{\Delta x} + \frac{\Delta t^3}{\Delta x^2})) + C(h^2 + \Delta t h^2 + \frac{\Delta t^2}{\Delta x} h^2 + \frac{\Delta t^3}{\Delta x^2} h^2 + \Delta t^4). \end{aligned}$$

Assuming again $\Delta t \leq \Delta x$, we have

$$e^n \leq \exp(C'T)e^0 + C(\Delta t^3 + h^2 + \frac{h^2}{\Delta t}).$$

The same remark as with CK2 is still valid. We can see that we are limited because of the terms $\frac{h^2}{\Delta t}$ and $\frac{\Delta t}{\Delta x}$. In order to be able to reach higher orders, we would have to use splines of superior degrees $m > 1$ to get terms in $\frac{h^{m+1}}{\Delta t}$ like in the other proofs of convergence, for example: ([1, 2])

4.5 Numerical results

In order to validate our new schemes, we have tested them on two standard test cases of plasma physics, the two stream instability and the bump on tail instability. We also compared them to the classical and knowledgeably robust Verlet scheme. Notice that because of the diffusivity of linear splines, we have used cubic splines for the distribution function.

For the two stream instability, the initial condition is given by

$$f_0(x, v) = \frac{1}{\sqrt{2\pi}} e^{-v^2/2} v^2 [1 - \alpha \cos(kx)],$$

with $k = 0.2$ and $\alpha = 0.05$. The computational domain is $[0, 2\pi/k] \times [-9, 9]$ which is sampled by $N_x = N_v = 128$ points. We used a time step $\Delta t = 0.1$ in the results of the left hand side of Figure 4.5.1 and of $\Delta t = 0.3$ on the right-hand side of the figure. We display the L^2 norm which reveals the dissipation of the scheme, the total momentum and the total energy. All of those are conserved in the continuous Vlasov-Poisson system. We do not display the number of particles which is conserved with an even better accuracy than the momentum. The momentum is exactly conserved by the scheme and up to about 10^{-13} in the simulation. This is due to roundoff errors and the truncation of the velocity space. The L^2 norm cannot be exactly conserved by any scheme using a phase space grid as soon as the grid does not resolve anymore the filaments. The Verlet scheme is our reference scheme here, and we observe that the results obtained with the CK schemes are very close, especially for the smallest time step. Moreover conservation properties are better for the third order CK3 than for the second order CK2.

For the bump-on-tail instability test case the initial condition writes

$$f_0(x, v) = \tilde{f}(v)[1 + \alpha \cos(kx)],$$

with

$$\tilde{f}(v) = n_p \exp(-v^2/2) + n_b \exp\left(-\frac{|v-u|^2}{2v_t^2}\right)$$

on the interval $[0, 20\pi]$, with periodic conditions in space. The initial condition f_0 is a Maxwellian distribution function which has a bump on the Maxwell distribution tail; the parameters of this bump are the following

$$n_p = \frac{9}{10(2\pi)^{1/2}}, n_b = \frac{2}{10(2\pi)^{1/2}}, u = 4.5, v_t = 0.5,$$

whereas the numerical parameters are $N_x = 128, N_v = 128, v_{max} = 9, \Delta t = 0.2$. The results are displayed in Figure 4.5.2. Here the momentum does not vanish, so that the results are not polluted by roundoff errors and the momentum is exactly conserved. The conclusion for the L^2 norm and the total energy is the same as in the Two Stream Instability test case. The potential or electric energy is a classical diagnostic for the bump on tail instability. The oscillations go on for a long time with all three time schemes, even though there is a slight energy increase for the CK2 scheme.

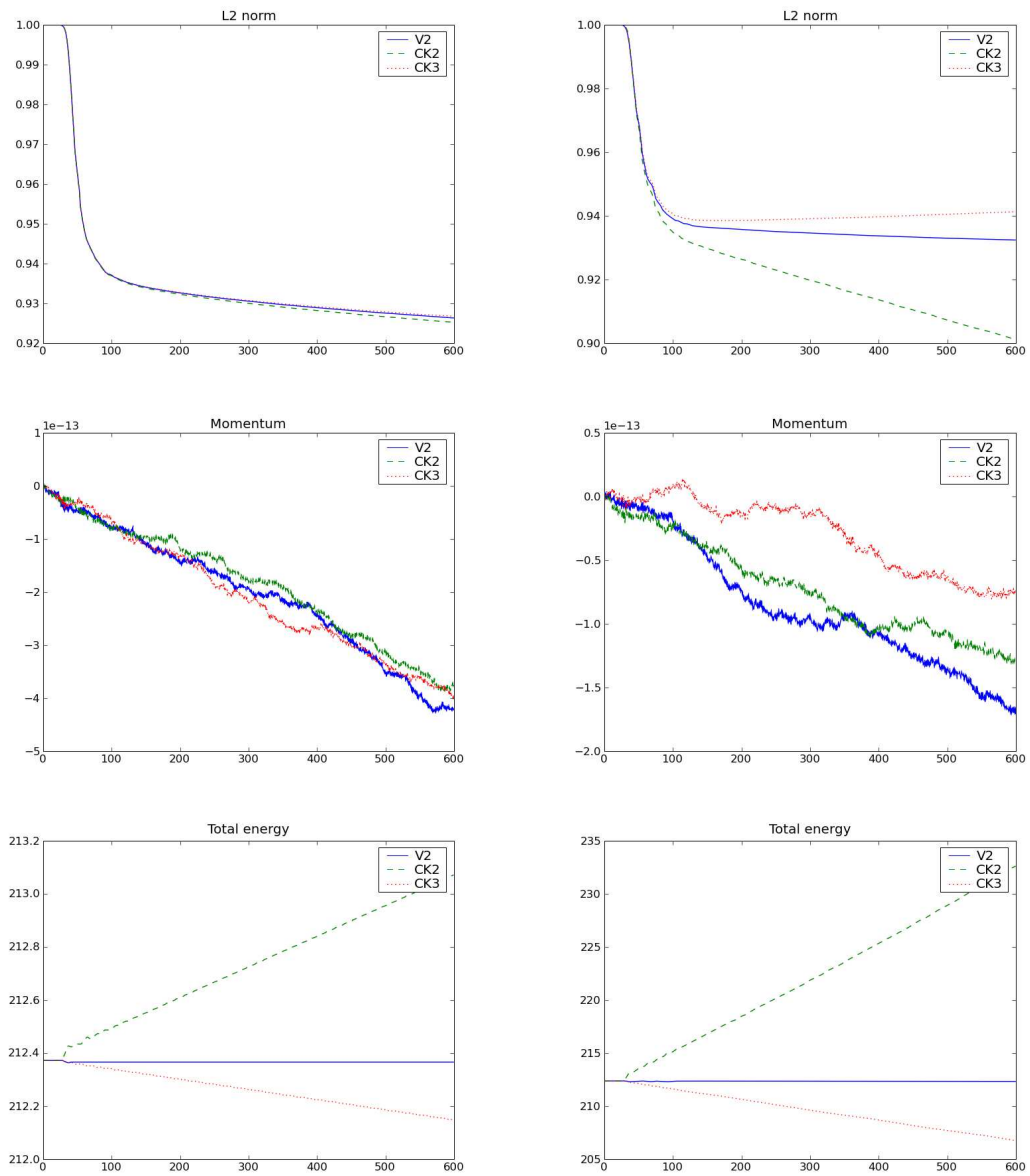


Figure 4.5.1: Two stream instability:

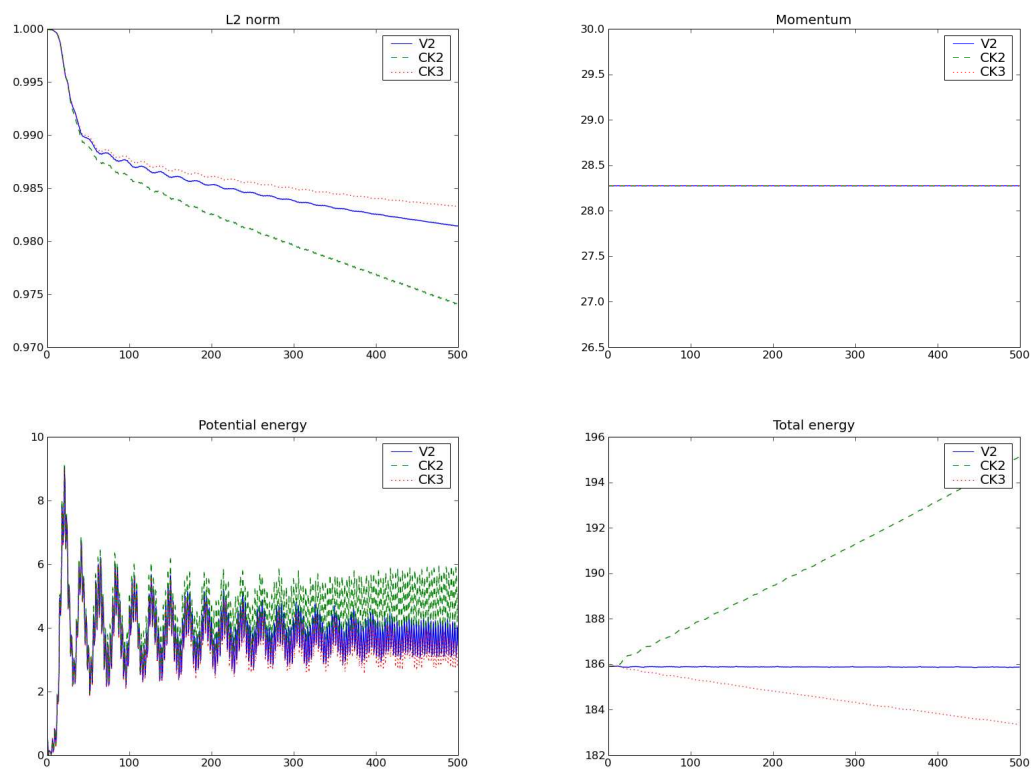


Figure 4.5.2: Bump on tail

4.6 Conclusion

In this paper, the proof of a L^1 convergence has been reached for linear spline interpolation. The originality, except from the choice of the L^1 norm is that the convergence has been reached for a non split method. In this paper, the computation of the characteristics has been made with the Verlet algorithm, or with a CK procedure, but the proof can be adapted to other algorithms such as Runge Kutta of any order. There remains for the moment some problems using splines of higher orders, especially concerning stability. This prevents us from reaching real high order algorithms. Numerical experiments that can be seen in [7], and confirmed here seem to prove that the method is also stable and convergent for cubic splines. Nevertheless, there remains a problem to preserve the l^1 norm of the coefficients $\omega_{i,j}$, since some of them can become non positive in the solving of the linear system with splines of degree higher than 2. Another way of tackling the problem will probably be needed.

Bibliography

- [1] N. BESSE, M. MEHRENBERGER, *Convergence of classes of high order semi-Lagrangian schemes for the Vlasov-Poisson system*, Math. Comput., **77**, pp. 93-123, (2008).
- [2] M. BOSTAN, N. CROUSEILLES, *Convergence of a semi-Lagrangian scheme for the reduced Vlasov-Maxwell system for laser-plasma interaction*, Numer. Math. (2009)
- [3] F. BOUCHUT, F. GOLSE, M. PULVIRENTI, *Kinetic equations and asymptotic theory*, Series in applied Math. P.G Ciarlet and P.L Lions (Eds) Gauthier Villars (2008)
- [4] C.K. BIRDSALL, A.B. LANGDON, *Plasma Physics via Computer Simulation*, Inst. of Phys. Publishing, Bristol/Philadelphia, 1991.
- [5] J.-A. CARILLO, F. VECIL, *Non oscillatory interpolation methods applied to Vlasov-based models*, SIAM Journal of Sc. Comput. **29**, pp. 1179-1206, (2007).
- [6] C. Z. CHENG, G. KNORR, *The integration of the Vlasov equation in configuration space*, J. Comput. Phys, **22**, pp. 330-3351, (1976).
- [7] N. CROUSEILLES, T. RESPAUD, E. SONNENDRUCKER, *A forward semi-Lagrangian method for the numerical solution of the Vlasov equation*, Comput. Phys. Comm., **180** (10), pp. 1730–1745, (2009)
- [8] C.J. COTTER, J. FRANK, S. REICH *The remapped particle-mesh semi-Lagrangian advection scheme*, Q. J. Meteorol. Soc., **133**, pp. 251-260, (2007)
- [9] G.-H COTTET, P.-A RAVIART, *Particle methods for the one-dimensional Vlasov-Poisson equations*, Siam J. Numer. anal. **21**, pp. 52-75, (1984)
- [10] B. DESPRÉS, *Finite volume transport Schemes*, Numerische Mathematik **108**, pp.529-556, (2008).
- [11] F. FILBET, E. SONNENDRÜCKER, P. BERTRAND, *Conservative numerical schemes for the Vlasov equation*, J. Comput. Phys., **172**, pp. 166-187, (2001).
- [12] F. FILBET, E. SONNENDRÜCKER, *Comparison of Eulerian Vlasov solvers*, Comput. Phys. Comm., **151**, pp. 247-266, (2003).
- [13] R.T GLASSEY, *The Cauchy problem in kinetic theory* SIAM, Philadelphia (1996)

- [14] V. GRANDGIRARD, M. BRUNETTI, P. BERTRAND, N. BESSE, X. GARBET, P. GHENDRIH, G. MANFREDI, Y. SARRAZIN, O. SAUTER, E. SONNENDRÜCKER, J. VACLAVIK, L. VILLARD, *A drift-kinetic semi-Lagrangian 4D code for ion turbulence simulation*, J. Comput. Phys., **217**, pp. 395-423, (2006).
- [15] S. REICH, *An explicit and conservative remapping strategy for semi-Lagrangian advection*, Atmospheric Science Letters **8**, pp. 58-63, (2007).
- [16] A. STANIFORTH, J. COTÉ, *Semi-Lagrangian integration schemes for atmospheric models - A review*, Mon. Weather Rev. **119**, pp. 2206-2223, (1991).
- [17] E. SONNENDRÜCKER, J. ROCHE, P. BERTRAND, A. GHIZZO *The semi-Lagrangian method for the numerical resolution of the Vlasov equation*, J. Comput. Phys., **149**, pp. 201-220, (1999).
- [18] M. ZERROUKAT, N. WOOD, A. STANIFORTH, *A monotonic and positive-definite filter for a Semi-Lagrangian Inherently Conserving and Efficient (SLICE) scheme*, Q.J.R. Meteorol. Soc., **131**, pp 2923-2936, (2005).
- [19] M. ZERROUKAT, N. WOOD, A. STANIFORTH, *The Parabolic Spline Method (PSM) for conservative transport problems*, Int. J. Numer. Meth. Fluids, **51**, pp. 1297-1318, (2006).

A charge preserving scheme for the numerical resolution of the Vlasov-Ampère equations.

5.1 Introduction

In order to describe the dynamics of charged particles in a plasma or in a propagated beam, the Vlasov equation can be used to calculate the response of the plasma to the electromagnetic fields. The unknown $f(t, x, v)$ which depends on the time t , the space x and the velocity v represents the distribution function of the studied particles. The coupling with the self-consistent electromagnetic fields is taken into account through the Maxwell's equations.

The numerical solution of such systems is most of the time performed using Particle In Cell (PIC) methods, in which the plasma is approximated by macro-particles (see [4]). They are advanced in time with the electromagnetic fields which are computed on a grid. However, despite their capability to treat complex problems, PIC methods are inherently noisy. This becomes problematic when low density or highly turbulent regions are studied. Hence, numerical methods which discretize the Vlasov equation on a grid of the phase space can offer a good alternative to PIC methods (see [8, 17, 18, 34, 7, 13, 28]).

An important issue for electromagnetic PIC or Vlasov solvers in which the fields are computed through the Maxwell's equations, is the problem of discrete charge conservation. The electric and magnetic fields via Ampère and Faraday's equations have to be computed in such a way that it satisfies a discrete Gauss law at each time step. Indeed, the charge and current densities computed from the particles (for PIC methods) or from f (for Vlasov methods) do not verify the continuity equation so that the Maxwell's equations with these sources might be ill-posed.

Two main issues have been explored in the literature, mainly in the PIC context. The first one consists in modifying the inconsistent electric field resulting from an ill-posed Maxwell solver (see [25, 26]). In the second approach, the current is computed in a specific way so as to enforce a discrete continuity equation (see [36, 1, 16, 35]). The second class of methods has the advantage

of being local and does not modify the electromagnetic field away from the source, which can generate errors in some applications.

More recently, Sircombe and Arber managed to create a 4D Vlasov-Maxwell charge preserving scheme using a split Eulerian approach (VALIS code described in [30]). They take full benefits of conservative methods by computing the current using the fluxes in space after each spatial advection. In addition to some specific properties that can be controlled through filters (positivity, monotonicity), conservative methods applied to multidimensional problems can be solved through the succession of unidimensional problems thanks to a directional splitting. Thus, conservative methods have proven very efficient for the solving of transport equations (for details see [10, 17, 18, 38, 9]). In this work, we also deal with a phase space grid to simulate the Vlasov equation, but using the Forward semi-Lagrangian method (FSL detailed in [11]) ; as explained in [11], since FSL bears similarities with PIC methods, we shall extend the approach of [36, 1, 14] to our FSL context. In a few words, the time-dependent current is averaged over the one-step trajectory of the particles (which correspond to the grid points in FSL).

The FSL approach has been developed on a cubic B-splines reconstruction. Different time algorithms are proposed to solve the characteristics of the Vlasov equations: Runge-Kutta or Cauchy-Kovaleskaya algorithms. As explained in [11] the main advantages of the FSL method are : *(i)* it is conservative (thanks to the partition of the unity), *(ii)* it can be easily extended to arbitrary high order time algorithms in its unsplit form (using CK algorithms), and *(iii)* it is equivalent to the BSL counterpart when 1D constant advectations are considered.

The coupling of FSL with charge preserving algorithms is the main goal of this work. We focus on the 1D Vlasov-Ampère and quasi-relativistic Vlasov-Maxwell models to show the feasibility and the advantages of the approach. The extension to the 2D Vlasov-Maxwell case will be the object of a future work in which we hope to present an alternative approach to the VALIS one presented in [30]. Here, we will see that if a discrete charge conservation is ensured and if the Poisson's equation is satisfied initially, then the electric field computed by the Ampère's equation automatically obeys the finite difference version of the Poisson's equation to machine precision without solving it. The key point is the computation of the current. For a given time computation of the characteristics (RK, CK), a numerical integration of the time-dependent current over the affine approximation of the characteristics is done. Since cubic B-splines are used, the current is polynomial of degree 3 so that a numerical integration using a Gaussian quadrature is exact. We are then able to prove that the so-computed current: *(i)* satisfies the continuity equation and *(ii)* generates (through the Ampère's equation) an electric field compatible with Poisson (without solving it). We then observe on numerical results that for a given time algorithms in FSL, the solution of the charge preserving scheme for the Vlasov-Ampère equation is equivalent to the solution of the Vlasov-Poisson equation. This is a first step towards more realistic 4D Vlasov-Maxwell simulations.

This paper is organized as follows. In the first part, the continuous problems of Vlasov-Poisson, Vlasov-Ampère and quasi-relativistic (QR) Vlasov-Maxwell 1D are presented. In the second part, the associated discrete problems and the numerical schemes to solve them are explained. Then, the charge preserving method will be detailed. Finally, numerical results will be displayed, especially a test case about 1D quasi relativistic Vlasov-Maxwell.

5.2 The continuous problem

5.2.1 The Vlasov-Ampère and Vlasov-Poisson models

Let us consider $f(t, x, v) \geq 0$ being the distribution function of electrons in phase-space, and $E(t, x)$ the self consistent electric field. We shall also consider an initially neutralizing population of immobile ions, in order to ensure the global neutrality of the plasma. Nevertheless, only the population of electrons will be taken care of in this work. The dimensionless periodical Vlasov-Ampère (resp. Poisson) system for this population of electrons reads:

$$\partial_t f + v \partial_x f + E(t, x) \partial_v f = 0, \quad (5.1)$$

$$\partial_t E(t, x) = -J(t, x) + \bar{J}(t) = - \int_{\mathbb{R}} v f(t, x, v) dv + \frac{1}{L} \int_0^L J(t, x) dx,$$

(resp.)

$$\partial_x E(t, x) = \rho(t, x) = \int_{\mathbb{R}} f(t, x, v) dv - 1, \quad (5.2)$$

where x and v are the phase space independent variables. Continuously, these two models are equivalent under the charge conservation condition:

$$\partial_t \rho(t, x) + \partial_x J(t, x) = 0. \quad (5.3)$$

A periodic plasma is considered, of period L so that $x \in [0, L]$, $v \in \mathbb{R}$, $t \geq 0$. The functions f and E are submitted to the following conditions:

$$f(t, 0, v) = f(t, L, v), \quad \forall v \in \mathbb{R}, \quad t \geq 0, \quad f(t, 0, v) = f(t, L, v),$$

$$E(t, 0) = E(t, L) \Leftrightarrow \frac{1}{L} \int_0^L \int_{\mathbb{R}} f(t, x, v) dv dx = 1, \quad \forall t \geq 0, \quad (5.4)$$

which translate the global neutrality of the plasma. In order to get a well-posed problem, a zero-mean electrostatic condition has to be added, which corresponds to a periodic electric potential:

$$\int_0^L E(t, x) dx = 0, \quad \forall t \geq 0, \quad (5.5)$$

and an initial condition:

$$f(0, x, v) = f_0(x, v), \quad \forall x \in [0, L], v \in \mathbb{R}. \quad (5.6)$$

Assuming that the electric field is smooth enough, equations (5.1), (5.2) and (5.4) can be solved in the classical sense as follows. For the existence, the uniqueness and the regularity of the solutions of the following differential system, the reader is referred to [5].

The motion of the particles is solved through the following first order differential system

$$\begin{aligned} \frac{dX}{dt}(t; (x, v), s) &= V(t; (x, v), s), \\ \frac{dV}{dt}(t; (x, v), s) &= E(t, X(t; (x, v), s)), \end{aligned} \quad (5.7)$$

where $(X(t; (x, v), s), V(t; (x, v), s))$ are the characteristic curves at time t which value at time s was (x, v) . These characteristics are the solutions of (5.7) at time t with the initial conditions:

$$X(s; (x, v), s) = x, \quad V(s; (x, v), s) = v. \quad (5.8)$$

The solution of problem (5.1), (5.4) is given by

$$f(t, x, v) = f_0(X(0; (x, v), t), V(0; (x, v), t)), \quad \forall x \in [0, L], v \in \mathbb{R}, t \geq 0. \quad (5.9)$$

Since $\partial(X, V)/\partial(x, v) = 1$, it follows

$$\frac{1}{L} \int_0^L \int_{\mathbb{R}} f(t, x, v) dv dx = \frac{1}{L} \int_0^L \int_{\mathbb{R}} f_0(x, v) dv dx = 1.$$

According to previous considerations, an equivalent form of the periodic Vlasov-Poisson problem is to find (f, E) , smooth enough, periodic with respect to x , with period L , and to solve the equations (5.2), (5.7), (5.8) and (5.9).

Introducing the electrostatic potential $\varphi = \varphi(t, x)$ such that $E(t, x) = -\partial_x \varphi(t, x)$, and setting $G = G(x, y)$ the fundamental solution of the Laplacian operator in one dimension, that is $-\partial_x^2 G(x, y) = \delta_0(x - y)$ with periodic boundary conditions, it comes

$$E(t, x) = \int_0^L K(x, y) \left(\int_{\mathbb{R}} f(t, y, v) dv - 1 \right) dy,$$

where

$$K(x, y) = -\partial_x G(x, y) = \begin{cases} y/L - 1, & \text{if } 0 \leq x < y, \\ y/L, & \text{if } y < x \leq L. \end{cases}$$

5.2.2 The quasi-relativistic Vlasov-Maxwell model

This model describes the motion of the electrons in the laser-plasma interaction context and has been recently introduced in the literature by the physicists [22]. To derive such a model, the key points are the following: starting from the Vlasov-Maxwell equations in one dimension in space (called x), and three dimensions in momentum, we make the assumption that the motions of interest are faster along the direction of propagation of the laser than in the associated transversal directions. Then, it is reasonable to consider that the electrons are monokinetic in the directions transversal to x . The derivation of this model is clearly explained in [3]. We also refer the reader to [20, 24, 19, 2] for more details. In particular, for the normalizations and the mathematical study, see [6]. After some computations (see [3]) one gets the QR 1D Vlasov-Maxwell system:

$$\frac{\partial f}{\partial t} + v(p) \frac{\partial f}{\partial x} + \left(E_x - \frac{\partial(|A|^2/2)}{\partial x} \right) \frac{\partial f}{\partial p} = 0,$$

where $v(p) = \frac{p}{\gamma(p)}$, $\gamma(p) = (1 + p^2)^{\frac{1}{2}}$ being the QR Lorentz factor, and $A = (0, A_y, A_z)$ being the vector potential.

Remark: In [3], the two other models (Non Relativistic and Full Relativistic) are also presented.

The Vlasov equation has to be coupled with the following 1D Maxwell's equations:

$$\begin{aligned}\frac{\partial E_y(t, x)}{\partial t} &= -\frac{\partial B_z(t, x)}{\partial x} + A_y(t, x)\rho_\gamma(t, x), \\ \frac{\partial E_z(t, x)}{\partial t} &= \frac{\partial B_y(t, x)}{\partial x} + A_z(t, x)\rho_\gamma(t, x).\end{aligned}$$

Note that $\rho_\gamma = \rho$ in the QR case.

$$\begin{aligned}\frac{\partial B_y(t, x)}{\partial t} &= \frac{\partial E_z(t, x)}{\partial x}, \\ \frac{\partial B_z(t, x)}{\partial t} &= -\frac{\partial E_y(t, x)}{\partial x}.\end{aligned}$$

The components of the vector potential are then computed:

$$\begin{aligned}\frac{\partial A_y(t, x)}{\partial t} &= -E_y(t, x), \\ \frac{\partial A_z(t, x)}{\partial t} &= -E_z(t, x).\end{aligned}$$

The longitudinal component of the electric field is obtained through the Poisson's equation:

$$\frac{\partial E_x(t, x)}{\partial x} = \int_{\mathbb{R}} f(t, x, p) dp - 1,$$

or equivalently under condition (5.3) through the Ampère's equation:

$$\frac{\partial E_x(t, x)}{\partial t} = -\int_{\mathbb{R}} v(p)f(t, x, p)dp + \frac{1}{L} \int_0^L J(t, x) dx, = -J(t, x) + \bar{J}(t).$$

Initial conditions have to be added for the previous equations:

$$\begin{aligned}f(0, x, p) &= f_0(x, p), \quad (x, p) \in \mathbb{R}^2, \\ (E, A, \partial_x A)(0, x) &= (E_0, A_0, A_1)(x), \quad x \in \mathbb{R}\end{aligned}$$

The trajectories of the particles are solved through the following system:

$$\begin{aligned}\frac{dX}{dt}(t; (x, p), s) &= v(P(t; (x, p), s)), \\ \frac{dP}{dt}(t; (x, p), s) &= (E(t, X(t; (x, p), s)) - \frac{\partial(|A|^2/2)}{\partial x}(t, X(t; (x, p), s))),\end{aligned}\tag{5.10}$$

where $(X(t; (x, p), s), P(t; (x, p), s))$ are the characteristic curves at time t which value at time s was (x, p) , solutions of (5.10) at time t with the initial conditions:

$$X(s; (x, p), s) = x, \quad P(s; (x, p), s) = p.$$

5.3 The discrete problems

In this section, the overall strategy of the FSL algorithm is presented. As detailed in [11], it is composed of two main steps: computation of the characteristics forwardly, and remapping of the distribution function on a phase space grid (deposition step).

First, the deposition step will be recalled. Then, time algorithms will be detailed for both models (1D Vlasov-Ampère and 1D Vlasov-Maxwell), *i.e.* how to advance the characteristics together with the update of the electromagnetic fields.

5.3.1 Deposition step

The two models have this step in common, the slight difference is that the characteristics are velocity ones for Vlasov-Ampère and impulsion ones for Vlasov-Maxwell. Thus, the deposition step shall be given for Vlasov-Ampère. Changing all v and V with p or P and solving (5.10) instead of (5.7) is merely needed to get this step for Vlasov-Maxwell.

A grid of the phase-space will be given, with N_x and N_v the number of points in the x direction $[0, L_x]$ and the v direction $[-v_{\max}, v_{\max}]$. We then define

$$\Delta x = L_x/N_x, \quad \Delta v = 2v_{\max}/N_v, \quad x_i = i\Delta x, \quad v_j = -v_{\max} + j\Delta v.$$

The discrete distribution function is initialized this way:

$$f_{i,j}^0 = f_0(x_i, v_j).$$

Then, if the values of f at time t^n are known on the grid, the discrete distribution function between time $[t^n, t^{n+1}]$ is a projection onto a cubic B-splines basis:

$$f(t, x, v) = \sum_{k,l} \omega_{k,l}^n S(x - X(t; x_k, v_l, t^n)) S(v - V(t; x_k, v_l, t^n)). \quad (5.11)$$

$(X(t; x_k, v_l, t^n), V(t; x_k, v_l, t^n))$ are the characteristics at time t , solutions of the two dimensional system (5.7), which origin at time t^n was the grid point (x_k, v_l) . The $\omega_{k,l}^n$ are the coefficients of the projection of f^n onto the spline basis. The cubic B-spline S is defined as follows

$$6S(x) = \begin{cases} (2 - |x|)^3 & \text{if } 1 \leq |x| \leq 2, \\ 4 - 6x^2 + 3|x|^3 & \text{if } 0 \leq |x| \leq 1, \\ 0 & \text{otherwise.} \end{cases}$$

Knowing the end of the characteristics, the distribution function is updated this way:

$$\begin{aligned} f(t^{n+1}, x_i, v_j) &= \sum_{k,l} \omega_{k,l}^n S(x_i - X(t^{n+1}; x_k, v_l, t^n)) S(v_j - V(t^{n+1}; x_k, v_l, t^n)), \\ &= \sum_{k,l} \omega_{k,l}^{n+1} S(x_i - x_k) S(v_j - v_l). \end{aligned}$$

Adding boundary conditions (for example the value of the normal derivative of f at the boundaries), a set of linear systems in each direction is obtained, from which the weights $\omega_{k,l}^n$ can be

computed as in [34, 21]. This phase will be called the deposition one. We detail in the next sequel two strategies to compute the characteristics numerically. Let us remark that the FSL method is conservative thanks to the partition of the unity property of B-splines. Moreover, when one-dimensional constant advections are considered, the forward approach is equivalent to the backward one, which is in turn equivalent in this case to its conservative counterpart (PSM: Parabolic Splines Method introduced in [38]). See [10] for more details about this last equivalence.

5.3.2 General time algorithms

Vlasov-Ampère

At time t^n ; x^n, v^n, E^n, f^n are known. We first have to solve:

$$\begin{aligned}\frac{dX}{dt}(t; (x, v), s) &= V(t; (x, v), s), \\ \frac{dV}{dt}(t; (x, v), s) &= E(t, X(t; (x, v), s)),\end{aligned}\tag{5.12}$$

with (x_k, v_l) as initial values.

Runge-Kutta 2 To compute the end of the characteristics starting at (x_k, v_l) , a Runge-Kutta 2 algorithm can be applied. It reads

- Step 1: $\tilde{x}_{k,l}^{n+1} = x_k + \Delta t v_l$,
- Step 2: $\tilde{v}_{k,l}^{n+1} = v_l + \Delta t E(t^n, x_k)$,
- Step 3: $x_{k,l}^{n+1} = x_k + \frac{\Delta t}{2}(v_l + \tilde{v}_{k,l}^{n+1})$,
- Step 4: $v_{k,l}^{n+1} = v_l + \frac{\Delta t}{2}(E(t^n, x_k) + E(t^{n+1}, \tilde{x}_{k,l}^{n+1}))$.

In order to perform the last step of the Runge-Kutta 2 algorithm, the electric field at time t^{n+1} is needed. In the classical way, $x_{k,l}^{n+1}$ is used to compute ρ^{n+1} , and then the Poisson's equation is solved to compute the new electric field. We will see later how E is advanced for a charge preserving algorithm and the resolution of the Ampère's equation. After this step, the deposition is made.

Cauchy-Kovalevsky procedure The strategy was developed in [29] and more details can be found there. The idea is to get high order approximations of the characteristics using Taylor expansions in time. And then, using the charge conservation equation, and higher velocity moments of the Vlasov equation, it becomes possible to replace time derivatives with terms containing only spatial derivatives and moments at time t^n . All these sources can be easily computed. Up to third order these Taylor expansions in time lead to:

$$X^{n+1} = X^n + \Delta t V^n + \frac{\Delta t^2}{2} E^n(X^n) + \frac{\Delta t^3}{6} \frac{d}{dt} E(X(t), t)|_{t=t^n},$$

$$V^{n+1} = V^n + \Delta t E^n(X^n) + \frac{\Delta t^2}{2} \frac{d}{dt} E(X(t), t)|_{t=t^n} + \frac{\Delta t^3}{6} \frac{d^2}{dt^2} E(X(t), t)|_{t=t^n}.$$

In order to be able to compute all the terms of these expansions the two first total time derivatives of $E(X(t), t)$ are needed. The first one is

$$\begin{aligned} \frac{d}{dt} E(X(t), t) &= \frac{\partial E}{\partial t}(X(t), t) + \frac{dX}{dt}(t) \frac{\partial E}{\partial x}(X(t), t), \\ &= -J(X(t), t) + \bar{J}(t) + V(t)\rho(X(t), t), \end{aligned}$$

where $\rho(x, t) = \int f(x, v, t) dv - 1$, $J(x, t) = \int f(x, v, t)v dv$ and $\bar{J}(t) = 1/L \int_0^L J(x, t) dx$. Indeed, the Poisson's equation yields $\partial_x E = \rho$ and integrating the Vlasov equation with respect to velocity, yields the charge conservation equation $\partial_t \rho + \partial_x J = 0$. Hence taking the derivative of the Poisson's equation with respect to time and using this equation we get

$$\partial_x (\partial_t E + J) = 0.$$

From which is obtained, as $\int_0^L E(x, t) dx = 0$:

$$\partial_t E = -J + \bar{J}.$$

The second total time derivative of $E(X(t), t)$ writes

$$\begin{aligned} \frac{d^2}{dt^2} E(X(t), t) &= -\partial_t J(X(t), t) - V(t)\partial_x J(X(t), t) + \frac{d\bar{J}}{dt}(t), \\ &+ E(X(t), t)\rho(X(t), t) + V(t)(\partial_t \rho(X(t), t) + V(t)\partial_x \rho(X(t), t)). \end{aligned}$$

To get rid of time derivatives, the strategy is to replace them with space derivatives. Concerning ρ , the charge conservation equation (5.3) is used:

$$\partial_t \rho(X(t), t) = -\partial_x J(X(t), t).$$

In order to compute the time derivative of the current J in terms of spatial derivatives, the Vlasov equation (5.1) is used, multiplied with v , and integrated with respect to v . This leads to

$$\partial_t J + \partial_x I_2 + E \int_{\mathbb{R}} \partial_v f v dv = 0,$$

where $I_n(x, t) = \int_{\mathbb{R}} f(x, v, t)v^n dv$. Hence, since f vanishes at infinity an integration by parts enables to get

$$\partial_t J(X(t), t) = -\partial_x I_2(X(t), t) + E(X(t), t)(1 + \rho(X(t), t)). \quad (5.13)$$

Moreover, the conservation of impulsion is respected in this model, so that:

$$\frac{d\bar{J}}{dt}(t) = 0. \quad (5.14)$$

In conclusion, a 3rd order Cauchy-Kovalevsky (CK3) time algorithm can be derived, following (5.3), (5.13), (5.14):

$$X^{n+1} = X^n + \Delta t V^n + \frac{\Delta t^2}{2} E^n(X^n) + \frac{\Delta t^3}{6} \varphi^n(X^n, V^n).$$

and

$$V^{n+1} = V^n + \Delta t E^n(X^n) + \frac{\Delta t^2}{2} \varphi^n(X^n, V^n) + \frac{\Delta t^3}{6} \phi^n(X^n, V^n).$$

where

$$\varphi^n(X^n, V^n) = V^n \rho^n(X^n) - J^n(X^n) + \bar{J}, \quad (5.15)$$

$$\phi^n(X^n, V^n) = \partial_x I_2(X^n, t^n) - E^n(X^n) - 2V^n \partial_x J(X^n, t^n) + (V^n)^2 \partial_x \rho(X^n, t^n).$$

Remark 7. Obviously, in order to get a second order algorithm (CK2), you just keep the terms until Δt^2 included.

With CK procedures, the characteristics can be solved immediately at the beginning of the time step, since everything needed is at once available. Once you know x^{n+1} , you can compute ρ^{n+1} and compute E^{n+1} like in RK with the Poisson's equation.

QR 1D Vlasov-Maxwell

Suppose that at time t^n : $f^n, E_x^n, B_{y,z}^n, A_{y,z}^n, E_{y,z}^{n-\frac{1}{2}}, x^n, p^n$ are known. A Yee algorithm (see [12]) will be used for the solving of the electromagnetic fields. The general time algorithm writes:

- Advance electric field $E_{y,z}$ on a time step:

$$E_{y,i}^{n+\frac{1}{2}} = E_{y,i}^{n-\frac{1}{2}} - \frac{\Delta t}{\Delta x} (B_{z,i+\frac{1}{2}}^n - B_{z,i-\frac{1}{2}}^n) + \Delta t A_{y,i}^n \rho_{\gamma,i}^n,$$

$$E_{z,i}^{n+\frac{1}{2}} = E_{z,i}^{n-\frac{1}{2}} + \frac{\Delta t}{\Delta x} (B_{y,i+\frac{1}{2}}^n - B_{y,i-\frac{1}{2}}^n) + \Delta t A_{z,i}^n \rho_{\gamma,i}^n.$$

- Advance the magnetic field $B_{y,z}^n$ on a time step:

$$B_{y,i-\frac{1}{2}}^{n+1} = B_{y,i-\frac{1}{2}}^n + \frac{\Delta t}{\Delta x} (E_{z,i}^{n+\frac{1}{2}} - E_{z,i-1}^{n+\frac{1}{2}}),$$

$$B_{z,i-\frac{1}{2}}^{n+1} = B_{z,i-\frac{1}{2}}^n - \frac{\Delta t}{\Delta x} (E_{y,i}^{n+\frac{1}{2}} - E_{y,i-1}^{n+\frac{1}{2}}).$$

- Advance the vector potential $A_{y,z}^n$ on a time step:

$$A_{y,i}^{n+1} = A_{y,i}^n - \Delta t E_{y,i}^{n+\frac{1}{2}},$$

$$A_{z,i}^{n+1} = A_{z,i}^n - \Delta t E_{z,i}^{n+\frac{1}{2}}.$$

- First step of RK2 algorithm for the characteristics, using $F(t, x) = -A_y(t, x)B_z(t, x) + A_z(t, x)B_y(t, x)$. :

$$\begin{aligned}\tilde{x}_{k,l}^{n+1} &= x_k + \Delta t v(p_l), \\ \tilde{p}_{k,l}^{n+1} &= p_l + \Delta t (E_{x,k}^n + F^n(x_k)), \\ x_{k,l}^{n+1} &= x_k + \frac{\Delta t}{2} (v(p_l) + v(\tilde{p}_{k,l}^{n+1})).\end{aligned}$$

- Compute E_x^{n+1} on a time step using the Poisson's equation.
- End of RK2 algorithm

$$p_{k,l}^{n+1} = p_l + \frac{\Delta t}{2} (E^n(x_k) + F^n(x_k) + E^{n+1}(x_{k,l}^{n+1}) + F^{n+1}(x_{k,l}^{n+1})).$$

- Deposition.

5.4 The charge preserving algorithms

In the previous section, it was seen that the electric field has to be updated thanks to the Poisson's equation. In this section, we are going to explain how to update E solving the Ampère's equation without solving the Poisson's one, but ensuring it is satisfied thanks to charge preserving algorithms.

5.4.1 Solving the electric field, Ampère vs Poisson

Let us precise that for all methods, the field will be computed on the dual mesh $(x_{i+\frac{1}{2}})_{i \in \mathbb{N}}$ on which $(E(t^n, x_{i+\frac{1}{2}}))$ is supposed to be known. In order to get $(E(t^n, x_i))$, linear or cubic spline interpolation is used. The key is how E^{n+1} is computed. Let us begin with the Ampère's equation. Up to second order accuracy in time, its approximation reads:

$$E(t^{n+1}, x_{i+\frac{1}{2}}) = E(t^n, x_{i+\frac{1}{2}}) - \Delta t (J_{i+\frac{1}{2}}^{n+\frac{1}{2}} + \bar{J}).$$

The way J is calculated will be explained later. The considered finite difference discrete approximation of the Poisson's equation reads:

$$E(t^{n+1}, x_{i+\frac{1}{2}}) = E(t^{n+1}, x_{i-\frac{1}{2}}) + \Delta x \rho_i^{n+1}. \quad (5.16)$$

Let us prove now that if the discrete charge conservation is enforced, the electric fields computed with Poisson or Ampère are equal.

Lemma 18. *The two methods will be actually the same if the charge and current densities verify the discrete charge conservation equation of second order derived from a Yee algorithm:*

$$\frac{\rho_i^{n+1} - \rho_i^n}{\Delta t} + \frac{J_{i+\frac{1}{2}}^{n+\frac{1}{2}} - J_{i-\frac{1}{2}}^{n+\frac{1}{2}}}{\Delta x} = 0. \quad (5.17)$$

Proof: Let us prove that if Poisson is true at time t^n , and discrete charge conservation (5.17) is verified, E with Poisson and Ampère at time t^{n+1} will be equal. Using the Ampère's equation and (5.17)

$$\begin{aligned} E^{n+1}(x_{i+\frac{1}{2}}) - E^n(x_{i+\frac{1}{2}}) &= -\Delta t(J_{i+\frac{1}{2}}^{n+\frac{1}{2}} + \bar{J}), \\ \frac{\rho_i^{n+1} - \rho_i^n}{\Delta t} + \frac{J_{i+\frac{1}{2}}^{n+\frac{1}{2}} - J_{i-\frac{1}{2}}^{n+\frac{1}{2}}}{\Delta x} &= 0, \end{aligned}$$

so that

$$\begin{aligned} -\Delta t(J_{i+\frac{1}{2}}^{n+\frac{1}{2}} - J_{i-\frac{1}{2}}^{n+\frac{1}{2}}) &= E^{n+1}(x_{i+\frac{1}{2}}) - E^n(x_{i+\frac{1}{2}}) - E^{n+1}(x_{i-\frac{1}{2}}) + E^n(x_{i-\frac{1}{2}}), \\ &= \Delta x(\rho_i^{n+1} - \rho_i^n). \end{aligned}$$

Hence, if Poisson is satisfied at time t^n , *i.e.*

$$E^n(x_{i+\frac{1}{2}}) - E^n(x_{i-\frac{1}{2}}) = \Delta x \rho_i^n,$$

Poisson is automatically satisfied at time t^{n+1} ,

$$E^{n+1}(x_{i+\frac{1}{2}}) - E^{n+1}(x_{i-\frac{1}{2}}) = \Delta x \rho_i^{n+1},$$

which is what was required.

5.4.2 Charge conservation

As it was proved in the last subsection, if E is initialized through Poisson, the problem can be solved on each time step with Ampère, without solving the Poisson's equation if the charge and current densities satisfy (5.17). Now a way to compute compatible ρ and J is proposed:

Compute ρ : Let us explain first how ρ is computed: Once $(x_{k,l}^{n+1})$ is known, it is possible to compute ρ on the mesh using a deposition:

$$\rho(t^{n+1}, x_i) = \sum_{k,l} \omega_{k,l}^n S(x_i - X(t^{n+1}; (x_k, v_l), t^n)) - 1.$$

Then, (5.16) is solved and $E(t^{n+1}, x_{i+\frac{1}{2}})$ can be computed for each i , adding the zero-mean condition (5.5).

Compute J - Discrete charge conservation: The discrete charge conservation equation will be used in order to find J ; following Villasenor Buneman and Barthelmé [36, 1]:

$$\begin{aligned}
\frac{\rho_i^{n+1} - \rho_i^n}{\Delta t} &= \frac{1}{\Delta t} \int_{t^n}^{t^{n+1}} \partial_t \rho(x_i, t), \\
&= \frac{1}{\Delta t} \sum_{k,l} \omega_{k,l}^n \int_{t^n}^{t^{n+1}} \frac{d}{dt} S^3(x_i - X_{k,l}(t)) dt, \\
&= -\frac{1}{\Delta t} \sum_{k,l} \omega_{k,l}^n \int_{t^n}^{t^{n+1}} \frac{dX_{k,l}(t)}{dt} S^3(x_i - X_{k,l}(t)) dt, \\
&= -\frac{1}{\Delta t \Delta x} \sum_{k,l} \omega_{k,l}^n \int_{t^n}^{t^{n+1}} \frac{dX_{k,l}(t)}{dt} (S^2(x_{i+\frac{1}{2}} - X_{k,l}(t)) - S^2(x_{i-\frac{1}{2}} - X_{k,l}(t))) dt, \\
&= -\left(\frac{J_{i+\frac{1}{2}}^{n+\frac{1}{2}} - J_{i-\frac{1}{2}}^{n+\frac{1}{2}}}{\Delta x} \right),
\end{aligned}$$

where $X_{k,l}(t) = X(t; (x_k, v_l), t^n)$, and S^2 the quadratic B-spline. S^2 and S^3 are linked using:

$$\frac{dS^3(x)}{dx} = S^2\left(x + \frac{1}{2}\right) - S^2\left(x - \frac{1}{2}\right).$$

This formula comes from the derivation of the convolution product defining $S^3 = S^2 * S^0$, which makes appear two Dirac mass. Let us remark that this update of ρ depends on the time derivative of the characteristic curves. This is linked with the algorithm used to solve them. In the following paragraphs, we present for various time algorithms (CRK for charge Runge-Kutta, CCK for charge Cauchy-Kovalevsky) the way to compute J .

Runge-Kutta for Vlasov-Ampère: CRK2: What has to be understood is that the only things that matter in the particle trajectory are the beginning and the ending point of it. Then, you can derive one method for each way of approaching the trajectory with the proper beginning and ending points. For the sake of simplicity, the characteristics will be linearly approached. In that purpose, let us set:

$$X_{k,l}(t) = x_k + \frac{t - t^n}{2} (v_l + \tilde{v}_{k,l}^{n+1}),$$

so that

$$\frac{dX_{k,l}(t)}{dt} = \frac{1}{2} (v_l + \tilde{v}_{k,l}^{n+1}).$$

Thus,

$$J_{i+\frac{1}{2}}^{n+\frac{1}{2}} = \frac{1}{2\Delta t} \sum_{k,l} \omega_{k,l}^n (v_l + \tilde{v}_{k,l}^{n+1}) \int_{t^n}^{t^{n+1}} S^2(x_{i+\frac{1}{2}} - X_{k,l}(t)) dt. \quad (5.18)$$

The integral in (5.18) has to be computed exactly. Supposing a CFL condition $v_{\max} \Delta t \leq \Delta x$, the particle cannot get through more than one cell, so that the integrated function is a polynomial

of degree 2. Thus, since the Gauss' formula with two points : $\int_{-1}^1 f(x)dx \approx 1/2(f(1/\sqrt{3}) + f(-1/\sqrt{3}))$ remains exact on polynomials till degree 3:

$$\begin{aligned} \int_{t^n}^{t^{n+1}} S^2(x_{i+\frac{1}{2}} - X_{k,l}(t))dt &= \frac{\Delta t}{2} \int_{-1}^1 S^2(x_{i+\frac{1}{2}} - X_{k,l}(\frac{\Delta t}{2}u + t^{n+\frac{1}{2}}))du, \\ &= \frac{\Delta t}{2} \left(S^2\left(x_{i+\frac{1}{2}} - X_{k,l}(t^{n+\frac{1}{2}} + \frac{\Delta t}{2\sqrt{3}})\right) + S^2\left(x_{i+\frac{1}{2}} - X_{k,l}(t^{n+\frac{1}{2}} - \frac{\Delta t}{2\sqrt{3}})\right) \right). \end{aligned}$$

To conclude, setting:

$$J_{i+\frac{1}{2}}^{n+\frac{1}{2}} = \frac{1}{4} \sum_{k,l} \omega_{k,l}^n \left(v_l + \tilde{v}_{k,l}^{n+1} \right) \left(S^2(x_{i+\frac{1}{2}} - X_{k,l}(t^{n+\frac{1}{2}} + \frac{\Delta t}{2\sqrt{3}})) + S^2(x_{i+\frac{1}{2}} - X_{k,l}(t^{n+\frac{1}{2}} - \frac{\Delta t}{2\sqrt{3}})) \right).$$

allows to preserve charge.

Cauchy-Kovalevsky for Vlasov-Ampère: CCK:

In order to be able to follow high order algorithms easily, a linear approximation of the characteristic curve will also be applied, following (5.15):

$$X_{k,l}(t) = x_k + (t - t^n)v_l + \Delta t(t - t^n)E^n(x_k) + \frac{\Delta t^2}{2}(t - t^n)\varphi^n(x_k, v_l),$$

so that

$$\frac{dX_{k,l}(t)}{dt} = v_l + \Delta t E^n(x_k) + \Delta t^2 \varphi^n(x_k, v_l) := D_{k,l}^n.$$

Thus,

$$J_{i+\frac{1}{2}}^{n+\frac{1}{2}} = \frac{1}{\Delta t} \sum_{k,l} \omega_{k,l}^n D_{k,l}^n \int_{t^n}^{t^{n+1}} S^2(x_{i+\frac{1}{2}} - X_{k,l}(t))dt.$$

Using the same exact computation of the integral thanks to the Gauss' points leads to:

$$J_{i+\frac{1}{2}}^{n+\frac{1}{2}} = \frac{1}{2} \sum_{k,l} \omega_{k,l}^n D_{k,l}^n \left(S^2(x_{i+\frac{1}{2}} - X_{k,l}(t^{n+\frac{1}{2}} + \frac{\Delta t}{2\sqrt{3}})) + S^2(x_{i+\frac{1}{2}} - X_{k,l}(t^{n+\frac{1}{2}} - \frac{\Delta t}{2\sqrt{3}})) \right).$$

Runge-Kutta 2 for Vlasov-Maxwell

This algorithm is the same as Runge-Kutta 2 for Vlasov-Ampère, changing v_l and $\tilde{v}_{k,l}^{n+1}$ in $v(p_l)$ and $v(\tilde{p}_{k,l}^{n+1})$. Therefore, the current which leads to a charge preserving algorithm writes:

$$J_{i+\frac{1}{2}}^{n+\frac{1}{2}} = \frac{1}{4} \sum_{k,l} \omega_{k,l}^n (v(p_l) + v(\tilde{p}_{k,l}^{n+1})) \left(S^2(x_{i+\frac{1}{2}} - X_{k,l}(t^{n+\frac{1}{2}} + \frac{\Delta t}{2\sqrt{3}})) + S^2(x_{i+\frac{1}{2}} - X_{k,l}(t^{n+\frac{1}{2}} - \frac{\Delta t}{2\sqrt{3}})) \right).$$

Summary:

Supposing x^{n+1} known, ρ is computed thanks to a deposition, then J is computed with the previous expressions. There, E can be advanced thanks to the Ampère's equation, and automatically obeys the Poisson's one.

Remark 8. Note that the previous algorithms can be extended to the 4D case, using the following splitting strategy:

- Solve $\partial_t f + v_x \partial_x f + E_x \partial_{v_x} f = 0$ using one of the previous charge preserving algorithm.
- Solve $\partial_t f + v_y \partial_y f + E_y \partial_{v_y} f = 0$ using one of the previous charge preserving algorithm.
- Solve $\partial_t f + v_y B_z \partial_{v_x} f - v_x B_z \partial_{v_y} f = 0$, using a Boris scheme.

Let us also remark, that no prediction will be needed using a Yee algorithm for the solving of the Maxwell's equations, so reasonable CPU time can be hoped compared to standard algorithms.

5.5 Numerical results

5.5.1 Introduction

We will test our algorithms with the classical test cases already used in [11]. Let us give a few details about the following diagnostics. First, concerning the CFL condition, it will be said that $\text{CFL} < 1$ when $v_{\max} \Delta t < \Delta x$ and $\text{CFL} > 1$ when $v_{\max} \Delta t > \Delta x$. What we call charge conservation will be the difference between ρ computed with the distribution function and ρ computed thanks to J and the charge conservation equation:

$$cc^{n+1}(i) := \int_{\mathbb{R}} f^{n+1}(x_i, v) dv - (\rho^n(x_i) + 1 - \frac{\Delta t}{\Delta x} (J_{i+\frac{1}{2}}^{n+\frac{1}{2}} - J_{i-\frac{1}{2}}^{n+\frac{1}{2}})).$$

Finally what is called Ampère Poisson equivalence is the difference between the electric field computed with Ampère and Poisson after 1000 iterations:

$$ap^{n+1}(i) := \frac{E^{n+1}(x_{i+\frac{1}{2}}) - E^{n+1}(x_{i-\frac{1}{2}})}{\Delta x} + (\rho^n(x_i) + 1 - \frac{\Delta t}{\Delta x} (J_{i+\frac{1}{2}}^{n+\frac{1}{2}} - J_{i-\frac{1}{2}}^{n+\frac{1}{2}})).$$

The classical Runge-Kutta 2 (resp Cauchy-Kovalevsky 2 and 3) algorithms, developed in section 3.2, coupled with a resolution of the electric field with Poisson will be called RK2 (resp CK2 and CK3). The RK2 and the Cauchy-Kovalevsky algorithms with charge conservation, developed in section 4, will be denoted respectively CRK2, CCK2 and CCK3.

5.5.2 Linear Landau damping

The initial condition associated to the scaled Vlasov-Poisson equation has the following form

$$f_0(x, v) = \frac{1}{\sqrt{2\pi}} \exp(-v^2/2)(1 + \alpha \cos(kx)), \quad (x, v) \in [0, 2\pi/k] \times \mathbb{R},$$

where $k = 0.5$ is the wave number and $\alpha = 0.001$ is the amplitude of the perturbation, so that linear regimes are considered here. A cartesian mesh is used to represent the phase space with a computational domain $[0, 2\pi/k] \times [-v_{\max}, v_{\max}]$, $v_{\max} = 6$. The number of mesh points in the spatial and velocity directions is designated by $N_x = 64$ and $N_v = 64$ respectively. For the

charge conservation algorithms, $\Delta t = 0.03$ so that the CFL condition is satisfied and $\Delta t = 0.1$ are considered (the CFL is violated in this latter case).

On Fig. 5.5.1, the implemented solution of the L^2 norm of the electric field: $1/2\|E(t)\|_{L^2}^2$ with the Runge-Kutta algorithm without charge conservation presented in section 3.2, and the Runge-Kutta algorithm with charge conservation presented in sections 3.2 and 4 with $\text{CFL} < 1$ are displayed in log scale. It can be observed that the two curves are nearly the same. Moreover, the theoretical damping associated to $k = 0.5$, which is -0.1533 is added in order to ensure that the solution corresponds to the predicted damping. On the same figure is plotted the same result with a CFL condition superior than 1 for RK2 and CRK2, which proves that the problem comes from the violation of the CFL condition in the charge algorithm. In particular, we also plot on Fig. 5.5.2 and on Fig. 5.5.3 the charge conservation and the Ampère-Poisson equivalence with on the left $\text{CFL} < 1$, and on the right $\text{CFL} > 1$. These results are issued from the RK algorithm and are given after 1000 iterations.

For the CK algorithm, we just plot on Fig. 5.5.4 on the left the electric energy and the theoretical damping for CK2 presented in section 3.2 and CCK2 presented in section 4, with $\text{CFL} < 1$, and the same on the right for CK3 and CCK3 developed in the same sections. The curves are overlaid, as it was expected.

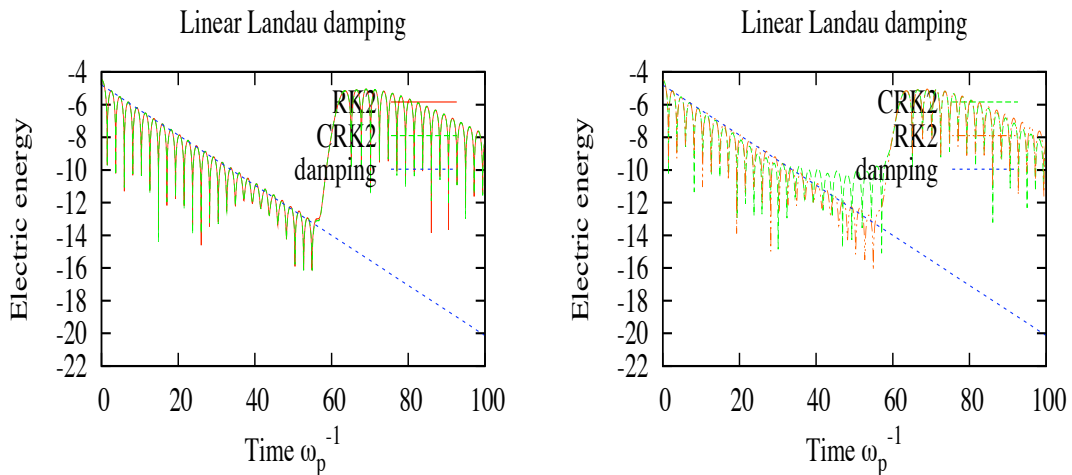


Figure 5.5.1: Linear Landau damping for $k = 0.5$ $N_x = N_v = 64$, $\Delta t = 0.03$ (left); $\Delta t = 0.1$ (right).

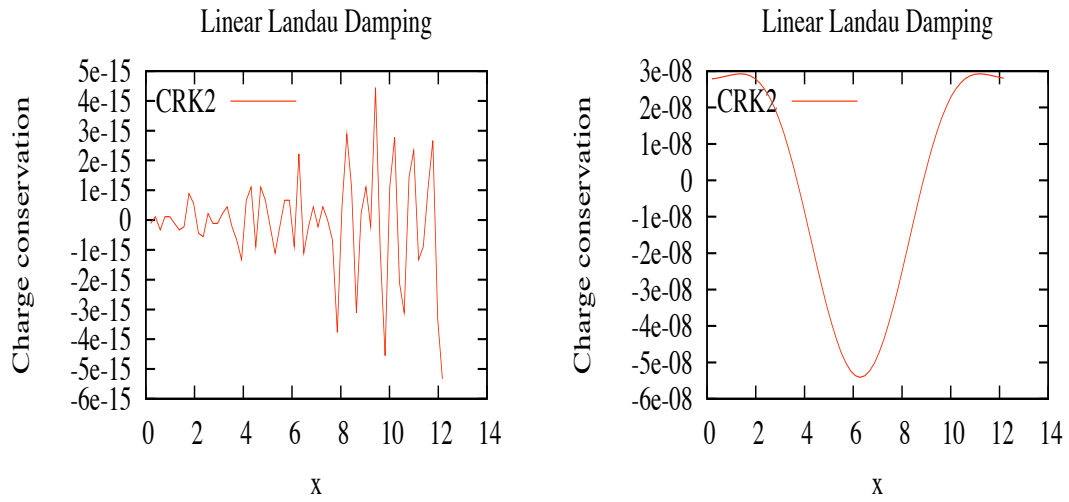


Figure 5.5.2: Charge Conservation $N_x = N_v = 64$, $\Delta t = 0.03$ (left); $\Delta t = 0.1$ (right), 1000 iterations.

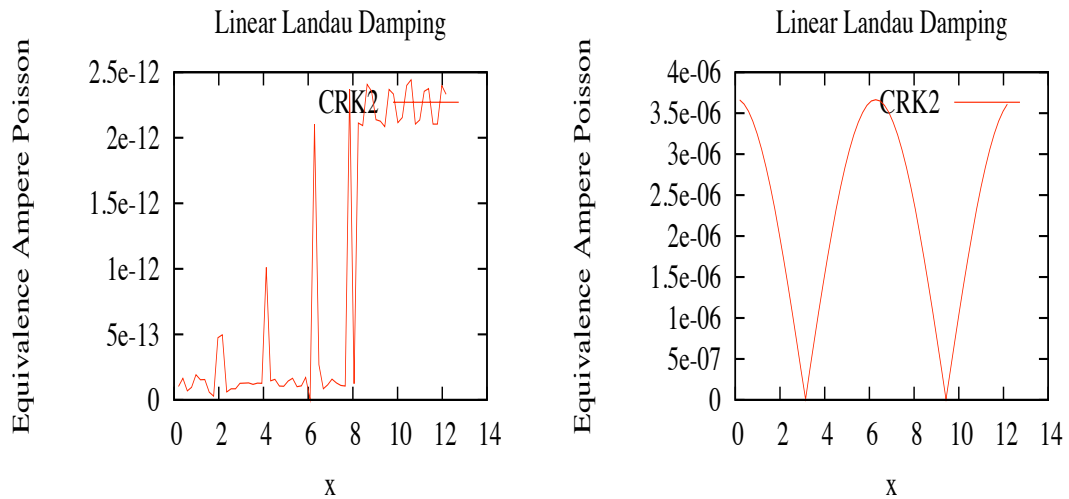


Figure 5.5.3: Ampère-Poisson equivalence, $N_x = N_v = 64$, $\Delta t = 0.03$ (left); $\Delta t = 0.1$ (right), 1000 iterations.

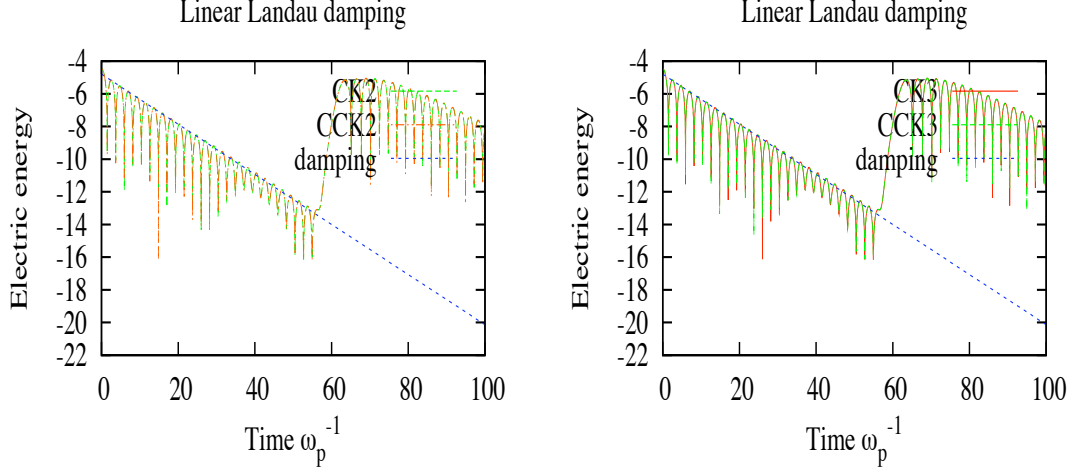


Figure 5.5.4: Electric energy for CK2 (left) and CK3 (right) $N_x = N_v = 64$, $\Delta t = 0.03$.

5.5.3 Two stream instability

This test case simulates two beams with opposite velocities that encounter (see [18, 27]). The corresponding initial condition can be given by

$$f_0(x, v) = \mathcal{M}(v)v^2[1 - \alpha \cos(kx)], \quad \mathcal{M}(v) = \frac{1}{\sqrt{2\pi}} \exp\left(-\frac{v^2}{2}\right),$$

with $k = 0.5$ and $\alpha = 0.05$. The computational domain is $[0, 2\pi/k] \times [-9, 9]$ which is sampled by $N_x = N_v = 128$ points. For the charge conservation algorithms developed in section 4, CFL imposes $\Delta t < 0.0109$, so the case $\text{CFL} < 1$ will be made with $\Delta t = 0.01$, and $\text{CFL} > 1$ with $\Delta t = 0.1$. We are interested in the electric energy $1/2\|E(t)\|_{L^2}^2$, which will be displayed in log scale. The same quantities as for the previous test cases are plotted on Fig. 5.5.5, 5.5.6, 5.5.7 and 5.5.8. The results are really precise for RK and CK, even in long time, under the assumption $\text{CFL} < 1$ with the charge algorithms presented in section 4. The results show a poor precision for the case $\text{CFL} > 1$. On Fig. 5.5.9, the L^2 norm of the solution and the first moment in v are displayed for $\Delta t = 0.1$. The L^2 norm cannot be exactly conserved by any scheme using a phase space grid as soon as the grid does not resolve anymore the filaments, but the developed algorithms perform well, and have similar precision. Differences should appear taking bigger time steps, as it will be seen in the next test case. The first moment is exactly conserved for CK, which has been proved theoretically in [29]. For RK2, there is a slight decrease of the first moment, and for RK3 a small increase which remains acceptable.

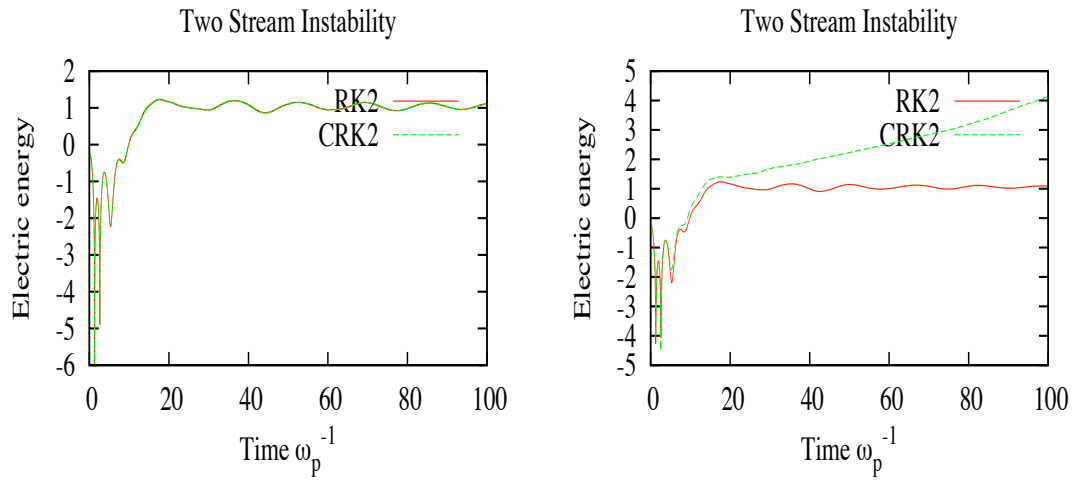


Figure 5.5.5: Electric energy: $N_x = N_v = 128$, $\Delta t = 0.01$ (left), $\Delta t = 0.1$ (right).

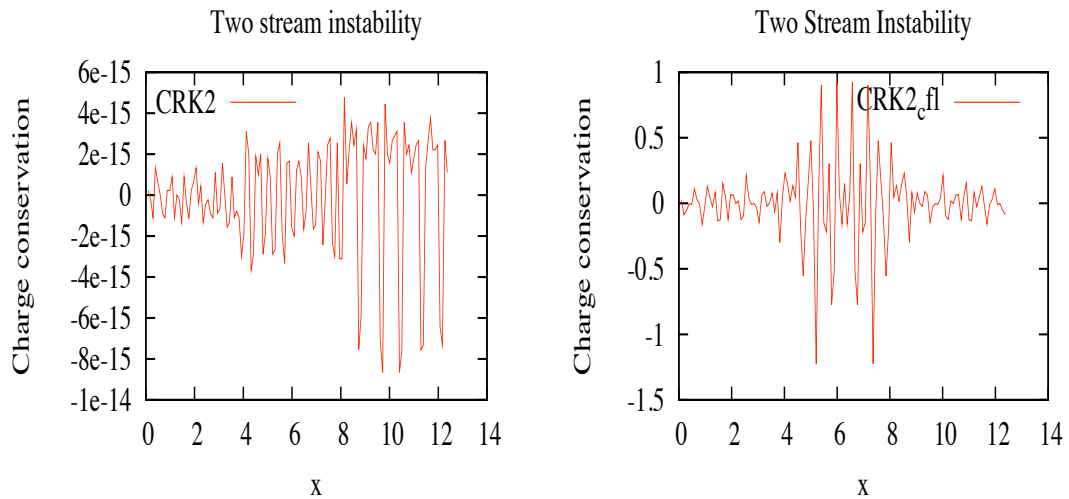


Figure 5.5.6: Charge conservation: $N_x = N_v = 128$, $\Delta t = 0.01$ (left), $\Delta t = 0.1$ (right), 1000 iterations.

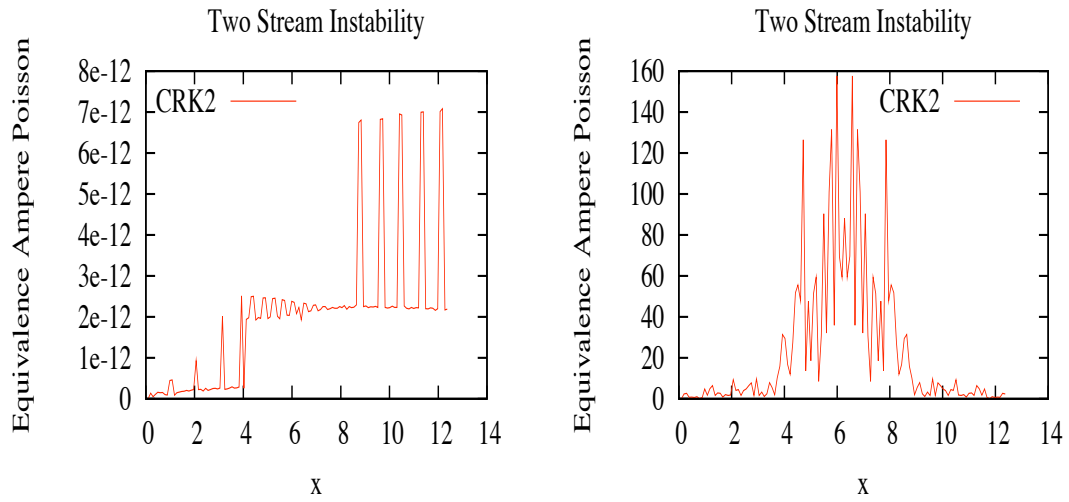


Figure 5.5.7: Ampère-Poisson equivalence, $N_x = N_v = 128$, $\Delta t = 0.01$ (left), $\Delta t = 0.1$ (right), 1000 iterations.

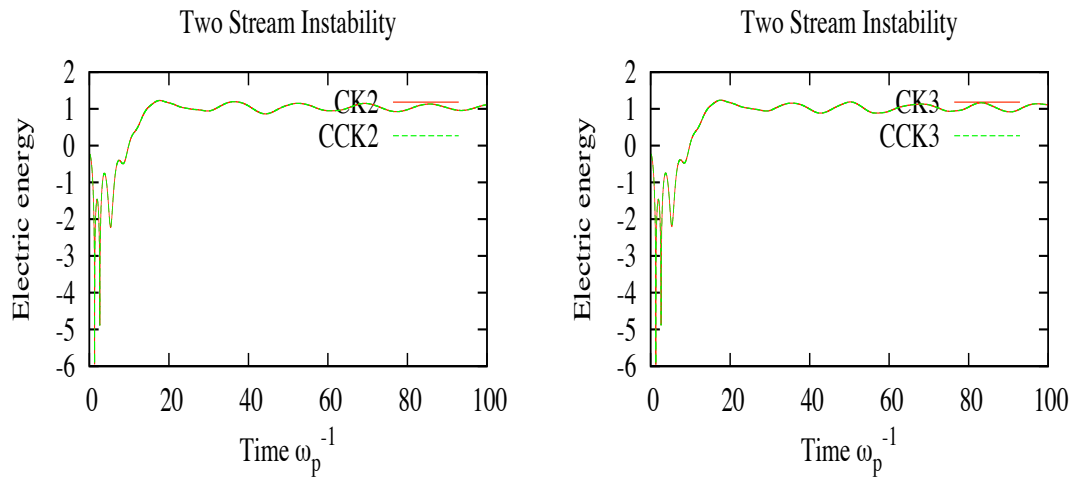


Figure 5.5.8: Electric energy CK2 (left) CK3 (right) $N_x = N_v = 128$, $\Delta t = 0.01$.

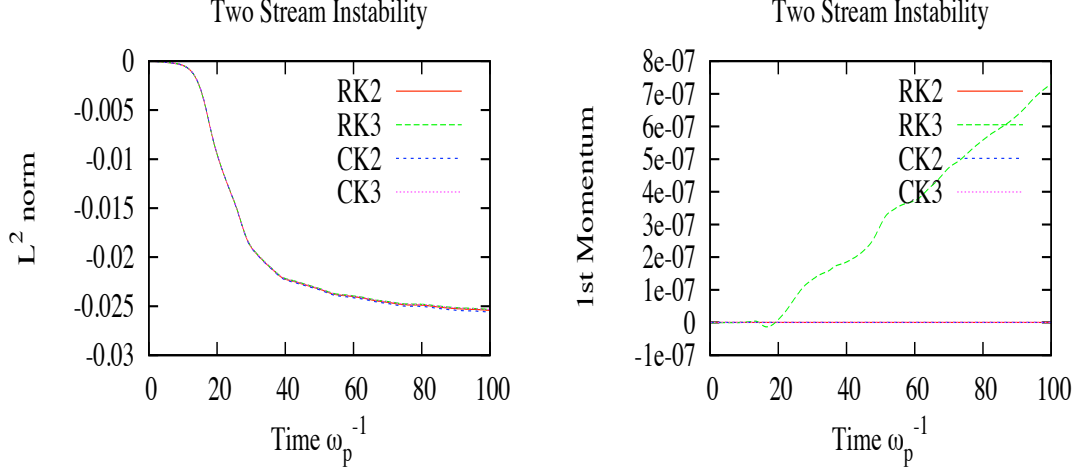


Figure 5.5.9: L^2 norm (left), First moment in v (right) $\Delta t = 0.1$.

5.5.4 Bump on Tail

Next, we can apply the scheme to the bump-on-tail instability test case for which the initial condition writes (see [32])

$$f_0(x, v) = \tilde{f}(v)[1 + \alpha \cos(kx)],$$

with $\alpha = 0.04$, $k = 0.3$ and

$$\tilde{f}(v) = \frac{n_p}{\sqrt{2\pi}} \exp(-v^2/2) + \frac{n_b}{\sqrt{2\pi}} \exp\left(-\frac{|v-u|^2}{2v_t^2}\right),$$

on the interval $[0, 20\pi]$, with periodic conditions in space. The initial condition f_0 is a Maxwellian distribution function which has a bump on the Maxwell distribution tail; the physical parameters are the following

$$n_p = 0.9, n_b = 0.2, u = 4.5, v_t = 0.5,$$

whereas the numerical parameters are $N_x = 128$, $N_v = 128$, $v_{\max} = 9$. For the charge conservation algorithms, CFL imposes $\Delta t < 0.0545$, so the cases $\text{CFL} < 1$ will be made with $\Delta t = 0.05$, and $\text{CFL} > 1$ with $\Delta t = 0.2$. We still give the same diagnostics on Fig. 5.5.10, 5.5.11, 5.5.12 and 5.5.13. For this electric energy diagnostic, we expect oscillatory behavior of frequency equal to 1.05; moreover, since an instability will be declared, the electric energy has to increase up to saturation at $t \approx 20.95$ and to converge for large times (see [27, 32]). The results are really precise for RK and CK, even in long time, under the assumption $\text{CFL} < 1$ for the charge algorithms developed in section 4.

On Fig. 5.5.14, the L^2 norm of the distribution function and the entropy $-\int f \ln(f) dx dv$ are plotted for $\Delta t = 0.2$. These two quantities are known to be theoretically preserved. As it was already explained, this cannot be reached with our kind of numerical methods. The conservation properties are better for the third order CK3 and RK3 than for the second order

CK2 and RK2. Let us precise that more Δt increases, more these differences are important, and that the RK algorithms perform a bit better, but are more expensive computationally speaking.

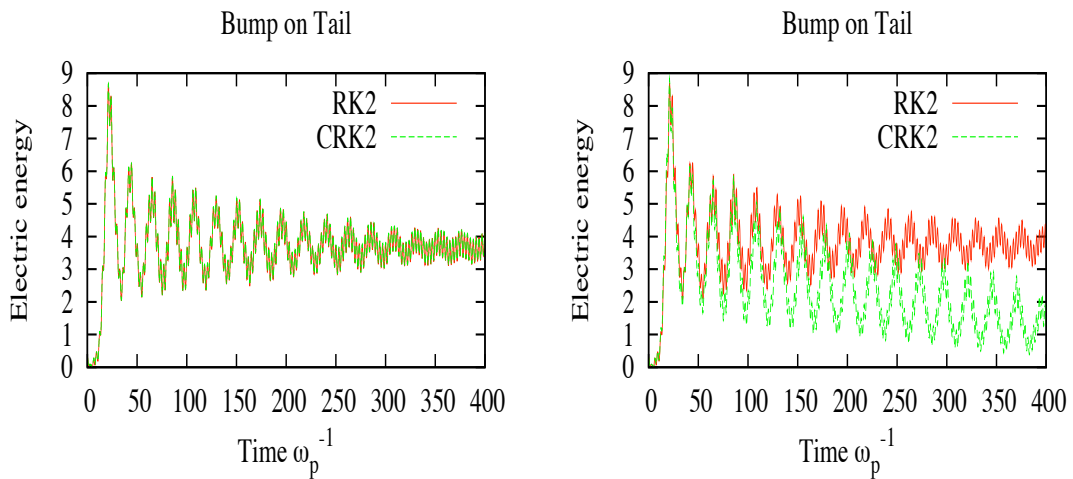


Figure 5.5.10: Electric energy $\Delta t = 0.05$ (left) $\Delta t = 0.2$ (right).

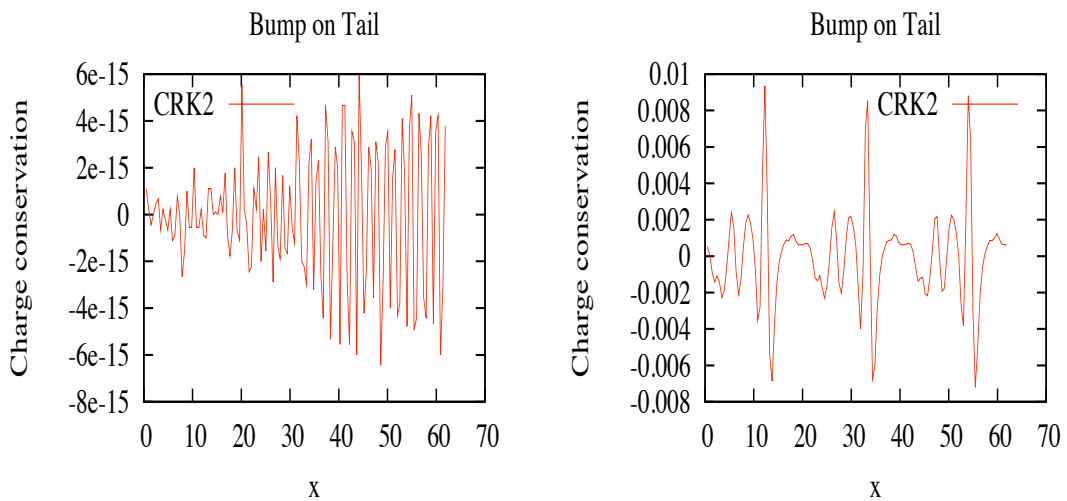


Figure 5.5.11: Charge Conservation $\Delta t = 0.05$ (left) $\Delta t = 0.2$ (right).

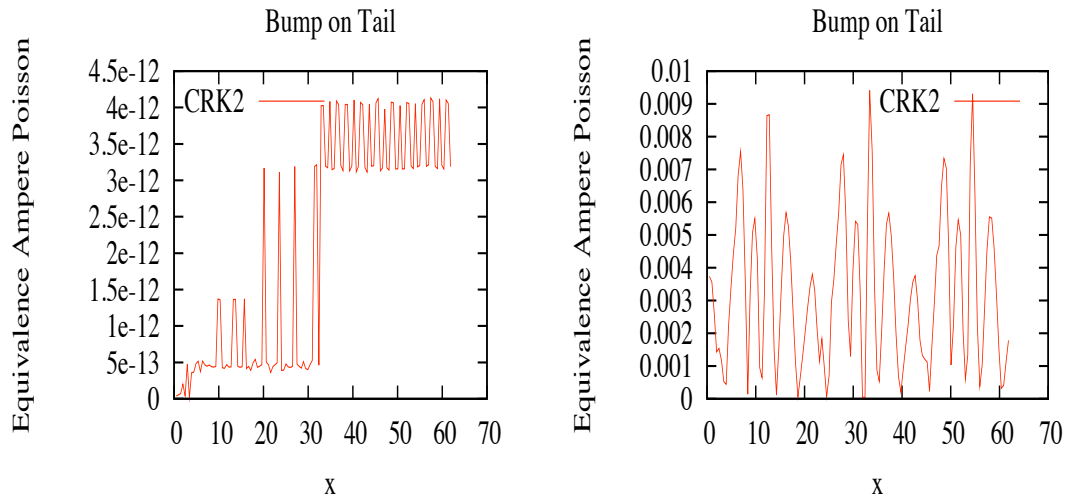


Figure 5.5.12: Ampère-Poisson equivalence $\Delta t = 0.05$ (left) $\Delta t = 0.2$ (right).

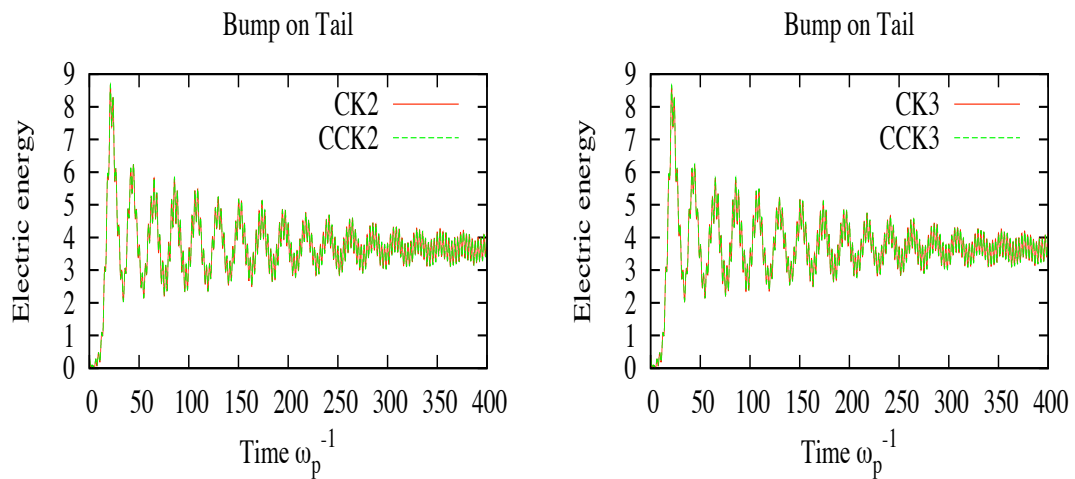
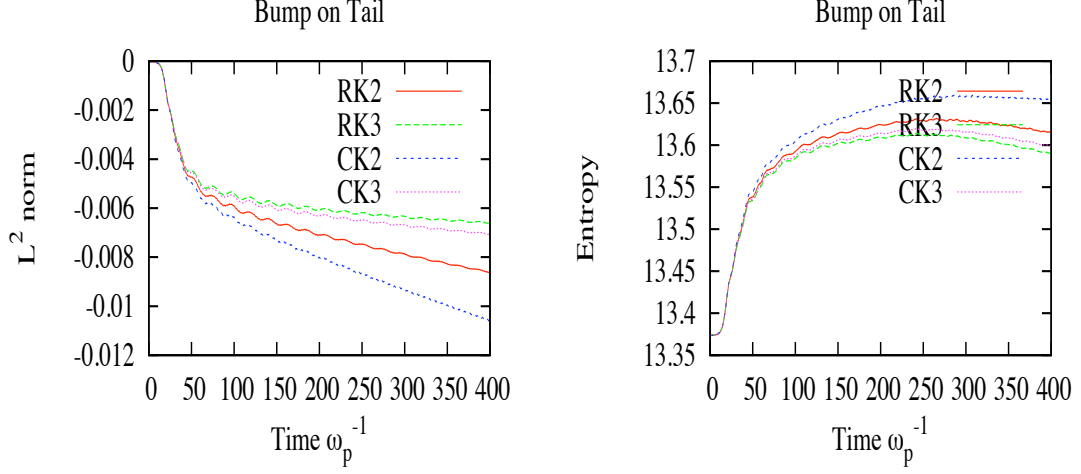


Figure 5.5.13: Electric energy $\Delta t = 0.05$, CK2 (left), CK3 (right).

Figure 5.5.14: L^2 norm (left), Entropy (right) $\Delta t = 0.2$.

5.5.5 QR Vlasov-Maxwell test case

The numerical method used to solve this test case was presented in section 2.2. Let us precise the numerical parameters used to perform this test case.

$$f^0(x, p) = \frac{1}{\sqrt{2\pi T}} \exp\left(-\frac{p^2}{(2T^2)}\right) (1 + \cos(kx)),$$

$T = 3keV$, and $k = \frac{1}{\sqrt{2}}$. A circularly polarized electromagnetic wave is initialized in a periodic domain with a quiver momentum $a_0 = \sqrt{3}$:

$$\begin{aligned} E_y^0(x) &= E_0 \cos(kx) & E_z^0(x) &= E_0 \sin(kx) \\ B_y^0(x) &= \frac{-k^* E_0}{\omega_0} \sin(kx) & B_z^0(x) &= \frac{k^* E_0}{\omega_0} \cos(kx) \\ A_y^0(x) &= -\frac{E_0}{\omega_0} \sin(kx) & A_z^0(x) &= \frac{E_0}{\omega_0} \cos(kx) \end{aligned}$$

where $k^* = k \operatorname{sinc}(\frac{k\Delta x}{2})$, and $\operatorname{sinc}(x) = \frac{\sin(x)}{x}$. We consider a pump wave of frequency ω_0 and wavenumber k_0 such that $\omega_0^2 = \omega_p^2/\gamma_0 + k_0^2 c^2$ is satisfied, with $\gamma_0 = 1 + a_0^2$. Choosing $k_0 c/m = 1/\sqrt{2}$, we obtain $\omega_0/\omega_p = 1$ (*i.e.* a ratio $n/n_c = 1$). ω_p is the plasma frequency, c the light velocity and n_c the critical density.

These physical parameters correspond to the most unstable mode, for more details about the test case, see [22, 23]. The numerical parameters are chosen as follows: the impulsion domain is $[-p_{\max}, p_{\max}]$, where $p_{\max} = 8.5$. The choice of k_0 determines the size of the periodic space domain which is taken equal to $[0, 2\pi\sqrt{2}]$, $N_x = 256$, $N_p = 256$, $\Delta t = 0.01$, which is under CFL condition.

We display on Fig. 5.5.15, 5.5.16, 5.5.17, 5.5.18, the distribution function at different times, for a Backward semi-Lagrangian algorithm, which shall be our reference, and our FSL charge conserving algorithm introduced in section 4. The two methods are difficult to compare with only this diagnostic, and seem to behave similarly. On Fig. 5.5.19, the mass conservation for BSL and FSL is plotted. FSL behaves far better, especially with long time scaling. Obviously, as the mass decreases, the charge cannot be conserved anymore, which is shown on Fig. 5.5.20, 5.5.21. Before the decrease of the mass, the FSL algorithm preserves charge exactly, and after the decrease, remains truly better. To conclude, on Fig. 5.5.22, 5.5.23 the integration of f with respect to x is displayed, at different times. At the beginning, the two curves are very close, but as time goes on, the two curves separate, and FSL remains more centered than BSL. For more details about comparisons between FSL and BSL, the reader is referred to [11].

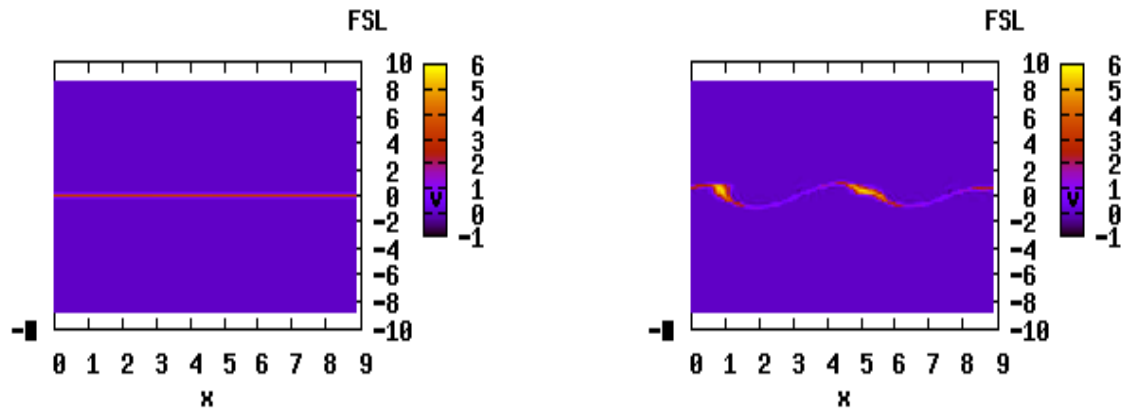


Figure 5.5.15: Distribution function at time = 10 and 22, $N_x = 256$, $N_p = 256$, $\Delta t = 0.01$.

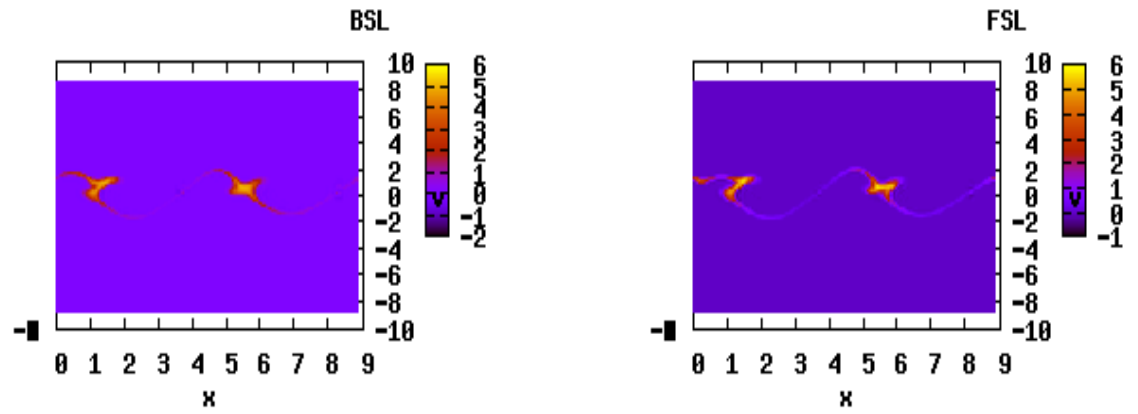


Figure 5.5.16: Distribution function at time = 23, BSL vs FSL, $N_x = 256$, $N_p = 256$, $\Delta t = 0.01$.

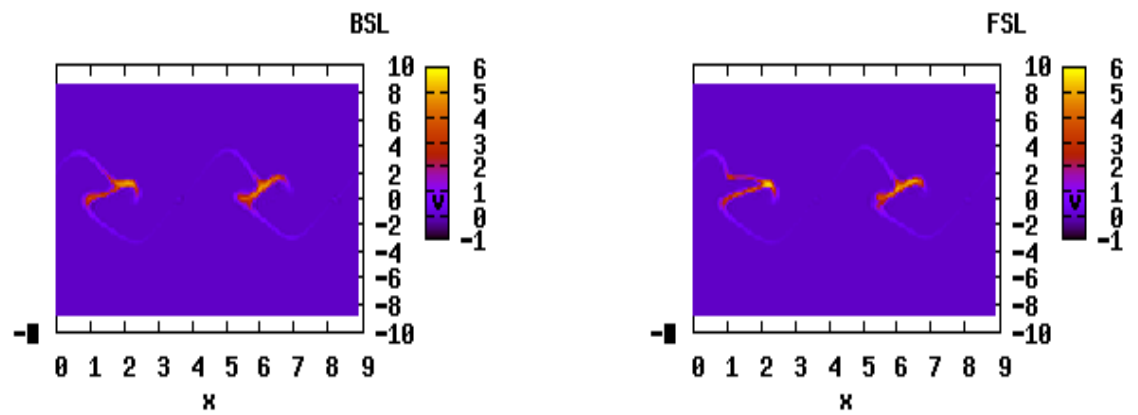


Figure 5.5.17: Distribution function at time = 24, BSL vs FSL, $N_x = 256$, $N_p = 256$, $\Delta t = 0.01$.

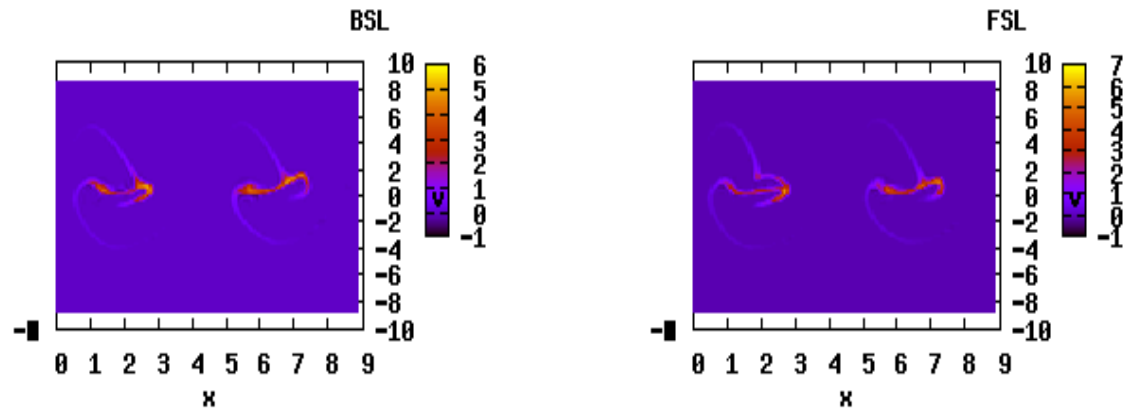


Figure 5.5.18: Distribution function at time = 25, BSL vs FSL, $N_x = 256$, $N_p = 256$, $\Delta t = 0.01$.

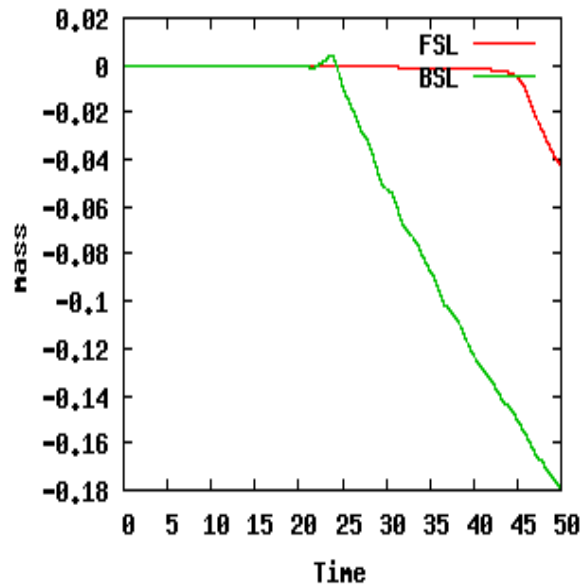


Figure 5.5.19: Mass, FSL vs BSL, $N_x = 256$, $N_p = 256$, $\Delta t = 0.01$.

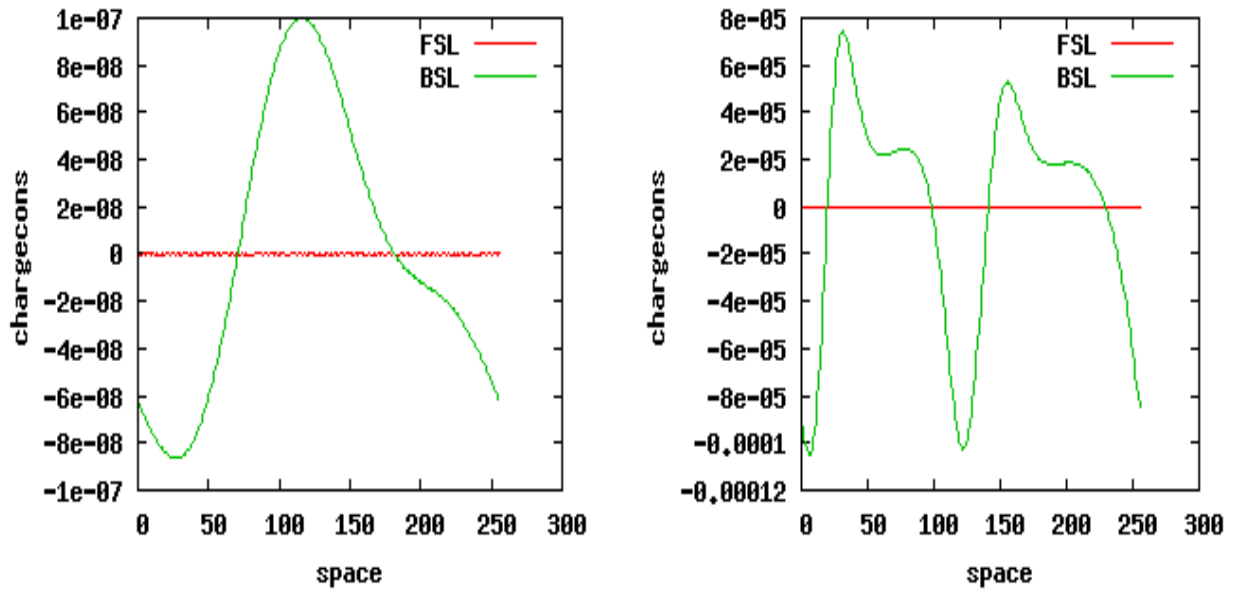


Figure 5.5.20: Charge conservation at time 10 and 20, BSL vs FSL, $N_x = 256, N_p = 256, \Delta t = 0.01$.

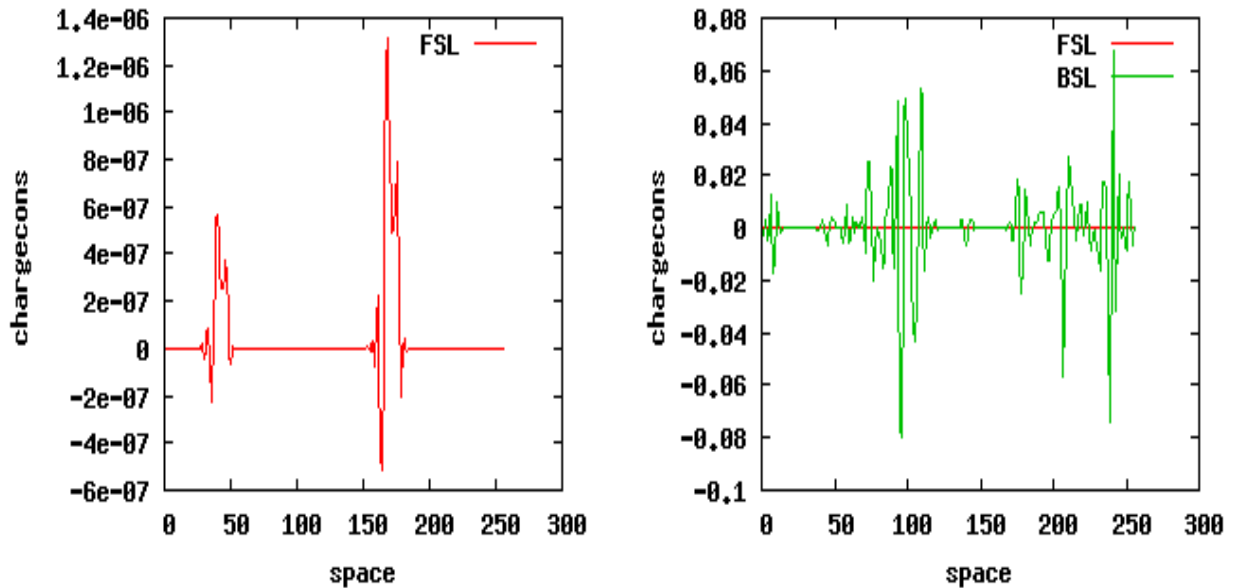


Figure 5.5.21: Charge conservation at time 26 and 30, BSL vs FSL, $N_x = 256, N_p = 256, \Delta t = 0.01$.

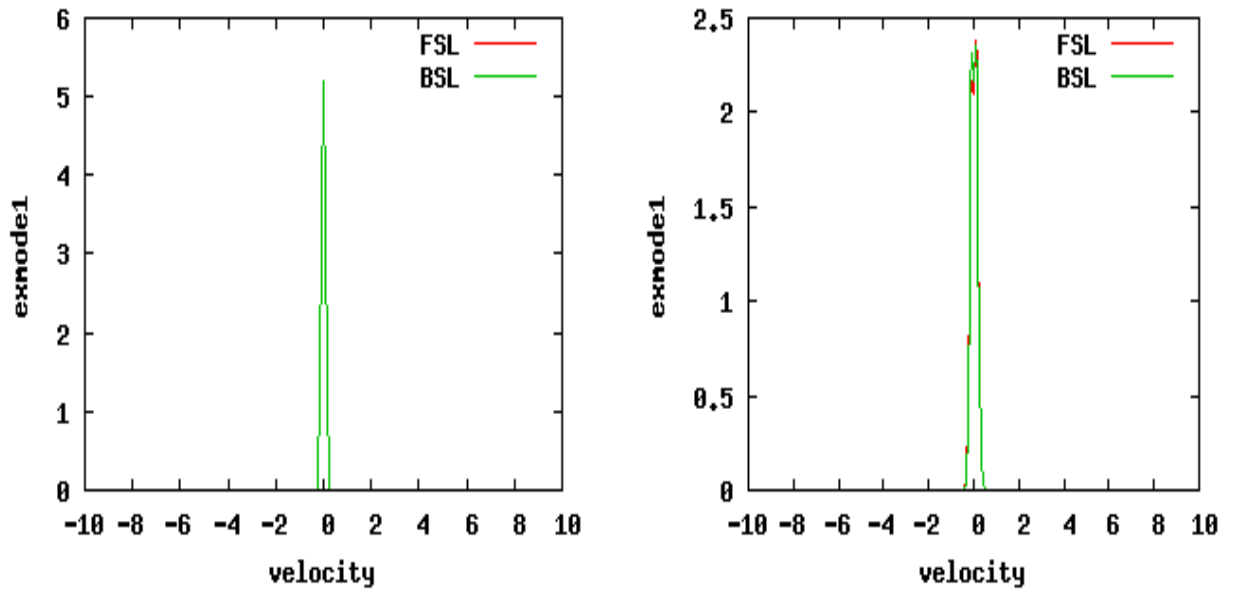


Figure 5.5.22: Integration of f along x , $t = 1000$ and 2000 , BSL vs FSL, $N_x = 256$, $N_p = 256$, $\Delta t = 0.01$.

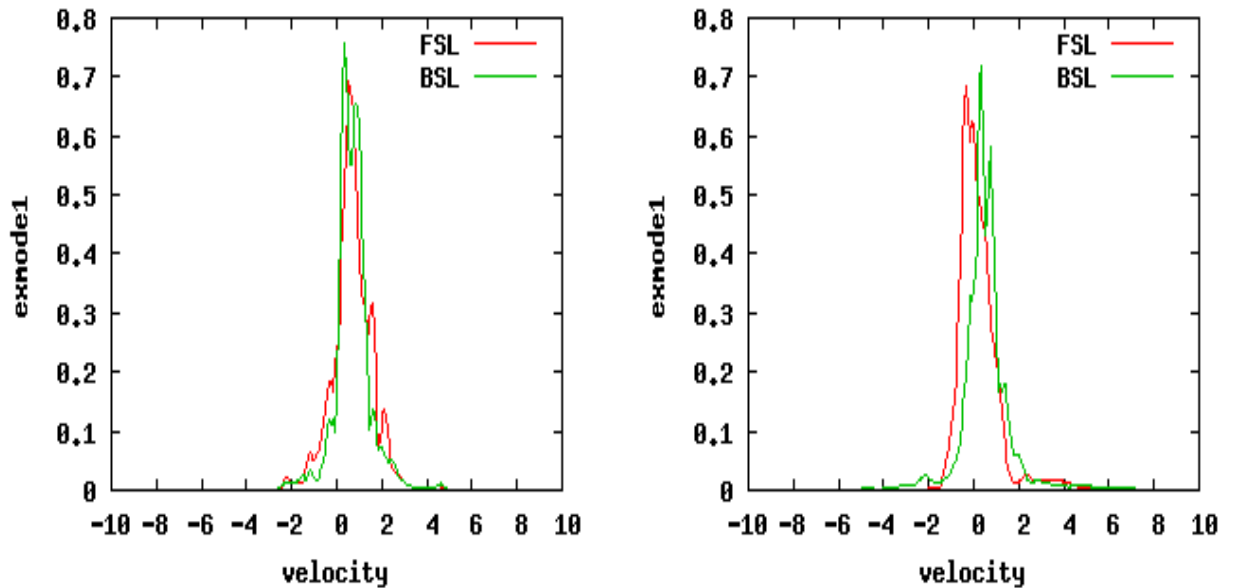


Figure 5.5.23: Integration of f along x , $t = 30$ and 40 , BSL vs FSL $N_x = 256$, $N_p = 256$, $\Delta t = 0.01$.

5.5.6 Numerical Synthesis

One of our goals was to compare these different algorithms in order to choose the best one for a prospective work in view of tackling the 4D case. First, it has to be said that the CK procedure is faster than the RK one, especially when you look for high order simulation, merely because there are no intermediate deposition steps, which is one of the most expensive step. Obviously, in CCK methods, a 2D deposition is made to compute J , therefore the CPU time is the same as the one of RK (see Table 1). The results concerning electric energy are really difficult to compare, and seem very good whatever algorithm you choose. We observe that the conserved quantities, like the L^2 norm of the distribution function are a bit better with RK, so CRK seems to be a good compromise between cost and accuracy. These methods are validated by these 1D test cases, and are encouraging for prospective work.

	RK2	RK3	Verlet	CK2	CK3	CRK2	CCK2	CCK3
64×64	27.1 s.	42.5 s.	26 s.	19 s.	20.8 s.	27.6 s.	27.1 s.	42.5 s.

Table 5.1: Comparison of the CPU time of the different method. 10000 iterations.

Moreover, with the last test case, with real Maxwell's equations, we see that a charge conserving FSL method is really better than a classical BSL one, which is entirely satisfying, and convincing for future work.

5.6 Conclusion

In this paper, charge preserving Forward semi-Lagrangian algorithms of second and third order for the characteristics have been developed, and the numerical results meet requirements for various test cases. In these cases, under a CFL condition, the two methods Vlasov-Poisson and Vlasov-Ampère have proven to be exactly the same, and the charge has proved to be preserved. A future work will be to design a 4D charge preserving FSL Vlasov-Maxwell scheme, especially comparing charge preserving algorithms developed in [30] with a procedure derived from this work, using a splitting scheme.

Bibliography

- [1] R. BARTHELMÉ, *Le problème de conservation de la charge dans le couplage des équations de Vlasov et de Maxwell*, Thèse de l'Université Louis Pasteur, 2005.
- [2] M. BOSTAN, N. CROUSEILLES, *Convergence of a semi-Lagrangian scheme for the reduced Vlasov-Maxwell system for laser-plasma interaction*, Numer. Math. **112**, no2, pp. 169-195 (2009).
- [3] M. BOSTAN, *Mild solutions for the relativistic Vlasov-Maxwell system for laser plasma interaction*, Quart. Appl. Math. **65**, pp. 163-187 (2007)
- [4] C.K. BIRDSALL, A.B. LANGDON, *Plasma Physics via Computer Simulation*, Inst. of Phys. Publishing, Bristol/Philadelphia, (1991).
- [5] F. BOUCHUT, F. GOLSE, M. PULVIRENTI, *Kinetic equations and asymptotic theory*, Series in applied Math. P.G Ciarlet and P.L Lions (Eds) Gauthier Villars (2008).
- [6] J. A. CARRILLO, S. LABRUNIE, *Global solutions for the one-dimensional Vlasov-Maxwell system for laser-plasma interaction*, Math. Models Methods Appl. Sci. **16**, pp. 19-57, (2006).
- [7] J.-A. CARRILLO, F. VECIL, *Non oscillatory interpolation methods applied to Vlasov-based models*, SIAM Journal of Sc. Comput. **29**, pp. 1179-1206, (2007).
- [8] C. Z. CHENG, G. KNORR, *The integration of the Vlasov equation in configuration space*, J. Comput. Phys, **22**, pp. 330-3351, (1976).
- [9] P. COLELLA, P.R. WOODWARD, *The Piecewise Parabolic Method (PPM) for gas-dynamical simulations*, J. Comput. Phys. **54** (1984) 174-201.
- [10] N. CROUSEILLES, M. MEHRENBERGER, E. SONNENDRÜCKER, *Conservative semi-Lagrangian schemes for the Vlasov equation*, J. Comput. Phys., **229**, no6, pp. 1927-1953 (2010).
- [11] N. CROUSEILLES, T. RESPAUD, E. SONNENDRUCKER, *A forward semi-Lagrangian method for the numerical solution of the Vlasov equation*, Comput. Phys. Comm. **180**, pp.1730-1745, (2009).
- [12] N. CROUSEILLES, A. GHIZZO, S. SALMON, *Vlasov laser-plasma interaction simulations with a moving grid*, INRIA Research Report number 6109 (2007).

- [13] C.J. COTTER, J. FRANK, S. REICH *The remapped particle-mesh semi-Lagrangian advection scheme*, Q. J. Meteorol. Soc., **133**, pp. 251-260, (2007).
- [14] J.W. EASTWOOD, *Virtual particle methods*, Comp. Phys. Comm., **64**, Issue 2, pp. 252-266, (1991).
- [15] N.V. ELKINA, J. BÜCHNER, *A new conservative unsplit method for the solution of the Vlasov equation*, J. Comput. Phys. **213** pp. 862, (2006).
- [16] T. ZH. ESIRKEPOV, *Exact charge conservation scheme for Particle-in-Cell simulation with an arbitrary form-factor*, Comp. Phys. Comm. **135**, pp. 144-153, (2001).
- [17] F. FILBET, E. SONNENDRÜCKER, P. BERTRAND, *Conservative numerical schemes for the Vlasov equation*, J. Comput. Phys., **172**, pp. 166-187, (2001).
- [18] F. FILBET, E. SONNENDRÜCKER, *Comparison of Eulerian Vlasov solvers*, Comput. Phys. Comm., **151**, pp. 247-266, (2003).
- [19] A. GHIZZO, P. BERTRAND, M.L. BEGUE, T.W. JOHNSTON, M. SHOUCRI, *A Hilbert-Vlasov code for the study of high-frequency plasma beatwave accelerator*, IEEE Transaction on Plasma Science, **24**, p. 370, (1996).
- [20] A. GHIZZO, P. BERTRAND, M. SHOUCRI, T.W. JOHNSTON, E. FIJALKOW, M.R. FEIX, *A Vlasov code for the numerical simulation of stimulated Raman scattering*, J. Comput. Phys. **90**, pp. 431-457, (1990).
- [21] V. GRANDGIRARD, M. BRUNETTI, P. BERTRAND, N. BESSE, X. GARBET, P. GHENDRIH, G. MANFREDI, Y. SARRAZIN, O. SAUTER, E. SONNENDRÜCKER, J. VACLAVIK, L. VILLARD, *A drift-kinetic semi-Lagrangian 4D code for ion turbulence simulation*, J. Comput. Phys., **217**, pp. 395-423, (2006).
- [22] F. HUOT, A. GHIZZO, P. BERTRAND, E. SONNENDRÜCKER, O. COULAUD *Instability of the time splitting scheme for the one-dimensional and relativistic Vlasov-Maxwell system*, J. Comput. Phys., **185**, pp. 512-531, (2003).
- [23] F. HUOT, A. GHIZZO, P. BERTRAND, E. SONNENDRÜCKER, O. COULAUD *Study of a propagation of ultraintense electromagnetic wave through plasma using semi-Lagrangian Vlasov codes*, IEEE Trans. on Plasma SC., **28**, (2000).
- [24] T.W. JOHNSTON, P. BERTRAND, A. GHIZZO, M. SHOUCRI, E. FIJALKOW, M.R. FEIX, *Simulated Raman scattering: Action evolution and particle trapping via Euler-Vlasov, fluid simulation*, Phys. Fluids B4, pp. 2523-2537, (1992).
- [25] B. MARDER, *A method for incorporating Gauss's law into electromagnetic PIC codes*, J. Comput. Phys. **68**, pp. 48-55, (1987).
- [26] C.-D. MUNZ, P. OMNES, R. SCHNEIDER, E. SONNENDRÜCKER, U. VOSS, *Divergence Correction Techniques for Maxwell Solvers Based on a Hyperbolic Model*, J. Comput. Phys., **161**, Issue 2, pp. 484-511, (2000).

- [27] T. NAKAMURA, T. YABE, *Cubic interpolated propagation scheme for solving the hyper-dimensional Vlasov-Poisson equation in phase space*, Comput. Phys. Comm., **120**, pp. 122-154, (1999).
- [28] S. REICH, *An explicit and conservative remapping strategy for semi-Lagrangian advection*, Atmospheric Science Letters, **8**, pp. 58-63, (2007).
- [29] T. RESPAUD, E. SONNENDRÜCKER *Analysis of a new class of Forward semi-Lagrangian schemes for the 1D Vlasov Poisson Equations*, HAL: hal-00442957, Submitted.
- [30] N.J. SIRCOMBE, T.D. ARBER, *VALIS: A split-conservative scheme for the relativistic 2D*; J. Comput. Phys., **228**, pp. 4773-4788 (2009).
- [31] M. SHOUCRI, *A two-level implicit scheme for the numerical solution of the linearized vorticity equation*, Int. J. Numer. Meth. Eng., **17**, p. 1525 (1981).
- [32] M. SHOUCRI, *Nonlinear evolution of the bump-on-tail instability*, Phys. Fluids, **22**, p. 2038-2039 (1979).
- [33] H. SCHMITZ, R. GRAUER, *Comparison of time splitting and backsubstitution methods for integrating Vlasov's equation with magnetic fields*, Comput. Phys. Commun. **175**, pp.86 (2006).
- [34] E. SONNENDRÜCKER, J. ROCHE, P. BERTRAND, A. GHIZZO, *The semi-Lagrangian method for the numerical resolution of the Vlasov equation*, J. Comput. Phys., **149**, pp. 201-220, (1999).
- [35] T. UMEDA, Y. OMURA, T. TOMINAGA, H. MATSUMOTO, *A new charge conservation method in electromagnetic particle-in-cell simulations*, Comp. Phys. Comm **156**, Issue1, pp. 73-85, (2003).
- [36] J. VILLASENOR, O. BUNEMAN, *Rigorous charge conservation for local electromagnetic field solvers*, Comp. Phys. Comm. **69**, pp. 306-316, (1992).
- [37] M. ZERROUKAT, N. WOOD, A. STANIFORTH, *A monotonic and positive-definite filter for a Semi-Lagrangian Inherently Conserving and Efficient (SLICE) scheme*, Q.J.R. Meteorol. Soc., **131**, pp 2923-2936, (2005).
- [38] M. ZERROUKAT, N. WOOD, A. STANIFORTH, *The Parabolic Spline Method (PSM) for conservative transport problems*, Int. J. Numer. Meth. Fluids, **51**, pp. 1297-1318, (2006).

Charge conserving conservative semi-Lagrangian methods for the relativistic Vlasov-Maxwell equations

6.1 Introduction

To describe the dynamics of charged particles in a plasma or in a propagating beam, the Vlasov equation can be used to calculate the response of the plasma to the electromagnetic fields. The unknown $f(t, \mathbf{x}, \mathbf{p})$ which depends on the time t , the space \mathbf{x} and the impulsion \mathbf{p} represents the distribution function of the studied particles. The coupling with the self-consistent electromagnetic fields is taken into account through the Maxwell's equations. Due to its nonlinear structure, analytical solutions are available only in few academic cases, and numerical simulations have to be performed to study realistic physical phenomena. Nowadays, mostly two classes of methods are used to investigate the behavior of the numerical solution of the Vlasov equation. On the one hand, Particle In Cell (PIC) methods, which are the most widely used, approach the plasma by macro-particles, the trajectories of which follow the characteristic curves of the Vlasov equation whereas the electromagnetic fields are computed by gathering the charge and current densities particles on a grid of the physical space (see [2]). On the other hand, Eulerian methods consist in discretizing the Vlasov equation on a grid of the phase space using classical numerical schemes such as finite volumes or finite elements methods for example (see [3, 8, 15, 6]). Although PIC methods can theoretically and potentially solve the whole 6 dimensional problem, it is well known that the inherent numerical noise makes difficult a precise description of low density regions, despite significant recent improvements. Hence, Eulerian methods offer a good alternative to overcome this lack of precision, even if problems of memory can arise when high dimensions problems are dealt with. In particular, Vlasov codes seem to be appropriate to study nonlinear processes. This last decade, gridded Vlasov solvers have been developed for 2D, 4D and even 5D phase space problems. Among them, the semi-Lagrangian method using a cubic spline interpolation (SPL) [15] and the Positive Flux Conservative (PFC)

method [7] have been implemented to deal with physical applications [9, 10, 16]. Recently, a parabolic spline method (PSM) has been introduced for transport equations arising in meteorology applications [18, 19]. This method benefits from the best approximation property of the SPL method and from the conservation of mass and positivity (by applying a suitable filter) of the PFC method. Conservative methods present a lot of advantages. In addition to the inherent conservative property, slope limiters can be introduced in the reconstruction to ensure some specific properties (positivity, monotonicity); moreover, since the conservative form of the equation is solved, multi-dimensional problems can be solved by a splitting procedure so that the solution of the full problem is reduced to a succession of solution to only one-dimensional problems. Obviously, this property is of great interest from an implementation and algorithmic point of view.

Nevertheless, all these kinds of methods lead to values of the charge and current densities which do not verify the discrete charge conservation equation. In order to properly simulate the physics of the Vlasov-Maxwell problem, it is well known that the charge conservation equation must be verified, so that the solutions of Ampère and Faraday automatically satisfy the electric Gauss' law. Thanks to a deposition scheme originally introduced by Villasenor and Buneman, charge conservation in PIC codes has been achieved. (See ([1, 17]) for details.)

Using conservative methods, Sircombe and Arber managed to create a 4D charge conserving algorithm [14] in the VALIS code. In the last chapter, we built a Forward semi-Lagrangian method for 1D problems, and the goal was to generalize it to 4D problems. In order to compare the results to the ones of VALIS, we have to compute all these 4D algorithms.

The following chapter is organized as follows. First, the relativistic 4D Vlasov-Maxwell equations are recalled, then finite volume form of semi-Lagrangian scheme is explained, and examples of reconstruction are given. In a third part, charge conservation finite volume scheme like in [?] is developed, and finally numerical results for the PSM method are given.

6.2 The relativistic Vlasov-Maxwell equations

We consider the motion of relativistic particles of charge q and mass m in their self-consistent electromagnetic field, which can be described by the relativistic Vlasov-Maxwell equations. Throughout the paper we shall study the two-dimensional model, which involves four phase space dimensions, namely x, y, p_x, p_y . In this case the unknown quantities are the particle distribution function $f(t, \mathbf{x}, \mathbf{p})$, the electric field $\mathbf{E}(t, \mathbf{x}) = (E_x, E_y, 0)$ and the magnetic field $\mathbf{B}(t, \mathbf{x}) = (0, 0, B_z)$, where we denote $\mathbf{x} = (x, y)$ and $\mathbf{p} = (p_x, p_y)$. Then the Vlasov equation reads

$$\frac{\partial f}{\partial t} + \mathbf{v}(\mathbf{p}) \cdot \nabla_x f + q(\mathbf{E}(t, \mathbf{x}) + \mathbf{v}(\mathbf{p}) \times \mathbf{B}(t, \mathbf{x})) \cdot \nabla_p f = 0, \quad (6.1)$$

where the particle velocity is defined by $\mathbf{v}(\mathbf{p}) = \frac{\mathbf{p}}{m\gamma}$ and the Lorentz factor $\gamma = \sqrt{1 + \frac{p_x^2 + p_y^2}{m^2 c^2}}$, with c the speed of light in vacuum. The initial condition $f(0, \mathbf{x}, \mathbf{p}) = f_0(\mathbf{x}, \mathbf{p})$ is given. The self-consistent electromagnetic fields $(\mathbf{E}(t, \mathbf{x}), \mathbf{B}(t, \mathbf{x}))$ are computed thanks to the Maxwell's

equations:

$$\frac{\partial \mathbf{E}}{\partial t} - c^2 \nabla \times \mathbf{B} = -\frac{\mathbf{J}}{\epsilon_0}, \quad (6.2)$$

$$\frac{\partial \mathbf{B}}{\partial t} + \nabla \times \mathbf{E} = 0, \quad (6.3)$$

$$\nabla \cdot \mathbf{E} = \frac{\rho}{\epsilon_0}, \quad (6.4)$$

$$\nabla \cdot \mathbf{B} = 0, \quad (6.5)$$

where ϵ_0 is the permittivity of free space. The sources of the Maxwell's equations, namely the charge density ρ and current density \mathbf{J} are computed from the particle distribution f and the uniform neutralizing Maxwellian background particles defined by their density $n_0(\mathbf{x}) = \int f_0(\mathbf{x}, \mathbf{p}) d\mathbf{p}$ thanks to

$$\rho(t, \mathbf{x}) = q \left(\int f(t, \mathbf{x}, \mathbf{p}) d\mathbf{p} - n_b(\mathbf{x}) \right), \quad \mathbf{J}(t, \mathbf{x}) = q \int f(t, \mathbf{x}, \mathbf{p}) \mathbf{v}(p) d\mathbf{p}. \quad (6.6)$$

Note that integrating the Vlasov equation with respect to the momentum variable \mathbf{p} yields

$$\frac{\partial \rho}{\partial t} + \nabla \cdot \mathbf{J} = 0, \quad (6.7)$$

which is called the continuity equation and expresses the local conservation of charge. In the continuous setting, provided this continuity equation is satisfied and Gauss' law (6.4) is satisfied at time $t = 0$, if the electric and magnetic fields are computed using only Ampere's law (6.2) and Faraday's law (6.3), Gauss' law is satisfied for all time. In general, numerical Vlasov-Maxwell solvers being PIC, Eulerian or semi-Lagrangian do not verify this and a correction scheme is generally used to enforce Gauss' law at all time step or from time to time, which induces causality problems for some applications as the correction scheme generally consists in solving an elliptic or parabolic problem [13] which propagates information at infinity speed.

A major aim of this paper will be to establish a discrete continuity equation verified by the discrete charge and current densities computed from the Vlasov solver compatible with the Maxwell solver, so that only Ampere's and Faraday's law will need to be advanced by our Maxwell solver, Gauss' law being a consequence of those.

6.3 Finite Volume form of a semi-Lagrangian scheme

6.3.1 Description of the conservative semi-Lagrangian scheme for constant coefficient advection in a Finite Volume formalism

We are now going to cast a conservative semi-Lagrangian scheme [6] for constant coefficient advection into a Finite Volume formalism. This will then enable us to construct charge conserving algorithms for a large class of split semi-Lagrangian schemes.

Let us consider constant coefficient 1D advections of the form

$$\frac{\partial f}{\partial t} + a \frac{\partial f}{\partial x} = 0. \quad (6.8)$$

Let us define uniformly spaced control cells $[x_{i-1/2}, x_{i+1/2}]$ with $x_{i+1/2} - x_{i-1/2} = \Delta x$. The unknown in a Finite Volume scheme will be the average value on a control cell that we shall denote by $f_j = \frac{1}{\Delta x} \int_{x_{j-1/2}}^{x_{j+1/2}} f(x) dx$.

In both Finite Volume and conservative semi-Lagrangian schemes, the first step is to reconstruct a piecewise polynomial function on each cell. We shall call f^R this reconstructed piecewise polynomial function. The reconstruction scheme does not matter for our purpose, it could be PPM, splines or something else (see next subsection), with limiters or not. The only property we shall need is that it is linked to the computed cell averages by $f_j = \frac{1}{\Delta x} \int_{x_{j-1/2}}^{x_{j+1/2}} f^R(x) dx$. We shall also assume that the CFL condition $\frac{a\Delta t}{\Delta x} \leq 1$ is verified.

In a Finite Volume scheme for the 1D advection equation (6.8), we compute

$$f_{i+1/2}^{n+1/2} = \frac{1}{\Delta t} \int_{t_n}^{t_{n+1}} f(t, x_{i+1/2}) dt = \frac{1}{\Delta t} \int_{t_n}^{t_{n+1}} f^R(x_{i+1/2} - a(t - t_n)) dt,$$

and by the change of variables $x = x_{i+1/2} - a(t - t_n)$:

$$f_{i+1/2}^{n+1/2} = \frac{1}{a\Delta t} \int_{x_{i+1/2}-a\Delta t}^{x_{i+1/2}} f^R(x) dx. \quad (6.9)$$

Integrating (6.8) on a control cell yields and between time t_n and t_{n+1} yields:

$$\begin{aligned} f_i^{n+1} &= f_i^n - \frac{a}{\Delta x} \int_{t_n}^{t_{n+1}} (f(t, x_{i+1/2}) - f(t, x_{i-1/2})) dt, \\ &= f_i^n - \frac{1}{\Delta x} \left(\int_{x_{i+1/2}-a\Delta t}^{x_{i+1/2}} f^R(x) dx - \int_{x_{i-1/2}-a\Delta t}^{x_{i-1/2}} f^R(x) dx \right). \end{aligned} \quad (6.10)$$

Let us denote by $f_{i+1/2}^{n+1/2}$ a numerical approximation of $\frac{1}{\Delta t} \int_{t_n}^{t_{n+1}} f(t, x_{i+1/2}) dt$. Then, using (6.9) and (6.10) our Finite Volume scheme becomes

$$f_i^{n+1} = f_i^n - \frac{a\Delta t}{\Delta x} (f_{i+1/2}^{n+1/2} - f_{i-1/2}^{n+1/2}). \quad (6.11)$$

On the other hand, for a conservative semi-Lagrangian scheme, the distribution function is updated using the relation

$$f_i^{n+1} = \frac{1}{\Delta x} \int_{X(x_{j-1/2})}^{X(x_{j+1/2})} f^R(x) dx,$$

where $X(x_{j+1/2})$ is the origin of the characteristic ending at $x_{j+1/2}$, that is in our case of constant advection at velocity a , $X(x_{j+1/2}) = x_{j+1/2} - a\Delta t$. Hence

$$\begin{aligned} f_i^{n+1} &= \frac{1}{\Delta x} \int_{x_{j-1/2}-a\Delta t}^{x_{j+1/2}-a\Delta t} f^R(x) dx, \\ &= \frac{1}{\Delta x} \left(\int_{x_{j-1/2}-a\Delta t}^{x_{j-1/2}} f^R(x) dx + \int_{x_{j-1/2}}^{x_{j+1/2}} f^R(x) dx - \int_{x_{j+1/2}-a\Delta t}^{x_{j+1/2}} f^R(x) dx \right), \\ &= f_i^n + \frac{1}{\Delta x} \left(\int_{x_{j-1/2}-a\Delta t}^{x_{j-1/2}} f^R(x) dx - \int_{x_{j+1/2}-a\Delta t}^{x_{j+1/2}} f^R(x) dx \right), \end{aligned}$$

which is the same expression as (6.10), so that both formalisms yield the same numerical scheme. Moreover, the finite volume flux $f_{i+1/2}^{n+1/2}$ can be expressed for a semi-Lagrangian scheme with respect to the reconstructed function f^R by

$$f_{i+1/2}^{n+1/2} = \frac{1}{a\Delta t} \int_{x_{j+1/2}-a\Delta t}^{x_{j+1/2}} f^R(x) dx.$$

In particular, if the reconstruction is performed using a primitive F^R of f^R , we have

$$f_{i+1/2}^{n+1/2} = \frac{1}{a\Delta t} (F^R(x_{j+1/2}) - F^R(x_{j+1/2} - a\Delta t)),$$

and the conservative scheme can write under a Finite Volume form:

$$f_i^{n+1} = f_i^n - \frac{a\Delta t}{\Delta x} (f_{i+1/2}^{n+1/2} - f_{i-1/2}^{n+1/2}).$$

6.3.2 Examples of reconstruction

Once the computation of the characteristics is done, we have to interpolate the primitive F^R of f^R . Knowing its values on the grid: $F_{i-\frac{1}{2}}^R$, $i \in [0, \dots, N]$ we want to compute $F^R(x)$. A periodic framework is considered, which imposes that:

$$F_{i-\frac{1}{2}}^R = F_{r-\frac{1}{2}}^R + qF_{N-\frac{1}{2}}^R, \quad \text{with } i = r + qN, \quad r \in [0, \dots, N-1], q \in \mathbb{Z}.$$

Then, an interpolation operator for $\alpha \in \mathbb{R}$: $\Lambda_\alpha: \mathbb{R}^{\mathbb{Z}} \rightarrow \mathbb{R}$ must be given, which satisfies:

$$\Lambda_k(f_i) = f_k, \quad k \in \mathbb{Z}$$

then, in a general case, we can write:

$$F^R(x) = \Lambda_{\alpha+\frac{1}{2}} f_{i-\frac{1}{2}}^R, \quad x = \alpha\Delta x.$$

Let us present the following classical reconstructions, like in [6]

Lagrange reconstruction Let $d \in \mathbb{N}$. The centered Lagrange reconstruction of degree $2d+1$ is:

$$\Lambda_\alpha(f_i) = \sum_{j=i-d}^{i+d+1} f_j l_j(\alpha), \quad i \leq \alpha < i+1, \quad l_j(\alpha) = \prod_{k=j-d, k \neq j}^{j+d+1} \frac{\alpha - k}{j - k},$$

which leads to

$$F^R(x) = \sum_{j=i-d}^{i+d+1} f_{j-\frac{1}{2}}^R L_j(x), \quad \forall x \in [x_{i-\frac{1}{2}}, x_{i+\frac{1}{2}}],$$

where

$$L_j(x) = \prod_{k=j-d, k \neq j}^{j+d+1} \frac{x - x_{k-\frac{1}{2}}}{x_{j-\frac{1}{2}} - x_{k-\frac{1}{2}}}$$

For $d = 1$, this reconstruction corresponds to the PFC method introduced in [7] in which the slope limiters step is not performed. This approach and similar ones have been also introduced in [11]. See [12] for a more complete bibliography.

Spline reconstruction The B-spline function is classically recursively defined by

$$B_d(x) = \int_{\mathbb{R}} B_{d-1}(t)B_0(x-t) dt, \quad B_0(x) = 1_{[-\frac{1}{2}, \frac{1}{2}]}(x)$$

The interpolation operator then writes:

$$\Lambda_\alpha(f_j) = \sum_{i \in \mathbb{Z}} \eta_i(f_j) B_d(\alpha - i),$$

which leads to:

$$F^R(x) = \sum_{i \in \mathbb{Z}} \eta_i B_d \left(\frac{x - x_{i-\frac{1}{2}}}{\Delta x} \right),$$

where the η_i coefficients are determined through the solving of a classical linear system (see [6]).

This approach (for $d = 3$) has been introduced in [19] as the Parabolic Spline Method. Their formulation refers to the reconstruction of the function g which is a C^1 piecewise parabolic function.

Hermite reconstruction We can consider a C^1 reconstruction of $F^R(x)$, using a Hermite interpolation operator:

$$\Lambda_\alpha(f_i) = f_i + f'_i \alpha + (f_{i+1} - f_i - f'_i) \alpha^2 + (f'_{i+1} + f'_i - 2(f_{i+1} - f_i)) \alpha^2 (\alpha - 1), \quad i \leq \alpha < i + 1,$$

The derivative value f'_j needs to be estimated. As in [8], we can use a fourth order accurate formula:

$$f'_j = \frac{1}{12\Delta x} (f_{j-2} - f_{j+2} + 8(f_{j+1} - f_{j-1})), \quad (6.12)$$

Note we can use a higher order formula, e. g. a sixth-order one:

$$f'_j = \frac{1}{60\Delta x} (f_{j+3} - f_{j-3} + 9(f_{j-2} + f_{j+2} + 45(f_{j+1} - f_{j-1}))). \quad (6.13)$$

This reconstruction with (6.12) (resp (6.13)) corresponds to the PPM method [4] (resp. [5]), in which the slope limiters step is not performed. We will denote it by PPM1, (resp. PPM2).

6.4 Charge conserving Finite Volume schemes

A discrete continuity equation is necessarily linked to the Maxwell solver, as the discrete curl and divergence operators need to be compatible. To this aim a first requirement of the Maxwell solver, is that the discrete divergence of the discrete curl vanishes. This property is in particular satisfied by the Yee solver on a staggered mesh.

On Fig. 6.4, the positions of the fields and the densities are displayed: $Ex_{i+1/2,j}$, $Ey_{i,j+1/2}$, $Bz_{i+1/2,j+1/2}$, $\rho_{i,j}$, $Jx_{i+1/2,j}$, $Jy_{i,j+1/2}$

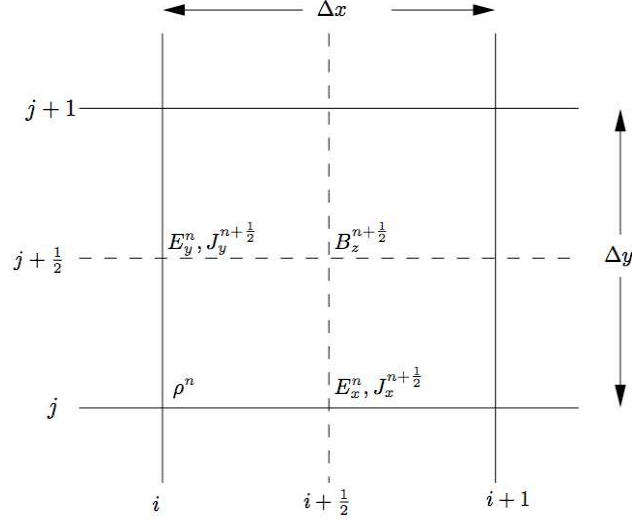


Figure 6.4.1: Positions of the fields and the densities for the 4D Yee scheme for Maxwell TE

The Yee scheme reads

$$\frac{B_{z_{i+1/2,j+1/2}}^{n+1/2} - B_{z_{i+1/2,j+1/2}}^{n-1/2}}{\Delta t} = \frac{E_{x_{i+1/2,j+1}}^n - E_{x_{i+1/2,j}}^n}{\Delta y} - \frac{E_{y_{i+1,j+1/2}}^n - E_{y_{i,j+1/2}}^n}{\Delta x}, \quad (6.14)$$

$$\frac{E_{x_{i+1/2,j}}^{n+1} - E_{x_{i+1/2,j}}^n}{\Delta t} = c^2 \frac{B_{z_{i+1/2,j+1/2}}^{n+1/2} - B_{z_{i+1/2,j-1/2}}^{n+1/2}}{\Delta y} - \frac{1}{\epsilon_0} J_{x_{i+1/2,j}}^{n+1/2}, \quad (6.15)$$

$$\frac{E_{y_{i,j+1/2}}^{n+1} - E_{y_{i,j+1/2}}^n}{\Delta t} = -c^2 \frac{B_{z_{i+1/2,j+1/2}}^{n+1/2} - B_{z_{i-1/2,j+1/2}}^{n+1/2}}{\Delta x} - \frac{1}{\epsilon_0} J_{y_{i,j+1/2}}^{n+1/2}. \quad (6.16)$$

The associate discrete Gauss' law will then read

$$\frac{E_{x_{i+1/2,j}}^n - E_{x_{i-1/2,j}}^n}{\Delta x} + \frac{E_{y_{i,j+1/2}}^n - E_{y_{i,j-1/2}}^n}{\Delta y} = \frac{1}{\epsilon_0} \rho_{i,j}^n. \quad (6.17)$$

Now, taking the discrete divergence of Ampere's law (6.15)-(6.16) yields

$$\begin{aligned} \frac{1}{\Delta t} \left(\frac{E_{x_{i+1/2,j}}^{n+1} - E_{x_{i-1/2,j}}^{n+1}}{\Delta x} + \frac{E_{y_{i,j+1/2}}^{n+1} - E_{y_{i,j-1/2}}^{n+1}}{\Delta y} - \frac{E_{x_{i+1/2,j}}^n - E_{x_{i-1/2,j}}^n}{\Delta x} - \frac{E_{y_{i,j+1/2}}^n - E_{y_{i,j-1/2}}^n}{\Delta y} \right) \\ = -\frac{1}{\epsilon_0} \left(\frac{J_{x_{i+1/2,j}}^{n+1/2} - J_{x_{i-1/2,j}}^{n+1/2}}{\Delta x} + \frac{J_{y_{i,j+1/2}}^{n+1/2} - J_{y_{i,j-1/2}}^{n+1/2}}{\Delta y} \right). \end{aligned}$$

Let us now assume that we have, at all time steps t_n , a discrete continuity equation reading

$$\frac{\rho_{i,j}^{n+1} - \rho_{i,j}^n}{\Delta t} + \frac{J_{x_{i+1/2,j}}^{n+1/2} - J_{x_{i-1/2,j}}^{n+1/2}}{\Delta x} + \frac{J_{y_{i,j+1/2}}^{n+1/2} - J_{y_{i,j-1/2}}^{n+1/2}}{\Delta y} = 0, \quad (6.18)$$

then

$$\frac{1}{\Delta t} \left(\frac{E_{x_{i+1/2,j}}^{n+1} - E_{x_{i-1/2,j}}^{n+1}}{\Delta x} + \frac{E_{y_{i,j+1/2}}^{n+1} - E_{y_{i,j-1/2}}^{n+1}}{\Delta y} - \frac{E_{x_{i+1/2,j}}^n - E_{x_{i-1/2,j}}^n}{\Delta x} - \frac{E_{y_{i,j+1/2}}^n - E_{y_{i,j-1/2}}^n}{\Delta y} \right) = \frac{1}{\epsilon_0} \left(\frac{\rho_{i,j}^{n+1} - \rho_{i,j}^n}{\Delta t} \right).$$

So, if the discrete Gauss law (6.17) is satisfied at time t^n , it follows that

$$\frac{E_{x_{i+1/2,j}}^{n+1} - E_{x_{i-1/2,j}}^{n+1}}{\Delta x} + \frac{E_{y_{i,j+1/2}}^{n+1} - E_{y_{i,j-1/2}}^{n+1}}{\Delta y} = \frac{1}{\epsilon_0} \rho_{i,j}^{n+1},$$

which is the discrete Gauss law at time t_{n+1} .

As a consequence, for the discrete Gauss law (6.17) to be automatically satisfied, when the discrete electromagnetic field is computed using Yee's scheme, the discrete charge and current densities computed with the discrete distribution function obtained by a Vlasov solver need to verify the discrete continuity equation (6.18).

Sircombe and Arber [14] showed that this could be enforced for a split-eulerian Vlasov solver using the PPM method of Colella and Woodward [4] by computing \mathbf{J} from the fluxes needed by the algorithm in the configuration space advections. Let us now show that this idea can be applied for general Finite Volume schemes. Although this is not necessary to obtain a discrete continuity equation, we shall only consider schemes which are split between configuration space and momentum space advections, as those are a lot more convenient to use in practice.

The split scheme will lead us to solve alternatively

$$\frac{\partial f}{\partial t} + \mathbf{v}(\mathbf{p}) \cdot \nabla_x f = 0, \quad (6.19)$$

and

$$\frac{\partial f}{\partial t} + q(\mathbf{E}(t, x) + \mathbf{v}(\mathbf{p}) \times \mathbf{B}(t, x)) \cdot \nabla_p f = 0, \quad (6.20)$$

The second equation does not modify ρ as can be seen integrating with respect to momentum. Hence it should not provide any direct contribution to \mathbf{J} either for the discrete continuity equation to be satisfied. We shall only require that the discrete solver exactly conserves ρ at all grid points, which is the case for all conservative solvers.

Let us now look at the advection in configuration space (6.19). For each given \mathbf{p} it is a constant coefficient advection.

Remark 9. For a, b constants, the operators $a \frac{\partial}{\partial x}$ and $b \frac{\partial}{\partial y}$ commute, so that the splitting is exact for constant coefficient 2D advection at the continuous level. However, there might be differences at the discrete level, but there should be not loss of order.

This applies in particular for the configuration space advection for fixed \mathbf{p} . Indeed, in this case it is equivalent to perform one 2D advection or two 1D advections in arbitrary order. As the latter is simpler and less costly, it is the solution which should be chosen.

Finally, we only need to consider constant coefficient 1D advections of the form

$$\frac{\partial f}{\partial t} + a \frac{\partial f}{\partial x} = 0.$$

Using last section, a Finite Volume or equivalently a conservative scheme writes in this case:

$$f_i^{n+1} = f_i^n - \frac{a\Delta t}{\Delta x} (f_{i+1/2}^{n+1/2} - f_{i-1/2}^{n+1/2}),$$

with

$$f_{i+1/2}^{n+1/2} = \frac{1}{a\Delta t} \int_{x_{i+1/2}-a\Delta t}^{x_{i+1/2}} f^R(x) dx.$$

Note that the actual computation of $f_{i+1/2}^{n+1/2}$ makes up the specific Finite Volume scheme, this could be done with an upwind scheme or the PPM scheme or others described in previous section. For our purposes, it will be sufficient to consider this generic form of the Finite Volume scheme.

Let us now come back to our split Vlasov solver, for which a Finite Volume scheme of the form (6.11) will be used in the x and y advection steps and any conservative scheme in the \mathbf{p} advection step. We discretize the distribution function on a 4D grid with uniform steps in each direction, denoting by i the x index, j the y index, k the p_x index and l the p_y index. Starting from $f_{i,j,k,l}^n$ at time step t^n , the algorithm reads,

$$\begin{aligned} f_{i,j,k,l}^{n,1} &= f_{i,j,k,l}^n - \frac{v_x(\mathbf{p}_{k,l})\Delta t}{2\Delta x} (f_{i+1/2,j,k,l}^{n,1/2} - f_{i-1/2,j,k,l}^{n,1/2}), \\ f_{i,j,k,l}^{n,2} &= f_{i,j,k,l}^{n,1} - \frac{v_y(\mathbf{p}_{k,l})\Delta t}{2\Delta y} (f_{i,j+1/2,k,l}^{n,3/2} - f_{i,j-1/2,k,l}^{n,3/2}), \\ f_{i,j,k,l}^{n,3} &\leftarrow f_{i,j,k,l}^{n,2} \text{ using a conservative advection in } \mathbf{p} \text{ space,} \\ f_{i,j,k,l}^{n,4} &= f_{i,j,k,l}^{n,3} - \frac{v_y(\mathbf{p}_{k,l})\Delta t}{2\Delta y} (f_{i,j+1/2,k,l}^{n,7/2} - f_{i,j-1/2,k,l}^{n,7/2}), \\ f_{i,j,k,l}^{n+1} &= f_{i,j,k,l}^{n,4} - \frac{v_x(\mathbf{p}_{k,l})\Delta t}{2\Delta x} (f_{i+1/2,j,k,l}^{n,9/2} - f_{i-1/2,j,k,l}^{n,9/2}). \end{aligned}$$

where

$$\begin{aligned} f_{i+1/2,j,k,l}^{n,1/2} &= \frac{2}{v_x(\mathbf{p}_{k,l})\Delta t} \int_{x_{i+1/2}-v_x(\mathbf{p}_{k,l})\frac{\Delta t}{2}}^{x_{i+1/2}} f^n(x, y_j, v_{x_k}, v_{y_l}) dx, \\ f_{i,j+1/2,k,l}^{n,3/2} &= \frac{2}{v_y(\mathbf{p}_{k,l})\Delta t} \int_{y_{j+1/2}-v_y(\mathbf{p}_{k,l})\frac{\Delta t}{2}}^{y_{j+1/2}} f^{n,1}(x_i, y, v_{x_k}, v_{y_l}) dy, \\ f_{i,j+1/2,k,l}^{n,7/2} &= \frac{2}{v_y(\mathbf{p}_{k,l})\Delta t} \int_{y_{j+1/2}-v_y(\mathbf{p}_{k,l})\frac{\Delta t}{2}}^{y_{j+1/2}} f^{n,3}(x_i, y, v_{x_k}, v_{y_l}) dy, \\ f_{i+1/2,j,k,l}^{n,9/2} &= \frac{2}{v_x(\mathbf{p}_{k,l})\Delta t} \int_{x_{i+1/2}-v_x(\mathbf{p}_{k,l})\frac{\Delta t}{2}}^{x_{i+1/2}} f^{n,4}(x, y_j, v_{x_k}, v_{y_l}) dx. \end{aligned}$$

Now, the discrete charge density is linked to the discrete distribution function by

$$\rho_{i,j} = q\Delta p_x \Delta p_y \sum_k \sum_l f_{i,j,k,l}.$$

So, using the previous algorithm we can relate $\rho_{i,j}^{n+1}$ to $\rho_{i,j}^n$ by summing the different lines with respect to k, l . Then, we get

$$\begin{aligned} \frac{1}{q\Delta p_x \Delta p_y} \rho_{i,j}^{n+1} &= \sum_{k,l} f_{i,j,k,l}^{n+1} \\ &= \sum_{k,l} f_{i,j,k,l}^{n,4} - \frac{\Delta t}{2\Delta x} \sum_{k,l} v_x(\mathbf{p}_{k,l}) (f_{i+1/2,j,k,l}^{n,9/2} - f_{i-1/2,j,k,l}^{n,9/2}) \\ &= \sum_{k,l} f_{i,j,k,l}^{n,3} - \frac{\Delta t}{2\Delta y} \sum_{k,l} v_y(\mathbf{p}_{k,l}) (f_{i,j+1/2,k,l}^{n,7/2} - f_{i,j-1/2,k,l}^{n,7/2}) \\ &\quad - \frac{\Delta t}{2\Delta x} \sum_{k,l} v_x(\mathbf{p}_{k,l}) (f_{i+1/2,j,k,l}^{n,9/2} - f_{i-1/2,j,k,l}^{n,9/2}) \end{aligned}$$

Then the conservativity of the advection in \mathbf{p} space yields $\sum_{k,l} f_{i,j,k,l}^{n,3} = \sum_{k,l} f_{i,j,k,l}^{n,2}$. Then, proceeding in the same manner with the first two steps of the algorithm we finally get

$$\begin{aligned} \frac{1}{q\Delta p_x \Delta p_y} \rho_{i,j}^{n+1} &= \sum_{k,l} f_{i,j,k,l}^n - \frac{\Delta t}{2\Delta y} \sum_{k,l} (v_y(\mathbf{p}_{k,l}) (f_{i,j+1/2,k,l}^{n,7/2} + f_{i,j+1/2,k,l}^{n,3/2} - f_{i,j-1/2,k,l}^{n,7/2} - f_{i,j-1/2,k,l}^{n,3/2}) \\ &\quad - \frac{\Delta t}{2\Delta x} \sum_{k,l} (v_x(\mathbf{p}_{k,l}) (f_{i+1/2,j,k,l}^{n,9/2} + f_{i+1/2,j,k,l}^{n,1/2} - f_{i-1/2,j,k,l}^{n,9/2} - f_{i-1/2,j,k,l}^{n,1/2})). \quad (6.21) \end{aligned}$$

Let us now denote by

$$J_{x_{i+1/2,j}}^{n+1/2} = q\Delta p_x \Delta p_y \sum_{k,l} v_x(\mathbf{p}_{k,l}) \cdot \frac{1}{2} (f_{i+1/2,j,k,l}^{n,9/2} + f_{i+1/2,j,k,l}^{n,1/2}), \quad (6.22)$$

$$J_{y_{i,j+1/2}}^{n+1/2} = q\Delta p_x \Delta p_y \sum_{k,l} v_y(\mathbf{p}_{k,l}) \cdot \frac{1}{2} (f_{i,j+1/2,k,l}^{n,7/2} + f_{i,j+1/2,k,l}^{n,3/2}). \quad (6.23)$$

Then (6.21) becomes

$$\frac{\rho_{i,j}^{n+1} - \rho_{i,j}^n}{\Delta t} + \frac{J_{x_{i+1/2,j}}^{n+1/2} - J_{x_{i-1/2,j}}^{n+1/2}}{\Delta x} + \frac{J_{y_{i,j+1/2}}^{n+1/2} - J_{y_{i,j-1/2}}^{n+1/2}}{\Delta y} = 0,$$

which is exactly the discrete continuity equation (6.18) needed by the Yee scheme. Hence expressions (6.22)-(6.23) provide an expression of the discrete current density \mathbf{J} consistent with a Finite Volume Vlasov solver and that satisfies a discrete continuity equation.

6.5 Numerical results

We will present the linear Landau damping used with the PSM method introduced in section 6.3.2., which will enable us to check that Gauss' law is indeed satisfied at the discrete level.

The initial condition writes:

$$f(x, y, p_x, p_y) = (1 + \epsilon \cos(k_x x)) \frac{1}{2\pi} \exp(-0.5(p_x^2 + p_y^2)).$$

This corresponds to a Maxwellian perturbed along the x -direction. The domain will be $[0, \frac{2\pi}{k_x}] \times [0, \frac{2\pi}{k_y}] \times [-6, 6]^2$, where $k_x = k_y = 0.5$. $\epsilon = 0.01$ will be considered.

The numerical parameters will be:

$N_x = N_y = 128$ or 256 , and $N_{p_x} = N_{p_y} = 32$. $\Delta t = 0.01$, which is under CFL condition.

On Fig. 6.5.1 is plotted the electric energy for both number of points in the spatial domain, and the theoretical damping which is here -0.1533 . It can be remarked that the method is alright since the damping fits the oscillations. It has to be precised that as the number of points in the spatial dimensions increase, the method becomes more and more accurate dealing with really small values.

On Fig. 6.5.2 and 6.5.3 the charge conservation is displayed at different times for $N_x = N_y = 128$, $N_{p_x} = N_{p_y} = 32$. The charge is preserved up to 10^{-10} , which is acceptable. This diagnostic was also realized with $N_x = N_y = 256$, and the results are about the same.

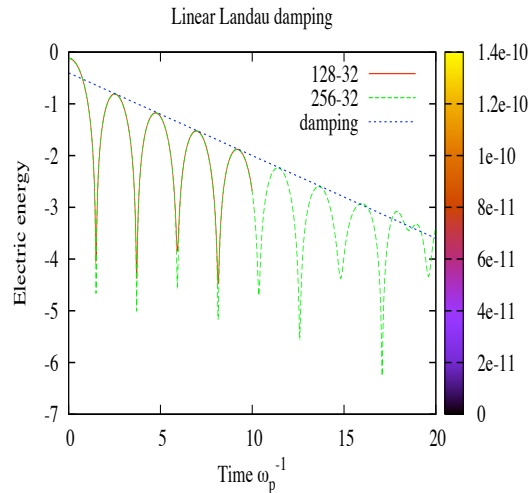


Figure 6.5.1: Electric Energy, $N_x = N_y = 128$ or 256 , $N_{p_x} = N_{p_y} = 32$, $\Delta t = 0.01$

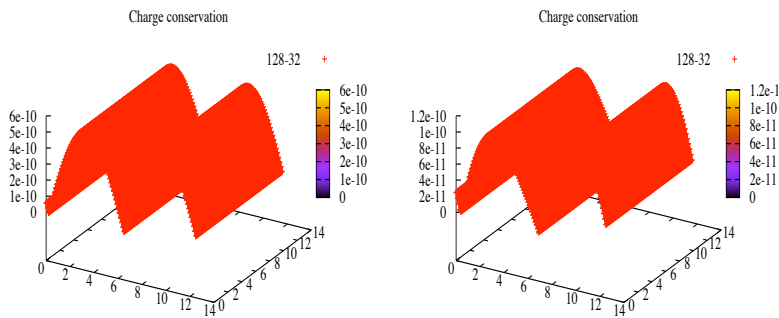


Figure 6.5.2: Charge Conservation, $N_x = N_y = 128$, $N_{p_x} = N_{p_y} = 32$, $\Delta t = 0.01$ after 1000 iterations (left), 5000 iterations (right)

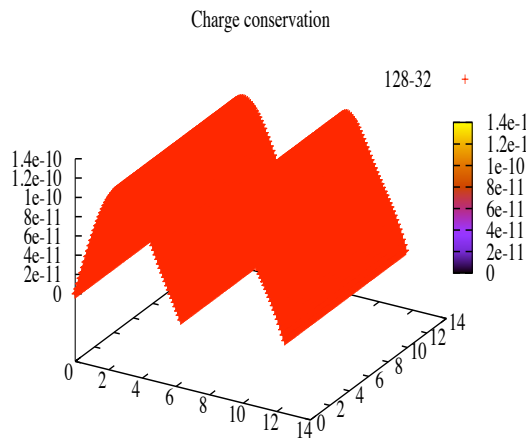


Figure 6.5.3: Charge Conservation, $N_x = N_y = 128$, $N_{p_x} = N_{p_y} = 32$, $\Delta t = 0.01$ after 10000 iterations

6.6 Conclusion and perspectives

The charge preserving algorithm proposed in [14] has been implemented for the particular case of a reconstruction using the Parabolic Spline Method introduced in [19]. The numerical results obtained are encouraging. These results will be further compared with a reconstruction using PPM or PFC, and with the FSL algorithms introduced in chapter 5, using a splitting strategy. Our expecting is that the FSL method will be quicker and easier than the conservative one, but maybe less accurate.

Bibliography

- [1] R. BARTHELMÉ, *Le problème de conservation de la charge dans le couplage des équations de Vlasov et de Maxwell*, Thèse de l'Université Louis Pasteur, 2005.
- [2] C.K. BIRDSALL, A. B. LANGDON, *Plasma Physics via Computer Simulation*, Inst. of Phys. Publishing, Bristol/Philadelphia, (1991).
- [3] C. Z. CHENG, G. KNORR, *The integration of the Vlasov equation in configuration space*, J. Comput. Phys, **22**, pp. 330-3351, (1976).
- [4] P. COLELLA, P.R. WOODWARD, *The Piecewise Parabolic Method (PPM) for gas-dynamical simulations*, J. Comput. Phys. **54** (1984) 174–201.
- [5] P. COLELLA, M. D. SEKORA, *A limiter for PPM that preserves accuracy at smooth extrema*, J. Comput. Phys., **227**, 7069-7076, (2008).
- [6] N. CROUSEILLES, M. MEHRENBERGER, E. SONNENDRÜCKER, *Conservative semi-Lagrangian schemes for the Vlasov equation*, J. Comput. Phys., **229**, no6, pp. 1927-1953 (2010).
- [7] F. FILBET, E. SONNENDRÜCKER, P. BERTRAND, *Conservative numerical schemes for the Vlasov equation*, J. Comput. Phys., **172**, pp. 166-187, (2001).
- [8] F. FILBET, E. SONNENDRÜCKER, *Comparison of Eulerian Vlasov solvers*, Comput. Phys. Comm., **151**, pp. 247-266, (2003).
- [9] A. GHIZZO, P. BERTRAND, M.L. BEGUE, T.W. JOHNSTON, M. SHOUCRI, *A Hilbert-Vlasov code for the study of high-frequency plasma beatwave accelerator*, IEEE Transaction on Plasma Science, **24**, p. 370, (1996).
- [10] V. GRANDGIRARD, M. BRUNETTI, P. BERTRAND, N. BESSE, X. GARBET, P. GHENDRIH, G. MANFREDI, Y. SARRAZIN, O. SAUTER, E. SONNENDRÜCKER, J. VACLAVIK, L. VILLARD, *A drift-kinetic semi-Lagrangian 4D code for ion turbulence simulation*, J. Comput. Phys., **217**, pp. 395-423, (2006).
- [11] J. LAPRISE, A. PLANTE, *A class of semi-Lagrangian integrated-mass (SLIM) numerical transport algorithms*, Mon. Wea. Rev. **123**, pp. 553-565, (1995).

- [12] P. H. LAURITZEN, *An inherently mass-conservative semi-implicit semi-Lagrangian model*, PhD thesis, Department of Geophysics, University of Copenhagen, Denmark, September, 2005.
- [13] C.-D. MUNZ, R. SCHNEIDER, E. SONNENDRÜCKER, U. VOSS, *Maxwell's equations when the charge conservation is not satisfied*, C. R. Acad. Sci. Paris Sér. I Math. **328**, no. 5, pp. 431-436, (1999).
- [14] N.J. SIRCOMBE, T.D. ARBER, *VALIS: A split-conservative scheme for the relativistic 2D Vlasov-Maxwell system*, J. Comput. Phys. **228**, pp. 4773-4788, (2009).
- [15] E. SONNENDRÜCKER, J. ROCHE, P. BERTRAND, A. GHIZZO, *The semi-Lagrangian method for the numerical resolution of the Vlasov equation*, J. Comput. Phys., **149**, pp. 201-220, (1999).
- [16] T. UMEDA, M. ASHOUR-ABDALLA, D. SCHRIVER, *Comparison of numerical interpolation schemes for one-dimensional electrostatic Vlasov code*, J. Plasma Phys., **72**, pp. 1057-1060, (2006).
- [17] J. VILLASENOR, O. BUNEMAN, *Rigorous charge conservation for local electromagnetic field solvers*, Comp. Phys. Comm. **69**, pp. 306-316, (1992).
- [18] M. ZERROUKAT, N. WOOD, A. STANIFORTH, *A monotonic and positive-definite filter for a Semi-Lagrangian Inherently Conserving and Efficient (SLICE) scheme*, Q.J.R. Meteorol. Soc., **131**, pp 2923-2936, (2005).
- [19] M. ZERROUKAT, N. WOOD, A. STANIFORTH, *The Parabolic Spline Method (PSM) for conservative transport problems*, Int. J. Numer. Meth. Fluids, **51**, pp. 1297-1318, (2006).